UTILIZATION OF EUCALYPTUS PULP FIBERS IN CEMENTITIOUS MATERIALS

A Dissertation
Presented to
The Academic Faculty

by

Passarin Jongvisuttisun

In Partial Fulfillment
of the Requirements for the Degree
Doctor of Philosophy in the
School of Civil and Environmental Engineering

Georgia Institute of Technology
December 2014

UTILIZATION OF EUCALYPTUS PULP FIBERS IN CEMENTITIOUS MATERIALS

Approved by:

Dr. Kimberly E. Kurtis , Advisor
School of Civil and Environmental Engineering
Georgia Institute of Technology

Dr. Lawrence F. Kahn
School of Civil and Environmental Engineering
Georgia Institute of Technology

Dr. J. David Frost
School of Civil and Environmental Engineering
Georgia Institute of Technology

Dr. T. Russell Gentry
School of Architecture
Georgia Institute of Technology

Dr. Wilasa Vichit-Vadakan
Manager, Advanced Chemicals for Civil Engineering and Building Materials
SCG Chemicals

Date Approved: August 19, 2014

ACKNOWLEDGEMENTS

First and foremost, I would like to express my sincere gratitude to my advisor, Dr. Kimberly E. Kurtis for her advice, knowledge and many insightful discussions and suggestions. I am grateful for her understanding, wisdom, patience, enthusiasm and encouragement and for pushing me farther than I thought I could go. I am fortunate to have worked with her. I would also like to thank Dr. Wilasa Vichit-Vadakan for her guidance and encouragement to have me pursue such an incredible experience. The joy and enthusiasm they have for their research were motivational for me. I am also thankful for the excellent example they have provided as mentors. I would also like to thank my thesis committee members sincerely Dr. Lawrence Kahn, Dr. David Frost, and Dr. Russell Gentry. I extremely appreciate their assistance and suggestions throughout my research and their time, interest, and helpful comments and insightful questions.

I also gratefully acknowledge the funding source, the Siam Cement Group (SCG) that made my Ph.D. work possible. I am grateful for the assistance provided by Jeremy Mitchell for his help with large-scale experiment setups and Dr. Johannes Leisen for his help with NMR/MRI experiments. All undergraduate research assistants are thanked for their valuable contributions to this research.

My time was made enjoyable in large part due to the many friends that became a part of my life. I am especially grateful for the members of the Kurtis group who have contributed remarkably to my personal and professional time at Georgia Tech, Dr. Robert Moser, Dr. Andrea Mezencevova, Dr. Boyeon Lee, Dr. Amal Jayapalan, Dr. Chris Shearer, Nathan Mayercsik, Bradley Dolphyn, Elizabeth Nadelman, Alvaro Paul, Mehdi

Rashidi, Ahmad Shalan, Gun Kim, and Behnaz Zaribaf. Also, to Daniela Estrada for her friendship and for listening and giving me words of encouragement. To Dr. Jazalyn Dukes and others for their friendship. To Jane Chisholm for her support. She was always there for me to give suggestions on my communication skills.

Most importantly, I would like to thank my family for all their love and encouragement. For my parents who raised me with love and supported me in all my pursuits. I dedicate this dissertation to the memory of my mother Chumjai Jongvisuttisun for her unconditional love through her life. You are always on my mind. To my father Manoo Jongvisuttisun for his love, support, and patience. Mrs. Patcharawilai Pongwishulada and Mr. Pichet Sahachaiyunta for understanding, supporting and being there for me these past four years.

TABLE OF CONTENTS

CHAPTER 8: CONCLUSIONS AND FUTURE RESEARCH

LIST OF TABLES

LIST OF FIGURES

LIST OF SYMBOLS

$A(T_k)$	Distribution of the relaxation time k
C_3A	Tricalcium aluminate phase (cement chemistry notation)
CH	Calcium hydroxide (cement chemistry notation)
C-S-H	Calcium silicate hydrates (cement chemistry notation)
C (x,t)	Chloride concentration of concrete
C_s	Surface chloride concentration of concrete
C_0	Initial chloride concentration of concrete
D_a	Apparent chloride diffusion coefficient
erf	Error function
E_{st}	Modulus of the elasticity of steel
f	Mass of dry fiber
f/c	Dry fiber mass-to-cement ratio
G_x	Gradient along the x-axis
G_y	Gradient along the y-axis
G_z	Gradient along the z-axis
k	Absorption capacity
k_A	Assumed absorption capacity
$\bar{L}_n$	Arithmetic mean length
$\bar{L}_w$	Weight-weighted mean length
l_i	Length class i
MC	Moisture content

M_{CEM}	Mass of cement proportioned for the mixture
M_F	Mass of as-received fiber
M_w	Mass of mixing water
M_o	Local sample magnetization
n	Total number of fiber
n_i	Number of fiber in the l_i
R_{os}	Outer radius of the steel ring
R_{oc}	Outer radius of the specimen
R_{is}	Inner radius of the steel ring
S	Local image intensity
s/c	Sand-to-cement volume ratio
t	The exposure time (h, hours)
t_p	Phase encoding time
T_k	Relaxation time k
T_1	Spin-lattice relaxation time, longitudinal relaxation time
T_2	Spin-spin relaxation time, transverse relaxation time
T_2^*	Effective spin-spin relaxation time
T_E	Echo time
w/c	Water-to-cement ratio
w/cm	Water-to-cementitious materials ratio
$(w/c)_{eff}$	Effective water-to-cement ratio
w_e/c	Entrained water-to-cement ratio
w_e/cm	Entrained water-to-cementitious materials ratio

x	Depth below the exposed surface
ε_i	Noise of the signal at i
ε_{st}	Strain in the steel ring
σ_{max}	Maximum residual tensile stress

LIST OF ABBREVIATIONS

ACI	American Concrete Institute
AFM	Atomic force microscopy
AR-glass	Alkali-resistant glass
ASSHTO	American Association of State Highway and Transportation Officials
ASTM	American Society for Testing and Materials
BKF	Bleached kraft pulp
BSF	Bleached soda pulp
CTL	Chloride threshold limit
CPMG sequence	Carr-Purcell-Meiboom-Gill sequence
DI water	Deionized water
EDS	Energy-dispersive X-ray spectroscopy
ESCA	Electron spectroscopy for chemical analysis
ESEM	Environmental scanning electron microscope
FE-SEM	Field-emission scanning electron microscope
FID	Frequency induction decay
FOV	Field of view
FQA	Fiber quality analyzer
FSP	Fiber saturation point
FTIR	Fourier transform infrared spectroscopy
FWHM	Full width at half maximum

HPFRCC	High performance fiber-reinforced cement composites
HR water	Hard-to-remove water
ICP	Inductively coupled plasma spectroscopy
ICP-OES	Inductively coupled plasma/optical emission spectroscopy
IC water	Internal curing water
IR sequence	Inversion recovery sequence
LOI	Loss on ignition
LWA	Lightweight aggregates
MRI	Magnetic resonance imaging
NMR	Nuclear magnetic resonance
NPE	Non-process elements
PES	Polyethersulfone
PFG	Pulsed field gradient
PP	Polypropylene
PVA	Polyvinyl alcohol
QXRD	Quantitative X-ray diffraction
RCPT	Rapid chloride permeability test
RD	Repetition delay time
RF, rf	Radio frequency
SAP	Superabsorbent polymers
SCF	Semi-chemical pulp
SCMs	Supplementary cementitious materials
SEM	Scanning electron microscope

SNR	Signal-to-noise ratio
SPI	Single point imaging
SPRITE	Single-point-ramped imaging with T_1-enhancement
SSD	Saturated surface dry
TAPPI	Technical Association of the Pulp and Paper Industry
TE	Echo time
TGA	Thermogravimetric analyzer
TMP	Thermomechanical softwood pulp
TR	Repetition time
TRLC	Total residual lignin content
UHPFRCC	Ultra high performance fiber-reinforced cement composites
UKF	Unbleached kraft pulp
USF	Unbleached soda pulp
VP-SEM	Variable-pressure scanning electron microscope
WRV	Water retention value
X-ray CT	X-ray computed tomography
XPS	X-ray photoelectron spectroscopy
XRF	X-ray fluorescence

SUMMARY

With the growing interest in renewable materials, the use of plant-based fibers as reinforcement in cementitious materials has been increasing. Plant-based fiber-cement composites are now found in products such as extruded non-pressure pipes and non-structural building materials such as siding, cladding, and soffit panels. Because of their consistency in quality and compatibility with cementitious matrices, pulped wood fibers, rather than untreated fibers, are an attractive source for renewable fiber reinforcement. Further, with a capacity of 54 million tons per year, pulped wood fibers can be produced on a scale to meet the demand of the construction industry.

Until now, most research efforts have focused on longer-length softwood pulps rather than on shorter-length hardwood pulps. However, not all regions have access to softwood pulps, and the greater availability of hardwood fibers in some developing tropical regions has just prompted interest in evaluating their use in fiber-cement composites. However, to date, these initial studies have focused almost exclusively on mechanical properties, not on early-age properties.

This study evaluates the use of hardwood eucalyptus pulps as internal curing agents and early-age cracking mitigators of cementitious composites. Based on the results, the maximum efficiency of such pulps in cement-based matrices can be achieved by the careful characterization and dosing of eucalyptus pulps and testing of pulp-cement composites. Results suggest that their internal curing efficiency depends more on their physical morphology than their chemical compositions. The results from *in situ* NMR/MRI experiments further confirm the finding that wood pulp, within the same

species, that has a thick cell wall is more beneficial for internal curing applications. The results show that such pulps release their free water in their lumen structure within 25 hours of hydration. Thus, for the hydration reaction beyond 25 hours, free water in small cell wall pores and bound water in the cell wall are responsible for mitigation of self-desiccation of a cement matrix.

Further studies on early-age interaction of eucalyptus pulps with cements also found that such pulps can selectively absorb and desorb ions from the pore solution of cement and precipitate calcium products on their surface, which ultimately can enhance hydration reaction. A more thorough understanding of the interactions between hardwood pulps and cements at early ages allows for optimization of the use and selection of hardwood fibers and tailoring of post-processing methods of fiber so that they can enhance the early age behavior of this growing class of composite materials.

When uniformly dispersed in cementitious composites, pulps have been shown to successfully mitigate self-desiccation in a cementitious matrix and increase resistance to early age shrinkage and cracking. The eucalyptus pulp-reinforced mortars exhibited a lower rate of stress development and lengthened time-to-cracking of about 1.6 and 2.3 times as long as the control mortar, respectively. The initial crack width also decreased by up to 88% in eucalyptus pulp-reinforced samples, which suggests the possibility of assisting self-healing in an appropriate mix design. Here, a series of experiments clarifies the role of hardwood eucalyptus pulps on the mitigation of early-age cracking by the combination of an increase in early tensile capacity, reduction in elastic modulus, and improvement of post-cracking toughness, all of which combine to mitigate early-age cracking.

Finally, to more broadly understand the potential implications of hardwood eucalyptus pulp fiber reinforcement on the performance of concrete, the effects of such pulp on compressive strength and permeability of concrete were also examined. Because of their internal curing capability, hardwood pulp was found to increase the compressive strength of air-cured concrete mixes, but the addition of hardwood pulp also seems to increase permeability of concrete. However, by using the Life 365 service life prediction model, the service life of the hardwood pulp-concrete seems to be least affected by curing condition indicating their robustness against field curing. Therefore, standard curing can underestimate the performance of eucalyptus pulp-cement composites and a curing procedure that resembles the actual field curing is necessary to reflect the actual performance of such fiber-cement composites.

Overall, the findings indicate that eucalyptus pulps can ultimately enhance the early-age properties of cementitious composites by providing internal curing against self-desiccation and reinforcements by crack bridging. Results from air cured samples also confirm the enhancement of pore space through the increase of degree of hydration and the decrease of microcracking due to shrinkage mitigation.

CHAPTER 1

INTRODUCTION

1.1 Background

Eucalyptus, a hardwood native to Australia, is now cultivated all over the world, including South America, North America, and Asia. With average annual growth rates up to 30m^3/ha/year at crop rotations of 7-15 years [1], the increase in plantations dedicated to this genus can be attributed to its "a) rapid growth on poor sites with low rainfall, b) ability to coppice readily, c) ability to tolerate periodic water logging and some soil salinity, and d) the usefulness of the wood for a range of purposes" [2]. Moreover, as it provides a balance in water consumption and promotes biodiversity, eucalyptus is an inexpensive, some have claimed that eucalyptus is an ideal hardwood species for sustainability. In addition, because it has a high capacity to capture carbon as a result of its higher growth rate and denser structure, eucalyptus, compared to other species, is more efficient at capturing carbon dioxide, fixing carbon, and generating oxygen per unit of volume [3]. For example, while a Scots pine tree can capture only about 0.0291 tons of carbon dioxide per year, a eucalyptus tree can capture up to 0.1359 tons [3].

Eucalyptus is increasingly used in a variety of applications, including papermaking. Its long history in the paper industry derives from the relatively good qualities of the fiber at a relatively low market price [4]. Juvenile eucalyptus trees reach maximum pulping strength properties at just six years of age. Because they have lower extractives content and thus require fewer cooking chemicals, younger eucalyptus trees are preferred for the kraft chemical pulping process. In contrast to the more established

use of eucalyptus in the paper industry, the use of eucalyptus pulp fibers in construction materials such as cement composites, mortar, and concrete has attracted considerable interest, but only in recent years with increasing demand for alternative, fast-growing, economical natural fiber that can enhance sustainability in construction materials. However, when compared to other types of plant-based fiber used in cementitious materials such as bamboo, sisal, and pine, the scientific literature related to the use of eucalyptus fiber is relatively limited.

Because the traditional objective of fiber reinforcement in cementitious materials is to improve the tensile capacity of composites, studies examining plant-derived reinforcements have focused on relatively long-length plant-based fibers such as jute, coconut, bagasse, sisal, and pine, not eucalyptus fibers. Compared to other fibers used in cementitious materials, the fiber length of eucalyptus is shorter, as presented in Table 1.1. That is, while most common fibers such as steel, alkali-resistant (AR) glass, and polymer fibers, used to reinforce cement-based materials, range from 6 to 76 mm in length, eucalyptus fibers measure only 0.6 to 1.2 mm in length [5, 6]. However, recent studies have shown that although the length of eucalyptus pulp is relatively short, the higher number of fibers per volume or weight found with a short-length fiber can provide effective crack-bridging, which contributes to an improvement in the mechanical performance of cement composites after aging [5]. Thus, while eucalyptus fiber may not improve the mechanical properties of concrete as much as longer natural fibers, it can be used as effective reinforcement in a wider range of finer-structured cementitious composites such as stucco, plaster, or mortar.

Moreover, although many studies have demonstrated that natural-plant-based fibers improve the performance of cementitious materials in many aspects, including toughness and crack resistance, not all fibers can be used on a large commercial scale because of the availability and variety of the fibers. Since the large-scale production of mortar and concrete requires a significant quantity of raw materials, the availability of fiber is a general prerequisite for the successful use of such fibers in mortar and concrete. Fiber from different sources or locations can contain various chemical components that eventually complicate the control of the hydration reaction. Therefore, the homogenization of the chemical constituents of fiber is another crucial requirement in the industrial-scale production of fiber-cement composites.

Use of wood-derived fibers obtained from large-scale commercial pulping mills could solve the problems of both the availability and variability in the chemical composition of natural fibers, rendering the use of pulps more practical for wider use in mortar and concrete than perhaps other bio-derived fibers. Since the capacity and quality of products in pulp mills are monitored to maintain consistency, variability in fibers derived from commercial pulping processes can be understood and controlled. Because of these advantages, many studies have examined the use of softwood pulps as reinforcements in cement paste, mortar, and concrete. However, this is not the case with hardwood pulps because they are shorter (i.e., lengths of 1 to 1.7 mm) than softwood pulps (e.g., pine pulp lengths are typically 2.5-4 mm [7]), which may limit their potential to improve the tensile strength and deformation capacity of the composites [8]. Therefore, few studies have examined eucalyptus pulps, despite their greater availability in some regions.

Another potential application of eucalyptus fibers is the mitigation of early-age shrinkage cracking in concrete. Several studies have demonstrated that wood-derived materials including pulp fiber can mitigate the autogenous shrinkage of concrete by providing internal curing water [9-11]. In concrete, “the first 48 hours are very important for [its] performance” [12]. During this period, the loss of water, both from the hydration reaction and drying causes concrete to shrink and can lead to cracking. Early cracks resulting from autogenous deformation caused by self-desiccation can increase permeability and gradually decrease durability. To overcome this problem, particularly for dense and low water-to-cement ratio cement-based materials in which external curing is not effective [13], the concept of internal curing water has drawn considerable interest. By incorporating highly absorptive materials such as lightweight aggregate (LWA) and super-absorbent polymers (SAP), internal curing water is distributed on demand throughout the paste as supply water for the hydrating cement paste. Thus, this additional supply of water partially or completely compensates for the loss of water and reduces early shrinkage [14]. Eucalyptus fibers, like other wood-derived fibers, can absorb considerable amounts of water which could potentially be used for internal curing.

Table 1.1 – Typical properties of fibers and their usages, adapted from [8]

Fiber	Length (mm)	Diameter (μm)	Specific gravity	Modulus of elasticity (GPa)	Tensile strength (GPa)	Typical production methods	Common applications
Steel	6.4-76 [15]	5-500	7.84	200	0.5-2.0	Premix	Cladding panels, slabs, pipes, prefabricated slabs
Alkali-resistant glass (AR-glass)	25-40 [16]	9-15	2.6	70-80	2-4	Premix, hand spray, and centrifugal casting	Cladding panels, box elements, roof tiles, pavement, and pipes
Polypropylene (PP)	6-60 [17]	25-1000	0.92-0.96	3.5-10	0.08-0.6	Premix, shotcrete, Hatschek	Cladding panels, sheets, roof tiles, piles
Polyvinyl alcohol (PVA)	6-12	14-650	1.3	23-36	0.8-1.5	Hatschek	Cladding panels, sheets, roof tiles
Jute	1800-3000	10-20	N/A*	N/A	0.25-0.35	Premix, laying	Sheets, roof tiles
Sisal [18]	N/A	N/A	1.37	15.2	0.34-0.37	Premix, laying	Sheets, roof tiles
Pine pulp	0.5-4.5 [19]	5-25 [19]	~1.5	N/A	~0.9	Hatschek	Sheets, roof tiles
Asbestos (Chrysolite)	N/A	0.02-0.4	2.6	164	3.1	Hatschek	Pipes, sheets, roof tiles
Eucalyptus	0.6-1.2 [6]	12-30 [6]	~1.5	35 [20]	N/A	N/A	N/A
Cement matrix (for comparison)	N/A	N/A	1.5-2.5	N/A	0.003-0.007	N/A	N/A

*N/A = not available

Because of their physical and chemical structures, plant-based fibers are capable of absorbing water in the form of both free and weakly bound water and then releasing water into the cement matrix during hydration. Prior research has demonstrated the abilities of different types of pulp fiber (e.g., softwood thermomechanical pulp, softwood kraft pulp, and specialty cellulose fibers) to mitigate autogenous shrinkage in cement paste and mortar [10]. However, the features of these fibers – both chemical and physical – affecting their efficacy as internal curing agents remain relatively unexplored. It is also unclear if the results obtained from prior studies of softwood fiber would also be applicable to hardwood species such as eucalyptus. With a more thorough understanding of the relationship between fiber properties and internal curing efficacy, the selection, the dosing, and even the design of pulp fiber for internal curing would be more precise.

Depending on the chemical constituents and morphology of fibers, plant-based fibers can interact with cement, affecting its early hydration behavior. These potential interactions must be understood so that early age behavior can be anticipated and/or controlled. Since hemicellulose and lignin can retard cement hydration, using fiber with a high content of these two constituents can significantly delay the initial and final setting times of cementitious composites [21-24]. Moreover, the surfaces of the fibers might serve as nucleation sites, and/or the hygroscopicity of the fibers could locally absorb and/or desorb highly alkaline pore water, affecting the concentration of free ions available for cement hydration [25]. Therefore, greater clarification of the interactions of pulp fibers in a cement matrix at an early age will facilitate the optimization of fiber processing methods for enhancing the behaviors of their composite materials.

Because of the substantial benefits of eucalyptus fiber, its use in cementitious materials is expected to increase. Although a number of studies have focused more on the mechanical and long-term performance of eucalyptus fiber-reinforced composites, research pertaining to the nano-to-microscale chemical and physical interactions between fibers and cement is limited. In addition, and perhaps, in part, as a result of the lack of fundamental study of fiber-cement interactions, the effects of eucalyptus fibers on the early-age properties and restrained-shrinkage cracking behaviors of cementitious composites remain relatively unclear.

1.2 Research Motivation

Because they are abundant, economical, and renewable, eucalyptus pulps have attracted interest in the recent decade. As a promising substitute or partial replacement for long-length fiber, eucalyptus fibers used in cementitious materials should become more common in the near future. Prior research has examined the potential of eucalyptus pulps as alternative reinforcement in cement-based composites but, to date, the majority of research efforts have focused more on the mechanical and long-term performance of cement-based composites. The effects of eucalyptus pulps on the early age properties, transport properties, and restrained shrinkage cracking behaviors of cementitious composites remain relatively unclear.

In addition to being used as reinforcement, eucalyptus pulps may be used as internal curing agents to mitigate early-age cracking caused by self-desiccation in high performance concrete. However, since their use as internal curing agents has not been explored, it is not clear if eucalyptus pulps can be used as effective internal curing agents. Moreover, since cement pore solution is highly ionic, improved understanding of such interactions between pulp fibers and the highly ionic concrete pore solution is important for developing pulp fibers for applications in cement-based materials. This will ultimately allow the optimization of fiber processing methods that enhance behaviors of this growing class of composite materials.

1.3 Objectives

The objective of this research is to enhance the understanding of the potential for eucalyptus fibers to mitigate early-age shrinkage and restrained cracking common in cementitious materials. Thus, the proposed study aims to examine both early-age properties, such as the internal curing capacity of fibers and the interactions of fibers with a cement matrix, and the potential for crack deflection and bridging during early-age shrinkage. A key component of this research is the extension of the use of eucalyptus pulps for internal curing and the reinforcement of cementitious materials. The study employs test methods whose purpose is to clarify the complex roles of fiber properties on the cement matrix, which have not been previously addressed in the literature.

Specifically, the purposes of this research are as follows:

1. To examine, through a combination of experiments, the underlying effects of the chemical composition and physical structure of the fiber on internal curing performance by evaluating five treatments of commercially available pulp fiber: unbleached soda pulp, bleached soda pulp, unbleached kraft pulp, bleached kraft pulp, and semi-chemical pulp.
2. To evaluate the mechanisms underlying the release and the movement of water as well as the migration of pore solution ions during the internal curing process.
3. To assess the role of eucalyptus pulps in early-age cracking mitigation.
4. To evaluate the potential of eucalyptus fibers for the mechanical reinforcement of finer structured cementitious composites such as stucco, plaster, and mortar.

1.4 Organization of Dissertation

The following chapters discuss the background, results, and conclusions of this research program. The structure of this dissertation is outlined below.

- Chapter 2 presents a thorough overview of the literature concerning the properties of wood pulps and their potential effects on cementitious materials. The review focuses on the background of the pulping process, the concept of internal curing, the transport of water through wood pulp, the interactions of natural fibers and cement-based matrix at early ages, and the shrinkage and its effects on cracking behaviors of fiber- and natural fiber-reinforced composites.
- Chapter 3 presents a summary of experimental details that outlines the various aspects of this study, from fiber characterization to mechanical testing.
- Chapter 4 presents the morphology and chemical properties of eucalyptus pulps used in this study and their effects on internal curing performance. Based on the internal curing performance, the candidate pulps are selected for further studies.
- Chapter 5 presents a more thorough evaluation of the early-age interactions between eucalyptus pulps and cement and the migration of internal curing water during internal curing.
- Chapter 6 presents the potential of eucalyptus pulps to mitigate early-age cracking in crack-prone mortar under a restrained condition. The ability of eucalyptus pulps combined with their capacity to provide internal curing is evaluated through a series of restrained shrinkage tests, early age mechanical tests, and characterization.

- Chapter 7 presents the effects of eucalyptus pulps on internal curing in concrete, on the compressive strength of concrete, and on the durability of internally-cured eucalyptus fiber-reinforced concrete. Results from bulk chloride diffusion are used for service life calculation, which indicates the effect of eucalyptus pulps on durability of concrete.
- Chapter 8 provides a summary of the research performed in this dissertation and the key conclusions. Future research areas are recommended, based on the major research findings.

CHAPTER 2

LITERATURE REVIEW

Like other types of wood, eucalyptus contains four main chemical components − cellulose, hemicellulose, lignin, and extractives − that contribute to fiber properties. Pulp or wood-derived fiber, the fundamental product of wood predominately used in papermaking, is obtained from a pulping process, in which process conditions, both pulping and bleaching, have profound effects on the chemical composition and morphology of the pulp. Therefore, the first topic in this section deals mainly with pulping processes. Then, the current literature concerning early age behaviors in cementitious composites – internal curing and fiber-cement interactions and the transport of water and pore solution in pulps – as well as shrinkage behaviors and some mechanical properties will be reviewed and discussed.

2.1 Pulping Process

According to ACI544.1R [15], plant-based fibers are available in two forms, i.e., unprocessed and processed fibers. Unprocessed plant-based fibers such as coconut, sisal, bamboo, and other vegetable fibers can be found predominantly in low cost cementitious composites, in which long-term performance is not the case, while processed fibers, usually refer to wood pulp fibers, are more common in large scale commercial production. Compared to unprocessed fibers, wood pulps from either chemical or mechanical pulping processes are relatively shorter, but usually stronger and perform

better during long aging in a cement environment, mostly because of the removal of lignin and extractives during the pulping process [8].

During pulping, wood fibers are extracted and separated from wood chips by rupturing the bond between these fibers by using chemical, mechanical, and thermal treatments. Table 2.1 shows general information about various common pulping processes. Chemical pulping processes such as the soda, sulfite, and kraft processes aim at removing lignin and other materials binding individual cells. These processes do not require any mechanical treatment. Therefore, the physical structure of the fibers is less likely to be altered than in mechanical pulping processes. In the soda pulping process, wood chips are cooked under pressure in a caustic soda solution that dissolves most of the lignin in the wood with some effects on the cellulose and hemicellulose. The soda pulp, a product of the soda pulping process, is relatively soft and bulky, so it is generally used in books, magazines, and envelopes. Because of its superior delignification selectivity resulting in a high quality pulp, the kraft process accounts for over 80 percent of the chemical pulp produced in the U.S. [26] and has almost replaced the soda process. Kraft pulping involves the digestion of wood chips at a specific temperature and pressure in a mixture solution of caustic soda (sodium hydroxide) and sodium sulfide, or “white liquor”. Kraft pulping produces a pulp with strong fibers used in applications such as brown paper bags, in which strength and wear and tear resistance are essential. Although the kraft pulping process produces high quality pulps, it has been emits sulfurous emissions and generates low pulp yield.

In contrast to these treatments which use chemistry to separate individual fiber, mechanical pulping processes such as thermomechanical and refiner mechanical

processes require mechanical energy to tear fiber out of the wood chips. The most well-known mechanical pulp process is high-temperature refining, or thermomechanical process. Because chemical reagents are not involved in mechanical pulping processes, thermomechanical pulp (TMP) fibers contain more lignin and hemicellulose than chemically treated fibers, which result in the lower alkaline resistance. In addition, because the use of the mechanical process for defibrating individual fiber, mechanical pulps are weaker than fibers obtained from other methods.

Semi-chemical pulping combines both chemical and mechanical treatments Therefore, semi-chemical pulping involves two steps: 1) digesting the wood chips with chemicals and 2) refining fibers mechanically, most often by using disc refiners. The process exhibits the intermediate range of pulp yields from 55 to 85 percent, which ranges between mechanical and chemical pulping. The degree of delignification can be designed for certain pulp yields, which is the weight of pulp obtained from a given weight of wood on an oven-dry basis, and specific properties.

Table 2.1 – Classification of pulping processes [27]

Mechanical Pulping	**Semi-chemical Pulping**	**Chemical Pulping**
Treatment using mechanical energy (heat treatment may be involved)	A combination of chemical and mechanical treatments	A combination of chemical and heat treatments
Yield - high (90-95%)	Yield – medium (55-90%)	Yield - low (40-55%)
Short, weak, unstable, impure fibers; difficult to bleach	Fiber properties depend on process	Long, strong, stable, pure fibers; easy to bleach
Processes: - Stone groundwood - Refiner - Thermomechanical	Processes: - Neutral sulfite - semi-chemical - High-yield kraft	Processes: - Kraft - Sulfite - Soda

Bleaching is a process aimed at increasing whiteness and cleanliness of pulps with two approaches, removing residual lignin or destroying some of the chromophoric groups in pulps. For chemical pulps, bleaching continues the delignification process to remove any residual lignin that has not been extracted in prior chemical processing while preserving carbohydrates yield. Bleaching chemicals such as chlorine, sodium hypochlorite, and ozone break down the lignin molecule and disrupt lignin-carbohydrate bonds into small water-or alkali-soluble parts. However, in contrast to chemical pulps, the aim of bleaching of mechanical pulps is to remove color from pulps with little yield loss by reducing or oxidizing chromophores (colored species) to leucochromophores (uncolored species). Therefore, bleaching chemicals such as sodium hydrosulfite and peroxides do not solubilize any appreciable amount of lignin, but rather chemically change colored molecular structures to a colorless structure. Essentially, bleaching does not affect the length of the fibers. However, it does change some fiber properties. It reduces the linear density and the strength of the fibers and increases the refinability.

2.2 Internal Curing Capability and Autogenous Shrinkage

In 1957, the concept of internal curing was introduced. The concept is based on the assumption that well-distributed, moisture-rich materials, such as lightweight aggregates, will transfer their absorbed water to the paste during hydration, as the paste self-desiccates [28]. This concept became popular when Robert Philleo used the term “internal curing” for the first time in 1991:

> "Either the basic nature of Portland cement must be changed so that self-desiccation is reduced, or a way must be found to get curing water into the interior of high strength structural members. A partial replacement of fine aggregate with saturated lightweight fines might offer a promising solution." [29]

In recent studies, since the early-age cracking of concrete remains a significant problem in structures, especially in high-performance concrete in which the relatively low water-to-cement ratio (w/c) compared to normal concrete is used, internal curing technology is considered to be one of the technological challenges of field applications in the future [14].

Internal curing technology compensates for insufficient utilization or applicability of conventional external curing methods, such as water-saturated covering. Since the penetration of water is limited to the concrete near-surface in dense, low water-to-cementitious materials (w/cm < 0.42) concrete, conventional curing methods may eliminate autogenous shrinkage in small cross-sections but not in those thicker than about 50 mm because the penetration of water is limited. To overcome this limitation, two strategies have been developed to make use of internal reservoirs of water. One strategy that has been investigated more extensively is based on the use of mineral-based lightweight aggregate (LWA) while the other is based on the use of water-absorbing polymers. These highly absorptive LWA or "super absorbent" polymeric materials (SAP) provide a set of water-filled reservoirs within the concrete that supply water on demand to the hydrating cement paste from the time when the concrete is mixed until the time when moisture equilibrium is achieved. Recent studies have demonstrated the use of fine

LWA and fine natural pozzolans for internal curing, which are being increasingly used in concrete [30-32]. The extra supply of water compensates for the loss of water by self-desiccation and reduces autogenous shrinkage [14].

The ability of the absorptive material for internal curing can be evaluated by performing an autogenous shrinkage experiment. Numerous studies have provided measurements of autogenous deformation in various types of paste, mortar, and concrete with LWA and SAP [33-41]. The mechanisms of both common absorptive materials are well established, that is, The mechanisms controlling the internal curing capacity of SAP are combinations of the swelling ratio, ion filtration, and the inter-particle spacing of the SAP [40, 42-44], while those of LWA are combinations of capillary suction, vapor diffusion, and capillary condensation [29, 42], as illustrated in Figure 2.1 and Figure 2.2.

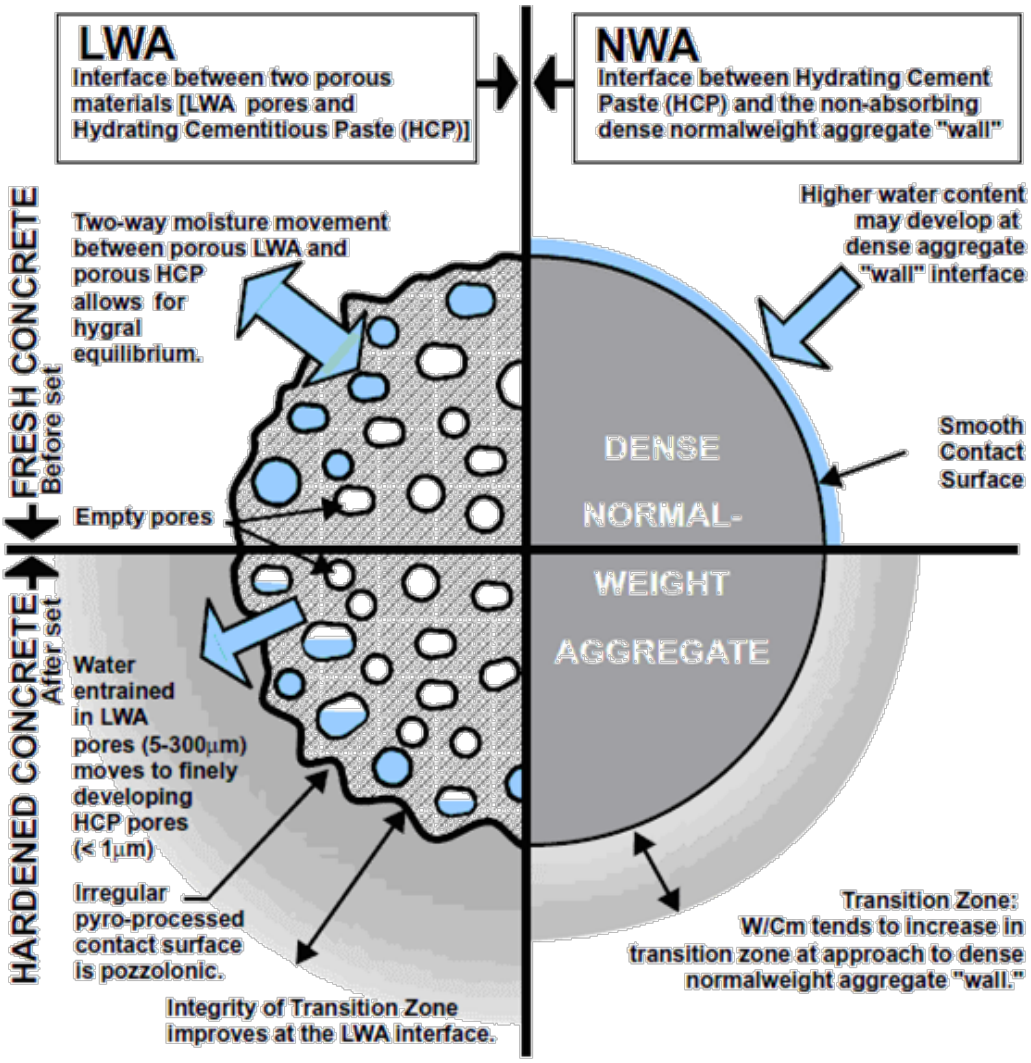

Figure 2.1 – The mechanism of water transport from LWA to surrounding paste compared with that of normal aggregate [39].

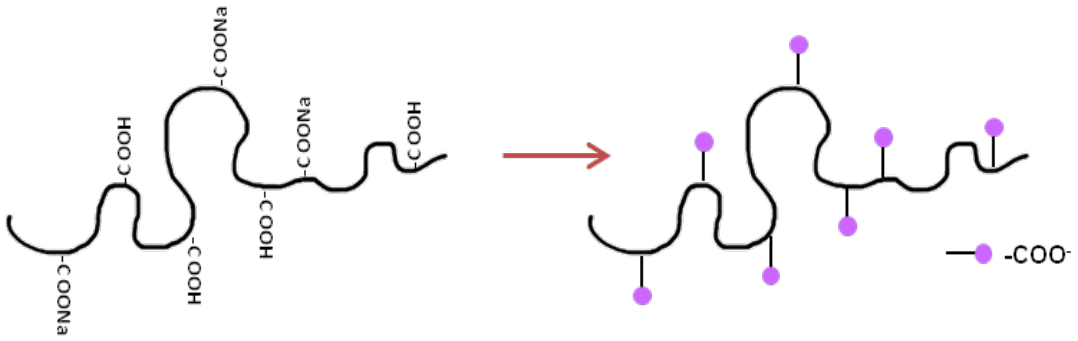

I. Soluble metal cations in cement pore solution deprotonates carboxylic groups (-COOH, -COONa) which create negative charges along polymer chains

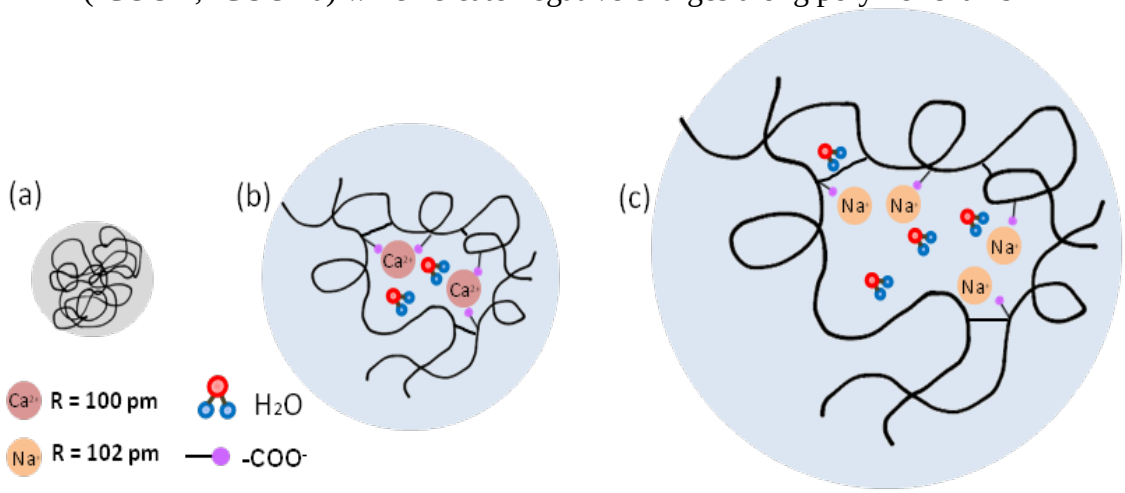

II. Schematic of the swelling behavior of SAP: (a) SAP in a collapsed state ; (b) SAP in Ca^{2+} solution; (c) SAP in Na^{+} solution, adapted from [44].

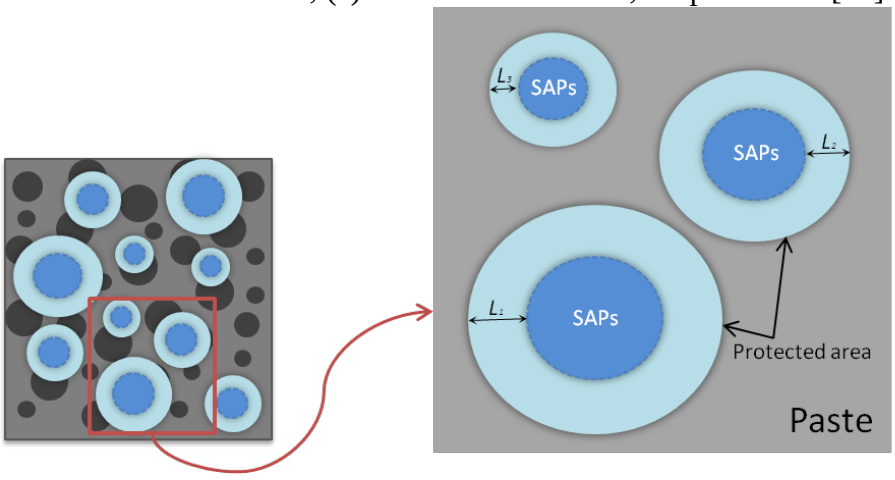

III. Schematic of inter-particle spacing and protected paste area, adapted from [42].

Figure 2.2 – Three main mechanisms that control the internal curing behavior of SAP.

In recent years, based on the key characteristic of internal curing agents that requires the capability of retaining water as a reservoir and the hygroscopic properties of wood, as well as the potential for wood-derived fibers to act as reinforcement, wood-derived materials are attracting more interest as internal curing agents. Because of their hygroscopic property, cellulose fibers absorb water from a fresh concrete mixture and then desorb that water back into the hydrating cement paste, ideally at a time and rate suitable for mitigating early shrinkage. Since the structure of wood pulps contains both small pores of about 0.08 μm in the cell wall and a large lumen pore of about 8 μm [45], wood pulps have an ability to attract free water. Illustrated in Figure 2.3, the structural properties of cellulose fibers such as their pores and lumen can hold free water while the composition of their chemicals such as cellulose and hemicelluloses can create a bond with water, called "weakly bound water." By using NMR relaxometry to observe the distribution of water in wood, Cheumani et al. [46] also reported that 4 types of water – bound water, free water present in the cell-wall pores, in the lumen, and in the vessels – appear in hardwood fiber.

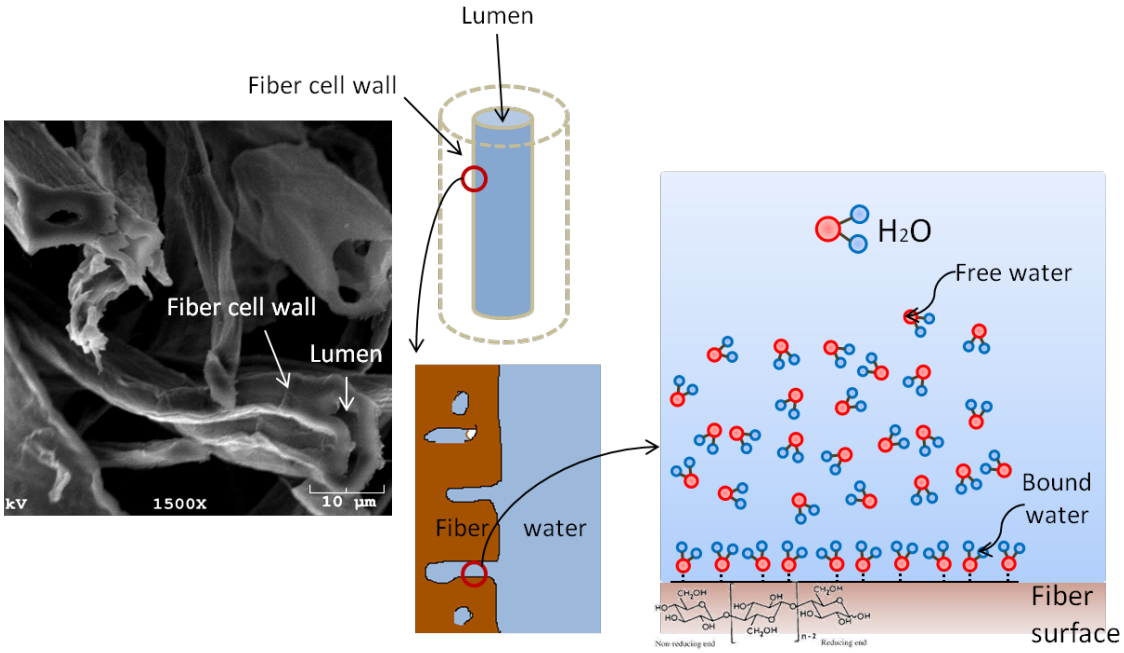

Figure 2.3 – Schematic of free and bound water in a fiber.

By using wood fibers as internal curing agents, the fibers must release both free and weakly bound water absorbed in the fibers into the cement matrix to mitigate the self-desiccation problem of low water-to-cementitious ratio (w/cm) matrix. To reduce autogenous shrinkage and investigate its effects on compressive strength, Mohr et al. [9] evaluated the role of pulp fibers and wood powder as internal curing agents in cement pastes. They found that thermomechanical softwood pulp (TMP) fiber and wood powder were more effective at reducing autogenous shrinkage than superabsorbent polymers, but at high mass fractions, TMP tended to adversely affect the compressive strength of cement pastes because of an increase in air voids resulting from fiber clumping.

Recently, Kawashima and Shah [11] reported on the ability of a commercially available specialty softwood-derived cellulose fiber (UltraFiber 500) to mitigate autogenous shrinkage, but in order to efficiently mitigate autogenous shrinkage the cementitious matrix must have sufficiently high fiber volume with adequate dispersion.

Because fibers are dispersed better in mortar than cement paste, the addition of a 1 percent cellulose fiber to mortar resulted in a 13 percent reduction in autogenous deformation after 7 days; by contrast, the addition of one percent cellulose fiber to cement paste did not show any measurable reduction in autogenous deformation.

Unlike LWA and SAP, the information pertaining to the mechanisms controlling internal curing capacity of wood fiber is rather limited. Although several studies have attempted to clarify the internal curing behaviors of wood pulps, the fact that physical and chemical properties of wood fibers are complex, no concrete conclusion has been made. To evaluate the mechanisms of wood fibers function as internal curing agents, Mezencevova et al. [10] examined the effects of softwood fiber compositions and structures – as varied through chemical treatment of TMP – on internal curing properties. They compared the early hydration behaviors and autogenous shrinkage test results of the cement paste of chemically-treated fibers – holocellulose TMP and α-cellulose TMP – to those of ordinary TMP-cement pastes. The primary chemical compositions of holocellulose TMP are cellulose and hemicellulose while that of α-cellulose TMP is only cellulose. Since each chemical composition can bind water differently, they expected that their results would clarify the effects of chemical compositions on the internal curing performance of wood fiber. However, based solely on their results, they could not make a sound conclusion because of the difficulty in separating chemical and morphological effects. Since transport processes of water from fibers to cement are complex, to better understand these complex relationships information about the morphology and compositions of fibers must be obtained and related to observed early age behaviors. For example, because of its open structure that contains many hydroxyl and acetyl groups

hemicellulose is the most hydrophilic constituent in wood fibers. Therefore, high water absorption and adsorption is expected in fibers having high hemicellulose content. However, the removal of hemicellulose results in greater fiber cell wall porosity, increasing the amount of both mesopores and macropores, Thus, an increase in the absorption of water into fiber can also be expected as the hemicellulose content decreases [47]. Moreover, the thickness of cell wall may have an effect on the rate of moisture ingress from the lumen through the cell wall. It is also not clear if the conclusions from the results of experiments on softwood fibers can be generalized to hardwood species such as eucalyptus.

In addition, because the qualities of pulp fibers depend on how they are processed, the influence of pulping on the internal curing capacity of fiber could be important because even in the same type of wood, the morphology and composition of its pulp can be altered by processing, which could have significant effects on the ability of the fibers to limit autogenous shrinkage. By identifying the relationships between the parameters of fiber and changes in autogenous shrinkage, one should be able to explain the mechanism by which cellulosic materials function as internal curing agents and thus the selection, the dosing, and even the design of pulp fiber for internal curing would be more precise.

2.3 The Transport of Water and Pore Solution in Wood Pulp

Since wood pulps are hygroscopic materials, they absorb or desorb water to equilibrate themselves with the surrounding humidity. Depending on their ultrastructure and chemical compositions, water can be accommodated in pulps by various processes including capillaries sorption and diffusion. Wood pulps contain two classes of pores. Relatively large pores, or fiber's lumen, range from 0.1 to 100 μm in size, exist inside the fibers and relatively small pores of size less than 0.1 μm present in the cell walls of the pulp, both of which are responsible for both capillary flow and diffusion [48]. Moreover, in an electrolytic solution like cement pore solution, even simple ions in water can either swell or shrink the cell wall of pulp, changing the effective size of pore space [49-51], and thus affect the diffusion in the cell wall. Pulps can also act as semi-permeable membrane [52]. Therefore, during the hydration reaction of cement, changes in the concentration of the counter-ions in cement pore solution can create osmotic pressure affecting the absorption and adsorption of water through osmosis. These interrelated mechanisms – capillary, diffusion, and osmosis – influence transition of water from wood pulps to cement and affects their internal curing performance.

Although, in a system of pulp-water suspension, the sorption of water in wood pulps is complicated, it is more straightforward than in a system of pulp-cement pore solution system. Pulps hold water in their structure as bound water and capillary water. While bound water is adsorbed by chemical constituents, capillary water is absorbed by the pore network. Water enters the pore network by capillary flow and water vapor transports through the fibers by diffusion. These processes – absorption and adsorption – take place simultaneously in pulp-water suspension.

Unlike water, the pore solution of cement-based materials is highly concentrated alkaline electrolyte. When cement mixes with water, it releases ions (e.g. calcium, sodium, potassium, and sulfate) and almost immediately turns into a complex alkali- and sulfate- bearing solution [53]. Thus, fibers disperse in concentrated alkaline solution. Although in general, the low levels of alkali ions can swell pulps, the high levels of ions can decrease swelling because of the suppression of electrostatic and osmotic forces. [50, 51]. The pore size of cell wall decreases when pulp is at the swollen state, which then reduces the water-holding capacity. The high levels of ion concentration, otherwise, tend to widen pores and increase the water-holding capacity. In fact, the water-holding capacity of cellulose pulps increases when the pH of the solution increases [54].

Moreover, the metal ions can also associate themselves with bound carboxylate groups. Although both water and alkali have high affinity for cellulose, alkali with the aid of water solvent, unlike pure water, can penetrate the crystalline structure of cellulose, which increases the absorption capacity [55]. The sorption is also accompanied by an appreciable selective adsorption. Davidson and Nevill [56] have reported the order affinity of various cations for the carboxyl groups of oxycellulose as fellow:

$$Ba > Ca > Ag > Tl > K > Na > Li > N(CH_4)_4.$$

As hydration reaction of cement proceeds, concentration of pore solution change continuously [57]. Therefore, the selective adsorption may ultimately affect the absorption capacity of such pulps in a cement pore solution as the changes in the concentration creates an osmotic flow. Thus, in a cement pore solution, the transport of water and pore solution ions are controlled by selective adsorption, capillary absorption, diffusion, and osmosis.

2.4 Interactions of Natural Fibers and a Cement-Based Matrix at Early Ages

Depending on the chemical constituents of fibers, the addition of wood fibers to cement-based materials could affect the early hydration behavior of cement. The potential for retardation has been examined. Since fiber components, hemicellulose and lignin, can retard cement hydration reaction, using fiber with high hemicellulose and lignin content significantly delays the initial and final setting times of composites. Govin et al. [23, 24] found that polysaccharides from wood could be hydrolyzed by alkali media and converted into numerous carboxylic acids, known to be powerful set-retarding agents. In their study, the calorimetric curves revealed that hydration of the silicate phases was significantly inhibited and therefore delayed by wood fiber inclusion. The results from infrared spectroscopy also showed a strong delay in the precipitation of calcium silicate hydrates (C-S-H) in the wood fiber-cement mixture. The Fourier transform infrared spectroscopy (FTIR) spectra of fiber-cement pastes hydrated for 24 hours showed only a slight change in the relative intensity of Si-O bending vibration at 525 cm^{-1}, which indicated very little polymerization of the silicates. Soroushian and Marikunte [58] evaluated the initial and final setting times of cement pastes containing softwood kraft pulps, hardwood kraft pulps, and mechanical pulps. They found that softwood and hardwood kraft pulps with a lower amount of lignin slightly increased only the final setting time while mechanical pulps considerably increased both the initial and final setting times of the cement paste. Their finding demonstrated the effect of lignin on the hydration reaction.

Not only do chemical compositions influence the early hydration behaviors of a cement matrix, but the morphology of wood fibers does, too. The surface of the fibers

might serve as nucleation sites, or the hygroscopicity of the fibers could locally absorb and/or desorb highly alkaline pore water, affecting the amount of free ions precipitating nearby. Pereira et al. [25] found that a lignocellulosic substrate of eucalyptus globules labill or "blue gum" could act as a cation exchange substrate, which adsorbs cations such as Ca^{2+}, Na^{+}, and K^{+} from filtrated cement solution. Therefore, they suggested that these locally absorbed calcium ions on the wood surface might impair or retard the hydration reaction.

However, interaction(s) between fiber and cement could also lead to potential acceleration in early hydration via nucleation, local absorption, adsorption, or desorption. As shown in Figure 2.4, the chemical shrinkage of fiber-cement pastes – where fiber absorption is accounted for to maintain a constant w/cm – are higher than the ordinary paste. The slightly greater chemical shrinkage in fiber-cement pastes indicates some complex early-hydration behaviors. For example, the higher chemical shrinkage of fiber-cement pastes could result from surface nucleation or from an osmotic effect related to the variation in concentration of the solution in the hydrating cement pastes' capillary pores and the fiber lumen. In addition, until the paste densifies sufficiently, water ponding on the surface could be absorbed through interconnected fibers and porosity, providing external water for further hydration. This effect, related to the experimental set up, could increase the chemical shrinkage of fiber-cement pastes. The experiments provided evidence that the early hydration reactions and shrinkage behaviors of fiber-cement pastes are complex. Therefore, further studies correlating hydration reactions with early-age behaviors should be performed with the technique that does not contain an artifact form the experimental set up. In particular to better understand the interactions

between fibers and cement at very early ages, a non-destructive technique would be the best technique to completely observe the water dynamics of wood fiber/cement system during hydration.

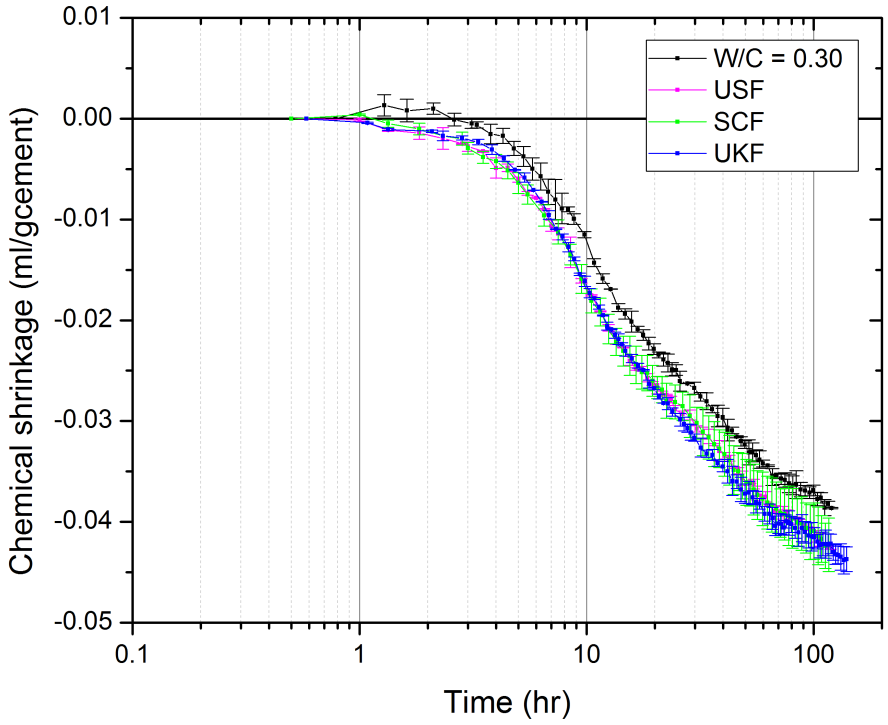

Figure 2.4 – Chemical shrinkage of the cement pastes compared with that of fiber-cement pastes of unbleached soda fiber (USF), semi-chemical fiber (SCF) and unbleached kraft fiber (UKF).

The water dynamics of hydrating cement at very early ages can be non-destructively monitored by nuclear magnetic resonance (NMR) and magnetic resonance imaging (MRI) techniques. These fast and potentially non-invasive techniques are based on measurements of the relaxation of specific atomic nuclei from an electromagnetically excited state to their natural state. Although proton NMR was first used in cement pastes by Kawachi et al. [59] in 1955 for studying of cement hydration, the use of proton NMR in cement-based materials has become popular only since the early 1980s in several

applications such as studying the structure of hydrated phases, determining the pore structure and pore size distribution of cement pastes, and observing the kinetics of the hydration processes. MRI was introduced in porous materials by Gummerson et al. [60], in 1979 for monitoring the dynamics of the internal water distribution in inorganic porous materials during capillary flow. Currently, ^{1}H relaxation MRI has been used to monitor the ingress, the drying, and the distribution of water in a cementitious matrix on a micron-scale resolution. Here, its sensitivity to water distribution will be used to monitor the distribution and the dynamic of internal curing water in cement pastes at early ages.

Unlike other tomographic techniques such as x-ray computed tomography (x-ray CT), the most recent development in combining NMR/MRI provides a method of obtaining not only the three-dimensional distribution of a liquid phase but also physical-chemical information by examining NMR spectra and relaxation times. Moreover, information pertaining to pore sizes, range from an angstrom up to about 10 micron [61], and surface areas in cement paste can be obtained by analyzing magnetic-resonance relaxation times, which are very sensitive to changes in both the molecular environment and molecular mobility. After the application of an RF pulse, nuclear spins, to return to their equilibrium state, transfer their magnetic energy to surroundings, referred to as "relaxation." The analysis of relaxation times – the spin-lattice relaxation time (longitudinal relaxation, T_1), the spin-spin relaxation time (transverse relaxation, T_2), and the effective spin-spin relaxation time (T_2^*) – provides information pertaining to the structure of the material. These relaxation processes occur simultaneously and can be used in studying the water dynamic in cementitious systems. In this research, potential

applications include the monitoring of internal curing water consumption in low w/c fiber-cement paste.

Although NMR observations of solid materials are more difficult than those of soft materials because of their relatively short relaxation times, several studies have successfully applied NMR to monitor the setting, hydration, and porosity evolution of cement, mortar, and concrete [46, 62-66]. Wang et al. [62] demonstrated the use of NMR to detect the setting of cement and the depletion of water during cement hydration. They continuously monitored the setting process by observing the evolution of the (T_1) distribution with an inversion recovery (IR) sequence, but they assessed the content of free water molecules in capillary pores and physically bound water with a simple one-pulse acquisition sequence. The authors found that the time derivative of optimum T_1, that is, the modal value of the T_1 distribution, correlated with the percolation of the solid network determined by using the Vicat needle test method. They found that the reduction in the signal amplitude of the one-pulse sequence was proportional to free water consumption, so it could be used as an indicator of the hydration process.

In an advanced stage of hydration, the photon frequency induction decay (FID) of a portland cement paste can be divided into three main components: 1) a component with a relatively long T_2 representing water in the micropores and layers, 2) a component with an intermediate T_2 representing the bonded water in the gel phase, and 3) a component with a very short T_2 representing the protons of the solid OH groups and the water of crystallization. Three main modes of the T_2 separated by an order of magnitude above 1 ms, 100 μs, and 10 μs are assigned to water molecules that are physically bound in capillary pores, interlayer water in the C-S-H gel structure, and water that is chemically

combined with the hydrated cement matrix, respectively. However, since the chemically bound water in the gel phase, which has significantly short T_2, is difficult to observe, most studies have focused on the detection of physically bound water in the confined pore structure of cement paste. The two components of capillary water provide information that facilitates the monitoring of the hydration behavior of cementitious materials.

To clarify the internal curing mechanism of alginate, a natural polysaccharide, in cement, Friedemann et al. [67] performed ^{1}H NMR experiments of T_2 and self-diffusion of physically bound water. They performed the T_2 relaxation studies using the Carr-Purcell-Meiboom-Gill (CPMG) sequence and the diffusion studies using pulsed field gradient (PFG) NMR. For CPMG, they set the echo time (T_E) to 100 μs so that only water in the capillary and gel pores could be detected. By analyzing the T_2 distribution, the authors found that the transportation of entrained water from alginate to the cement matrix starts at the onset of the accelerated period of the hydration reaction and, depending on the amount of entrained water, ends within 20 hours or continues for 14 days. In addition, by combining one-dimensional NMR imaging with PFG NMR diffusometry, the authors were able to monitor the reduction in the self-diffusion coefficient of physically bound water in cement pastes over time. However, the diffusion studies were not sensitive enough to capture the difference between diffusion coefficients of the control samples and those of the internally cured samples.

Recently, Cheumani et al. [46] investigated wood-cement interactions taking place in wood-cement composites during hydration by using low-field NMR relaxometry. They observed water in wood, the transformation of water from wood to cement, the

transformation of capillary pore water into hydrates and gel pores, and its transformation into a cement matrix. They found that although hardwood contained three types of pore water – T_2 of 4.1-6.9 ms, 19.9-43.7 ms, and 164-279 ms – assigned to water in small pores found in the cell wall, the wood cell lumen, and the wood vessels, respectively, large pores filled with water only when the water content in the wood was sufficiently high. They also observed the migration of water, especially free water, from wood to cement in wood-cement composites rather than phenomena associated with cement hydration alone. At the end of the process, depending on the initial water content, some of the water, in the form of free or bound water, was retained in the wood.

Although Cheumani et al. have demonstrated that the NMR relaxometry technique is a powerful tool that can be used for probing water in wood-cement composites and optimizing the wood-cement system, the results of some of their experiments remain unclear. The presence of lignin in wood and the effects of wood hygroscopic properties on initial water content, both of which can affect their results. Since they used toluene-ethanol solution and water to remove extractives from wood, most of the lignin might remain in the wood cell structure. However, the presence of lignin in the wood cell structure affects experimental results because lignin could delay the initial and final setting times of composites, as demonstrated in several studies [68]. The wood's hygroscopic properties can also change the bulk w/c of composites. Depending on its initial water content, wood can absorb water during mixing and desorb it to cement later on. Therefore the water available to cement during mixing was changed, which in turn affected results.

Since MRI permits three-dimensional imaging with minimal sample preparation and provides information on the liquid phase, MRI is attracting an interest among cement and concrete researchers. However, as mentioned before, since the nuclear spin relaxation times of water in porous materials are significantly short, the use of MRI for imaging fluids in porous materials, like cement and concrete, is much more complicated than that of bulk liquids in a biological tissue. The signal data of the water in porous materials by using conventional pulse- and gradient-echo techniques contain a relatively poor signal-to-noise ratio (SNR) because the transverse relaxation times of the cement matrix are considerably shorter than the echo time due to the strong chemical and physical bonds between fluid molecules and hydrated cement matrix. Since the pore solution of cement contains a high concentration of paramagnetic ions such as Na^+, K^+ and Ca^{2+}, Greener et al. [69] found that the T_2 of the mixing water that has not yet formed a part of hydration product of white cement paste at about 12 min after mixing is approximately 40 ms, which is considerably shorter than that of free water in which the T_2 is about 3s. Therefore, the traditional standard techniques such as a spin-echo technique cannot provide a high spatial resolution signal. However, some studies have provided strong evidence that other techniques such as a single point imaging (SPI) and a single-point ramped imaging with T_1-enhancement (SPRITE) can be used to measure the profiles of water in building materials such as plaster, mortar, and concrete.

Unlike conventional MRI techniques, SPI is a pure phase encoding technique that detects a single point of frequency induction decay within a short time after the pulse is excited. The gradients along the x, y, and z axes, (G_x, G_y and G_z, respectively) are activated before a radio frequency (RF) pulse is applied. This RF pulse rotates the net

magnetization of the magnetic field by 90^{o}. The gradient along each axis is consecutively changed in steps while the others are kept constant. Therefore the density of spins, as a function of position, is phase encoded along the gradient direction, so that a particular phase in the NMR signal corresponds to a particular position on the axis. The signals which are proportional to the density of the spins are Fourier transformed to the final spatial image. Pure phase encoding is insensitive to signal loss, artifacts, and distortions due to time-varying magnetization and chemical shift; therefore, SPI techniques are often used for acquiring images of the hydration reaction of porous materials. The encoding times of an SPI experiment can be only 10 to 100 μs, so signal data gathered from such an experiment are insensitive to distortion. Although images from MRI have lower resolution than those from the electron micrographs, Jaffer et al. [70] showed that SPI technique is sensitive enough for imaging cement pastes. The signal was very sensitive to water concentration gradient and allowed monitoring of diffusion of water into the paste sample. They also presented a reasonable image of the major cracks and their interconnectivity of the sample with a resolution of 312 μm × 312 μm × 624 μm per voxel. Moreover, with more detailed calibration of the MRI images by information obtained from environmental scanning electron microscope (ESEM) they could identify the features that are not clear such as unhydrated particle, calcium hydroxide, and calcite crystals.

Although SPI experiments provide good resolution with high SNR, the 2D and 3D imaging of samples by SPI technique is time consuming because the technique generates only one k-space data point per excitation. To overcome this problem, Balcom et al. [71] developed another method based on the SPI technique called “SPRITE.” While

this technique is also insensitive to resolution loss and distortion resulting from susceptibility, chemical shift, and field inhomogeneity, its imaging speed is much faster than SPI because SPRITE can acquire an entire k-space data line with a single gradient waveform. They suggested that the acquisition time for a 3D imaging of a concrete sample with about 3 cm diameter could be as low as 15 seconds [72]. The local image intensity from SPI and SPRITE is given by Eq. 3.1.

$$S = M_0 \cdot e^{\frac{t_p}{T_2^*}} \cdot \left(\frac{1 - e^{\frac{TR}{T_1}}}{1 - cos\theta \cdot e^{\frac{TR}{T_1}}} \right) \cdot sin\theta \qquad \text{Eq. 3.1}$$

where S is the local image intensity, M_0 is the local sample magnetization, TR is the repetition time between RF pulses, t_p is the encoding time at which a single data point is recorded after an RF pulse, and θ is the rotation angle of the sample magnetization caused by the RF excitation pulse. Since TR is always longer than T_1 for cement and concrete, Eq 3.1 can be simplified to Eq 3.2, which is a straightforward equation for rapidly determining fluid content in porous matrix

$$S = M_0 \cdot e^{\frac{t_p}{T_2^*}} \cdot sin\theta \qquad \text{Eq. 3.2}$$

This literature indicates that the NMR/MRI technique can be used to examine the hydration of the cement matrix and the behavior of fiber-cement paste upon exposure to water such as water ingress, drying, and distribution. Therefore, this proposed study will employ NMR/MRI technique to clarify the internal curing mechanism of wood fibers.

The sensitivity of MRI to water distribution will be used to monitor the distribution and the dynamic of internal curing water in cement pastes, while the proton NMR relaxometry will be applied to investigate the transformation of internal curing water into C-S-H gel water at early ages. Specifically, by applying NMR/MRI technique together with autogenous shrinkage experiments, there is an opportunity to reveal internal curing mechanisms of pulp fiber-cement composites that cannot be captured by the use of other techniques. Such this understanding will potentially enhance the use of pulp in cementitious materials by guiding the selection, dosing and design of pulp for a specific propose.

2.5 Unrestrained and Restrained Shrinkage Behaviors of Fiber-Reinforced Composites

During its service life, cementitious materials are subject to volume changes caused by factors such as the hydration reaction, self-desiccation, and moisture loss. When cement hydrates, the total volume of hydrated products is lower than that of unreacted cement and water, which causes chemical shrinkage, as illustrated in Figure 2.5. Chemical shrinkage is inevitable (i.e., it occurs independent of environment or w/c) and continuously occurs at a microscopic scale as long as the hydration reaction proceeds. Self-desiccation is predominant in a low water-to-cement ratio matrix (w/c < 0.42) in which external water is not available, either due to curing conditions or matrix density. Therefore, cement consumes water from capillary pores for further hydration, creating a noticeable uniform reduction in volume, or “autogenous shrinkage” or “self-desiccation” shrinkage, as shown in Figure 2.5. Drying shrinkage is a phenomenon that results when cement, mortar, concrete, and fiber-reinforced composites lose their water to

surroundings. The loss of water creates capillary pressure, leading to contraction in the volume of a specimen. The magnitude of drying shrinkage depends on environmental conditions such as temperature and relative humidity. In addition to these factors, chemical reactions such as carbonation also contribute to volume changes in cementitious materials. However, the proposed study will focus more on shrinkage caused by the hydration reaction, self-desiccation, and moisture loss.

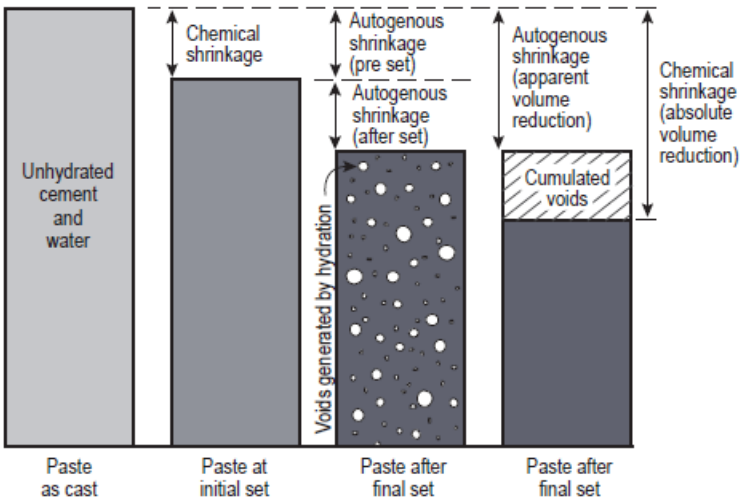

Figure 2.5 – Chemical and autogenous shrinkage volume changes of cement paste [68].

Unrestrained drying shrinkage, also called “free shrinkage,” is a condition in which concrete and mortar shrink freely without any external restraint. When a specimen is free to shrink, tensile stress does not develop and cracking does not occur. However, a concrete and mortar member is normally restrained by other members such as connecting members, the foundation, and reinforcements, which do not allow them to shrink, resulting in significant stresses in the specimen. Although aggregates provide volume stability to concrete which reduce the potential of cracking, since cementitious materials

are weak in tension, concrete will eventually crack as a result of the development of tensile stresses.

Cracking, an inevitable phenomenon of mortar and concrete, can range from micro-scale to macro-scale. Starting with microcracking, these small cracks continue to develop as the stress increases and then begin to coalesce to form a single localized crack in the concrete. In most cases, cracks do not significantly affect the mechanical efficiency of concrete structures, but they drastically reduce the durability of concrete because they create interconnecting flow paths while increasing concrete permeability. The progression of cracks allows more water and aggressive chemical ingress into the concrete, which accelerates further deterioration.

Despite the many transport processes in concrete such as diffusion, permeability, electro-migration, thermal-migration, osmosis, and capillary suction, both diffusion and permeability are most commonly used as key indices for assessing the durability of concrete because they indicate the transport processes of ions and water through concrete, respectively. Diffusion is a transport process driven by concentration gradients of chemical ions through saturated concrete without the flow of water. Therefore, mass diffusivity, the so-called “diffusion coefficient,” is the ability of substances or dissolved ions to flow along a medium of interest. Permeability is defined as the rate of the pressure-driven flow of fluid into a porous solid, and the permeability of concrete refers to the rate of entry or movement of fluid containing aggressive substances into concrete [73]. Both diffusivity and permeability are microstructure dependent and have a strong correlation with interconnected pores and flaws. For uncracked concrete, both the w/cm and the degree of hydration play an important role in controlling interconnected porosity,

which in turn relates to the permeability of concrete. The lower w/cm and the higher degree of hydration result in lower permeability. However, cracks generate alternate flow paths that allow more water and deteriorating substances into concrete and its reinforcements. Thus, cracked concrete is more vulnerable to the processes of deterioration than uncracked concrete.

Since cracks affect the durability of structures, many researchers focus on testing of the potential of cracking in mortar and concrete. Several test methods, both with unrestrained and restrained conditions, are capable of identifying the potential for cracking in mortar and concrete. The simplest test method is the measurement of the change in the length of samples without any restraint. This standard test method, ASTM C157 [74] "Standard test method for length change of hardened hydraulic cement mortar and concrete," evaluates free shrinkage. While the results of the free shrinkage test provide some insight about the driving force behind drying shrinkage cracking, one cannot predict the cracking behavior of mortar and concrete in the field by analyzing only free deformation data. However, the results of the free shrinkage test combined with a stochastic approach and numerical models could predict the cracking potential of concrete [75], but it is still not applicable to fiber-reinforced concrete because of several additional factors such as the initiation of cracking and the role of toughening. Furthermore, in fiber-reinforced cement paste, mortar, and concrete, the cracking tendency is a combination of the effects of free shrinkage and fiber reinforcement.

Restrained shrinkage tests of mortar and concrete are more complex than free shrinkage tests in several ways. For example, the extent of cracking depends on surroundings and restraint conditions [76] and the degree of restraint must be sufficient to

generate stress that induces cracking. Moreover, the degree of restraint, the behavior of drying, and the development of stress in tests depend on specimen geometry and boundary conditions [77-82]. Because the combination of several phenomena such as hydration, drying, and the evolution of mechanical properties affects the stress state, the analysis of restrained cracking becomes more difficult. However, if researchers properly design and perform a restrained test, one can obtain useful results and determine the cracking tendency. To understand the cracking behavior of mortar and concrete, many researchers have developed restrained tests based on several specimen geometries such as linear, ring, and flat specimens.

The linear restrained shrinkage test normally consists of a set of long-slender specimens, each of which is cast with either one or two fixed ends. If only one end is fixed, another end is free to move and controlled by using equipment that applies and records the force required to keep the specimen at a constant length [81, 83]. The applied load and the known cross-sectional area are converted to restrained shrinkage stress. If both ends are fixed, the test results normally find the time-to-cracking, the crack width or area, and the crack pattern [80, 82, 84]. A specimen that cracks later and has a smaller crack width represents better performance.

The most common restrained shrinkage test method is referred to as “restrained ring testing” in the standard ASTM C1581 [85] “Standard Test Method for Determining Age at Cracking and Induced Tensile Stress Characteristics of Mortar and Concrete under Restrained Shrinkage.” As a result of drying, concrete tends to shrink, but the shrinkage is restrained by a steel ring that creates internal uniform pressure: hoop tensile stress and radial compressive stress. If strain gauges are attached on the inner steel ring, the

residual stress that develops from the restraint can be quantified, presenting an advantage over the linear method. Cracks that result from the restrained ring test can be observed and measured with a microscope.

While the ring test remains the most widely used as a quality control test for assessing the shrinkage cracking potential of a concrete mixture, its metallic ring does not physically or chemically represent real substrates. Therefore, several researchers have designed experimental methods with mortar cast on concrete or brick substrates for more realistic mortar/substrate systems [86, 87]. The distribution of strain in cementitious materials, which is related to its composition and microstructure, can be observed by using image analysis (i.e., the digital image correlation technique). This technique, which allows deformation to be visualized and linked to specific microstructural features, provides additional insight into the mechanisms of deformation, illustrated in Figure 2.6 (work by Lopez et al. [88]). While Figure 2.6b shows the elastic strain map of a normal strength concrete specimen subject to applied stress, Figure 2.6c and Figure 2.6d present the creep and shrinkage strain map after the application of stress after one day and 28 days, respectively. More recently, Mauroux et al. [87] have investigated the early-shrinkage behavior of plastering mortar. They used the mapping of strain heterogeneity, shown in Figure 2.7, to measure the extent of damage.

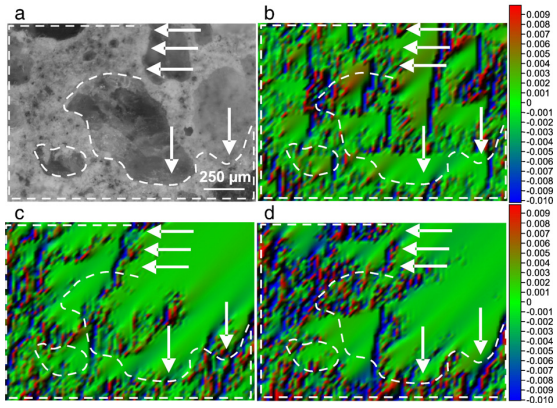

Figure 2.6 – (a) Region of interest obtained at high magnification on a specimen under 9.7 MPa stress, (b) an elastic strain map, (c) a one-day creep and shrinkage strain map, and (d) a 28-day creep and shrinkage strain map [88].

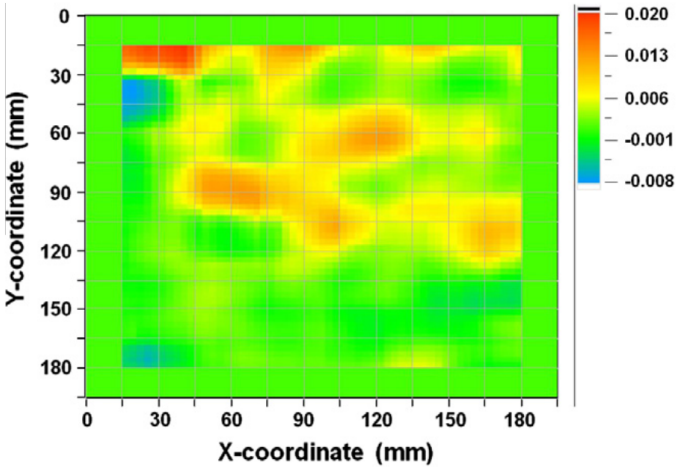

Figure 2.7 – Local surface variation map during free shrinkage after 10 h of drying [87].

Although the main sources of cracking are stresses induced by restrained drying shrinkage, the combination of several phenomena such as hydration and drying and the evolution of mechanical properties affect the development of stress at an early age, making the early-age cracking more difficult to analyze. Therefore, in this study additional tests including split tension, modulus of elasticity, and free shrinkage will be performed to thoroughly evaluate the effects of eucalyptus fiber on shrinkage behaviors.

2.6 Shrinkage Cracking of Natural Fiber-Reinforced Cementitious Materials

One of the most efficient technologies that control many types of cracks of all ages is fiber reinforcement, which can be classified in terms of its end effect: the control of plastic shrinkage cracking up to the time of setting of the concrete and the mitigation of cracking in hardened concrete between hardening and long-term maturity. The effect of fiber reinforcement depends on the type and amount of fiber in concrete. For example, controlling plastic shrinkage cracking requires a low content of fibers (approximately 0.1% by volume) with a low modulus of elasticity. However, hardened concrete requires both higher content and higher modulus fibers to maximize the efficiency of the reinforcing fibrous system.

Generally, at a low volume fraction (<1%), fibers are used to reduce shrinkage cracking; at a moderate volume fraction (1-2 %), they increase the modulus of rupture, fracture toughness, and impact resistance; and at a high volume fraction (>2%), they produce the strain-hardening mechanisms of composites. These composites are often referred to as “high-performance fiber-reinforced cement composites (HPFRCC)” or “ultra-high performance fiber-reinforced cement composites (UHPFRCC).” Another advantage of fiber is that it provides the toughening mechanism of concrete, referred to as “fiber bridging.” Unlike plain concrete, fiber-reinforced concrete does not break immediately after the initiation of the first crack. It does break, however, when fibers are pulled out or deboned. Since pullout and debonding play an important role in the fiber-bridging mechanism, from material and structural points of view, optimizing the bond between the fiber and the matrix requires a delicate balance. If the fibers have a weak bond with the matrix, they can slip out under a low load contributing very little to crack

bridging. On the other hand, if the bond with the matrix is too strong, the fibers may break before they dissipate energy. Therefore, the interface between fiber and cement is crucial.

According to several studies, the inclusion of cellulose fibers at 0.5 and 1 percent by volume of concrete and mortar does not affect their drying shrinkage behavior [11, 89]. Another study reported an increase in the free shrinkage of natural fiber-reinforced mortar [90]. The additional shrinkage was attributed to the shrinkage of natural fiber when it released water during drying, and an increase in the porosity of the matrix because of the addition of natural fibers. Filho et al. [90] reported that the type of natural fiber affected free shrinkage. They found that the addition of 3 percent sisal fiber increased drying shrinkage by 27 percent, which was 8.2 percent higher than the drying shrinkage of coconut fiber-reinforced concrete.

Although natural fibers were found not to reduce the drying shrinkage, many publications reported their effectiveness at mitigating restrained shrinkage-induced cracking [11, 89, 91]. Sarigaphuti et al.[89] showed that the addition of fibers at a 0.5 percent volume to concrete can delay the onset of cracking. Based on their experiments, pulp fiber-reinforced rings delayed cracking up to six days compared to plain concrete while polypropylene reinforced concrete delayed cracking by only three days. The maximum crack width of pulp fiber-reinforced concrete was only 55 percent of plain concrete. Soroushian [91] found that a 0.2 percent volume of pulp fiber delayed the initiation of cracking in a concrete sample up to 26 days. Kawashima and Shah [11] also reported 57 and 86 percent reductions in the crack width of the cellulose fiber-reinforced mortar and concrete, respectively.

In this study, although the length of eucalyptus pulp is relatively short compared to other cellulose-based fibers used in mortar and concrete, it is worth examining the mechanical properties of eucalyptus fiber-reinforced mortar because such pulp may improve some mechanical properties and/or reduce potential of cracking of cementitious materials at early ages. Since eucalyptus trees grow rapidly and they can adapt to a variety of conditions and regions, if eucalyptus fibers can be used as a substitute or partial replacement for long-length fibers, they will benefit cementitious materials more than any other type of cellulose-based fibers.

CHAPTER 3

EXPERIMENTAL DETAILS

3.1 Overview of Research Plan

The goal of the study is to evaluate the potential of eucalyptus pulps for the mitigation of early-age shrinkage and restrained cracking in cementitious materials. Therefore, experiments were designed to fully address the effects of such pulps on cementitious materials from the fundamental perspective. Overall, the experiments can be divided into three major tasks of work. The initial work task, which is related to objective 1, focused on evaluation of internal curing performance among eucalyptus fibers from different processes to select the candidate fibers for further studies. The second task, which is related to objective 2, focused on the early age behaviors of pulp-fiber cement composites, both the effects of fiber on hydration reaction of cement and the migration of water and pore solution ions during internal curing. The final work task, which is related to objectives 3 and 4, aimed to examine the performance of eucalyptus pulps for the mechanical reinforcement of fine structured cementitious composites and its use in concrete structures. Experimental details for the sample preparation and testing are described in this chapter. A sketch showing the steps of the study program is presented in Figure 3.1.

Task 1 (Objective 1): Evaluating the effects of the fiber chemical composition and the physical structure on internal curing performance.

Early-age cracking resulting from self-desiccation is as a major problem in concrete structures with low w/c and low w/cm. One strategy to mitigate such a problem is internal curing based on the use of absorptive materials such as LWA, SAP, and wood-derived materials, to provide a set of water-filled reservoirs within the concrete that supply water on demand to the hydrating cement paste. Because of significant research efforts on the use of LWA and SAP for internal curing, the key mechanisms controlling the performance of LWA and SAP on internal curing are successfully identified, while those of wood pulps remain unclear. Since the properties of wood pulps are more complex than that of the LWA and SAP, wood pulps can hold water in the lumen and the cell-wall pores and bound water to their chemical compositions, which creates difficulty in identifying the key mechanisms underlying the performance of pulps on internal curing.

In this task, experiments were designed to determine a most significant parameter that can serve as an indicator for comparing the efficiency of pulps for internal curing applications. This parameter was selected based on the analysis of fiber characteristics such as morphology, chemical composition, and absorption capacity, together with the internal curing behavior of the fiber-cement pastes (i.e. autogenous shrinkage). Five different treatments of commercially available eucalyptus pulp were evaluated and compared for the selection of candidate pulps for further studies. These fibers – unbleached kraft pulp, bleached kraft pulp, unbleached soda pulp, bleached soda pulp, and semi-chemical pulp – were collected from common chemical processes used for

eucalyptus pulping (i.e. kraft pulping, soda pulping, and semi-chemical pulping). The alteration from pulping process including bleaching may affect the performance of such pulps in cement-based materials.

Task 2 (Objective 2): Evaluating the mechanisms underlying the early-age interactions between pulp and cement and the migration of water and pore solution ions during internal curing.

Once the candidate pulps were selected based on results in the first task, more experiments were conducted to gain a thorough understanding of the interactions between eucalyptus pulp and cement. For preliminary investigation of interactions between pulp and cement, chemical shrinkage of fiber-cement pastes was compared with that of the plain cement paste. Then, mechanisms underlying such interactions were proposed.

Chemical interactions between fiber and cement at early ages were evaluated using nanocharacterization techniques. In this effort, atomic force microscopy (AFM), scanning electron microscopy/energy dispersive x-ray spectroscopy (SEM/EDS), and x-ray photoelectron spectroscopy (XPS) were used in combination to quantify variation in the elemental composition of fiber, through its structure and after its introduction to cement. Surface morphology of the pulp was observed using AFM and SEM while the surface chemistry and the way in which that chemistry changes at the surface region were evaluated using XPS. In addition to fiber alterations, inductive coupled plasma/optical emission spectroscopy (ICP/OES) was used to determine the concentrations of the elements in the pore solution of cement before and after fiber immersion.

For the in-depth clarification of the internal curing mechanism of eucalyptus pulp, the migration of water or pore solution during internal curing was nondestructively

monitored by nuclear magnetic resonance (NMR) and magnetic resonance imaging (MRI) techniques. The NMR/MRI techniques together with autogenous shrinkage and isothermal calorimetry measurements revealed the internal curing mechanisms of pulp fiber-cement composites that could not be captured by the use of other techniques.

Task 3 (Objectives 3 and 4): Examining the performance of eucalyptus pulps for the mechanical reinforcement of mortar and the use of its in concrete.

Because of its short length, only a few scientific publications pertaining to the use of eucalyptus pulp in mortar and concrete are available. Most of the experimental results pertaining to the effect of eucalyptus pulp in the mitigation of cracking in mortar and concrete have not yet been sufficiently explored. However, since its short length can facilitate uniform dispersion of fiber thorough out a matrix, this property warrants further examination. This research focused on possible applications of eucalyptus pulps in mortar and concrete; therefore, several experiments were designed and conducted to examine the potential of eucalyptus pulps to reinforce fine structures such as mortar stucco and the effect of such pulps in concrete.

Given the hypothesis that although eucalyptus fibers may not improve the long-term tensile capacity of mortar, they could enhance some tensile capacity at very early ages and, thus, reduce the potential for cracking. So, one possible application of eucalyptus pulp is the enhancement of some early-age properties of mortar when the mortar is not mature and prone to crack under restrained shrinkage conditions. Therefore, this work compared the performance of eucalyptus pulps on the early-age cracking mitigation in ordinary types of mortar to that in mortar containing a more common internal curing agent, superabsorbent polymer (SAP). Both the ability of eucalyptus pulp

to reinforce and its capacity to provide internal curing were evaluated through a series of restrained shrinkage tests, early age mechanical tests, and characterization. By following ASTM C1581, the study examined the potential for the cracking of eucalyptus-reinforced mortar and quantified the development of internal stress developed from the restraint. Cracks that result from the restrained steel ring were observed and measured. Strain sensors were used to monitor the development of stress during restrained shrinkage and provided an assessment of the time of cracking. Although the main sources of cracking were stresses induced by restrained drying shrinkage, the combination of various phenomena such as hydration and drying and the development of mechanical properties affected the development of stress at an early age, making early-age cracking more difficult to be analyzed. Therefore, additional tests, including split tension, modulus of elasticity, and free shrinkage were performed to thoroughly evaluate this behavior.

The effects of eucalyptus pulp on the flexural performance of mortar were examined by performing three-point bending tests on fiber-reinforced mortar at different volume fractions of eucalyptus pulp. The area under the load-deflection curve after the first crack of eucalyptus fiber-reinforced mortar, known as "post-cracking toughness," indicated whether eucalyptus can increase the toughness of mortar. For further investigation, microscopy techniques, both scanning electron microscopy (SEM) and variable-pressure electron microscopy (VP-SEM) were employed to establish a relationship between fiber morphology with toughening mechanisms and crack propagation.

To evaluate the use of eucalyptus fibers in concrete, this study compared compressive strength and the chloride transport properties of internally-cured eucalyptus

fiber-reinforced concrete to those of the unreinforced and SAP-blended concrete. Based on the electron migration of ASTM C1202, a “standard test method for electrical indication of concrete's ability to resist chloride ion penetration,” and bulk diffusion tests of ASTM C1556, a “standard test method for determining the apparent chloride diffusion coefficient of cementitious mixtures by bulk diffusion," the effect of such pulp on electron migration were examined. The bulk diffusion coefficients determined in this study were used in Life-365 software to estimate the service life of a reinforced concrete structure. The results provided more insight into which applications that eucalyptus pulps be used in concrete or does it can ever be used in concrete.

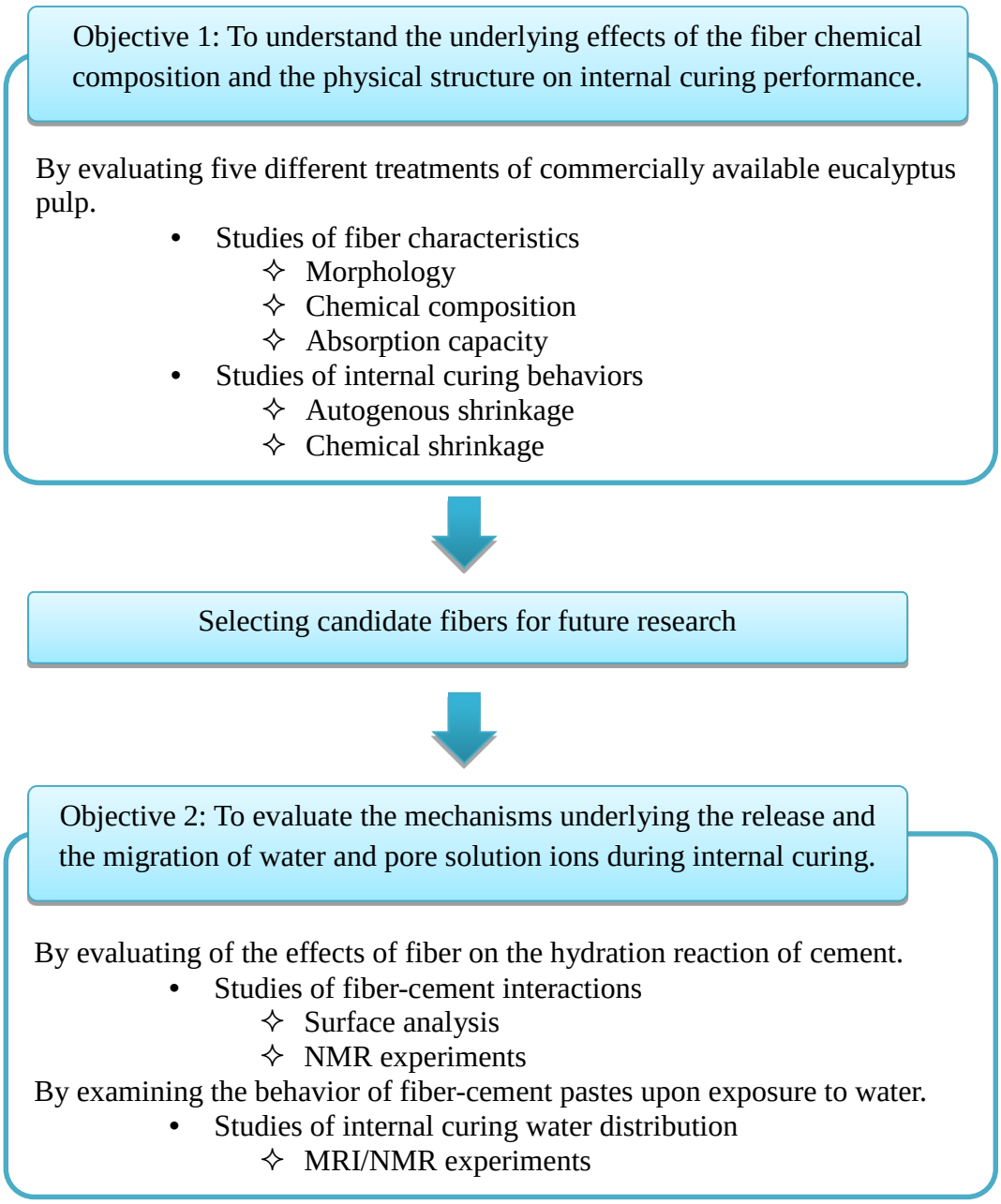

Figure 3.1 – Scope of experimental program.

Objective 3: To assess the role of pulp fiber in early-age cracking mitigation.
&
Objective 4: To evaluate the potential of eucalyptus fibers for mechanical reinforcement of cementitious composites.

By evaluating the mechanical properties of mortar and concrete

- Mortar properties
  - ✧ Flexural toughness
  - ✧ Restrained shrinkage
  - ✧ Free shrinkage
  - ✧ Elastic modulus
  - ✧ Tensile strength
- Concrete properties
  - ✧ Compressive strength

By examining the effects of eucalyptus fibers on the durability of concrete

- Studies of chloride permeability
  - ✧ Surface resistivity
  - ✧ Rapid chloride permeability tests (RCPT)
  - ✧ Bulk diffusion

Figure 3.1 – Scope of experimental program (continued).

CHAPTER 4

THE EFFECTS OF THE FIBER CHEMICAL COMPOSITION AND PHYSICAL MORPHOLOGY ON INTERNAL CURING PERFORMANCE

4.1 Introduction

While native to Australia, eucalyptus is now grown in most parts of the world in tropical and subtropical climates (e.g., North and South America, Africa, Mediterranean, Middle East, and Southeast Asia) and is of considerable interest to researchers and environmentalists alike because of their fast growth rate, which makes them highly renewable. Recently, Tonoli et al. [5] demonstrated the advantages of eucalyptus pulps as a reinforcement of cementitious materials; these include their high dispersibility and effective crack bridging. However, the internal curing performance of eucalyptus pulps had not been examined in their or other studies.

This chapter evaluates the effect of variations in processing conditions of hardwood Eucalyptus camaldulensis fibers to produce five fibers—unbleached soda pulp, bleached soda pulp, unbleached kraft pulp, bleached kraft pulp, and semi-chemical pulp—and their performance as internal curing agents. The structure and composition of five different fiber variants were first evaluated by image analysis and thermal analysis techniques. Each of these fibers results from different processing of the same hardwood eucalyptus species. Then, the internal curing capacities of the fibers measured through standard autogenous shrinkage testing are compared to fiber composition and

morphology, to better clarify the complex roles these factors play in providing internal curing to cement-based materials.

4.2 Materials and Methods

4.2.1 Materials

Eucalyptus camaldulensis (or River Red gum) fibers, sourced from Southeast Asia, were evaluated in this study. Fibers from five common commercial treatments, varying the types of chemicals used and the use of mechanical action during treatment – unbleached soda pulp (USF), bleached soda pulp (BSF), unbleached kraft pulp (UKF), bleached kraft pulp (BKF), and semi-chemical pulp (SCF) – were collected from commercial papermaking processes. The effect of internal restraint was evaluated by comparing the autogenous shrinkage test results of pulp fiber-cement pastes with that of the polypropylene fiber-cement paste (Grace MicroFiber^{TM}), chopped to approximately 0.5-1.5 mm in length (e.g., approximately the same length as the pulp fibers) to isolate the influence of the internal curing from any internal restraint provided by the fibers. The diameter of the polypropylene fiber was approximately 20-25 μm, which is slightly larger than the hardwood pulp fibers, but reasonably similar.

The fiber-cement samples tested in this study by calorimetry and autogenous shrinkage experiments were prepared by mixing the as-received, never dried, fibers with ASTM Type I/II portland cement (Lafarge, North America) and deionized water (DI water, resistivity of 18.2 MΩ.cm) at a fixed w/c of 0.30. The oxide analysis was performed by X-ray fluorescence (XRF, Bruker AXS S8 Tiger) spectrometry. The oxide composition of the cement is (percentage by mass): 19.73% SiO_2, 4.82% Al_2O_3, 3.16% Fe_2O_3, 62.41% CaO, 3.64% MgO, 2.99% SO_3, 0.08% Na_2O, 0.48% K_2O, and 2.2% LOI.

The crystalline phases of cement were determined by performing quantitative X-ray diffraction analysis (QXRD, Bruker AXS D4 Endeavor) with the Rietveld method using TOPAS software. The crystalline phase composition of the cement is (percentage by mass): 52.6% alite, 20.7% belite, 3.7% aluminate, 11% ferrite, 0.1% lime, 2.3% portlandite, 2.6% periclase, 0.6% arcanite, 0.4% aphthitalite, 0.9% gypsum, 2.4% bassanite, and 2.7% calcite.

4.2.2 Image Analysis to Quantify Morphology of Eucalyptus Pulp Fibers

The cross-sectional dimensions of eucalyptus fibers were assessed by performing image analysis on scanning electron micrographs. Fiber morphological properties can be quantified effectively based on statistical image analysis with microscopy techniques [92, 93]. Samples for each of the fibers were dispersed in DI water, vacuum filtered at 74.5±3.5 kPa (22±1 in.Hg), and freeze-dried in order to eliminate clumping of the fibers, to prevent collapse of the fiber ultra-structures, and to preserve their microstructure. Freeze-dried fiber bundles were embedded in a hydrophilic aromatic acrylic resin (LR white embedding medium) and heat cured in a conventional oven at 60^{o}C for 24 hours. After the acrylic resin was polymerized, samples were ground using silicon carbide paper with a grit size of 320, 600, and 1200, and polished using a 1.0 and 0.3 micron of aluminum oxide powder. Images of polished samples were acquired with a Hitachi S-3700N variable pressure scanning electron microscope at 600X magnification with a 20kV accelerated voltage and 9-10 mm of working distance. Using the public-domain, Java-based image processing program ImageJ, gray-scale images were thresholded and converted to binary images, as shown in Figure 4.1. In the binary image, small particles, such as grinding debris and other fine materials, and split fibers were discarded. Then, the

modal values of the diameters of the fiber and lumen in the fitted data were determined based on a statistical analysis of 350 cross-sectional fiber images per fiber type.

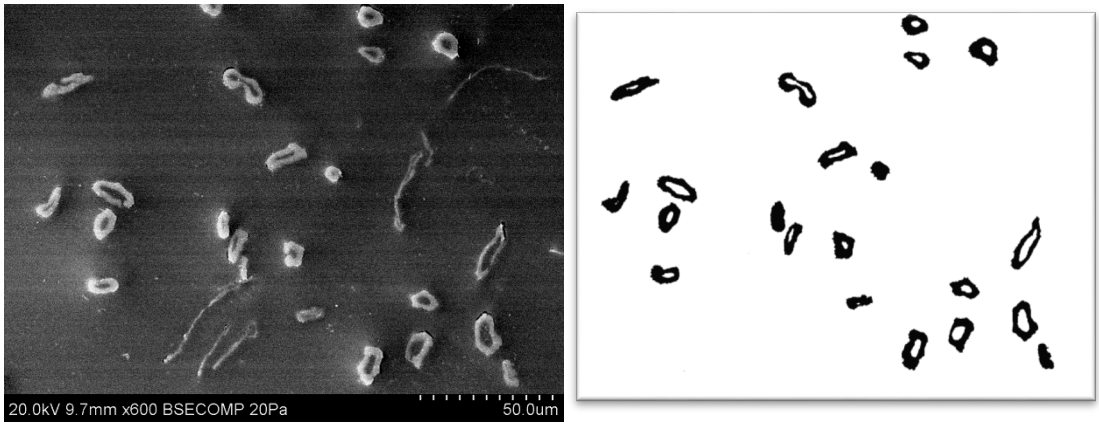

a. b.

Figure 4.1 – Typical cross-section of fibers embedded in an acrylic resin (a) gray-scale SEM image and (b) binary image for analysis.

4.2.3 Composition and Hard-to-Remove Water Analysis of Eucalyptus Pulp Fiber

The compositions of the five fiber types were determined through measurements of lignin content, cellulose-to-hemicellulose ratio, and hard-to-remove (HR) water content. The lignin content in fibers was determined by a kappa number test according to TAPPI Standard T236. The total residual lignin content (TRLC) was calculated according to TRLC = kappa number/6.546 [94]. Because the kappa numbers of bleached pulp were very small, the residual lignin content in both bleached fibers was assumed to be insignificant, as expected for this type of fiber processing. The ratio of cellulose-to-hemicellulose of each fiber was determined by measuring the weight change of samples during thermogravimetric analysis. As-received fibers were dried at 23±2^{o}C and 42 ±3%RH in a ventilation hood for 24 hours prior to the test. Samples were placed in a thermogravimetric analyzer (TGA), TA instrument Q5000IR. The nitrogen gas flow rate was 20 mL/min for both balance and sample chamber gas. Samples were heated up from

room temperature to 600°C at a constant heating rate of 10°C/min. Since the main decomposition temperature of hemicellulose and cellulose occurs mainly at 220-315°C and 315-400°C, respectively [95], the cellulose-to-hemicellulose ratio of the fibers was defined as the fraction of the percent weight change at 315-400°C to the percent weight change at 220-315°C.

In addition, for the purpose of understanding the use of pulp fibers for internal curing, it is important that relative availability of moisture provided by the fiber be assessed by measuring the HR water content. HR water can be defined as the moisture ratio (grams of water per gram of dry fiber) at the transition between the constant and the falling rate zones of evaporative changes in mass detected by during TGA [96]. Park et al. [96] proposed that the amount of HR water could be used as an indicator of the range in moisture content within which moisture loss from the fibers is controlled by internal diffusion. Therefore, this research will relate HR water to both fiber properties (e.g., fiber type, pore volume, and fiber wall thickness) and fiber-cement pastes properties, such as autogenous shrinkage. TGA was used to determine the HR water content in each fiber. The nitrogen gas flow rate was 20 mL/min for balance and sample chamber gas. Measurements of change in mass were made under isothermal conditions at 50°C until the weight change was negligible. The resolution of the instrument was 0.001 µg.

4.2.4 Fiber Quality Analysis

Fiber Quality Analyzer (FQA) was used to characterize the arithmetic mean length ($\bar{L}_n$), the weight-weighted mean length ($\bar{L}_w$), the fiber coarseness, and the length-weighted percent fines content for each pulp fiber. FQA is a widely used optical fiber analyzer that gathers information of fibers through projected images of the fibers in a

dilute suspension transported through the optical and imaging systems. Since the mass of dry fiber (f), the total number of fiber (n), and the number of fiber in the length class l_i (n_i) were known, the $\bar{L}_n$ and $\bar{L}_w$, could be calculated as follows:

$$\bar{L}_n = \frac{\sum n_i \, l_i}{n} \qquad \text{Eq. 4.1}$$

$$\bar{L}_w = \frac{\sum n_i \, l_i^3}{\sum n_i \, l_i^2} \qquad \text{Eq. 4.2}$$

Coarseness of the fiber is the "weight of fiber wall material in a specified fiber length" [27]. From FQA data, the mean value of fiber coarseness was:

$$Fiber\ coarseness\ (\frac{mg}{m}) = \frac{f \times 1000}{\bar{L}_n \times n} \qquad \text{Eq. 4.3}$$

The length-weighted percent fines content was calculated by dividing the total length of measureable fines (0.07 to 0.10 mm in length) by the total length of measureable fines and fibers. The maximum length of fine fraction set in this experiment was 0.1 mm.

4.2.5 Autogenous Deformation

The mix proportions for the control and fiber-cement paste samples were selected to maintain a constant amount of "entrained" water (e.g., water available for internal curing) with the constant amount of cement (by weight) and the w/c of 0.30, 0.31, and 0.32, listed in Table 4.1. The amount of fiber added to the cement paste depended on the absorption capacity (*k*) of the fiber, as determined by the method described by Johansen et al. [97]. Based on the assumptions that internal curing agents will absorb water from the mix to equilibrate at *k* and that they neither accelerate nor slow the rate of hydration,

the *k* of fibers can be calculated by comparing the early heat evolution data of the fiber-cement pastes to those of ordinary cement pastes at a similar water-to-cement ratio. Absorption of water by the internal curing agents would be expected to produce calorimetry curves similar to those for ordinary pastes at a lower w/c; thus, the amount of water absorbed can be used to calculate *k* for an internally cured paste of known composition.

To determine the *k* of fibers, fibers were first assumed to have *k* at 1. Then, using Eq. 4.4 and 4.5, the mass of mixing water (M_W) and the mass of as-received fibers (M_F) were calculated based on the mass of cement proportioned for the mixture (M_{CEM}), the moisture content of each fiber (MC, determined according to ASTM D4442-07 [98]), the assumed *k* (k_A), and dry fiber mass-to-cement ratio (f/c), Then, the early heat evolution data of fiber-cement pastes were compared to those of ordinary cement pastes to determine the effective w/c (w/c_{eff}). Then, the k_A of fibers was adjusted to the actual *k* of the fibers (Eq. 4.6 and 4.7).

$$M_w = M_{CEM} \times \left\{\frac{w}{c} - \left[\left(\frac{MC}{100} - k_A\right) \times \frac{f}{c}\right]\right\} \quad \text{Eq. 4.4}$$

$$M_F = M_{CEM} \times \frac{f}{c} \times \left(1 + \frac{MC}{100}\right) \quad \text{Eq. 4.5}$$

$$\Delta k = \frac{\frac{w}{c} - \frac{w}{c_{eff}}}{\frac{f}{c}} \quad \text{Eq. 4.6}$$

$$k = k_A + \Delta k \quad \text{Eq. 4.7}$$

The effectiveness of eucalyptus fibers as internal curing agents was examined through the comparison of autogenous shrinkage test results of fiber-cement pastes to

those of the cement pastes at three different water-to-cement ratios (w/c), i.e. w/c = 0.30, 0.31, and 0.32. The autogenous deformation was measured according to ASTM C1698-09 [99]. After mixing, the pastes were cast and sealed in corrugated polyethylene tubes having an outer diameter of 29 ± 0.5 mm with a length of 420 ± 5 mm. All of the samples were stored in an environmental chamber at 25^{o}C ± 1^{o}C during the entire test period. When the pastes reached the final set, determined according to ASTM C191-08 [100], measurements of the initial deformation were taken. The test data of fiber-cement pastes were compared with that of the control sample, which contained no internal curing agent.

Table 4.1 – Mix designs for the autogenous shrinkage measurements.

	Control			**Fiber-Cement Paste**								
	w/c 0.3	**w/c 0.31**	**w/c 0.32**	**USF**	**BSF**	**SCF**	**SCF 1%**	**UKF**	**UKF 1%**	**BKF**	**BKF 1%**	**PP 1%**
As-received MC[a] (%)	-	-	-	487	417	529	529	401	401	414	414	-
k	-	-	-	1	1	1.5	1.5	2	2	2	2	-
Cement (g)	1500	1500	1500	1500	1500	1500	1500	1500	1500	1500	1500	1500
Water (g)	450	465	480	391.95	402.45	412.10	393.15	434.93	419.85	433.95	417.90	450
Dry fiber (g) [Dry fiber-to-cement in mass percent]	-	-	-	15 [1]	15 [1]	10 [0.667]	15 [1]	7.5 [0.5]	15 [1]	7.5 [0.5]	15 [1]	15 [1]
As-received fiber (g)	-	-	-	88.05	77.55	62.90	94.35	37.58	75.15	38.55	77.10	15
w/c	0.3	0.31	0.32	0.3	0.3	0.3	0.3	0.3	0.3	0.3	0.3	0.3
w_e/c[b]	-	-	-	0.01	0.01	0.01	0.015	0.01	0.02	0.01	0.02	-

[a] The moisture content of fibers is expressed as a percentage of the oven-dry mass of fibers.

[b] The term w_e/c is the amount of entrained water to cement by mass.

4.3 Results and Discussion

To evaluate the internal curing performance of eucalyptus fibers, autogenous shrinkage experiments of cement pastes – w/c = 0.30, 0.31, and 0.32 – and fiber-cement pastes were performed. For more understanding of factors controlling the internal curing capacity of eucalyptus fibers, the autogenous shrinkage test results were then evaluated and analyzed in the context of fiber properties.

4.3.1 Fiber Properties

Table 4.2 summarizes results from the physical and chemical analysis of the fibers and provides data describing each fiber's diameter, the lumen diameter, the cell wall thickness, the fiber coarseness, the arithmetic mean fiber length, the weight-weighted mean fiber length, and the length-weight percent fines content, as well as other properties of each fiber, including *k*, the kappa number, the total residual lignin content, the cellulose-to-hemicellulose ratio, and the amount of HR water measured.

The frequency distributions of the fiber and lumen diameters obtained through the statistical image analysis previously described are shown in Fig. 4.2 and 4.3, respectively. By using OriginPro data analysis software, the discrete frequency distributions of the fiber diameter were fitted based on Pearson IV distribution, while that of the lumen diameter were fitted based on log-normal distribution. Fitting parameters were iterated until the fit converged (Chi-square tolerance value of 1E-9 was reached). The modal values for the fiber diameter and lumen diameter can be determined from the peak values, evaluated by using local maximum peak finding method, from curves fitted to the discrete frequency distributions shown in Figures 4.2 and 4.3, respectively. The cell-wall

thickness is the difference between the modal value of the fiber diameter and lumen diameter divided by two.

The weight-weighted mean fiber lengths, measured by using FQA, ranged from 0.68- 0.78 mm. The weight-weighted mean fiber length is more commonly used in paper science, because it is more related to sheet properties than other mean lengths [101]. Although the diameter of fiber, the thickness of cell wall, the density of cell wall, and the cross-section of fiber affect the coarseness of fiber, Table 4.2 shows that, the cell-wall thicknesses evaluated by image analysis seem well correlated with coarseness values evaluated by using FQA. A fiber that has high coarseness value could be expected to have a thick fiber wall [102].

Overall, the morphological properties resulting from the analysis of the fiber, determined from the image analysis and FQA, agree with prior research outcomes. Paavilainen et al. [103] reported that the properties of hardwood vary between 0.7-1.7 mm, 2.5-5 μm, and 15-40 μm for the fiber length, the cell wall thickness, and the fiber width, respectively. Specifically, the morphological characteristics of Eucalyptus camaldulensis pulps grown in northern India are a fiber length of 0.8±0.21 mm, a fiber width of 15±3.1 μm, a lumen diameter of 7.2±0.8 μm, and a cell wall thickness of 4.0±0.9 μm [6].

Among these fibers, it is worth noting the variation in chemical composition, particularly cellulose-to-hemicellulose ratio and lignin content. With regard to chemical composition, as expected, the lignin and hemicellulose content in the fiber decreased as the degree of chemical treatment increased. Both fully chemically-treated fibers (BSF, BKF) had relatively high cellulose and low lignin contents compared to their

corresponding unbleached fibers (USF, UKF), resulting in cellulose-to-hemicellulose ratios of approximately 4.5-6 and 3-4, respectively. In addition, due to its lowest level of chemical treatment (a mild chemical treatment followed by moderate mechanical refining) among five fibers tested, the SCF had the highest amount of both lignin and hemicellulose.

Fibers also vary in length-weighted percent fines content. Both soda fibers (USF, BSF) had the lowest fines content, while SCF had the highest, likely due to the mechanical aspects associated with this form of processing which are absent in the other soda and kraft processing methods. Some variation in *k* was also noted. Both soda fibers (USF, BSF) had *k* of 1 while that of SCF and both kraft fibers (UKF, BKF) were 1.5 and 2, respectively. This can be implied that, based on dry fiber mass, the soda fibers, SCF, and kraft fibers absorb water about 1, 1.5, and 2 times their own weight, respectively. Of the parameters measured, *k* seems most well-linked to the lumen diameter, with the larger *k* found for fibers with the larger lumens. In addition, kraft fibers had a higher *k* of 2 perhaps because these fibers are characterized by a narrower cell wall thickness and a larger lumen diameter than soda fibers, with *k* of 1. These results coincide well with prior studies that found that the water retention value (WRV), the amount of water held in the fiber, determined by centrifuge method, decreased as the mean fiber wall thickness increased [104]. Since water is retained by capillarity inside the lumen, fibers with a thinner wall thickness and larger lumen diameter contain more water that could result in a higher *k.*

The fibers also varied in their proportion of HR water. While the SCF had the highest amount of HR water, the UKF had the lowest amount. While there is no clear

relationship between the measured *k* and the HR water content, variations in the fiber morphology and composition may influence the amount of HR water measured. Since the HR water is a combination of both bound water and some amount of free water that is located in small pores and capillaries, making it difficult to remove from fiber in the drying process, internal diffusion is considered to be the key mechanism for removal of HR water. Internal diffusion, then, depends on properties such as lumen diameter and volume, fiber wall thickness, fiber wall composition, and moisture content [105]. Therefore, both a smaller lumen diameter resulting in greater capillary tension and a thicker cell wall obstructing the diffusion of water to the surface contribute to a higher amount of HR water. From Table 4.2, a thicker cell wall thickness of soda fibers appears to correspond with the higher amount of HR water. In addition to the thickness of the cell wall, the higher HR content in the SCF could also be related to the higher lignin content. Since the lignin (and some hemicellulose) removal results in increased fiber wall porosity [106, 107], therefore, the higher lignin content in SCF could be interpreted that the cell wall of SCF is denser than other fiber types resulting in the slower moisture diffusion to the fiber surface.

Table 4.2 – Fiber properties.

Fiber Properties	Types of Fibers				
	USF	**BSF**	**UKF**	**BKF**	**SCF**
k[a]	1	1	2	2	1.5
Kappa number	20-22	N/A[e]	25	N/A[e]	150-160
Lignin content (%)	3-3.3	N/A[e]	3.82	N/A[e]	23-24.5
Cellulose-to-hemicellulose ratio[b]	3.99	5.89	3.01	4.49	1.05
HR water content[b] (g/g dry fiber)	1.44±0.11	1.45±0.01	1.30±0.02	1.37±0.09	1.76±0.06
Fiber diameter[c] (μm)	12.914	12.524	12.602	12.797	14.124
Lumen diameter[c] (μm)	5.067	4.716	5.341	5.341	5.380
Cell wall thickness[c] (μm)	3.924	3.904	3.631	3.728	4.372
Coarseness[d] (mg/m)	0.065	0.064	0.059	0.062	0.119
Arithmetic mean length[d] (mm)	0.471±0.01	0.463±0.01	0.481±0.01	0.481±0.00	0.418±0.00
Weight-weighted mean length[d] (mm)	0.690±0.02	0.778±0.09	0.734±0.04	0.771±0.05	0.684±0.01
Length-weighted percent fines content[d] (%)	0.73±0.00	0.77±0.01	0.93±0.05	0.88±0.03	1.12±0.03

[a]*k* of fibers were determined by performing isothermal calorimetry tests.

[b]Cellulose-to-hemicellulose ratio and HR water content of fibers were determined by measuring the weight change of samples in TGA.

[c]Fiber morphological properties—fiber diameter, lumen diameter, and cell wall thickness—were evaluated by performing an image analysis.

[d]Fiber qualities—coarseness, arithmetic mean length, weight-weighted mean length, and length-weighted percent fines content—were determined by using FQA.

[e]The kappa numbers of bleached fibers were very small. Therefore, the residual lignin content in bleached fibers was assumed to be negligible.

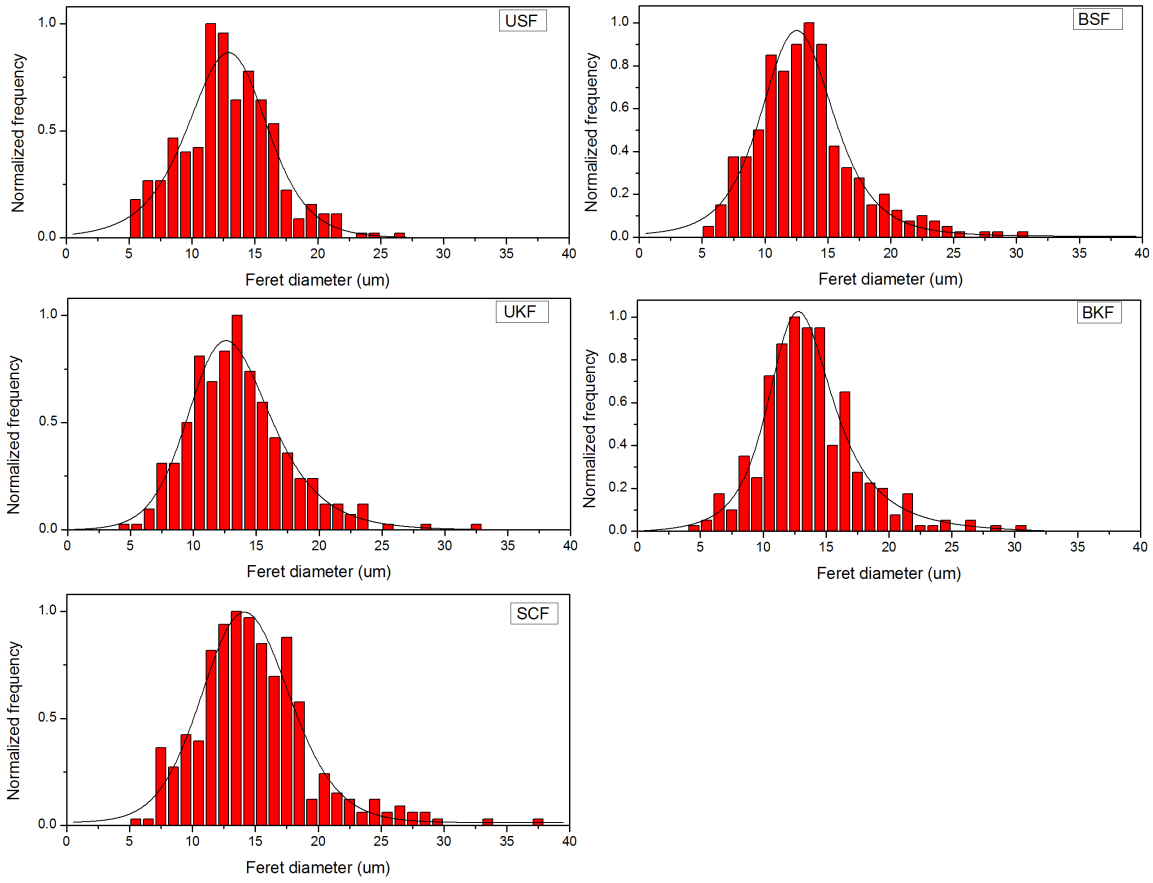

Figure 4.2 – Frequency distribution of the fiber diameters (µm) from the image analysis.

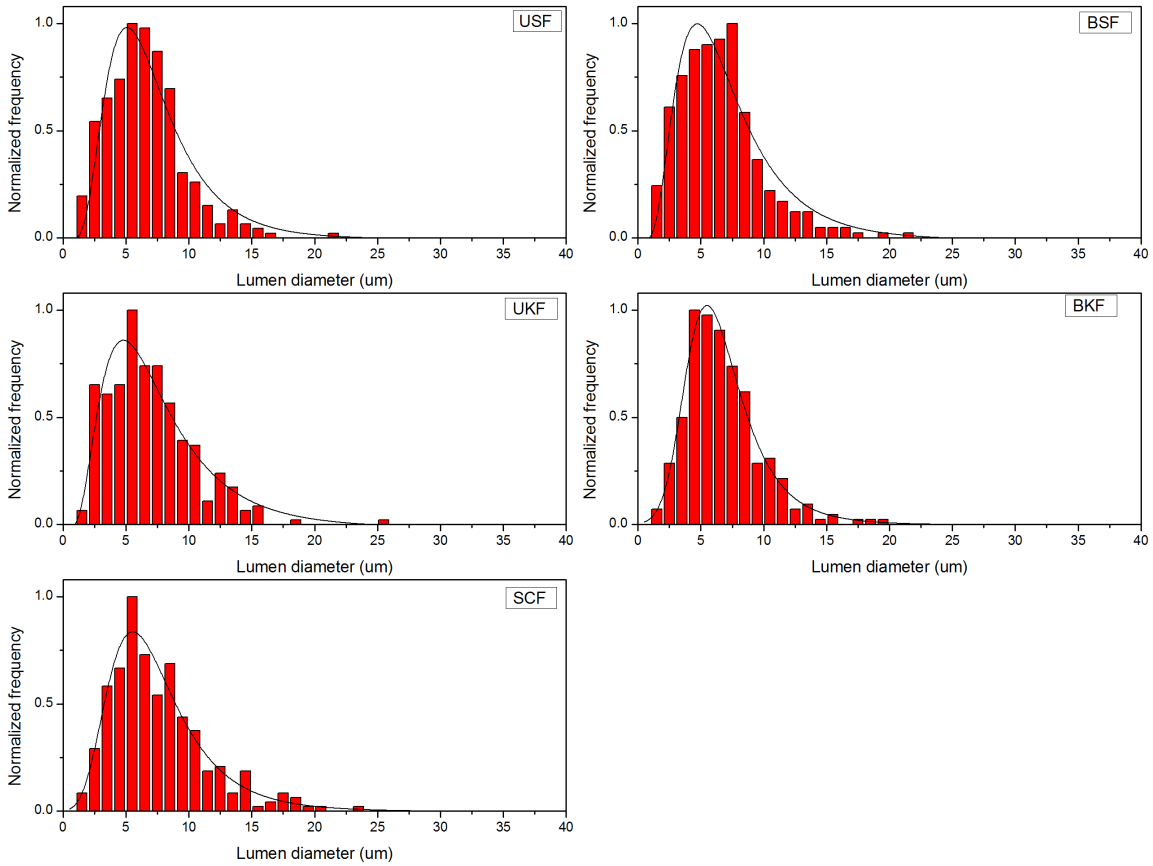

Figure 4.3 – Frequency distribution of the lumen diameters (μm) from the image analysis.

4.3.2 Effect of Fibers on Early-Age Hydration

Figure 4.4 presents the effects of the incorporation of fiber on the rate of the hydration of cement paste assessed by isothermal calorimetry. The mix design (i.e., water contents) of the fiber-cement pastes were adjusted corresponding to *k* of each fiber (Table 4.2). With these adjustments, the addition of the fibers to the cement paste did not greatly affect the hydration rate of cement as expected, since the moisture expected to be absorbed by each fiber was accounted for in the mix design. Although the inclusion of BSF and BKF delayed the onset of the C_3S hydration peak by 20 to 40 minutes, respectively, the cumulative heat of hydration over the first 40 hours did not vary much

among the pastes (Figure 4.5). By 50 to 60 hours, the overall hydration of the fiber-cement pastes was slightly higher (~2-5% at 60 hours) than that of the control mix (w/c = 0.30), providing some evidence that the internal curing offered by the fibers promotes early cement hydration.

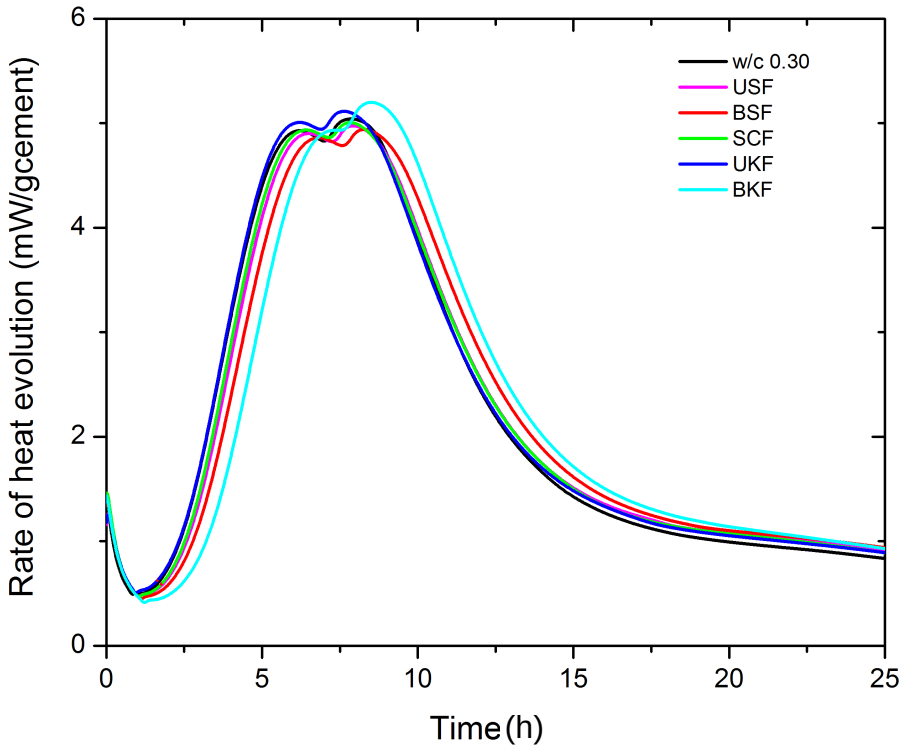

Figure 4.4 – Heat released from the cement paste compared with that of the fiber-cement pastes.

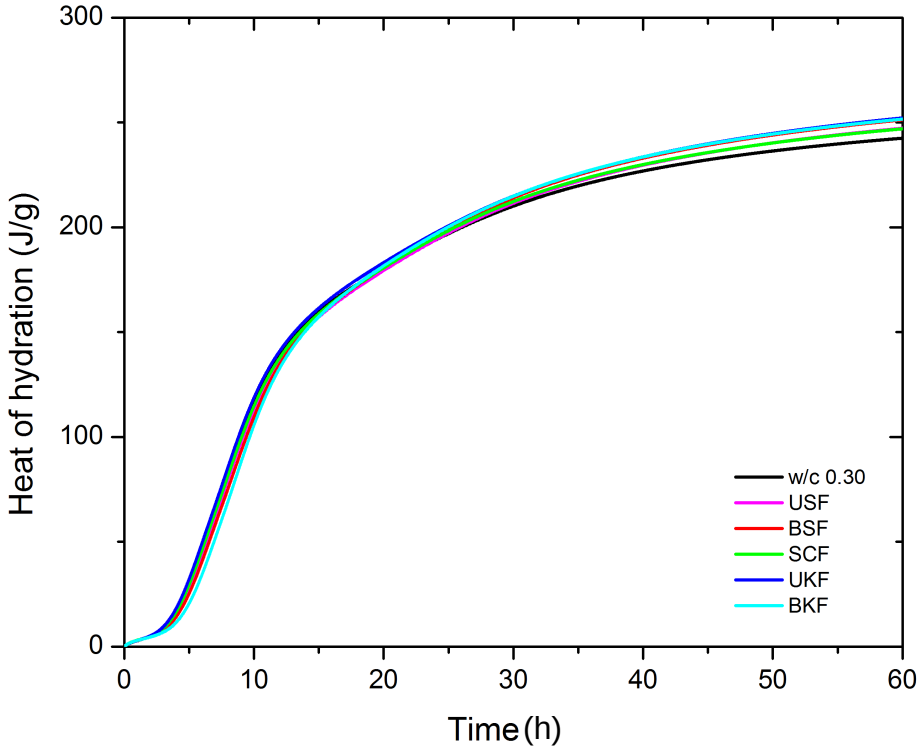

Figure 4.5 – Cumulative energy released from the cement paste compared with that of the fiber-cement pastes.

Accounting for only *k*, the preliminary results suggest that of the five eucalyptus variants examined kraft fibers and SCF are most advantageous for internal curing. However, a more comprehensive assessment of the potential of these fibers as internal curing agents necessitates further data pertaining to composition and morphology as well as measurements of early age deformation, as will be discussed subsequently.

4.3.3 Setting Time and Autogenous Shrinkage Behaviors of Fiber-Cement Pastes

The capacities of the fibers to offset autogenous shrinkage by internal curing were compared through measurements of deformation made after the final set. The final set times of fiber-cement pastes, which were prepared to contain 0.01 of entrained water per gram of cement (based upon each fiber's determined *k* at a fixed w/c of 0.30), are

compared to those of the cement pastes at w/c = 0.30 and 0.31 in Figure 4.6. Although lignin derivatives such as lignosulfonate could retard the hydration reaction of calcium silicate phases [108], the use of fiber containing a high amount of lignin such as SCF (nearly 23% lignin) did not extend the time to set. Instead, the setting times determined by using Vicat apparatus were generally the same. The exception is BKF, which extended the time to set by 40 minutes. This fiber also resulted in some offsets in the rate of hydration data obtained in isothermal calorimetry. Together, this provides evidence that the fiber has some effect on slowing early hydration. However, as seen in Figure 4.6, even BKF did not delay final set to the extent observed when increasing the w/c from 0.30 to 0.31, demonstrating that variations in setting time with the addition of eucalyptus fibers is minimal.

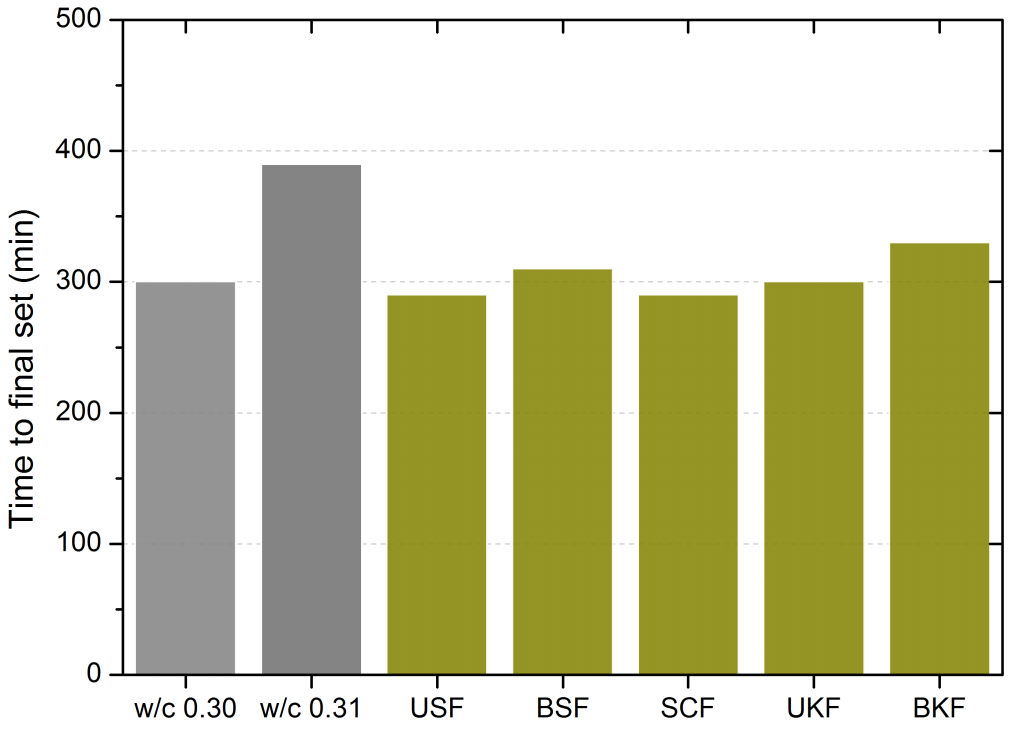

Figure 4.6 – Final setting time of the cement paste compared with that of the fiber-cement pastes at 0.01 of w_e/c.

Figure 4.7 compares the autogenous shrinkage of the cement paste and internally cured fiber-cement pastes, measured after the final setting. All of the fiber-cement pastes, shown in Figure 4.7, were prepared based on the determined *k* of the fibers; each contains w_e/c of 0.01. Within the first few hours after the final setting, the fiber-cement pastes exhibited a slightly higher (or more negative) autogenous strain than cement paste, indicating either greater shrinkage or perhaps less bleeding during this period [109]. Over time, the rates of the shrinkage of the fiber-cement paste specimens were lower than that of the cement paste at w/c of 0.30. This indicates that the fibers, also in a paste with w/c of 0.30, released water into the hydrating cement and reduced self-desiccation.

At about 28 days, the fiber-cement pastes exhibited autogenous strain of -652.05 ± 14.73 με, -652.58 ± 28.25 με, -791.52 ± 19.84 με, -809.09 ± 16.85 με, and -740.81 ± 36.88 με for the USF, BSF, SCF, UKF, and BKF, respectively, whereas cement paste at w/c of 0.30 underwent autogenous strain of about -867.77 ± 12.96 με. Examining the absolute deformation at 2 days shows that both kraft fibers and SCF, containing the same amount of entrained water as soda fibers, did not exhibit effective shrinkage reduction compared to the control paste (at w/c of 0.30). This can be taken to imply that reaching desirable internal curing efficiency requires higher dosage rates of the kraft fibers and SCF. It is also interesting in Figure 4.7 to note that the effectiveness of BKF to mitigate autogenous shrinkage decreases with time, suggesting that entrained water was perhaps released too early with this fiber.

Overall, these results show that of the treatments of eucalyptus camaldulensis examined here, both types of soda fibers with the lowest *k* values of 1 were most effective at limiting autogenous shrinkage, with a ~25% reduction in autogenous

shrinkage. Also, both of these internally cured pastes showed similar shrinkage deformation to the control cement paste at w/c of 0.32, as shown in Figure 4.8.

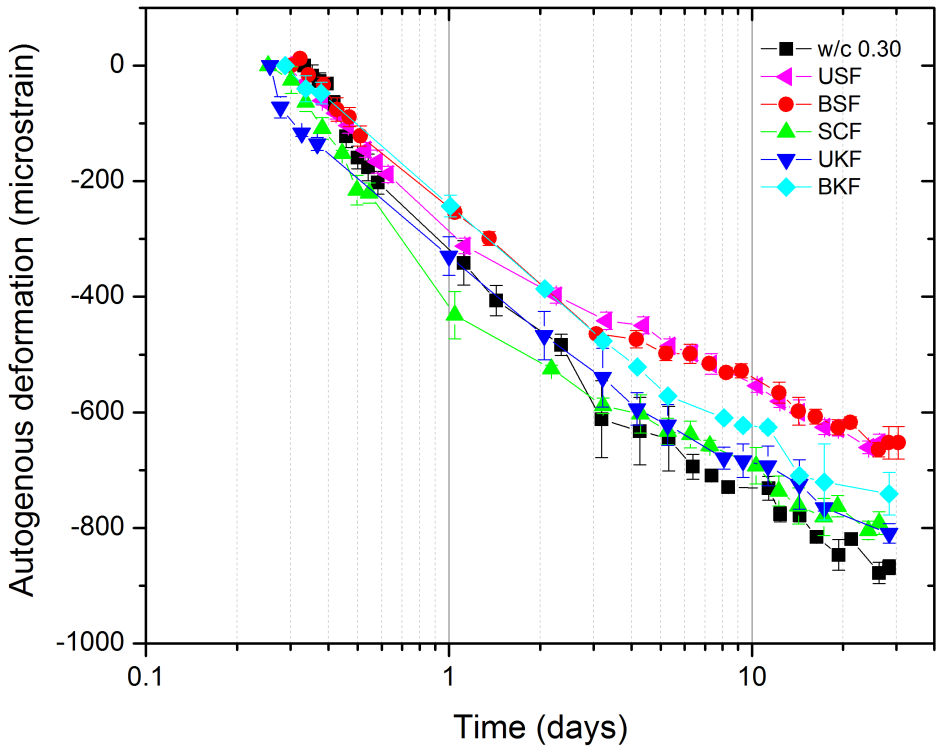

Figure 4.7 – Autogenous deformation of the cement paste compared with that of the fiber-cement pastes with 0.01 of w_e/c.

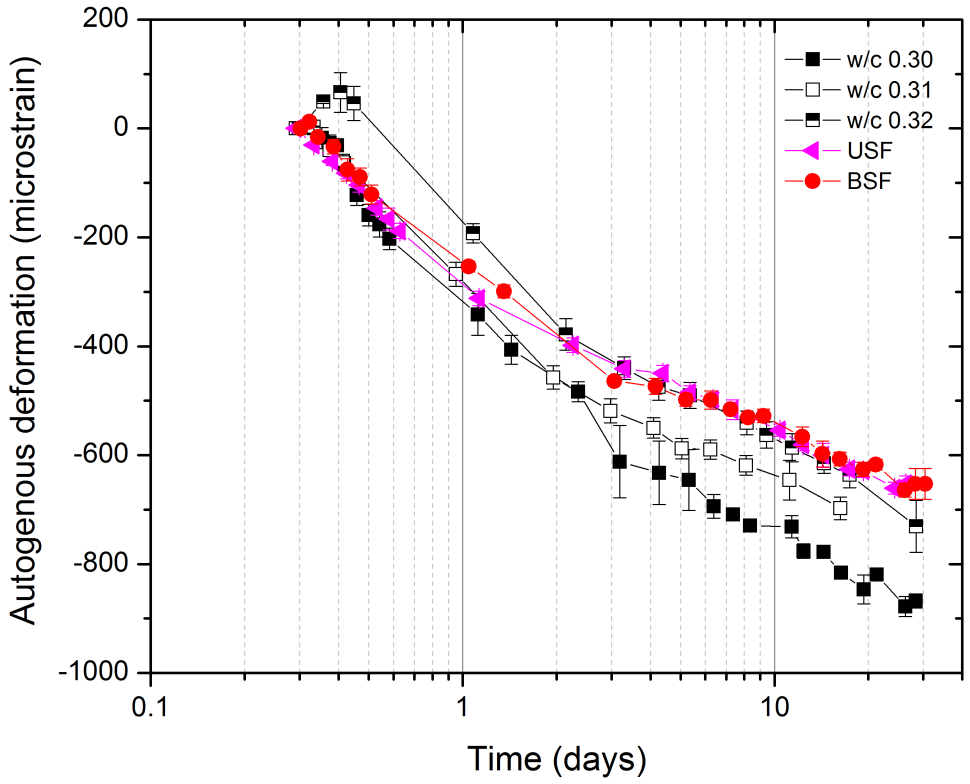

Figure 4.8 – Autogenous deformation of the cement pastes (w/c = 0.30, 0.31 and 0.32) compared with that of USF and BSF cement pastes at 0.01 of w_e/c.

When the dosage of kraft fibers and SCF was increased to a 1% dry mass fraction, corresponding to 0.02 and 0.015 of w_e/c, respectively, SCF at a greater entrained water capacity did not exhibit any enhancement in autogenous deformation, indicating that SCF is not effective for internal curing. However, kraft fibers, both UKF and BKF, exhibited behavior similar to that of soda fibers, at the lower w_e/c as shown in Figure 4.9. Since soda fibers and kraft fibers-cement pastes underwent similar autogenous deformation at equivalent fiber dosage rate (1% of dry fiber mass), the mechanical effect of fibers, i.e. internal restraint, could affect the autogenous deformation of the paste. Therefore, to study the effect of the addition of fiber on the internal restraint, the autogenous shrinkage of polypropylene (PP) fiber-cement paste, where the fiber length and diameter closely

approximate that of the pulp fibers but without internal curing capacity, was measured. As shown in Figure 4.9, at 28 days the PP fiber-cement paste underwent autogenous strain of -862±60 με and exhibited no shrinkage reduction compared to the control during the entire test period. These results suggest that the inclusion of short fibers does not provide substantial internal restraint to autogenous shrinkage. Although it should be noted that the elastic modulus of wood single-fiber in a dry state is one order of magnitude greater than that of PP fiber, the elastic modulus of wood single-fiber in a wet state is also one order of magnitude lower than that in a dry state [110]. Therefore, given that the longitudinal modulus of eucalyptus kraft in a dry state is approximately 35 GPa [20], the modulus of eucalyptus fibers in a saturated state, as they would be when added to mix water and in cement paste at very early ages, would be only about 3.5 GPa. The modulus of the pulp fiber, then, is close to that of the PP fiber used for comparison. (The elastic modulus of individual wood fibers in a dry state varies from 10 to 50 GPa [111], while that of Grace Microfiber^{TM} is 3.5 GPa.). This finding corresponds with a prior study which examined the efficiency of wood-derived powders and fibers for internal curing [9]. That study found that both short fibers and cellulose powder-cement pastes exhibited similar autogenous behaviors, thus they concluded that the addition of short fibers (less than 1.0 mm in length) does not provide any mechanical restraint to early age paste deformation.

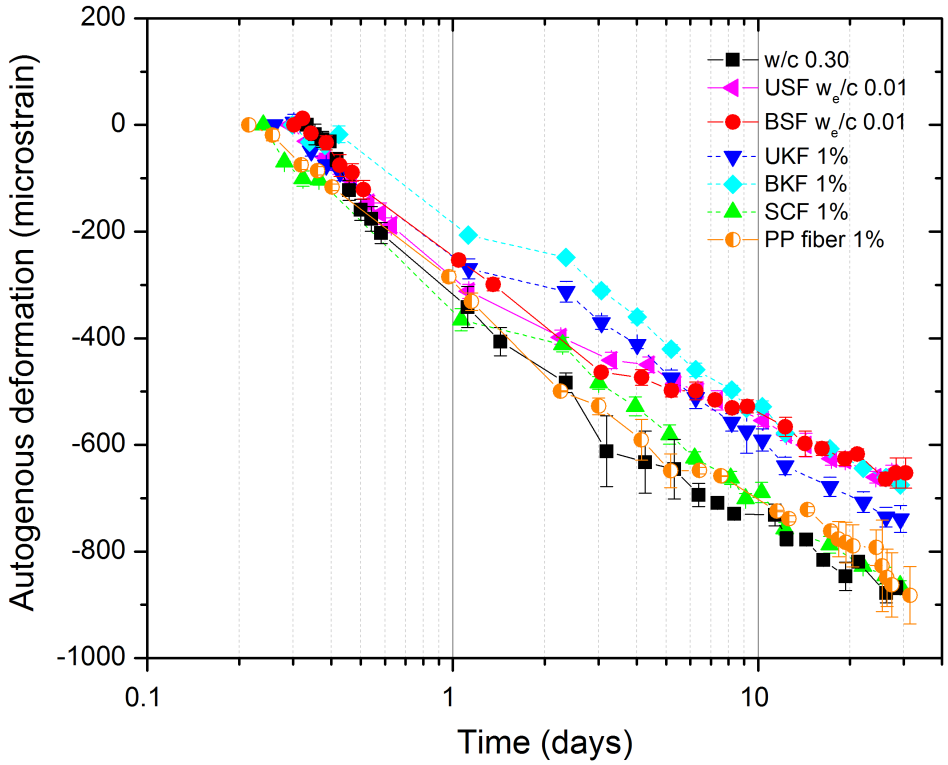

Figure 4.9 – Autogenous deformation of the cement paste compared with that of fiber-cement pastes at a 1% mass fraction of dry fiber.

Among the five fibers examined, both at the same nominal amount of entrained water and dry fiber mass percent, SCF was the least effective for internal curing and it is the only fiber subject to mechanical processing. Therefore, before discussing these results in light of the data regarding the composition and the morphology of the various fibers, it is worth examining the SCF case specifically. First, at $w_e/c = 0.01$, SCF-cement paste underwent a mere 8% reduction in autogenous shrinkage compared to control cement paste of w/c = 0.30. Second, the increasing dosage rate of SCF fiber to 1% dry mass fraction ($w_e/c = 0.015$) did not enhance any reduction in autogenous deformation. These behaviors were not expected, given that the SCF had the highest HR water content and a higher *k* than the soda fibers (which was more effective as an internal curing agent, as

noted previously). The relative ineffectiveness of the SCF can be attributed to fiber bundling (or poor dispersion). Fiber bundling in SCF is related to the method of fiber processing. Since its processing is limited to partial delignification and defiberization, SCF contains fiber bundles, illustrated in Figure 4.10a. Therefore, it is likely that the fibers could not be adequately dispersed. Therefore, entrained water absorbed by fibers was less likely to be well-distributed in SCF-cement paste. The correlation between dispersion and internal curing performance was also reported in prior studies [11, 33, 36, 112]. In addition to fiber bundling, the mechanical treatment in the semi-chemical pulping process leads to fiber fracture, shown in Figure 4.10b. This is also reflected in the higher fines content of SCF as compared to USF is shown in Figure 4.11 and Table 4.2.

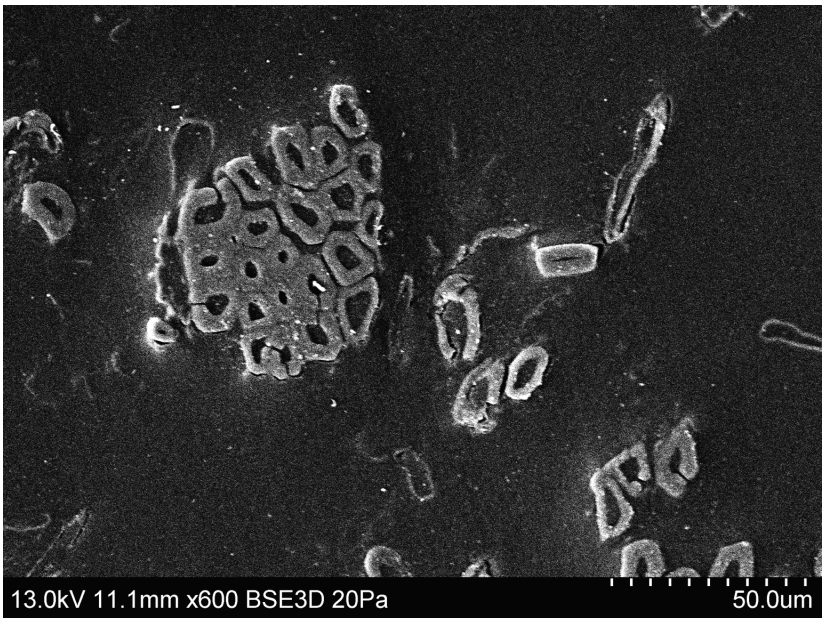

a)

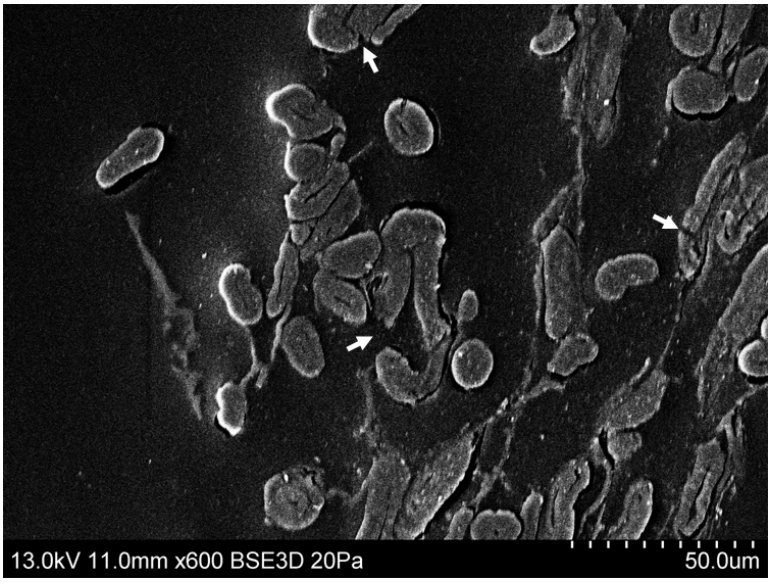

b)

Figure 4.10 – SEM cross-sectional images of SCF of a) fiber bundles and b) fiber fracture compared to c) a SEM cross-sectional image of USF.

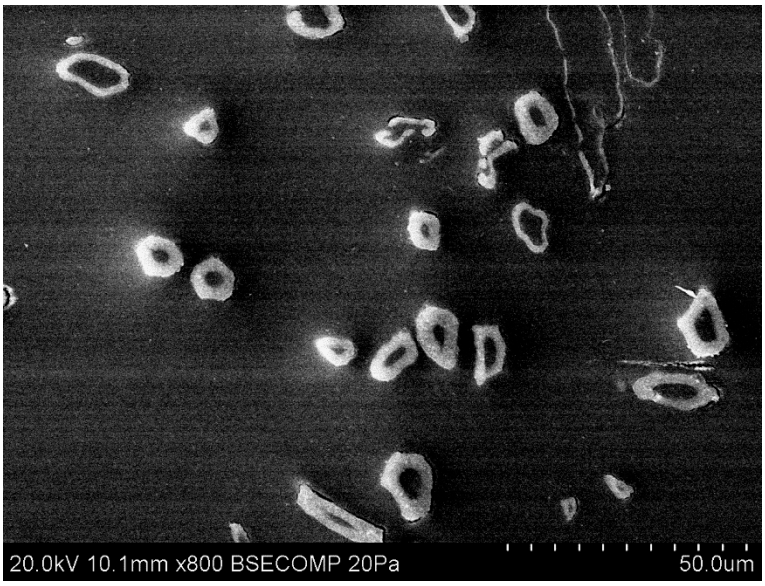

c)

Figure 4.10 – SEM cross-sectional images of SCF of a) fiber bundles and b) fiber fracture compared to c) a SEM cross-sectional image of USF. (Continued)

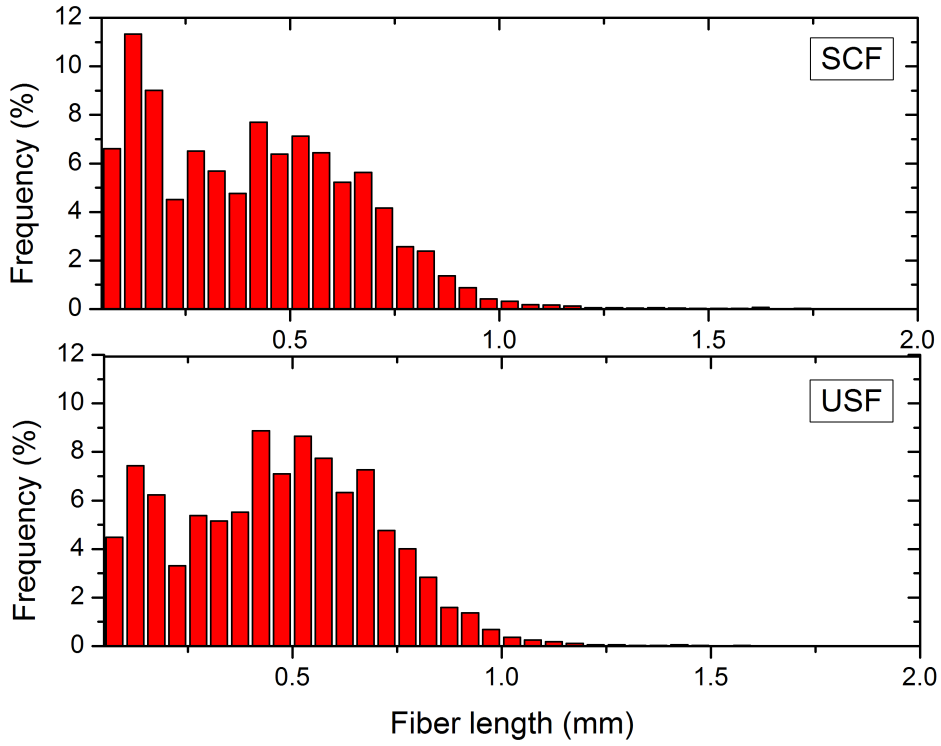

Figure 4.11 – Frequency distribution of percent fines content of SCF and USF observed by using FQA.

Considering in more detail the effects of fiber chemical composition and morphology, unbleached and bleached fibers from the same papermaking process, but having different ratios of cellulose-to-hemicellulose, exhibited almost the same internal curing behaviors (i.e. autogenous shrinkage behaviors and adsorption capacities). In contrast, the internal curing behaviors of fibers from different paper making processes such as USF and UKF (also BSF and BKF), having similar ratios of cellulose-to-hemicellulose, were dissimilar. Together, these observations suggest that the cellulose-to-hemicellulose ratio did not significantly affect the internal curing capacity of the fibers. Although hemicellulose is the most hydrophilic constituent in wood fibers, variations in hemicellulose content could result in several and sometimes competing effects. On one hand, due to its open structure that contains many hydroxyl and acetyl groups, hemicellulose can bind relatively large amounts of water. Therefore, high water absorption is expected in fibers having high hemicellulose content. On the other hand, the removal of hemicellulose results in greater fiber cell wall porosity, increasing the amount of both mesopores and macropores. Thus, an increase in the absorption of water into fibers can also be expected as the hemicellulose content decreases [47]. (However, the removal of hemicellulose may enable greater moisture binding by the remaining cellulose. Rowell and Stout [113] state that not only hemicellulose but also accessible cellulose, both non-crystalline and the surfaces of crystalline cellulose, is crucial in moisture sorption.) The increased porosity in the cell wall may be expected to influence the rate of moisture ingress from the lumen through the cell wall.

From the results in Figure 4.7, both soda fibers (USF and BSF), were more effective in mitigating autogenous shrinkage. Averaging the data from unbleached and

bleached fibers (i.e., neglecting chemical composition), reductions in autogenous shrinkage of nearly 25% for the soda fibers and 7% for the kraft fibers were found compared to ordinary paste (at w/c of 0.30). These findings imply that the internal curing efficiency of these eucalyptus fibers could be related more strongly to their physical morphology than variations in chemical composition of fibers. However, it should be recognized that changes in chemical composition imparted through fiber processing can influence physical structure. That is, the removal of hemicellulose and lignin through pulping can increase cell wall porosity, which can alter the rate of moisture transport from the lumen and cell wall to the surrounding cement pastes.

Here, taking all of the data on chemical composition and morphology into account, it is proposed that the relatively better performance of the soda fibers results from their morphology. Their greater cell wall thickness is thought to contribute to their higher HR water content than kraft fibers. Therefore, the soda fibers are believed to release their entrained water into the hydrating cement during the early hydration period at a slower rate than the kraft fibers. Making entrained water available at a slightly later age is believed to improve the efficacy of hardwood fibers for internal curing.

This mechanism differs from that generally accepted for saturated lightweight aggregates and SAPs in which higher water desorption rates are believed to be more favorable [42, 114]. However, since hardwood fibers are significantly smaller than lightweight aggregates and since they are added at higher dosages than SAPs[*], entrained water from well-dispersed pulp fibers is more readily available to surrounding volumes of hydrating cement. Another way of envisioning this is to imagine entrained water

[*] For internal curing application, at the same w_e/c, due to the lower *k* of pulp fibers, the dosage rate of fibers is higher than that of SAPs by about one order of magnitude.

diffusing from internal curing sources to the surrounding pastes. In the case of pulp fibers, due to their small size (high surface area-to-volume ratio) and relatively large number, the entrained water will be made available relatively rapidly to the surrounding paste. Therefore, for the hardwood fibers examined here, it is proposed that the rates of water release from a fiber with lower HR water content might be too fast to mitigate self-desiccation, as demonstrated by data for the BKF-cement paste (Figure 4.7).

And, one study on SAPs comes to a similar finding: Schrofl et al. [115] reports that the SAPs that showed slow release of pore solution to the hydrating paste are more effective in mitigating autogenous shrinkage than others SAPs that desorbed pore solution too early.

4.4 Conclusions

Results from an evaluation of the eucalyptus fiber properties and a comparison with the autogenous shrinkage experimental results show a correlation between the composition and morphology of these hardwood fibers and their internal curing capacity, with the following conclusions:

- Soda fibers, with their thicker cells walls which are correlated with their higher HR water content, exhibited better autogenous shrinkage mitigation than kraft fibers, even though their absorption capacity, *k,* was lower than kraft fibers.
- These results demonstrate that a slower rate of moisture release during early hydration, as indicated by HR water content, is preferable for internal curing with eucalyptus pulps. These results suggest that thicker cell walled fibers hold greater promise as internal curing agents.

- HR water content is a meaningful parameter for the assessment of pulp fibers as internal curing agents.
- In contrast to soda fibers, SCF fiber, despite its high HR water content, was not effective as an internal curing agent because of its unsuitable physical morphology (i.e., open lumens) and poor dispersability, indicating that the physical morphology of fibers and fiber dispersion should also be taken into account.
- Comparing between the effects of fiber's chemical composition and morphology, results indicate that the internal curing efficiency of eucalyptus fibers is related more strongly to their physical morphology than variations in chemical composition. However, further studies on lignin-rich fibers are needed to verify these findings across a wider range of fiber compositions.

Overall, these findings indicate the need for further studies on a wider range of fibers and comparisons of fibers to SAPs and LWAs. Such studies would examine whether thicker-walled cells in pulp fibers, especially fibers with greater HR water and lignin content, are more conducive to internal curing applications.

CHAPTER 5

THE EARLY-AGE INTERACTION BETWEEN EUCALYPTUS PULPS AND CEMENTS: THE KEY MECHANISMS CONTROLLING INTERNAL CURING PERFORMANCE

5.1 Introduction

Since the concept of using internal curing in high performance concrete has been developed over the past decade, the mechanisms of common absorptive materials – LWA and SAP – for internal curing are relatively understood. That is, the mechanisms controlling the internal curing capacity for LWA are combinations of capillary suction, vapor diffusion, and capillary condensation [29, 42], while those of SAP are combinations of the swelling ratio, ion filtration, and the inter-particle spacing of the SAP [40, 42, 44]. However, unlike LWA and SAP, the information pertaining to the mechanisms controlling internal curing capacity of wood fiber is rather limited. Because the properties, both physical and chemical, of wood fiber are complex and vary by fiber source and processing, understanding the mechanisms which most significantly influence internal curing has been challenging to determine.

Because the pore solution of cement is not pure water but rather an aqueous solution containing a variety of ionic species, the behaviors of wood pulps in a pore solution are more complicated than that in pure water. Pore solution ions can either swell or shrink the cell wall of pulp, changing the effective size of pore space [49-51], and thus affect the diffusion in the cell wall. Pulp can also act as a semi-permeable membrane [52]. Therefore, during the hydration reaction of cement, changes in the concentration of

the counter-ions in cement pore solution can create osmotic pressure affecting the absorption of water through osmosis. These interrelated mechanisms – capillary, diffusion, and osmosis – influence the transition of water from wood pulp fibers to the surrounding hydrating cement paste, affecting their internal curing performance.

Moreover, the surface area of eucalyptus pulp is high compared to other fillers added to cementitious materials. For example, while the surface area of bleached eucalyptus pulp (once dried) is about 60-100 m^2/g [116], that of the limestone filler at an average particle size of 0.7 μm and titanium dioxide with an agglomerate size of 0.58 μm are about 12 m^2/g and 35-65 m^2/g, respectively [117]. These two fillers can provide nucleation sites for hydrating cement and thus increase the early-hydration reaction. Therefore, the surface of eucalyptus pulp may also serve as nucleation sites for hydration products. Based on earlier results (see section 2.4.), it was found that the chemical shrinkage of eucalyptus-fiber cement pastes, shown in Figure 2.4, are slightly higher than that of plain cement paste. These findings suggest some complexities in early hydration behavior that are not captured by isothermal calorimetry. Although such complexities could have resulted from some surface nucleation or an osmotic effect related to differences in the concentration of the solution in both capillary pores and the fiber lumen, a more thorough examination would clarify this behavior.

Although the effects of wood pulps on the long-term performance of pulp-cement composites have been thoroughly studied [5, 118-120], the effects of wood pulp on early hydration reactions are not yet understood. There is also no evidence to support that conclusions based on softwood pulp would be applicable to hardwood pulp such as eucalyptus. This lack of fundamental understanding is one obstacle to optimizing and

tailoring the post-processing methods of such pulp to enhance the behavior of fiber-composite materials, such as internal curing efficiency. To clarify the underlying mechanisms of early-age interactions between eucalyptus pulps and cements, this chapter's aims are: 1) to investigate the migration of entrained water from eucalyptus pulps to hydrating cement paste and 2) to examine the chemical mechanisms underlying the evolving interactions between eucalyptus pulp and cement. This chapter focuses on such interactions, particularly at early ages, which remain relatively unexplored.

5.2 Migration of Entrained Water from Eucalyptus Pulp to Hydrating Cement Paste Characterized by Using Low-Field ^{1}H NMR

The underlying mechanical and chemical properties of fibers which affect the transition of water, including underlying mechanisms and the time and rate at which it occurs, are important for identifying and tailoring fibers for internal curing applications. However, compared to numerous studies on the net effect of internal curing or shrinkage behavior of cementitious composites, research in the area of internal curing mechanisms is rather limited largely because of the challenges in studying these processes *in situ*. Several techniques such as X-ray absorption, X-ray microtomography, and nuclear magnetic resonance have been used monitor the movement of water from internal curing agents to hydrated cement pastes and mortar [67, 121-126], bringing insight into the transition of entrained water. Those studies found that the transition of entrained water from the internal curing agents (i.e. LWA, hydrogels of polysaccharide, and SAP) to the paste mainly occurs during the early hydration reaction period, either within the acceleratory period [67, 122, 123], within the first 24 h of hydration [121, 125], or within 3 days [124, 126]. However, none of these studies have investigated wood pulps as

internal curing agents. Moreover, beside its effects on compressive strength and salt scaling resistance, the effectiveness of hydrogels of polysaccharide, which releases internal curing water within the acceleratory period, to mitigate autogenous shrinkage has not been reported.

Among methods that have been used to monitor the transport of entrained water, low-field ^{1}H NMR relaxometry is most convenient because the sample preparation is simple. Although NMR observations of solid materials are more difficult than those of soft materials because of their relatively short relaxation times, several studies have successfully applied NMR to monitor the internal curing mechanisms of LWA and polymer gel (alginate) and SAP [67, 122, 123, 126]. Recently, Cheumani et al. [46] investigated wood-cement interaction taking place in wood-cement composites during hydration by using low-field ^{1}H, but their work did not account for internal curing and the samples examined contained ground wood powder, not wood pulp. These initial studies do suggest the potential for ^{1}H NMR to provide new insights into the transport of water during internal curing in wood-fiber cementitious composites.

5.2.1 Materials and Methods

To investigate the mobility of water molecules and the water depletion of internal curing water in wood pulp-cement pastes, change in NMR signals – spin-spin relaxation times (T_2) and spin-lattice relaxation times (T_1) – of cement pastes are monitored at early ages. Results from internally cured cement pastes are compared to that of companion ordinary pastes. For comparison, isothermal calorimetry and magnetic resonance imaging (MRI) were performed on companion samples to provide complementary data regarding

reaction kinetics and water distribution, respectively, also at early ages (from mixing to 25 h of hydration).

5.2.1.1 Materials

Necessitated by the requirement for MRI, an ASTM C150 Type I white cement (Lehigh White Cement), was used in this study. In addition, to eliminate bleeding and to exacerbate autogenous shrinkage, metakaolin (Thiele Kaolin Sandersville, Georgia, USA) was used at 3% replacement for cement by mass. Table 5.1 provides their compositions, based upon oxide analysis obtained by X-ray fluorescence (XRF, Bruker AXS S8 Tiger) spectrometry and upon crystalline phase composition obtained by quantitative X-ray diffraction analysis (QXRD, Bruker AXS D4 Endeavor) with the Rietveld method using TOPAS software. The percentage of amorphous content in metakaolin was approximately 96%.

Table 5.1 – Oxide composition of white cement and metakaolin and crystalline phase composition of white cement (% by mass)

Oxide composition	**White cement**	**Metakaolin**	**Crystalline phase composition**	**White cement**
SiO_2	23.65	51.26	alite	68
Al_2O_3	2.09	44.43	belite	16.7
Fe_2O_3	0.38	0.41	aluminate	3.5
CaO	67.56	0.04	ferrite	0.1
MgO	0.80	0.16	lime	0.1
SO_3	2.10	0.05	portlandite	1.6
Na_2O	0.18	0.41	periclase	0.3
K_2O	0.04	0.09	arcanite	0.9
TiO_2	0.07	1.87	aphthitalite	0.2
P_2O_5	0.36	0.07	bassanite	1.5
MnO	0.02	0.07	anhydrite	2.1
SrO	0.12	0.01	ye'elimite	0.5
LOI	2.62	0.96	calcite	4.2
Insoluble residue	0.40	N/A		

Wood pulps used in this study were conventional unrefined unbleached Eucalyptus camaldulensis (or River Red gum) pulps collected from commercially soda pulping (USF) and kraft pulping (UKF) processes in Southeast Asia. While the moisture content (dry basis) of USF was 245%, that of the UKF was 370%. Both pulps were chemically treated. Therefore, they were high in cellulose and low in lignin. The kappa numbers of USF and UKF were 14.6 and 25, which give the total residual lignin contents of 2.23 and 3.82 percent, respectively. For the NMR measurement of wood pulp samples, the never-dried pulps were dried at 23±1°C in a chamber containing saturated $K_2CO_3.2H_2O$ salt solution (approximately 43% RH) and sampled for the measurement of T_2 relaxation at various drying times. To evaluate the moisture content of the pulps, immediately after the NMR experiments, pulps were dried at 105±1°C in an oven for 24 hours to a constant weight.

Table 5.2 presents the mixing proportion of control and pulp-cementitious paste samples evaluated in this study. Two control cementitious pastes were evaluated. One of which had water-to-cementitious materials ratio (w/cm) of 0.30, the other of which had w/cm of 0.34. The w/cm 0.30 paste corresponded to the basic w/cm of internally cured pulp-cement pastes while the w/cm 0.34 paste accounted for entrained water-to-cementitious materials ratio (w_e/cm). Therefore, the cementitious paste at w/cm of 0.34 had the same "total" amount of water available for a hydrating cementitious matrix (i.e., w/cm + w_e/cm) as internally cured pulp-cementitious pastes (i.e., 1% USF and 0.8% UKF-cementitious pastes).

Samples were mixed at room temperature (23±1°C). Fiber cementitious pastes were prepared by mixing the fiber with deionized water for a minute with a hand mixer;

subsequently, cement and metakaolin were added and mixing continued for another three minutes. Samples were then placed in the NMR tubes or calorimeter ampoule, sealed, and then transferred to the testing condition (30±1°C) at 30 min of hydration.

Table 5.2 – Composition of ordinary cementitious and fiber-cementitious pastes for heat of hydration and NMR measurements.

	Control		**Fiber-cement paste**		
	w/cm 0.3	**w/cm 0.34**	**1% USF (*k*=4)**	**2% USF (*k*=4)**	**0.8% UKF (*k*=5)**
White cement (g)	97	97	97	97	97
Metakaolin (g)	3	3	3	3	3
Water (g)	30	34	31.55	33.10	31.04
Moisture content of fiber (MC, %)	-	-	245	245	370
As-received fiber (g)	-	-	3.45	6.90	3.76
Water-to-cementitious materials ratio (w/cm)	0.30	0.34	0.30	0.30	0.30
Entrained water-to-cementitious materials ratio (w_e/cm)	-	-	0.04	0.08	0.04
ADVA455 (ml)	0.5	0.5	0.5	0.5	0.5

5.2.1.2 Heat of Hydration/Isothermal Calorimetry

Maintaining a consistent w/cm, particularly for fiber-cementitious pastes, requires that the amount of internal curing water available to the paste be accounted for during mixture proportioning. Therefore, the amounts of "entrained water" (e.g., water available for internal curing), which depend on the amounts of wood pulps in the paste as well as the intrinsic properties of these agents and the cementitious materials used [40, 44, 127], were quantified using the method suggested by [97] and the mix water masses adjusted accordingly. Same mixing procedure described in section 4.2, the heat of hydration of fiber-cementitious pastes was measured by isothermal calorimeter (TAM Air,

Thermometric AB) for 24 hours. The cumulative heat of hydration of fiber-cementitious paste was compared with that of the control cementitious pastes. The absorption capacity of USF was determined to be 4 while that of UKF was 5. Since the high efficiency polycarboxylate-based superplasticizer, ADVA455 (WR Grace), was added to enhance the workability of the fiber-containing pastes, the same amount was also added in each of the companion samples (5μL per gram of cementitious materials).

As companion to NMR measurements, the early hydration reaction of the pastes at $30 \pm 1^{o}C$ was monitored. The compositions of the control and fiber-cement paste samples for heat of hydration measurements at $30 \pm 1^{o}C$ are listed in Table 5.2. About 3-4 grams of paste was added to the ampoule, sealed, and placed in the calorimeter at 30 min.

5.2.1.3 Magnetic Resonance Imaging (MRI)

The distribution of evaporable water after setting was observed by MRI Scanner (Bruker PhamaScan®) equipped with a 7-T, 38 mm rf coil, and 90 mm horizontal-bore superconducting magnet. The series of 2D (64 x 64) images of cement paste samples – w/cm 0.30, w/cm 0.34, and 1% USF cementitious pastes – were taken by using single point imaging (SPI) method with the phase encoding time t_p of 119 μs, the repetition time TR of 10 ms, and a field of view (FOV) of 40 x 40 mm. The resolution of image was 625 x 625 μm/voxel. The t_p and TR were selected to yield a high resolution image [70]. The value of t_p was longer than the T_2 of solid phases (~20μs) and the T_2 of interlayer water (~100μs). Thus, only gel water and capillary water were detected.

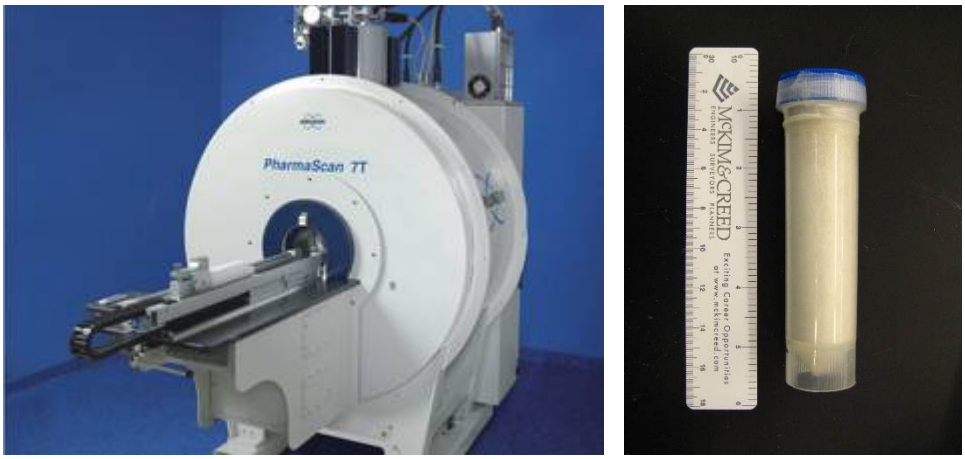

Figure 5.1 – The Bruker PhamaScan® and a sample holder for MRI measurements.

5.2.1.4 Low-field NMR Measurements

^{1}H NMR measurements were performed at resonance frequency of 23 MHz using low NMR field (MARAN Ultra 23) with a 25 mm radiofrequency (rf) probe operated at 30±1^{o}C. The changes in ^{1}H NMR relaxations of cement pastes with and without internal curing agent at early ages were monitored by repeated T_2 and T_1 relaxation experiments at 2 h time intervals from 1 h to 25 h of hydration. About 15 g of sample was filled into a 20 mm diameter NMR tube. Then, the sample tube was sealed to prevent the evaporation of water and placed in the NMR sample coil.

Figure 5.2 – The MARAN Ultra 23 and a sample holder for NMR measurements.

Spin-spin T_2 relaxation experiments were performed using the Carr-Purcell-Meiboom-Gill (CPMG) pulse sequence, $90^{o}_{x} - (\tau - 180^{o}_{y} - \tau)_{n}$, as shown in Figure 5.3. The experiment parameters were followed the procedure demonstrated in [46], in which the number of echoes (π pulses) was 600 and the inter-echo time (TE) was 200 μs. The length of the $\pi/2$ and π pulses was 6.1 and 12.2 μs, respectively. Since the solid-phase protons have short T_2 relaxation times of about 20 μs, at this TE length, the CPMG measurement detected only the ^{1}H NMR signal of liquid-phase protons in pulps, cement pastes and pulp-cement pastes.

To allow the nuclear spins to relax to equilibrium between each scan, a repetition delay time (RD) was set at 5 s. The 256 successive CPMG relaxation measurements were added together to improve the signal-to-noise ratio. For heterogeneous materials such as cement paste, the resulting relaxation is characterized by a multi-exponential decay, which can be described by a simplified quantum-mechanical model as:

$$X(t_i) = \sum_k A(T_k)\exp(-\frac{t_i}{T_k}) + \varepsilon_i \qquad \text{Eq. 5.1}$$

Where T_k and $A(T_k)$ correspond respectively to the relaxation times and the relaxation time distribution of the system having the noise of the signal represented by ε. The recorded transverse magnetization decays were analyzed with an inverse Laplace transformation program (provided by P. Callaghan, Victoria University of Wellington, New Zealand), which employs the regularized non-negative least square fit for the determination of the T_2 distribution.

The spin-lattice relaxation (T_1) was determined by using an inversion recovery pulse sequence. Decays comprised 20 echoes logarithmically distributed from 50 μs to 100 ms. The resulting T_1 data were collected from 16 scans and were analyzed with a regularized ILT using Winfit software (Bruker) that decomposes the T_1 distribution to the discrete distributions of spin-lattice relaxation times.

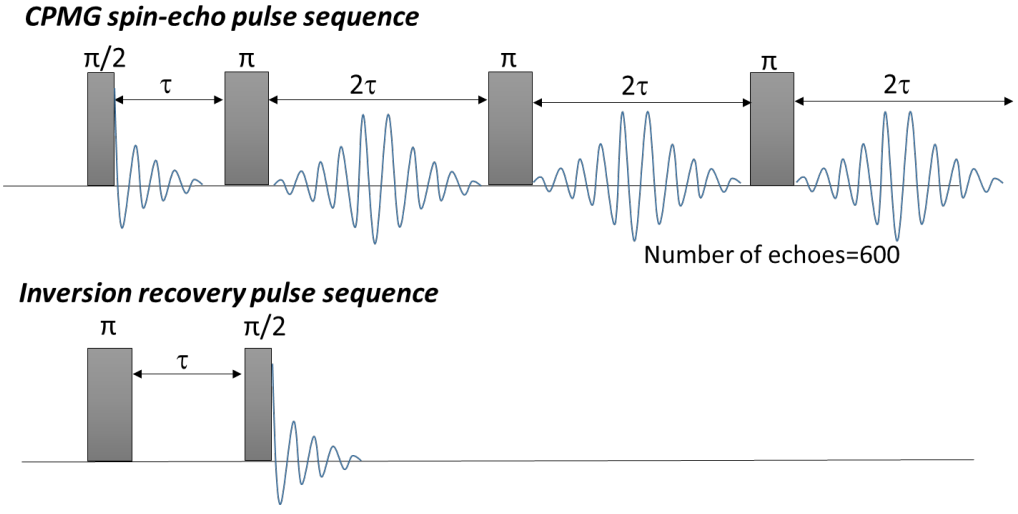

Figure 5.3 – The schematic representation of the Carr-Purcell-Gill-Meiboom multiple spin-echo pulse sequence and the inversion recovery pulse sequence for determining of T_2 and T_1, respectively.

5.2.2 Results

For a thorough clarification of the transport of entrained water from eucalyptus pulp to hydrating cementitious paste, several techniques – calorimetry, MRI, and NMR – were employed to characterize the behavior of eucalyptus pulps, cementitious pastes, and pulp-cementitious pastes. First, as companion to NMR measurements, the isothermal calorimetry was used to observe the early hydration reaction of the pastes. Then, MRI was used for the preliminary *in situ* comparison of water consumption among samples with and without eucalyptus pulp as internal curing agent (i.e., w/cm 0.30, 1% USF, and w/cm 0.34). Finally, the NMR measurement of T_2 relaxation on eucalyptus pulps and cementitious pastes provided a comprehensive demonstration of the transition of water from eucalyptus pulps to a hydrating cementitious matrix. By cross-referencing NMR results to the conventional calorimetry test results, details on water depletion resulting from hydration processes were revealed.

5.2.2.1 Early Hydration Reaction of Fiber-Cementitious Pastes

Figures 5.4 and 5.5 present the early hydration curves of cementitious paste samples. All results were normalized per g of cementitious materials. Each curve presented in Figures 5.4 and 5.5 represents the average of data of three replicates for each sample. Because of the external mixing, the system did not capture the initial heat peak associated with the induction period. From the figures, while overall hydration is not significantly suppressed, compared to the w/cm 0.30 cementitious paste the addition of eucalyptus pulps slightly delays the setting. However, the extent of the delay is similar to that noticed when increasing the water content, as seen in the w/cm 0.34 cementitious paste. At very early ages (<23 hours), eucalyptus pulps-cementitious pastes exhibited

lower heat release than that of w/cm 0.30 cementitious paste. However, the cumulative curves of USF-and UKF-cementitious pastes were higher than that of w/cm 0.30 cementitious paste at later ages (i.e., beginning at approximately 23-24 hours and 28 hours for cementitious pastes with w_e/cm of 0.04 and 0.08, respectively). Similar behavior was reported in cases for SAP and LWA internal curing agents [30, 37], in which, at approximately 24 hours, both LWA and SAP also yield higher cumulative heat release than the control paste. This perhaps indicates the additional hydration reaction associated with entrained water, which is available for further hydration.

Considering the early-age interaction between eucalyptus pulps and cement, from Figure 5.4, a small retardation of the main peak of USF- and UKF-cementitious pastes could result from the absorption of alkali ions, particularly Ca^{2+} in a white cementitious matrix, which dilutes the initial Ca^{2+} concentration in the pore solution, delaying the precipitation in the pore space [128]. Moreover, the height of the main peaks of both USF- and UKF-cementitious pastes are slightly higher than that of w/cm 0.30 and w/cm 0.34 pastes indicating greater reaction, which is perhaps facilitated by nucleation on the surface of eucalyptus pulps. From [128], it was reported that wood pulp fibers exchange ions with cement pore solution through their cell wall and some apparently crystalline products have been noted to nucleate on their surface at early ages. While these interactions depend on the cement and fibers combined, those prior findings do agree with the results here suggesting that internal curing with pulp fibers can enhance early hydration. (More details on sorption are in section 5.3.)

The effects of ion exchange capacity of SAP on hydration reaction, particularly on the induction period, have also been reported in [37]. Since SAP also exchanges its

ions with cement pore solution [44], it tends to lengthen the induction period of the SAP-cement paste as compared to the reference paste, but not as much as the paste with only water added. The same behavior is observed in this study, as the main peaks of USF- and UKF-cement pastes both with w_e/cm of 0.04 occurs between that for w/cm 0.30 and w/cm 0.34 cement pastes indicating that the desorption kinetics of wood pulps, or eucalyptus pulps, are similar to that observed in SAP. Therefore, the water held in both internal curing agents may gradually release when pores in the cement paste are emptied by self-desiccation [129].

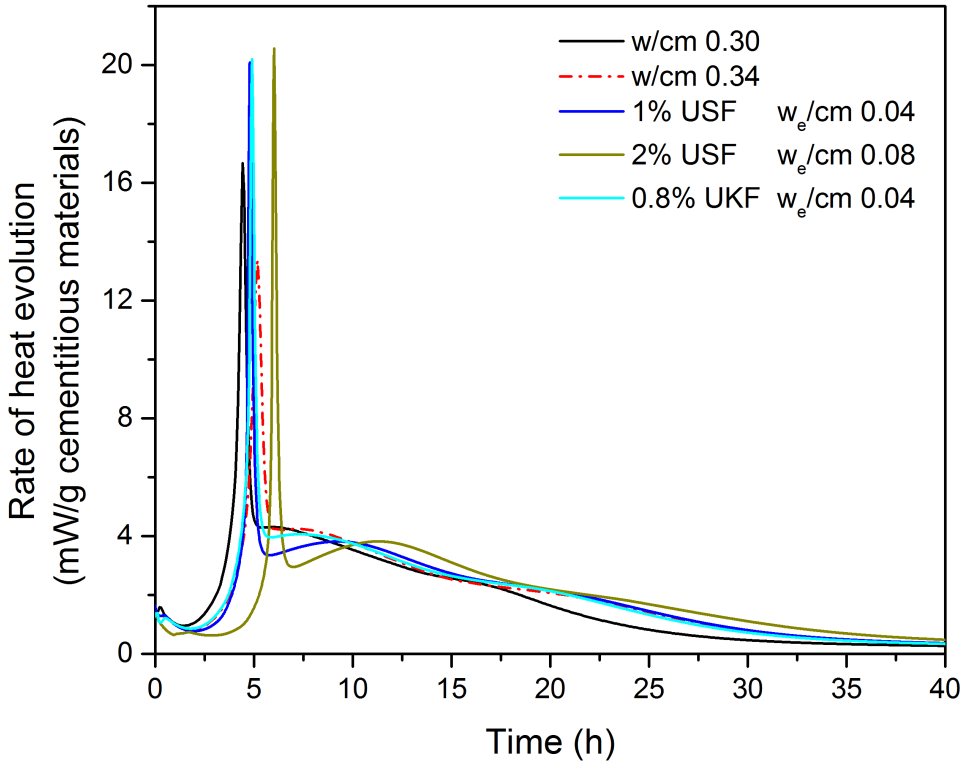

Figure 5.4 – Rate of heat evolution of fiber-cementitious pastes compared with that of plain cementitious pastes at w/cm 0.30 and 0.34.

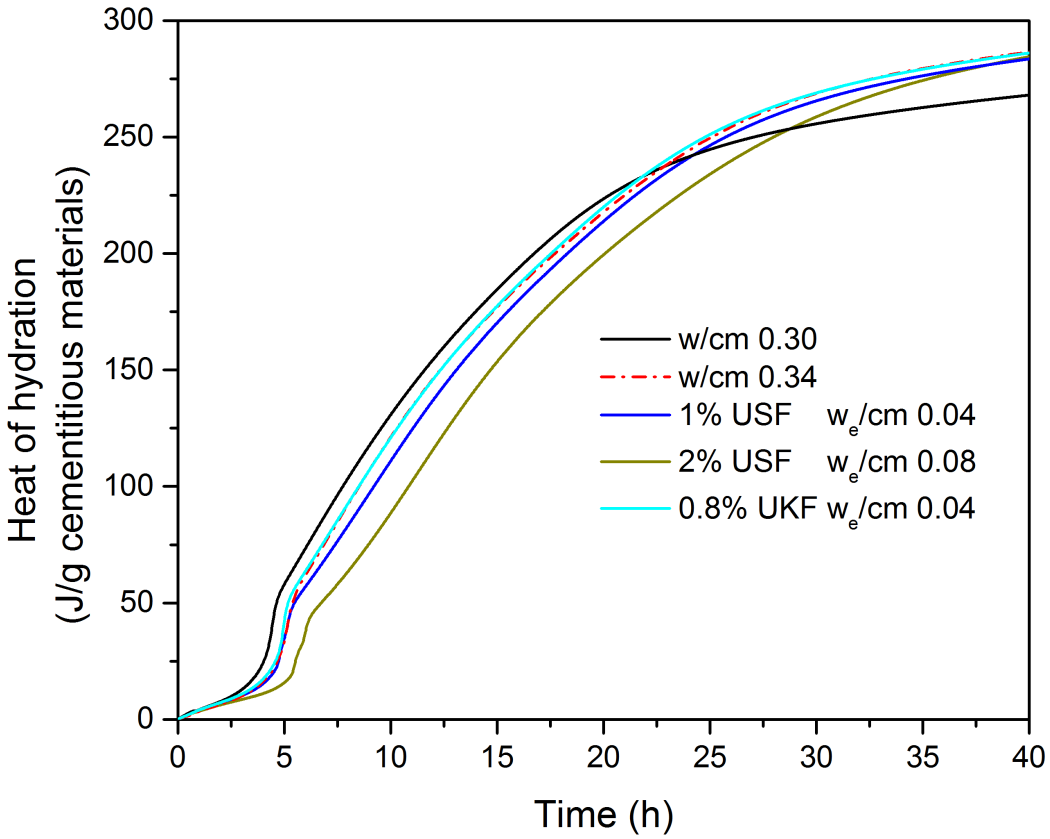

Figure 5.5 – Cumulative heat evolved of fiber-cementitious pastes compared with that of plain cementitious pastes at w/cm 0.30 and 0.34.

5.2.2.2 Magnetic Resonance Imaging (MRI)

To preliminarily observe the water depletion of internal curing cement paste, this study employed the SPI phase encoding technique to visualize the distribution of evaporable water (i.e. gel water and capillary water) in cementitious pastes, with and without internal curing agents, after setting. Figure 5.6 presents series of axial MRI slices at various hydration times. Since MRI is a water probe, the bright area in images indicates more water-filled space.

Figure 5.6 – Axial MRI slices of 1% USF-fiber cement pastes compared to that of the control cement pastes at various hydration times.

Time after mixing	**w/cm 0.30**	**1%USF**	**w/cm 0.34**
7h	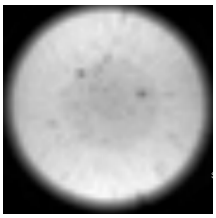	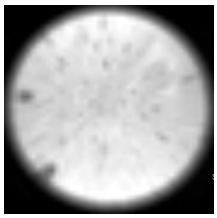	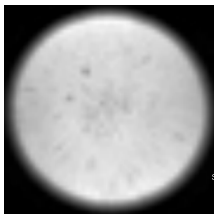
13h	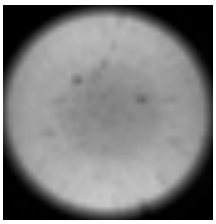	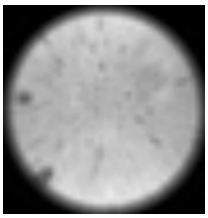	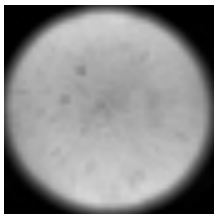
24h (1D)	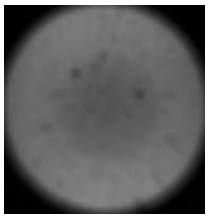	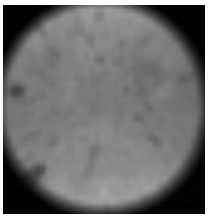	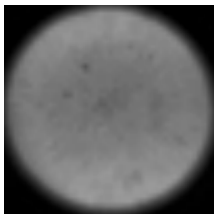
168h (7D)	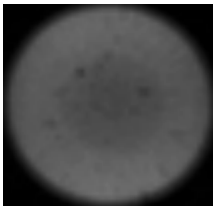	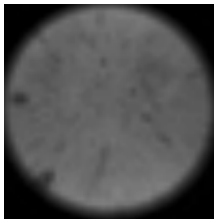	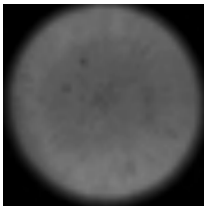
672h (28D)	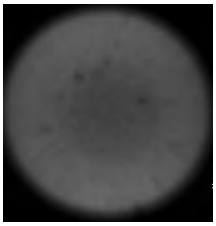	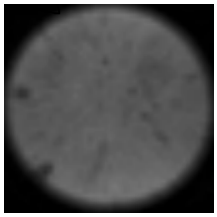	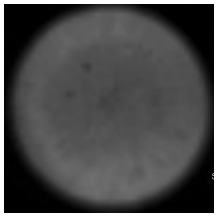

In the sealed condition, the amount of evaporable water decreases only due to the hydration reaction, as confirmed in [130]. Figure 5.7 present the change in MRI signal intensity of cementitious pastes. The signal was normalized by the intensity of each sample after setting (at 7 hours from mixing). From the figure, the rate of signal intensity

loss is highest at early ages or after setting up to 25 h of hydration. The w/cm 0.30 cementitious paste exhibited the highest loss of signal, which could result from both the hydration reaction and self-desiccation process. In case of the 1% USF-cementitious paste, the rate of its signal loss was similar to that of w/cm 0.34 cementitious paste. However, from 13hours to 240hours, the signal intensity of 1% USF-cementitious paste began to exhibit a higher rate of signal loss than that of w/cm 0.34 cementitious paste, which may demonstrate the migration of water from wood pulp into the hydrating cementitious matrix. After 240 hours, the signal of all samples becomes almost the same values.

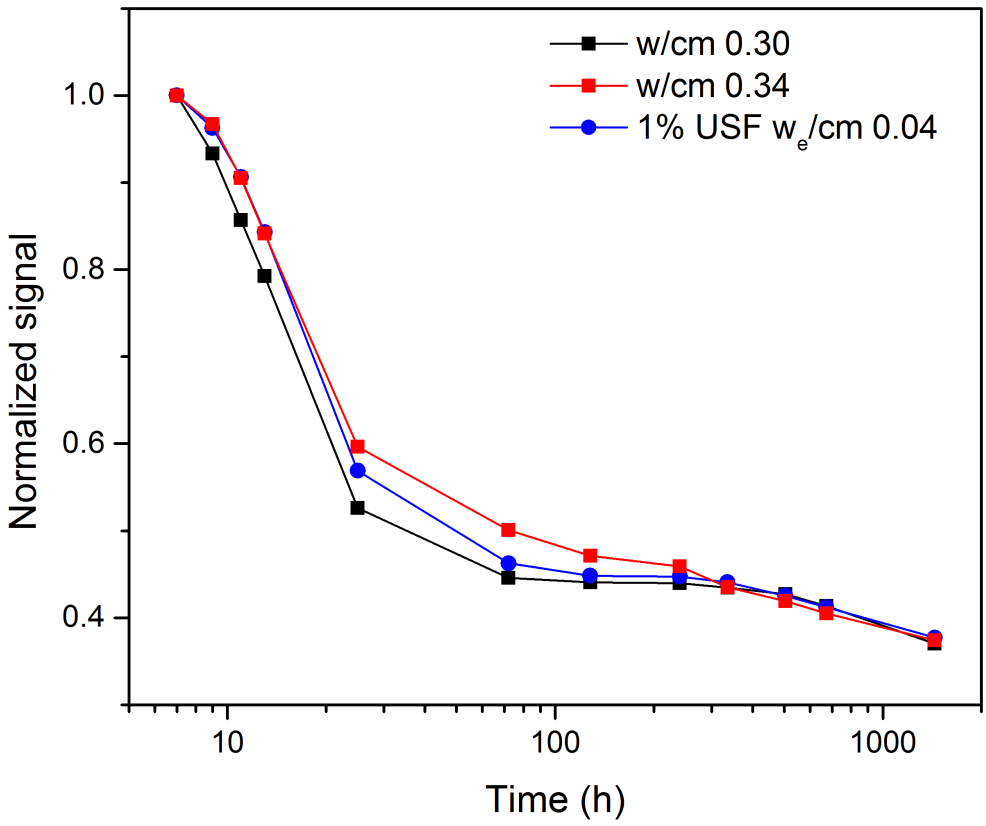

Figure 5.7 – Normalized evaporable water signal of 1% USF-cement paste compared to that of w/cm 0.30 and w/cm 0.34 cement pastes.

5.2.2.3 Dynamics of Water and Change in NMR Relaxation of Wood Pulp

Based on MRI measurements, from both Figures 5.6 and 5.7, as the intensity of w/cm 0.30 cementitious paste dissipated faster than that of 1%USF and w/cm 0.34 cementitious pastes, which confirms that the water held in eucalyptus pulp was gradually released as pores in the cementitious paste were emptied by self-desiccation. This section and beyond describe the migration of entrained water from wood pulps to hydrating cementitious paste, which was observed by NMR measurements. In addition, the key mechanisms that affect internal curing efficiency of eucalyptus pulps are proposed.

Figures 5.8 and 5.9 show the distribution of the T_2 relaxation of USF and UKF samples at various moisture contents. On an oven-dried basis, the initial or as-received moisture contents of USF and UKF were 245% and 370%, respectively. With environmental exposures to induce various degrees of drying (see section 5.2.1.1.), moisture contents (MCs) of 245%, 175%, 66%, 31%, and 5.5% were ultimately achieved for the USF and 370%, 268%, 154%, 42%, and 20% for the UKF.

Shown in Figure 5.9, the NMR signal of never-dried USF and UKF exhibited two peaks at about 1.9-3.4 ms and 4.9-76.33 ms. As reported in [46, 131], the T_2 at 0.8-1.4 ms, 4.1-6.9 ms, and 19.9-43.7 ms have been assigned to bound water absorbed in the cell wall, free water in the small pores and free water in the cell lumens, respectively. Therefore, in Figures 5.8 and 5.9, the first peak corresponded to bound water and the later peak ascribed to water held in small cell wall pores and free water in the fiber lumen.

When pulps were dried, the distribution of T_2 shifted toward the lower value and the proton concentration reduced, which indicates the loss of free water in the small pores and the fiber lumen, as shown in Figure 5.9. The figure clearly shows the sequence of

drying: that is, the removal of free water in the lumen, the removal of free water in the small pores, and the removal of bound water, as also suggested in [132].

It is proposed that this behavior is mainly controlled by capillary draw and water vapor diffusion, both resulting from a gradient in relative humidity (i.e., higher moisture content within the fiber than in the surrounding self-desiccating cementitious paste). Moreover, since pulps used in this study were never dried, the structure of their cell wall changed while they were losing water during drying. Typically, when drying, the fiber shrinks, lumen collapses, and pores close. These alterations confine the water in the fiber lumen, in the cell wall pores, and in the cell wall, and since the fluid in a confined space undergoes NMR relaxation at a faster rate than the bulk fluid [61], the NMR relaxation time reduces. Shown in Figure 5.8, when the USF pulp underwent drying from 245% MC to 5.5% MC, while the proton concentration of T_2 relaxation of the high T_2 was decreasing, that of the low T_2 was increasing; this suggests that the fiber cell wall collapsed resulting in more tightly bound water in the cell wall. Another possible explanation has been suggested [131]: that is, when the water content decreases, capillary action and water vapor produce a water layer on the surface of the lumen which does not exchange with the cell free water and consequently relaxes with a T_2 similar to that of the cell wall water and thus increases the amount of water associated with the fast T_2 region.

Figure 5.9 compares the distribution of T_2 relaxation for the two pulp types, at similar moisture contents. Typically, a sample which has thicker cell wall and smaller cell diameter should have higher T_2 population in short region than a sample that has thinner cell wall and larger cell diameter [131]. However, in this study, both USF and UKF exhibited almost identical T_2 distribution with only slight difference in proton

intensity, mainly due to the fact that both USF and UKF were produced from the same wood species, Eucalyptus camaldulensis. Therefore, even though they were produced by different pulping processes, their alterations in the morphology and the chemical compositions that affect the distribution of T_2 relaxation were not detectable in NMR measurement of wood pulp alone.

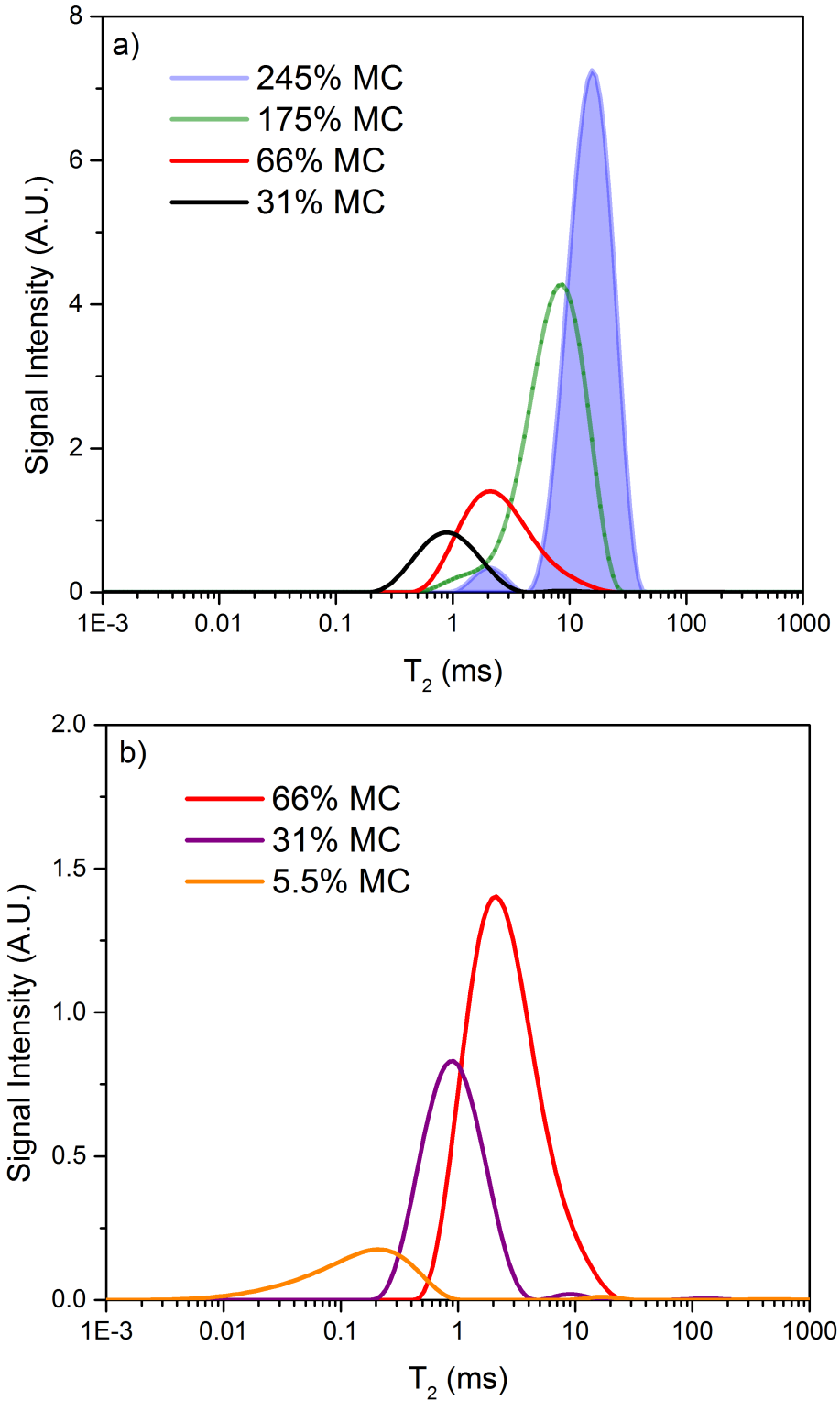

Figure 5.8 – Distribution of transverse relaxation time (T_2) of USF samples at different moisture contents (dry basis) a) at fiber saturation point (FSP) and beyond, b) below FSP.

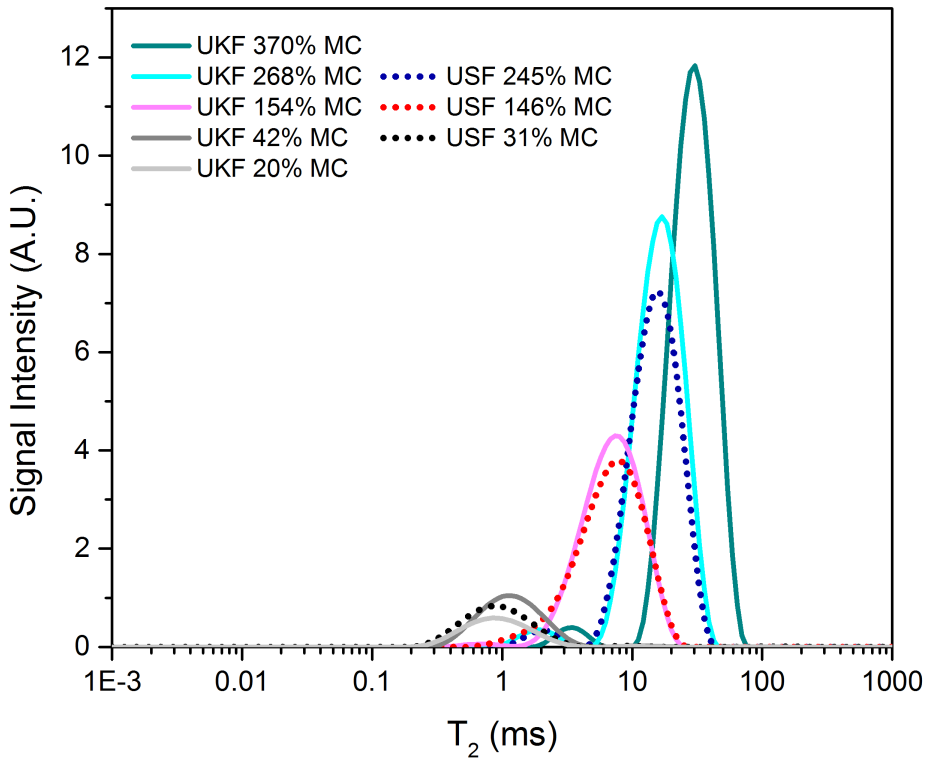

Figure 5.9 – Distribution of transverse relaxation time (T_2) of USF samples compared to UKF samples at similar moisture content (dry basis).

5.2.2.4 Change in NMR Relaxation in Hydrating Cementitious Pastes

Figure 5.10 presents the development of the multi-component T_2 distribution of 1% USF-cementitious paste sample, as well as companion ordinary cementitious paste (i.e., w/cm 0.30) over the early hydration period. As previously noted, the short relaxation times correspond to confined water and long relaxation times correspond to bulk water. Examining the ordinary cementitious paste first, at a few hours of hydration (i.e. from 1 hour to ~5 hours), the distribution of T_2 relaxation exhibited 3 peaks with the values of approximately 0.5 ms, 4-5 ms, and 400-500 ms. It is proposed that these may be assigned to bound water on the cement grain surfaces and free water that is held on cement grains by capillary tension (T_2 ~ 0.5 ms), bulk water (T_2 ~ 4-5 ms), and bleeding water (T_2 ~ 400-500 ms), respectively.

Since at the very early stage of hydration (i.e., after mixing up to before setting), only a relatively small fraction of the overall hydration of cementitious materials takes place, the reductions in capillary pore sizes are overwhelmed by the pore size reductions due to setting and local particle rearrangement. Therefore, the microstructure of cementitious paste is likely to be a suspension of rigid particles in solution with local agglomeration of connecting particles [133, 134]. Thus, unlike more mature cementitious paste that appears in the fast-diffusion or "surface-limited" regime [61], the NMR relaxation of very early age cementitious paste may appear in the slow-diffusion regime or "diffusion-limited" regime which is the characteristic of larger pores. In the slow-diffusion regime, the rate of relaxation at the surface is significantly shorter than the time taken for the molecules to diffuse in center of pores. Therefore, the magnetization decay has a multi-exponential character due to the substantial contribution of the surface-bound water. Moreover, due to the high specific surface area and porosity of metakaolin particles in these pastes, a significant amount of water may be absorbed into their porosity or adsorbed on their surface contributing to the short T_2 component (at $T_2 \sim 0.5$ ms).

In addition, comparing the short T_2 component of w/cm 0.30 cementitious paste with that of 1% USF cementitious paste, the proton concentration of the 1% USF-cement paste sample was slightly higher than that of the w/cm 0.30 paste sample suggesting some contributions of bound water in eucalyptus pulp in this T_2 region. While the majority of the T_2 component within a few hours after mixing were found in the intermediate T_2 region (~ 4-5 ms), a minor T_2 component appeared in the much longer T_2 region (~ hundreds of ms). The intermediate T_2 is characteristic of bulk water in the

hydrating space [135], whereas the longer T_2 component can associate with bleed water on the surface of samples. Although pure water has T_2 of about 2-3 s (or 2000-3000 ms) [136], bleed water from a cementitious matrix is strongly alkali and contains numerous ions including some paramagnetic and ferromagnetic impurities, which can shorten the T_2 relaxation time. Therefore, bleed water has the T_2 value lower than pure water.

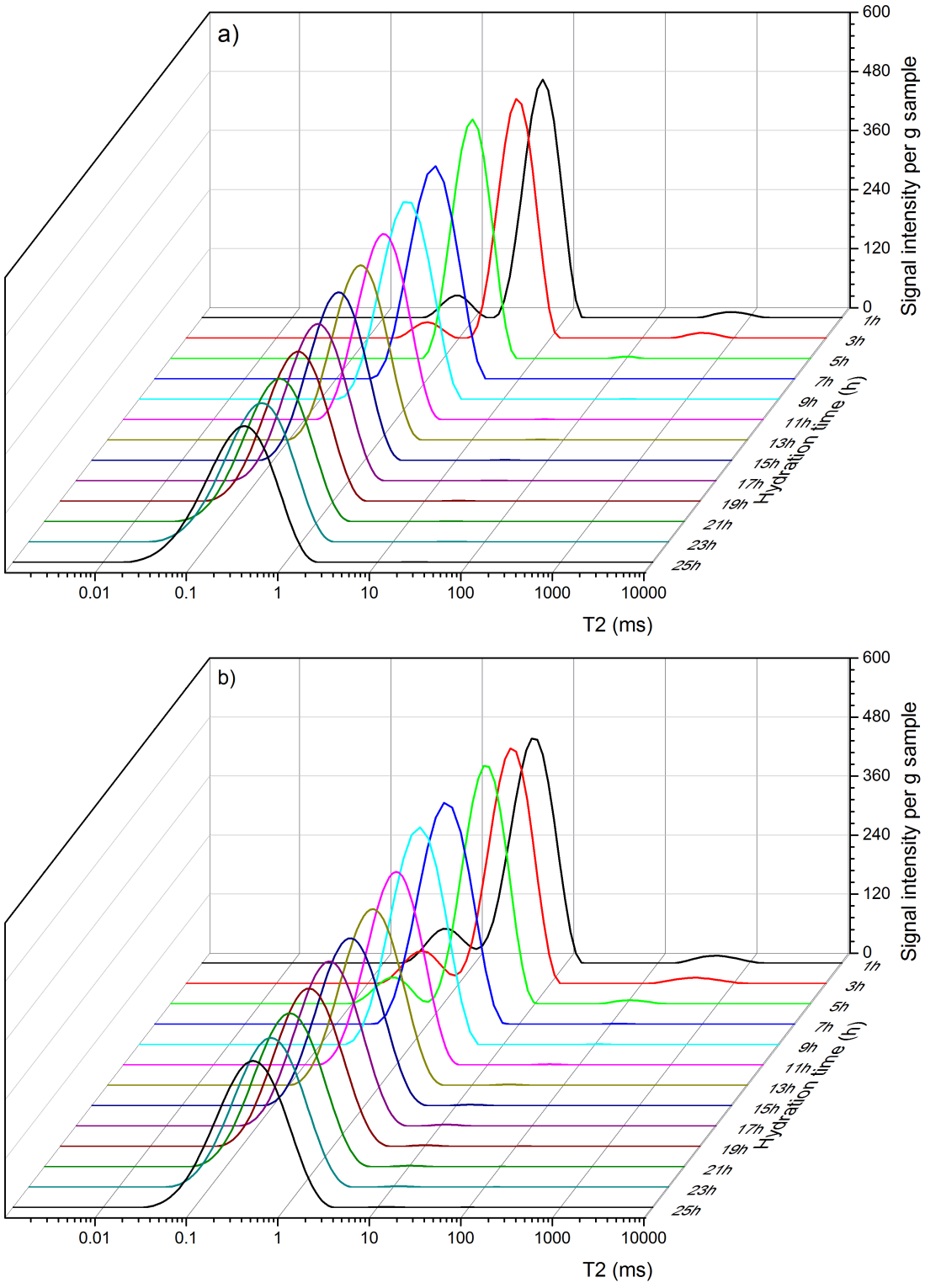

Figure 5.10 – The evolution of T_2 distribution during hydration of cementitious pastes a) plain cementitious paste (w/cm 0.30) and b) USF-cementitious paste at 1% USF (w/cm=0.30 and w_e/cm =0.04).

As the hydration reaction proceeds, hydration products develop both in water-filled space and on the surface of cement grains reducing the interparticle spacing, densifying the paste and thus decreasing the overall porosity and pore size. Thus, there is an associated change from the slow-diffusion to the fast-diffusion regime, in which the relaxation behavior is uniform over the entire – albeit finer – pores. Thus, the NMR signal at this study range, showed in Figure 5.10 after 7 h of hydration, behaved more like single-exponential relaxation decay and the T_2 component in the short region merged with the intermediate region.

Figure 5.11 demonstrates the evolution of optimum T_1 values. This concept has often been cited as an indicator of setting during cement hydration [62, 137]. Based on results reported in [62], the optimum T_1 value is sensitive to the formation of the solid network and thus its change relates to the penetration depth measured by Vicat needle. To simplify, the final setting is approximated as the point after the exponential changing prior to the stabilization of optimum T_1 value. (These are visualized in Figure 5.11 as points a, b, and c.) These points, then, imply that the final setting of w/cm 0.30 cementitious paste occurred at about 4-5 hours while that of w/cm 0.34, 1%USF and 0.8%UKF-cementitious pastes occurred at about 6 hours and that of 2%USF-cementitious paste occurred at about 6-7 hours. These values seem to correlate well to the T_2 relaxation measurements and to the results from calorimetry, in which the first hydration peaks occurred at about 1 hour apart (see Figure 5.4.).

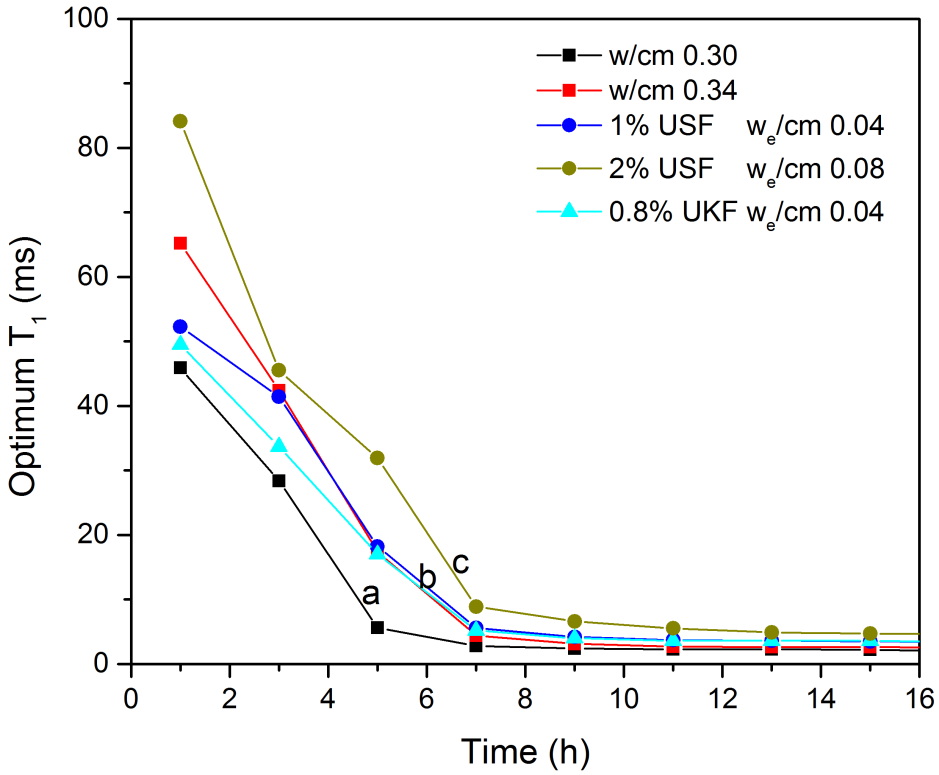

Figure 5.11 – The evolution of optimum T_1 values of fiber-cementitious pastes compared with that of plain cementitious pastes at w/cm 0.30 and 0.34. (The 2%USF-cementitious paste has w_e/c of 0.08).

5.2.2.5 Dynamic of Entrained Water during Early Hydration Period

Typically, when T_2 distribution is used to characterize the pore size distribution based on the fast exchange model, the analysis relies on the fact that all pores are saturated with pore solution. However, when applying the T_2 measurement on a cement matrix that undergoes self-desiccation, because of the empty porosity is created during sealed curing, the distribution of T_2 may not correlate with the actual pore size. Rather, in the case of self-desiccation, T_2 measurement may provide information about the change in pore size, the change in moisture content in the pores, and the transition of water from internal curing agents to a hydrating cementitious matrix.

Figures 5.12, 5.13, and 5.14 demonstrate the dynamic of entrained water during early hydration reaction of internally cured cementitious pastes.[†] The results shown for each cementitious paste were averaged from two samples. From these data, as the hydration proceeded, not only were the peaks decreased in their intensity but the peaks also shifted toward lower relaxation times. For example, the peaks of T_2 relaxation time of w/cm 0.30 cementitious paste, 1% USF cementitious paste, and w/cm 0.34 cementitious paste at 13 h of hydration were at about 0.6 ms, 0.84 ms, and 1.08 ms, at 19 h of hydration were at about 0.40 ms, 0.55 ms, and 0.60 ms, and at 25 h of hydration were at about 0.35 ms, 0.43 ms, and 0.43 ms, respectively.

As mentioned, in a saturated hydrating cementitious paste, using the fast exchange model, the T_2 of water-filled pores can be related to the pore dimension, and hence the decrease of T_2 relaxation times reveals the decrease in the size of capillary pores. However, in the absence of an external source of water and at low w/cm (w/cm < 0.42), there is not enough capillary water for the hydration of a cementitious matrix, leading to a reduction of the internal relative humidity (so called "self-desiccation") [138]. As the pore desiccates and/or empties, water is less mobile and can be associated with shorter T_2. Therefore, while interpreting the early T_2 relaxation of a hydrating cementitious matrix that undergoes self-desiccation, one should realize that the reduction of T_2 relaxation results from two mechanisms: 1) the decrease in the size of capillary pores due to the progression of hydration reaction and 2) the restricted mobility of water

[†]The analysis of T_2 component from CPMG measurement of the hydrated cement pastes yields three T_2 components associated with chemically bound water (~9μs), gel water (~80μs), and capillary water (~350μs). [135] However, it should be noted that, in this study while the CPMG echo time is long enough to detect only the liquid-phase protons, the solid-phase protons relax at T_2 relaxation times too short to be detected in this low-field NMR experiment.

in the capillary pores due to self-desiccation. Thus, the NMR results should be considered in the context of complimentary techniques such as calorimetry, for more clarification.

First, the distributions of the samples with eucalyptus pulps as internal curing agents exhibited two peaks. The major peak coincides with the capillary water in cementitious pastes without internal curing agent, and the minor peak corresponds to free water in the fiber lumen (see Figures 5.8 and 5.9). The main peaks of internally cured samples that contained the same amount of entrained water – 1%USF and 0.8%UKF – mostly overlapped each other, indicating their similar behavior. From Figures 5.12, 5.13, and 5.14, the position of the major peaks of 1% USF and 0.8% UKF-cementitious pastes, both of which have w_e/c of 0.04, appeared between w/cm 0.30 and w/cm 0.34 cementitious pastes. From 13 to 25 h of hydration, while the peaks of T_2 relaxation time of w/cm 0.30 cementitious paste shifted from 0.6 ms to 0.35 ms and that of w/cm 0.34 cementitious paste shifted from 1.04 ms to 0.45 ms, that of 1% USF and 0.8% UKF-cementitious pastes shifted from 0.84 to 0.43 ms. This reduction in T_2 relaxation time potentially indicates both the decrease in pore size due to the formation of hydration products and the consumption of capillary pore water due to hydration reaction.

Besides the effect of hydration reaction on pore size distribution, compared to the corresponding paste that contained the same amount of free water (w/cm 0.30) at 25 h of hydration, in which the cumulative heat of hydration of pastes were essentially the same, the main peaks of internally cured samples are higher and broader, suggesting that more water is available for hydrating cementitious matrix in these pastes. Since the peak amplitude is proportional to the proton population (or signal intensity), the content of water remaining in capillary pores can be determined by calculating the areas under the

peaks. The area under the main peak of w/cm 0.30, w/cm 0.34, 1% USF, 0.8% UKF, and 2% USF cementitious pastes were approximately 230, 332, 343, 345, and 587, respectively. The broadness of a peak can be described by the term full width at half maximum (FWHM), which is commonly used to represent the width of a peak of curve. The FWHM of w/cm 0.30, w/cm 0.34, 1% USF, 0.8% UKF, and 2% USF cementitious pastes were approximately 0.769, 0.985, 1.032, 1.039, and 1.745, respectively. Thus, the increase in the peak area and the width of internally cured cementitious pastes further demonstrates that more water is available in eucalyptus pulp-cementitious pastes than w/cm 0.30 and w/cm 0.34 cement pastes.

In addition, changes in the major peaks correlate with the changes of heat of hydration curves (Figures 5.4 and 5.5), in which the main peaks of the T_2 relaxation of eucalyptus pulp-cementitious pastes with w_e/cm of 0.04 occurred between that for w/cm 0.30 and w/cm 0.34 cementitious pastes. From 13 h to 25 h of hydration, the rate of change in the peak amplitude of eucalyptus pulp-cementitious pastes were slower than that of w/cm 0.34 paste. This perhaps can be viewed as an indication of the desorption kinetics of eucalyptus pulps when surrounded by the self-desiccating paste. The water held in eucalyptus pulp was gradually released while pores in the cement paste were emptied by self-desiccation and thus a reduction in the peak amplitude of T_2 relaxation occurred at a slow pace. In contrast to internally cured pastes, since w/cm 0.34 paste did not have internal curing agent, when self-desiccation occurred, capillary pores were emptied very rapidly. Therefore, the w/cm 0.34 cement paste exhibited the significant reduction in the peak amplitude of T_2 relaxation.

Unlike the migration of water from LWA that can be detected by the decreasing area of the water in such reference LWA sample [122], since the transition of T_2 relaxation times of wood pulp at different moisture contents somewhat overlaps with the T_2 relaxation times of capillary water of cementitious pastes, one should be cautious when interpreting these data in considering the migration of water from eucalyptus pulps. When comparing data for fiber-cementitious pastes in Figures 5.12, 5.13, and 5.14 and with that for the fibers alone in Figures 5.8 and 5.9, it is clear that eucalyptus pulps lose water in their lumen within 25 h of hydration. As no T_2 component in the cell lumen presented in all curves, most remaining water presented in the form of both bound water in the cell wall and free water in the cell wall pores. This water is then available for further cement hydration reaction, demonstrating the internal curing capacity of these fibers, which had been demonstrated through shrinkage studies in section 4.3.3 and in [139, 140]. And, for the first time, the time at which the internal curing water is provided from pulp fibers is understood.

In addition, details about kinetics of water release from eucalyptus pulps to hydrating cementitious paste may be clarified by considering the changes in minor peaks. The transition of water from the cell wall pores into the cell wall or the cementitious matrix is evidenced in the minor peaks. From 13 hours to 25 hours, the minor peaks shifted toward the major peaks indicating the diffusion and/or osmosis of water from eucalyptus pulps to the cementitious matrix. Although they contained the same amount of w_e/c, the rate of water loss from the cell wall pores of UKF was faster than that of USF as the minor peaks of 0.8%UKF tend to have lower T_2 value. This perhaps confirmed the results reported in section 4.4 and in [139, 140] that wood pulp that can hold a large

amount of water in its structure such as pulp that has a thick cell wall will be more beneficial for mitigating autogenous shrinkage because it will not release all water too early.

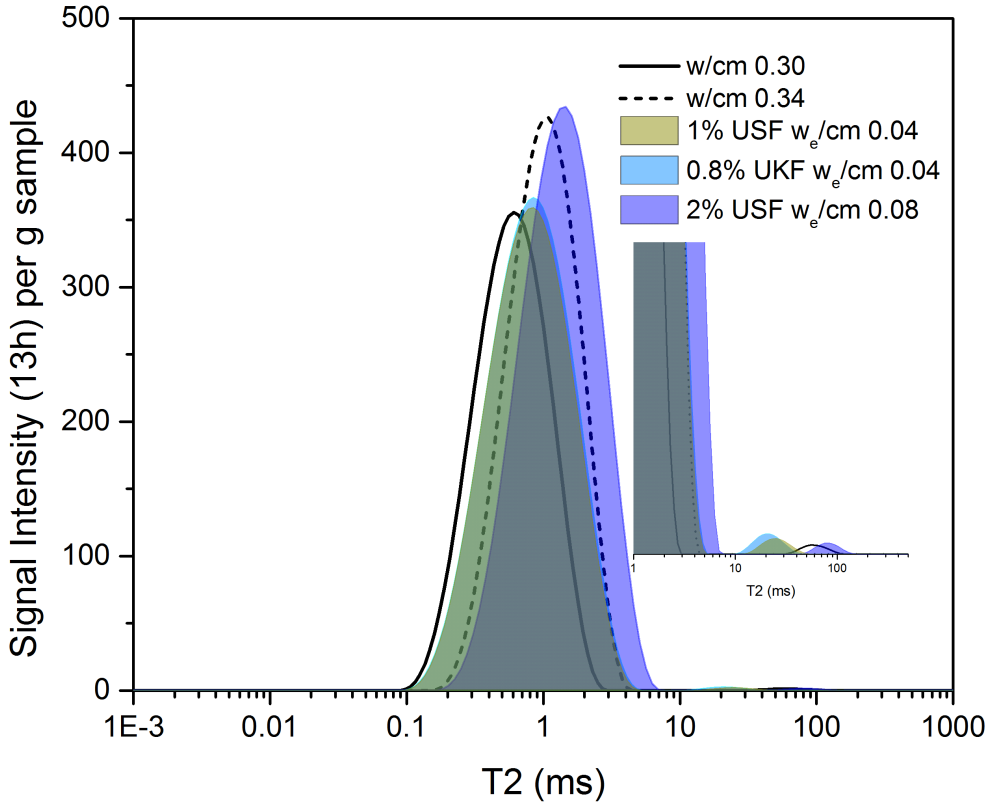

Figure 5.12 – Distribution of T_2 relaxation times of fiber-cementitious pastes compared with that of plain cementitious pastes at 13 h of hydration.

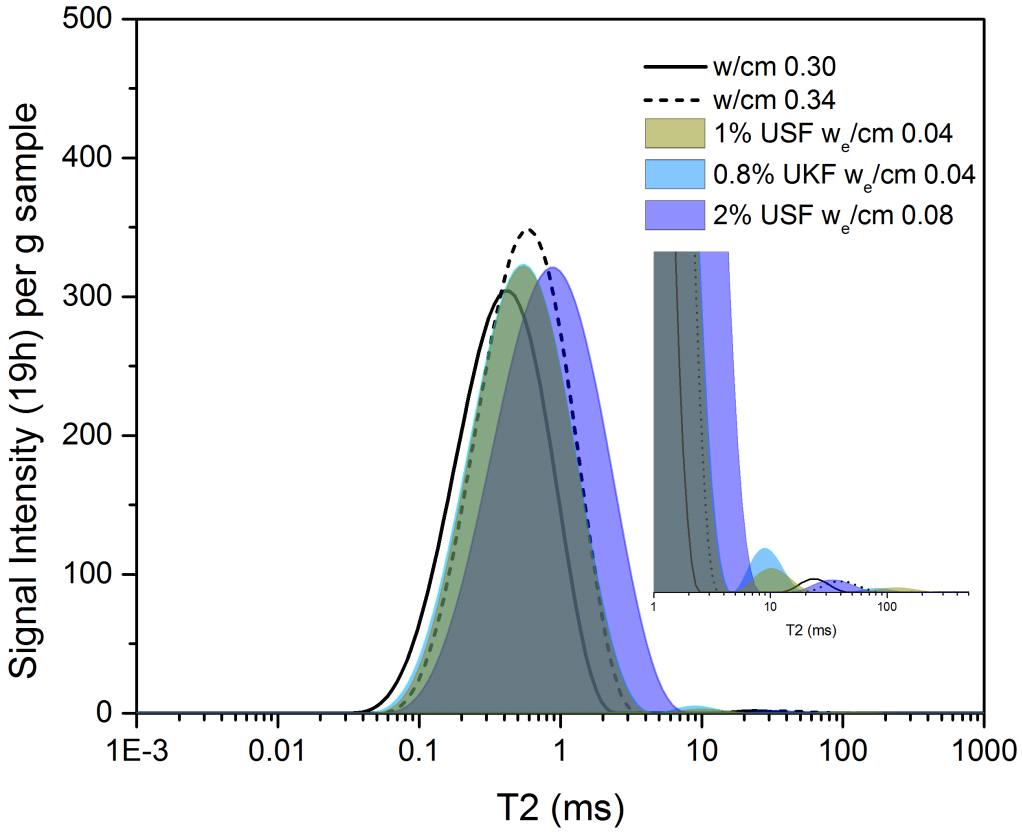

Figure 5.13 – Distribution of T_2 relaxation times of fiber-cementitious pastes compared with that of plain cementitious pastes at 19 h of hydration.

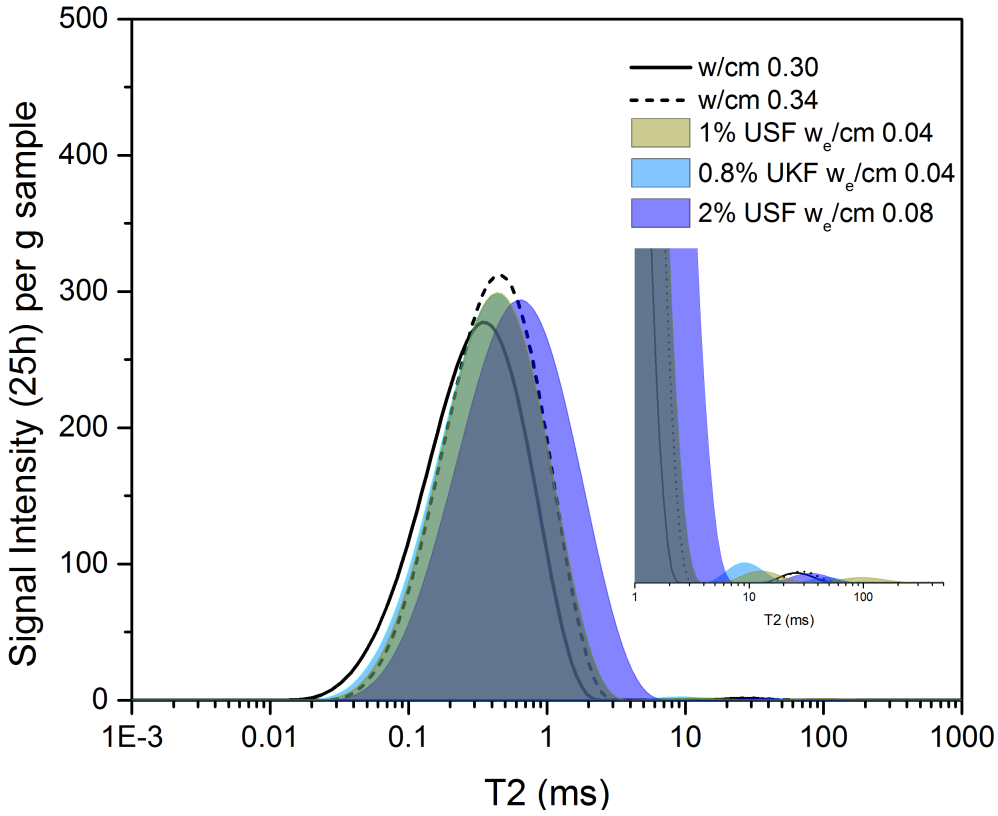

Figure 5.14 – Distribution of T_2 relaxation times of fiber-cementitious pastes compared with that of plain cementitious pastes at 25 h of hydration.

5.3 Sorption of Pore Solution Ions in Eucalyptus Pulps During Early Hydration of Cements

While the chemical compositions of plant-based fiber can influence cement hydration, the effects can be minimized in wood pulp derived from chemical processes, such as kraft and soda pulp. Since the content of lignin in the fiber generally decreases as the level of chemical treatment increases, chemically treated wood pulp rarely contains lignin and extractives. When wood pulp from a chemical process is used in cementitious composites, little or no change in setting time and heat of hydration, as observed by isothermal calorimetry, has been reported [9, 58, 139]. Therefore, at early ages, the effects of chemically treated wood fibers on hydration have been assumed to be minimal.

The assumption that chemically treated wood pulps do not interact with cement at early ages may not be applicable for internal curing applications, as several studies in pulp and paper science have suggested the ability of wood kraft pulps to sorb Na^{+} and Ca^{2+} from aqueous solution. The sorptivity of the pulp in the solution highly depends on pH and initial concentration [141, 142] and occurs competitively among the types of ions presented in a solution. Since cement pore solution is highly ionic, improved understanding of such interactions between pulp fibers and the highly ionic cement pore solution is important for developing pulp fibers for applications in cement-based materials. For example, the effectiveness of mitigation of self-desiccation may depend on the ionic absorption and desorption capacity of the pulp, such as has been found with SAP [44].

Because of the presence of ionizable groups (i.e., carboxylic acid and phenolic groups) in the cell wall of wood fibers, when suspended in water, wood pulps carry a

charge that is directly related to the ion-exchange capacity of the fibers [143]. The presence of charge on the surface of fiber is strongly related to the pH of solution. Carboxylic acid groups found in hemicellulose and cellulose structures are weakly dissociated and completely ionized at pH of ~7, whereas phenolic groups such as guaiacyl phenolics, syringyl phenolics, and condensed phenolics found in the lignin structure are ionizable at pH>7 due to their higher p*K*a values. Since the typical pH of the pore solution in cementitious materials is about 12-13, both carboxylic acid and phenolic groups would be almost completely ionized and available to exchange with cations. These ionizable groups of fiber are strongly related to the cation sorption capacity of the fibers [142]. Therefore, wood pulp would be expected to behave differently in deionized water and cement pore solutions, and thus determining the absorption capacity (i.e. the ability to absorb entrained water during mixing of wood pulp with cement) of wood pulp in water as reported in [11] may not be accurate.

Additional effort must be devoted to clarifying the chemical mechanism(s) underlying the evolving interactions between chemical pulp-based fibers and cement, which affect internal curing performance of chemically treated wood pulps. This section focuses on such interactions, particularly at early ages, which remain relatively unexplored. Therefore, even though the overall goal in this chapter is to examine whether or not eucalyptus pulps react with cement, the focus of the study is to determine the interactions between chemically treated eucalyptus pulps and pore solution ions.

5.3.1 Material and Methods

To clarify the mechanism(s) underlying the early-hydration reaction between chemically treated wood pulp and cement, this work aimed to observe and compare such interactions between chemically treated eucalyptus pulp with two types of cement (i.e., gray and white cements) by surface characterization techniques in combination with standard test methods. The elemental composition of eucalyptus pulp through its structure before and after its immersion in cement pore solutions was quantified and compared to that in deionized water (with a resistivity of 18.2 MΩ.cm).

5.3.1.1 Materials

Two types of portland cement were used in this study were: ASTM C150 Type I/II gray cement (Lafarge North America) and Type I white cement (Lehigh White Cement). Table 5.3 provides their compositions, based upon oxide analysis obtained by X-ray fluorescence (XRF, Bruker AXS S8 Tiger) spectrometry and crystalline phase composition obtained by quantitative X-ray diffraction analysis (QXRD, Bruker AXS D4 Endeavor) with the Rietveld method using TOPAS software.

Wood pulp used in this study was conventional unrefined, unbleached Eucalyptus camaldulensis (or River Red gum) pulp collected from a commercial soda pulping process in Southeast Asia. Since the pulp was chemically treated, it was high in cellulose and low in lignin. The kappa number of the pulp was 14.6, equal to a total residual lignin content of 2.23 percent. This USF pulp had an as-received moisture content (dry basis) of 245%.

Table 5.3 – Oxide composition and crystalline phase composition of gray and white cements (% by mass).

Oxide composition	**Gray cement**	**White cement**	**Crystalline phase composition**	**Gray cement**	**White cement**
SiO_2	19.73	23.65	alite	52.6	68
Al_2O_3	4.82	2.09	belite	20.7	16.7
Fe_2O_3	3.16	0.38	aluminate	3.7	3.5
CaO	62.41	67.56	ferrite	11	0.1
MgO	3.64	0.80	lime	0.1	0.1
SO_3	2.99	2.10	portlandite	2.3	1.6
Na_2O	0.08	0.18	periclase	2.6	0.3
K_2O	0.48	0.04	arcanite	0.6	0.9
LOI	2.27	2.62	aphthitalite	0.4	0.2
			gypsum	0.9	-
			bassanite	2.4	1.5
			anhydrite	-	2.1
			ye'elimite	-	0.5
			calcite	2.7	4.2

5.3.1.2 Quantitative Elemental Analysis

Cement pore solutions were extracted at early ages from cement pastes prepared at a water-to-cement ratio (w/c) of 0.30 by mass. With a hand mixer, 500 g of cement was mixed with the appropriate amount of water in a polyethylene bowl, which was purged with N_2 and sealed tightly. One hour after initial mixing, the cement pore solution was collected by vacuum filtration using 0.45 µm cellulose filters and 0.20µm polyethersulfone (PES) membranes. While small amounts of the pore solution were immediately diluted and acidified for ICP analysis, 10 ml of the pore solution was then transferred to a centrifugal tube containing 0.293 g of pulp, which equals approximately 0.085 g of oven-dry pulp. The tube was then purged with N_2, sealed with a cap, placed on a roller mixer, and rotated for 24 hours at 70 rpm to prevent segregation. After 24 hours,

the pulp was filtrated from the pore solution using 0.20 µm PES membranes washed with deionized water. Then, the pulp was freeze-dried for further analysis. For comparison, the same steps were followed when companion fiber samples dispersed in deionized (DI) water were prepared.

The concentration of the elements – Na, K, Ca, Al, S, and Si – in the pore solution with and without fibers was quantified by inductively-coupled plasma optical emission spectrometer (ICP-OES, Optima 8000, PerkinElmer). Detection limits for this device are parts per billion (ppb) for most elements, including calcium, sodium, and silicon. Shown in Table 5.4, wavelengths for the quantitative elemental analysis were selected according to ASTM C1301-95 [144]. The spectrometer was calibrated using Ca, Li, Na, Al, and Si standards in a nitric acid matrix diluted to 0.5, 10, 20, and 50, and 100 parts per million (ppm) for the measurements of Na, K, Ca, and S, and diluted to 0.4, 1, 2, and 4 ppm for the measurements of Al and Si. Yttrium was used as an internal standard. For each sample, two replicate pore solutions at dilutions of 10x and 100x were prepared and tested.

Table 5.4 – Wavelengths used to detect calcium, sodium, potassium, aluminum, sulfur, and silicon in the quantitative elemental analysis.

Element	**Wavelength (nm)**
K	766.491
Na	588.995
Ca	317.933
S (as SO_4^{2-})	180.669 (182.037)
Al	308.215
Si	251.611

5.3.1.3 Surface Analysis

The surface composition and variations in the near-surface region were observed using X-ray photoelectron spectroscopy (XPS), also known as electron spectroscopy for chemical analysis (ESCA). At least three locations for each sample were analyzed using K-alpha XPS (Thermo Scientific) in a scan area of 250 x 250 µm. An electron flood gun was used to compensate for the charging on the surface of pulp samples. The survey scan of the surface layer was used to quantify the apparent surface composition of USF. Data from the spectra were evaluated using the spectrometer's curving-fitting software (Avantage, Thermo Scientific). A Shirley background was assumed in all cases and an 80:20 Gaussian/Lorentzian peak shape was assumed for photoelectron peaks.

In addition to the composition, the morphology of the pulp samples was observed by scanning electron microscopy (Zeiss Ultra60 FE-SEM) and atomic force microscopy (Veeco AFM II Dimension 3100). For SEM, a freeze-dried fiber sample was attached to a sample holder, using solvent-free carbon conductive tabs, and then gold-coated by a sputter process (Hummer 6 gold/palladium sputterer.) Images of samples were acquired at magnification range from 800x to 35,000x and 5 kV of acceleration voltage and 9-10 mm of working distance. For AFM, a pulp sample was dispersed in deionized water for one minute using a hand mixer. A single drop of about 50 µL of pulp suspension was deposited on a covered glass slide and dried in a conventional oven at 60^{o}C for 24 hours to obtain a relatively flat sample. Samples were examined in tapping mode using a trihedral shape cantilever (µmasch NSC18) with a nominal spring constant of 2.8 N/m. Measurements were performed in a laboratory environment (23±1^{o}C and 50±5%RH).

5.3.2 Results

5.3.2.1 Quantitative Elemental Analysis

Table 5.5 presents results from quantitative elemental analysis of filtered samples before and after immersion in deionized water and cement pore solutions. The table compares initial concentrations of elements in the deionized water with those in the cement pore solutions. From the table, the sorption behavior of USF depends on the initial concentration of each composition in the solution. After 24 h of fiber immersion in deionized water, the concentrations of Ca, S, and Si increased while that of K and Na remained constant. From such behavior, it can be inferred that small amounts of Ca, S, and Si desorbed from the fiber into the water. In contrast in both cement pore solutions, the fiber took in K, Na, and Ca and lost greater concentrations of S, and Si than deionized water. These results confirm that at higher pH, more ionized sites are available on the cell wall of fibers, thus allowing USF to absorb or bind more cations.

The sulfur found in the pore solutions containing the fibers can be derived from several sources. Wood contains sulfur that organically combines in amino acids and other complexes, for example. Also, although the soda pulping process requires only sodium hydroxide as a cooking agent, soda mills commonly employ a small amount of sulfide in the pulping liquor [145]. Therefore, the presence of sulfur in soda pulp is typical.

As determined by ICP, the amount of sulfur reported is the “total” sulfur in each solution, which includes the amount of soluble sulfate (SO_4^{2-}), sulfite (SO_3^{2-}), and sulfide (S^{2-}). However, since the solubility of sulfates increase as degree of alkalinity increases [146], the amount of sulfur in a pore solution detected after the immersion of USF should increase significantly. Also the increase of SO_4^{2-} ion concentration in the pore solution may

affect the hydration of the tricalcium aluminate phase (C_3A) in cement, particularly at early ages [147].

As shown in Table 5.5, the effect of the alkaline pore solution on solubility of sulfates (and may also sulfite) appeared in both pore solutions of gray and white cement. The high amount of S released from the fiber in cement pore solution indicates that cement pore solutions perhaps solubilize sulfur compounds in USF to accommodate the influx of pore solution ions (i.e., K^+, Na^+, and Ca^{2+}).

Table 5.5 – Quantitative elemental analysis results; Concentrations of potassium, sodium, calcium, sulfur, aluminum, and silicon are given in mM.

	Deionized water		**Gray cement pore solution**		**White cement pore solution**	
	Before pH =7.56	**After pH =8.14**	**Before pH =12.94**	**After pH = 12.91**	**Before pH =12.51**	**After pH =12.45**
K	<0.01	<0.01	320.09	296.17	15.19	14.39
Na	<0.001	<0.001	41.46	38.71	17.45	15.03
Ca	0.03	0.07	10.47	8.00	58.43	35.40
S (as SO_4^{2-})	<0.009	0.60	163.16 (101.29)	205.58 (115.09)	58.78 (38.22)	74.47 (43.47)
Al	<0.001	0.01	0.025	0.024	0.039	0.026
Si	0.05	0.07	0.076	0.111	0.104	0.098

The effects of initial pore solution composition on the sorption of metal ions to USF are shown in Table 5.5. After exposure to the fibers, the changes in concentrations of K, Na, and Ca in the gray cement pore solution were 23.92, 2.75, and 2.47 mM, respectively, whereas that of the white cement pore solution were 0.8, 2.42, and 28.28 mM, respectively. Since pulp carries acid functional groups (e.g. phenolics, carboxylic acids and hexenuronic acids) that can be protonized, metal ions, known as non-process elements (NPE), including K^+, Na^+, and Ca^{2+}, can bind to the cell wall of fibers. Su et al. [148] determined the binding capacity of metal ions on kraft pulp at the pH of 4.5, in

which the order of affinity among three ions was $Ca^{2+}>>K^{+}\cong Na^{+}$.[‡] However, in this study, the effects of initial concentration play an important role on the ion selectivity of USF. In gray cement pore solution, more K^{+} was taken up, but in white cement pore solution, more Ca^{2+} was; in both cases, however, the greatest binding – in terms of reduction in concentration - occurred for the most abundant cation.

However, comparing relative reductions in concentration as a percentage, there appears in both the white and gray cement cases to be a preference for binding bivalent cations over monovalent. Assuming the equilibrium reactions of the ion exchange reaction between the functional groups present on the USF and metal ions are stoichiometric, the exchange of metal ions to hydrogen ions of divalent metal ions and monovalent metal ions will be 1:2 and 1:1 [148, 149], respectively. Therefore, in the pore solutions examined, Ca^{2+} will have higher affinity for acidic sites than a monovalent ion (e.g. Na^{+}, K^{+}). However, in gray cement pore solution, because of the high concentration of K^{+}, K^{+} ions likely occupy more acidic sites than that of K^{+} ions in white cement and seems to occupy more sites than that of Ca^{2+} ions. In contrast, in white cement pore solution, in which higher concentration of Ca^{2+} is significantly higher than K^{+}, USF binds more toward Ca^{2+} than other ions.

5.3.2.2 Surface Chemical Analysis

While pore solution ions clearly interact with the cell wall of USF, the nature of the interaction requires further study. For example, ions may combine to form precipitates on or within the USF cell wall. Therefore, to better understand these

[‡] In their work 14 metal ions – Pb^{2+}, Cu^{2+}, Cd^{2+}, Zn^{2+}, Ni^{2+}, Mn^{2+}, Ba^{2+}, Sr^{2+}, Ca^{2+}, Mg^{2+}, Rb^{+}, K^{+}, Na^{+}, Li^{+} – were loaded at 1.25 mmol to the 13.6 g oven dried pulp.

interactions, the surface of USF was examined chemically by XPS and structurally by SEM. Figure 5.15 shows the XPS spectrum of USF samples before and after 24 hours of exposure in deionized water compared to that after 24 hours in the cement pore solutions. From the figure, as expected, the spectrum of USF before immersion is dominated by carbon (C1s) and oxygen (O1s) peaks, which are the elements that make up the constituents of pulp, with slight peaks of silicon (Si2p and Si2s), shown in Figure 5.15a. After USF was immersed in deionized water for 24 hours, in Figure 5.15b, the surface of USF did not exhibit any detectable changes, with the same three elements (i.e. carbon, oxygen, and silicon) detected. On the other hand, after 24 hours of immersion in gray cement pore solution shown in Figure 5.15c, additional peaks at ~169, 347, and 293 eV, are found which are attributed to S2p, $Ca2p_{3/2}$, and $K2p_{3/2}$, respectively. Figure 5.15d presents XPS spectrum of USF sample after 24 hours of immersion in white cement pore solution. XPS shows additional peaks at around 347 eV, which corresponds to $Ca2p_{3/2}$ but no significant peaks of S2p, and $K2p_{3/2}$, in contrast to the gray cement case.

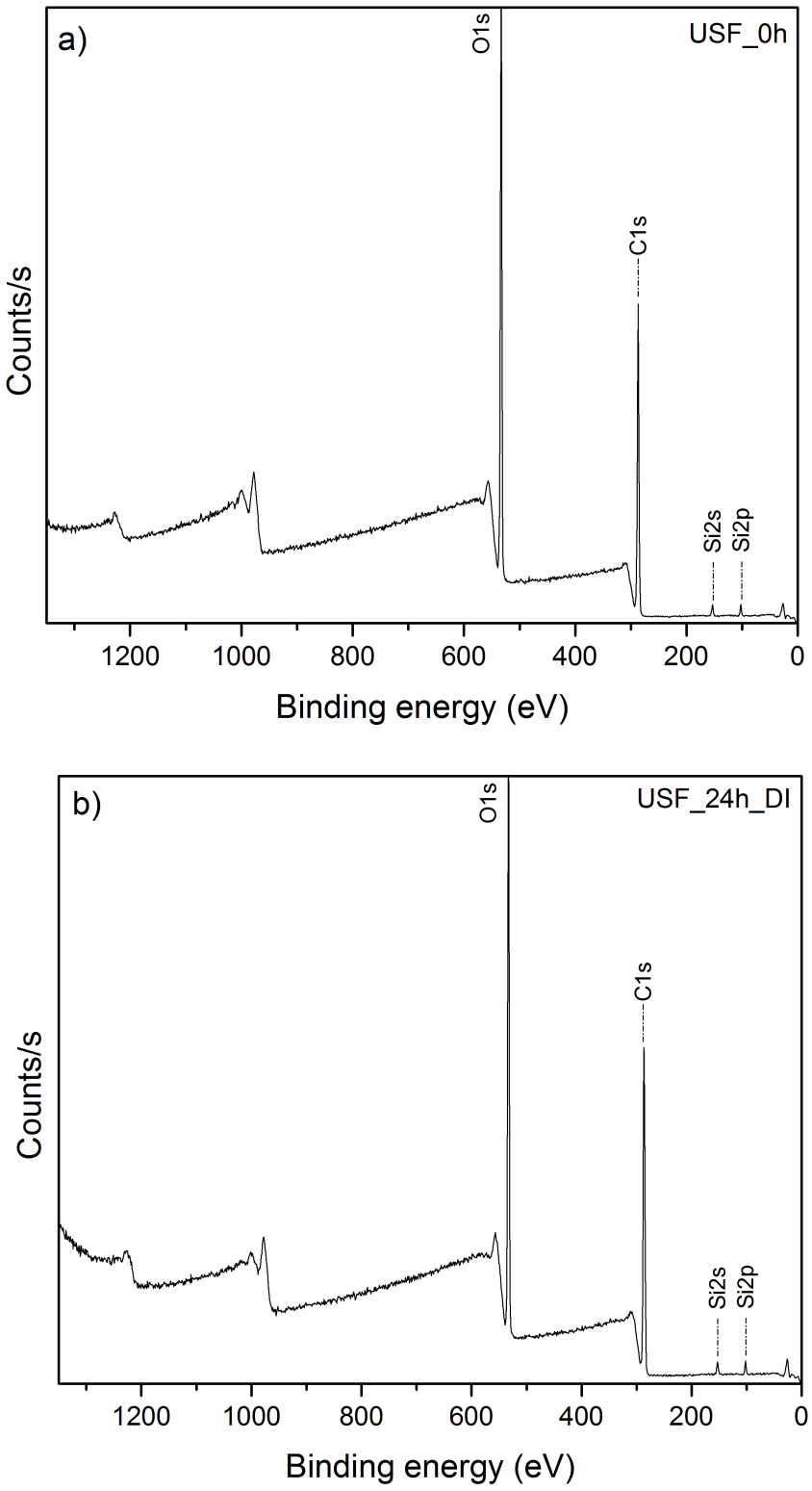

Figure 5.15 – XPS survey scans on the surface of USF samples a) unreacted USF, b) after immersion in deionized water, c) after immersion in the pore solution of gray cement, and d) after immersed in the pore solution of white cement.

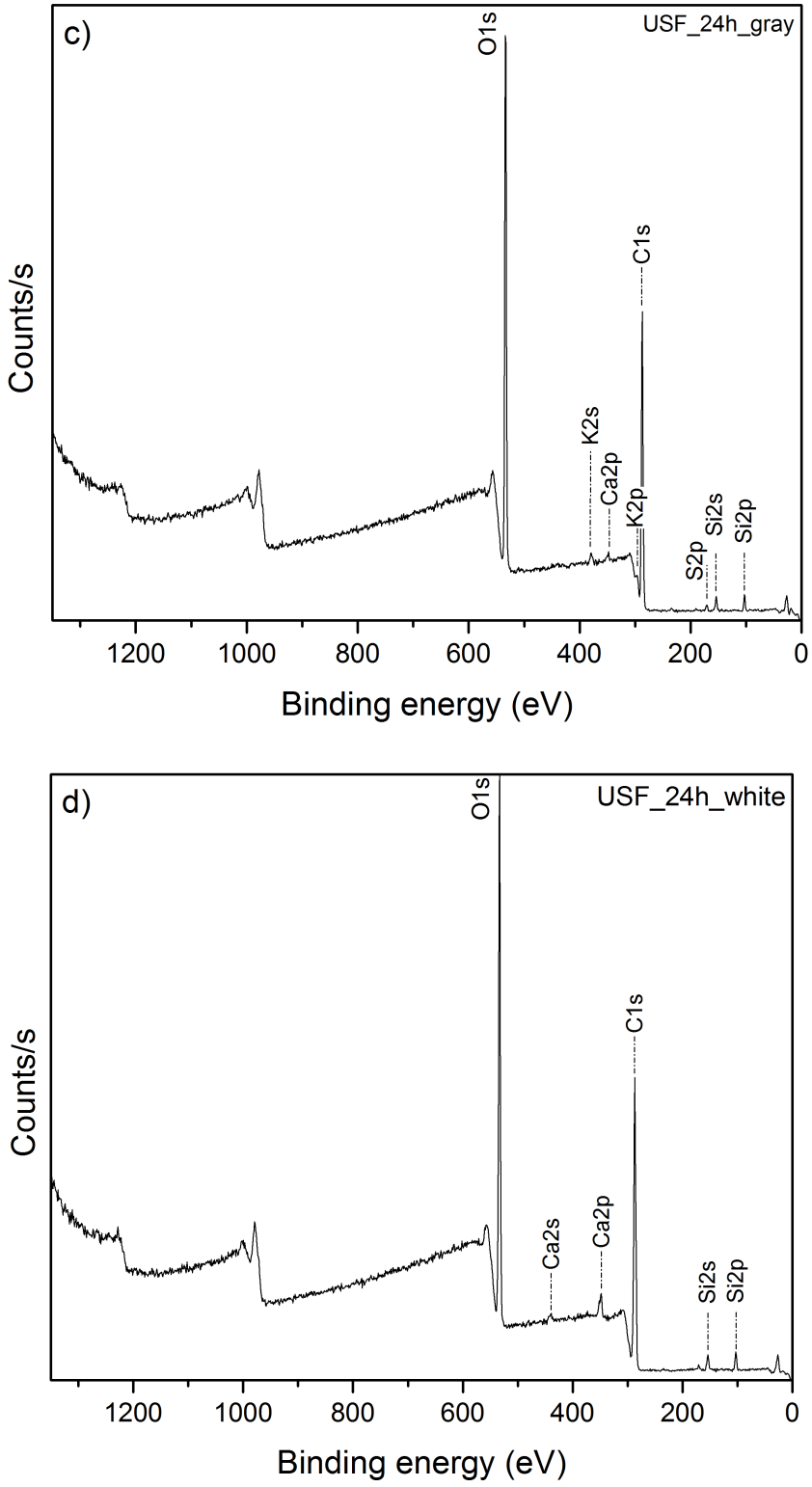

Figure 5.15 – XPS survey scans on the surface of USF samples a) unreacted USF, b) after immersion in deionized water, c) after immersion in the pore solution of gray cement, and d) after immersed in the pore solution of white cement. (continued)

Table 5.6 presents the elemental compositions and binding energies of the surface of USF before and after immersion. These results were averaged from three different locations on the surface of USF. While the atomic concentration of Ca, K, and S on the surface of the USF sample immersed in gray cement pore solution increased, only the atomic concentration of Ca on the surface of USF immersed in white cement pore solution increased. The change in atomic concentration of Ca indicates some precipitation of calcium products on the surface of USF.

Table 5.6 – Apparent surface composition of USF before and after immersed in DI water and cement pore solutions. The standard deviations from three sampling spots are in parentheses.

	Peak BE (eV)	**Atomic (%)**			
		Before immersion	**After 24 hours**		
			Deionized water	**Gray cement pore solution**	**White cement pore solution**
C1s	286-287	59.09 (2.74)	61.69 (2.19)	57.08 (1.55)	58.70 (0.51)
O1s	533-533.5	37.81 (3.80)	35.34 (2.72)	38.13 (1.63)	37.29 (0.76)
Si2p	102-103	3.11 (1.06)	2.97 (0.61)	2.52 (0.59)	2.82 (0.48)
Ca2p	347-348.5	-	-	0.27 (0.08)	1.19 (0.11)
S2p	168.9-169.1	-	-	1.07 (0.36)	0.28 (0.19)
K2p	293-293.5	-	-	0.94 (0.53)	-

5.3.2.3 Surface Morphology

An SEM image (Figure 5.16) of USF pulp before immersion in a solution shows that, despite their lack of refinement, external fibrillation is clearly seen and some microfibrils are found projecting from the surface. These microfibrils increase the surface area, and they may serve as nucleation sites onto which hydration products precipitate.

Cement hydration acceleratory effects associated with additional surface area, even with chemically inert materials, have been previously reported in [117] .

Figure 5.16 – An SEM image of USF fibers.

Figures 5.17, 5.18, and 5.19 present the surface morphology of USF fibers after 24 hours of immersion in deionized water, gray cement pore solution, and white cement pore solution, respectively. While immersed in deionized water, the USF fiber seems consistent with observations of fibrillation, also apparent when dry; no precipitates are noted. In figures 5.18 and 5.19, the presences of small, discrete apparently crystalline products are apparent on the surface of USF. Their collocation with microfibrils suggests that the fiber surface features may encourage nucleation of hydration products on the USF. These observations further demonstrate that the surface of USF is not inert in its early-age interaction in cementitious composites.

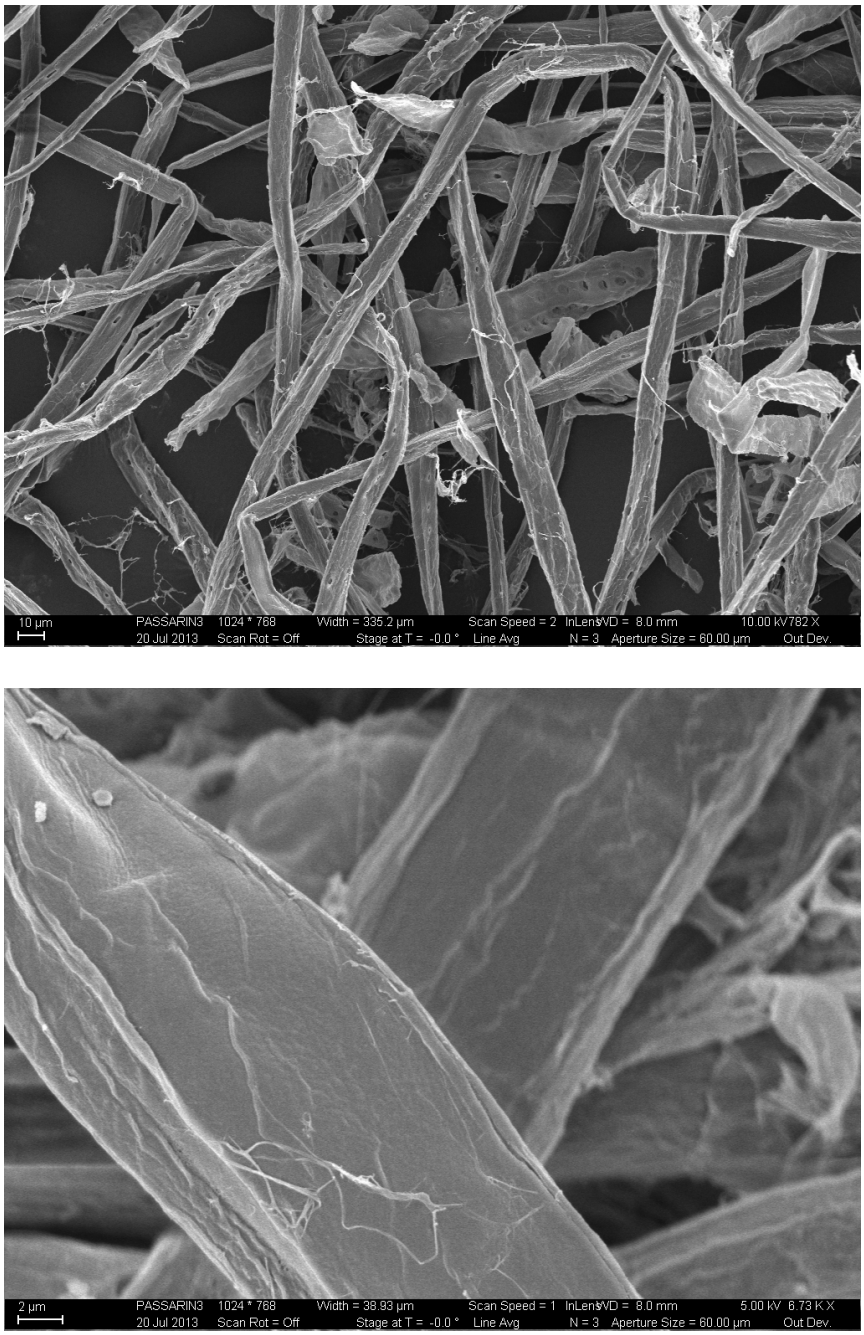

Figure 5.17 – Scanning electron micrographs of USF surfaces after 24 h of immersion in deionized water.

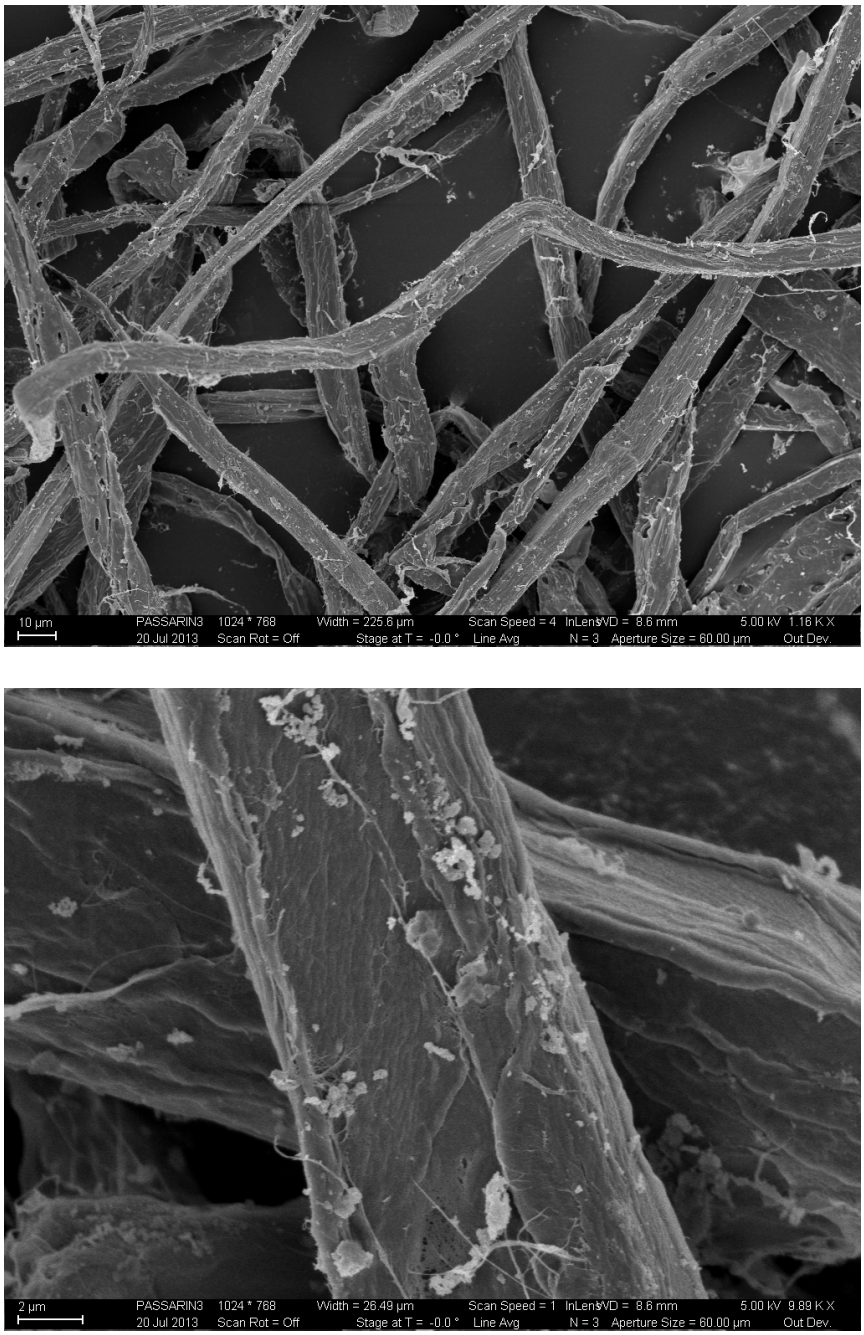

Figure 5.18 – Scanning electron micrographs of USF surfaces after 24 h of immersion in gray cement pore solution.

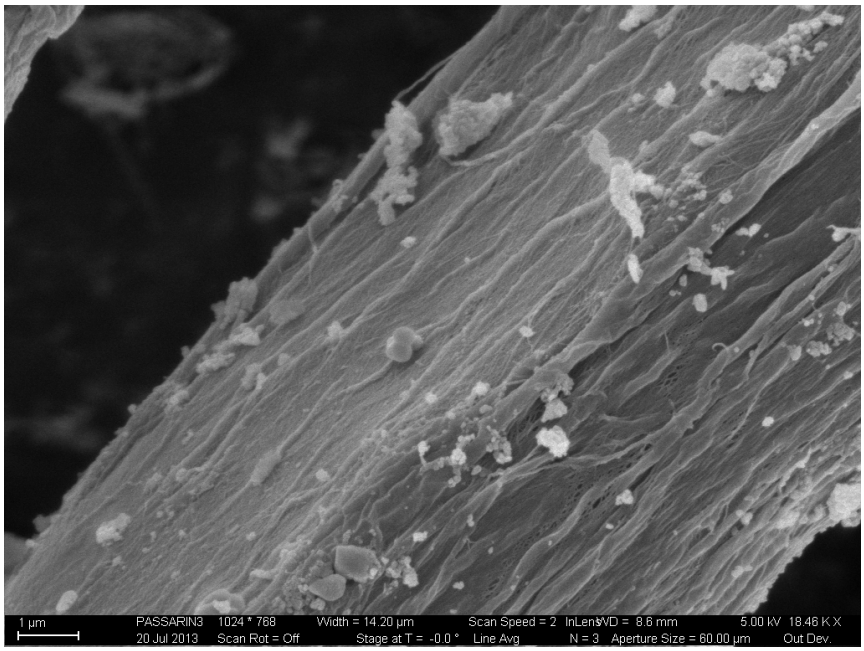

Figure 5.18 – Scanning electron micrographs of USF surfaces after 24 h of immersion in gray cement pore solution. (continued)

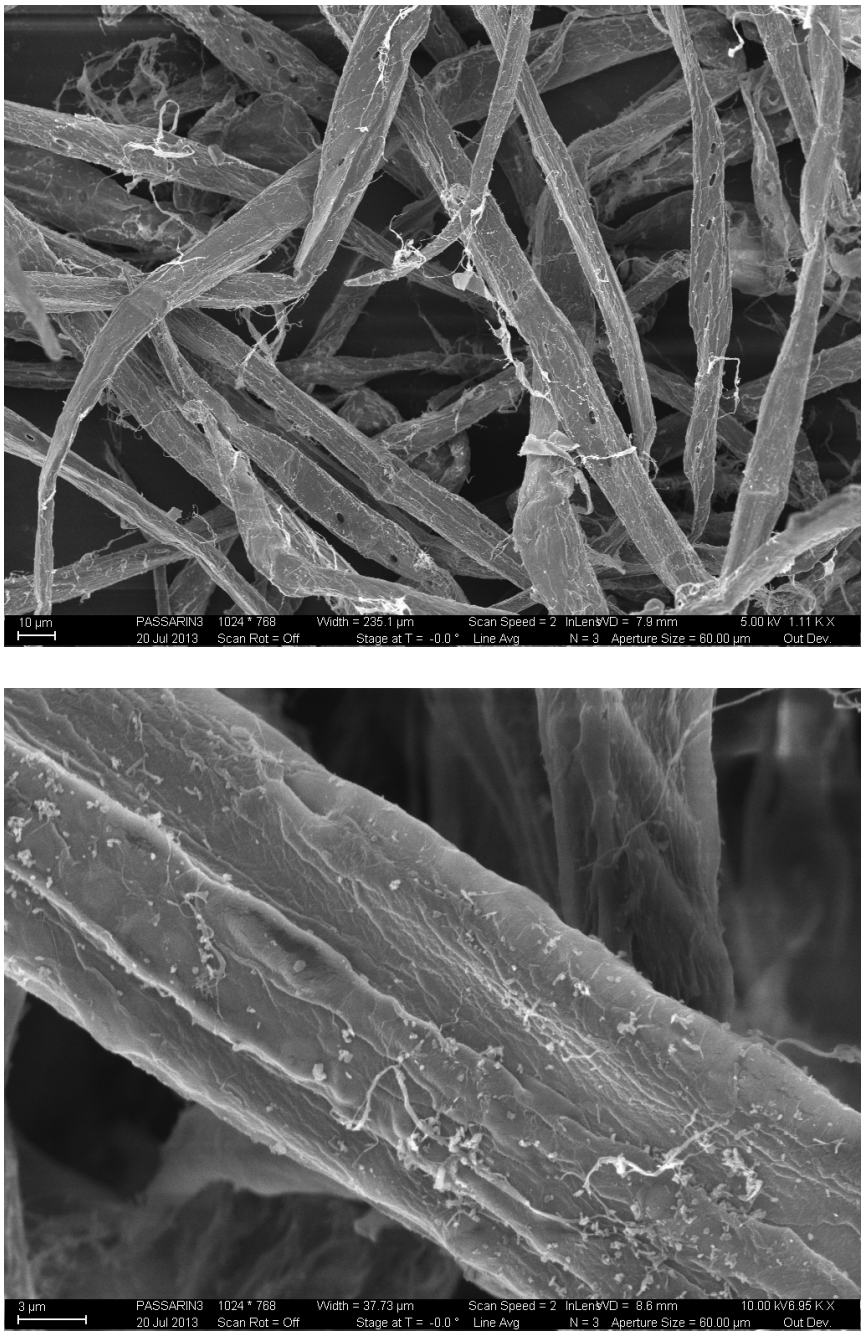

Figure 5.19 – Scanning electron micrographs of USF surfaces after 24 h of immersion in gray cement pore solution.

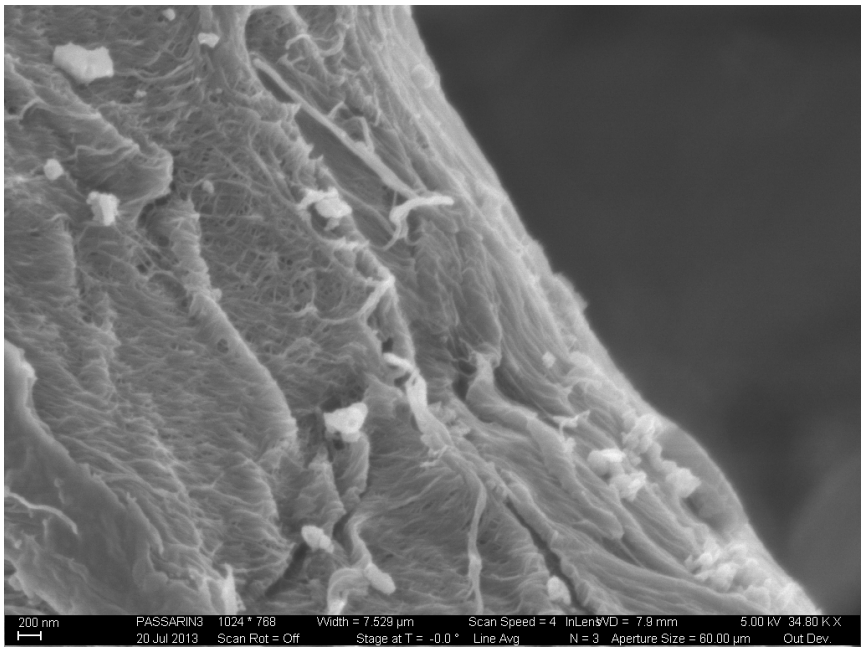

Figure 5.19 – Scanning electron micrographs of USF surfaces after 24 h of immersion in gray cement pore solution. (continued)

For more insights into the nature of precipitates, the topological properties of the USF surface was observed by AFM. Figures 5.20 and 5.21 show a selection of AFM scans of the surface of USF after immersion in deionized water and white cement pore solution, respectively. While the surface of USF fiber immersed in deionized water appears to be smooth, that of the USF fiber immersed in white cement pore solution contains irregular particles deposited on the surface. These particles' morphologies are both polygonal and rounded with sizes in the range of hundreds of nanometers and smaller. This size range conforms to the size of both calcium hydroxide (CH) and calcium silicate hydrate (C-S-H) found in [150], in which the size ranges of CH and C-S-H are in several dozen and hundreds of nanometers, respectively. Moreover, while the rounded particles conform to the shape of a C-S-H particle, the polygonal shape conforms to the shape of a CH crystal.

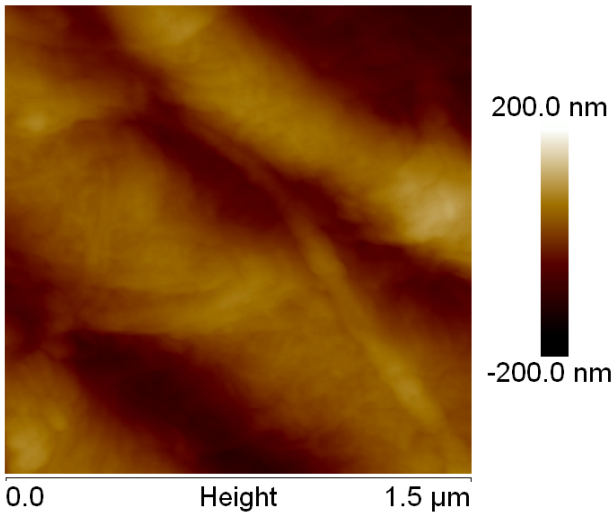

a)

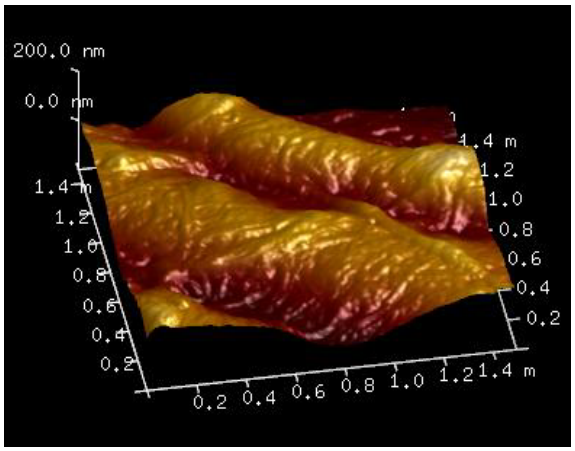

b)

Figure 5.20 – a) Two-dimensional (2D) and b) three-dimensional (3D) atomic force microscopy (AFM) images of USF pulp after 24 h of immersion in deionized water.

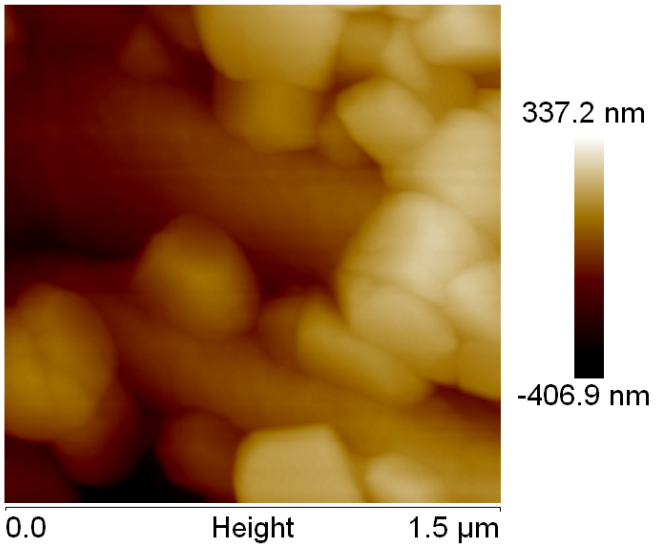

a)

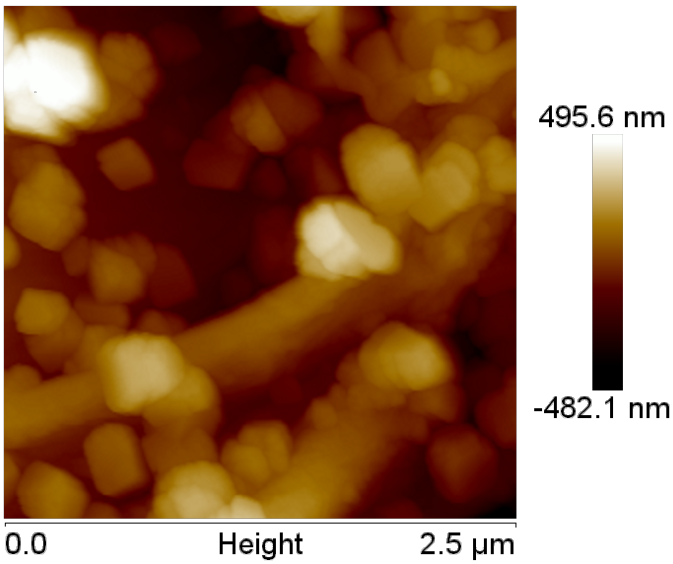

b)

Figure 5.21 – a), b), c) Two-dimensional (2D) and d) three-dimensional (3D) atomic force microscopy (AFM) images of USF pulp after 24 h of immersion in white cement pore solution.

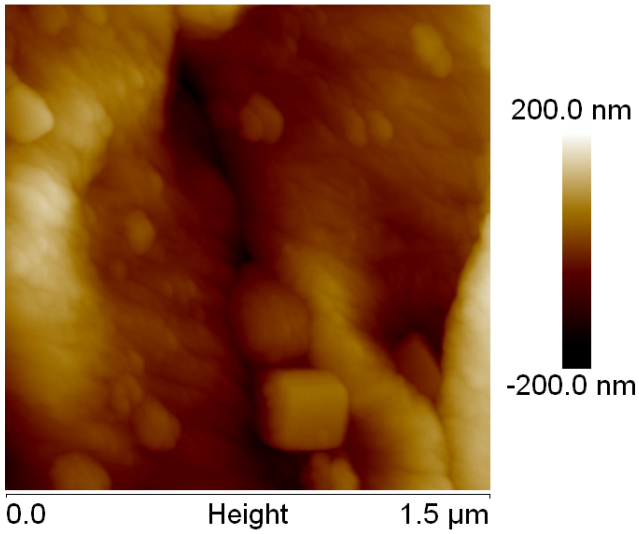

c)

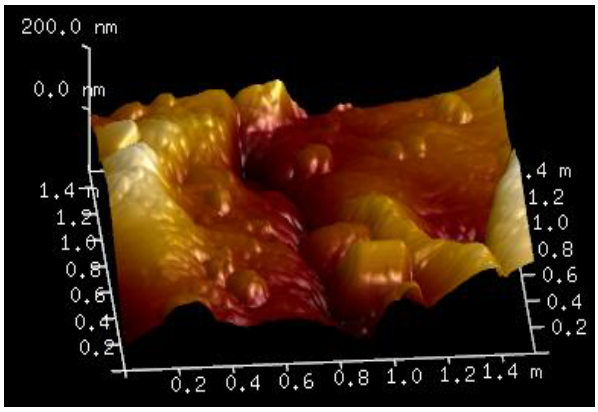

d)

Figure 5.21 – a), b), c) Two-dimensional (2D) and d) three-dimensional (3D) atomic force microscopy (AFM) images of USF pulp after 24 h of immersion in white cement pore solution. (Continued)

5.3.3 Discussion

Here, taking all of the data on quantitative elemental analysis and surface analysis into account, it is proposed that, in the pore solution of cement, eucalyptus pulp acts as a semi-permeable membrane in which its sorptivity depends on cement type. While in gray cement pore solution eucalyptus pulp absorbs more K^+, in white cement pore solution such pulp absorbs more Ca^{2+}. This effect should be taken into consideration for the use of

eucalyptus pulp in some applications, especially when using specialty cement such as white cement. For example, while the absorption capacities of USF and UKF in the gray cement were 1 and 2, respectively (see section 4.3.1.), those of USF and UKF in white cement were 4 and 5, respectively (see section 5.2.1.2.).

Besides the effects of the presence of other ions and initial concentration, if one assumes that the concentration of S obtained from the ICP wavenumber of 182.037 is associated to $CaSO_4$, from which supplied both Ca^{2+} and SO_4^{2-} to the pore solutions, the actual amounts of Ca^{2+} bound to USF in gray and white cement pore solutions are 16.27 and 28.28 mM, respectively. Then, based on the concentration of K, Na, and Ca measured by ICP, if one reverse calculates, the total charge associated with the ion exchange reaction of gray and white cement pore solutions are 59.21 and 59.78 mN, respectively. Therefore, the amount of Ca^{2+} adsorbed to USF in gray and white cement pore solutions are 1,914 and 3,327 mmol/kg of oven-dry USF. Based on data from Duong et al. [141] that sorption capacity of unbleached kraft fiber for Ca^{2+} at pH of 11 is about 200 mmol/kg of oven-dry fiber[§], thus, in this study, total charge of Ca^{2+} exceeds the maximum capacity of USF, suggesting that calcium may present in nonionic forms and some precipitation of calcium-containing compound may occur on the surface. This behavior has been recently found in [141, 149] and, in this study, is confirmed by XPS and AFM measurements.

Results from XPS show that relatively more K^+ and Ca^{2+} were bound to the USF than Na^+. The high solubility of potassium compounds suggests that K^+ does not precipitate on the surface but instead is bound in the fiber cell wall. However, in the case

[§] Since the value is based on experimental results on sorption isotherm of unbleached kraft fiber not unbleached soda fiber, this is meant for the approximate comparison.

of calcium, since the solubility of calcium compounds is low, calcium more likely precipitates on the surface of USF, as reported in [141]. The presence of sulfur atoms on the surface suggests that one of the possible forms that precipitate on USF surface can be sulfate-containing hydrate phases.

Although in this study, due to their small amount and size, the exact hydrated phases of precipitants have not yet been determined, the results suggest that the fiber surface can serve as nucleation sites for cement hydration products. Since the XPS results suggest that precipitants are calcium-rich phases, several possible hydrate phases are calcium silicate hydrate, calcium hydroxide, and sulfate-containing calcium hydrate phases. These precipitants may facilitate hydration reaction at early ages. For example, the presence of calcium hydroxide crystals on the surface could facilitate the growth of calcium silicate hydrate (C-S-H) [151], which could play an important role in controlling fiber-cement interfacial properties.

5.4 Conclusions

In this study, while the heat of hydration of cement pastes is captured by isothermal calorimetry, the transport of entrained water (or internal curing water) from eucalyptus pulp to hydrating cementitious paste is examined through a series of *in situ* MRI and NMR measurements. The behaviors of eucalyptus pulp as internal curing agent are summarized as follows:

- In the cementitious matrix examined in this study, free water from the eucalyptus fiber lumen contributes to internal curing within the first 25 h of hydration, while free water in the cell wall pores and bound water in the cell

wall contribute to later mitigation of self-desiccation shrinkage. These results point to the importance of cell wall thickness in internal curing with fibers.

- The addition of eucalyptus pulps did not affect the overall heat of hydration. The setting time was slightly delayed. However, at after 25 h of hydration the heat of pulp-cementitious pastes was higher than that of control paste of w/cm at 0.30, which indicates the additional hydration reaction due to internal curing. Quite similar behavior has been reported with the use of LWA and SAP.

- Preliminary MRI imaging confirms that eucalyptus pulp is well dispersed in the cement paste, at least at the resolution performed in this study, as demonstrated by the uniformity in MRI signal intensity for 1%USF-cementitious paste.

Although results from NMR/MRI measurements reveal the mechanisms underlying the migration of entrained water from eucalyptus pulps to hydrating cement paste, pulps not only absorb and desorb water but also interact with ions in the pore solution of cement. Such interaction would change the concentration of ions in their cell wall, which may promote osmosis. Therefore, to evaluate such interactions at early ages, nanocharacterization techniques were employed to compare fiber interactions in deionized water with those in cement pore solutions within 24 h of hydration. Based on results found in the study, several mechanisms are proposed:

- USF adsorbs cations from cement pore solution to its structure via ion exchange. Although adsorption of Ca^{2+} is preferable to Na^{+} and K^{+}, the

amount and type of ion adsorbed depends on the chemical compositions of the pore solution, which in turn depends on the cement composition.

- An increase in concentration of sulfur indicates dissolution of gypsum (and perhaps other sulfur-containing compounds) to accommodate the influx of pore solution ions. This increase in sulfur concentration in the pore solution may affect the hydration of calcium aluminate phase (C_3A) and should be further examined.

- From XPS analysis, changes in fiber surface chemistry were observed. The change in atomic concentration of Ca indicates some precipitation of calcium-containing products on the surface of USF, which corresponds with results from ICP analysis.

- SEM images reveal the presence of small, discrete crystals on the USF surface indicating some precipitation or nucleation on the surface of USF, in which the nucleation sites and the presence of surface asperities, including microfibrils, appear to be associated.

Overall, these results together show that there are important interactions occurring between the pulp and the surrounding pore solution, which depend upon the cement composition. As a result, when assessing the potential for internal curing performance, it is critical that the fibers be examined in a pore solution or cement matrix, rather than in water.

CHAPTER 6

EUCALYPTUS PULP FOR THE MITIGATION OF EARLY-AGE CRACKING

6.1 Introduction

Chapter 4 has demonstrated that eucalyptus pulps can provide internal curing in cementitious composites [9, 139]. Because of their physical and chemical structures, hardwood pulps are hygroscopic, taking up water as both free and weakly bound water which may then be released into the cement matrix during hydration, potentially contributing to the mitigation of autogenous shrinkage in cement paste and mortar of low w/c. Therefore, while eucalyptus pulps, one of hardwood species, may not significantly improve the mechanical properties of mortar and concrete as much as longer plant-based fibers they may enhance some early-age properties with the potential to limit the cracking of cementitious composites at early ages especially in a system that has a high cement content whereby the highest tensile stress-to-strength ratios are exhibited at the period between 24 and 48 hours after setting [152]. Therefore, due to their availability, consistency, dispersability, internal curing capability, and crack-arresting properties, hardwood fibers warrant further examination for use in cement-based construction materials.

This chapter compares the performance of eucalyptus pulp on early-age cracking mitigation in ordinary types of mortar to that in mortar containing a more common internal curing agent, superabsorbent polymer (SAP). Both the ability of eucalyptus pulp to reinforce and its capacity to provide internal curing are evaluated through a series of

restrained shrinkage tests, early age mechanical tests, and characterization. The overall goal is to better understand the roles of internal curing and reinforcement as they relate to shrinkage crack mitigation through the use of eucalyptus pulp fiber.

6.2 Materials and Methods

6.2.1 Materials

Unbleached soda pulp (USF) was obtained from a commercial soda-pulp mill located in Southeast Asia. The pulp was never dried, so it retained its structure. Key features include the kappa number of the pulp was 14.6, giving a total residual lignin content of 2.23 percent. The average length of the fiber was approximately 0.69 ± 0.02 mm. The as-received moisture content of the USF was 245%, determined according to ASTM D4442-07 [98]. The superabsorbent polymer used for comparison was a cross-linked acrylamide/acrylic acid copolymer, the most predominant type of SAP used for internal curing [44]. The SAP was in powder form and added to dry cement prior to mixing.

Mortar samples were prepared using commercially available ASTM Type I/II portland cement (Lafarge, North America), natural siliceous sand (Atlanta, Georgia, USA), and tap water. The oxide analysis of the cement was performed by x-ray fluorescence (XRF, Bruker AXS S8 Tiger) spectrometry. The oxide composition of the cement was (as percentage by mass) 19.73% SiO_2, 4.82% Al_2O_3, 3.16% Fe_2O_3, 62.41% CaO, 3.64% MgO, 2.99% SO_3, 0.08% Na_2O, 0.48% K_2O, and 2.2% LOI. The crystalline phases of cement, as identified by quantitative x-ray diffraction analysis (QXRD, Bruker AXS D4 Endeavor) with the Rietveld method using TOPAS software, was (as percentage by mass) 52.6% alite, 20.7% belite, 3.7% aluminate, 11% ferrite, 0.1% lime, 2.3%

portlandite, 2.6% periclase, 0.6% arcanite, 0.4% aphthitalite, 0.9% gypsum, 2.4% bassanite, and 2.7% calcite. The particle size distribution of the sand, shown in Figure 6.1, was adjusted to meet ASTM C897-05 requirements [153]. The oven-dry specific gravity was 2.62 and the fineness modulus was 2.68.

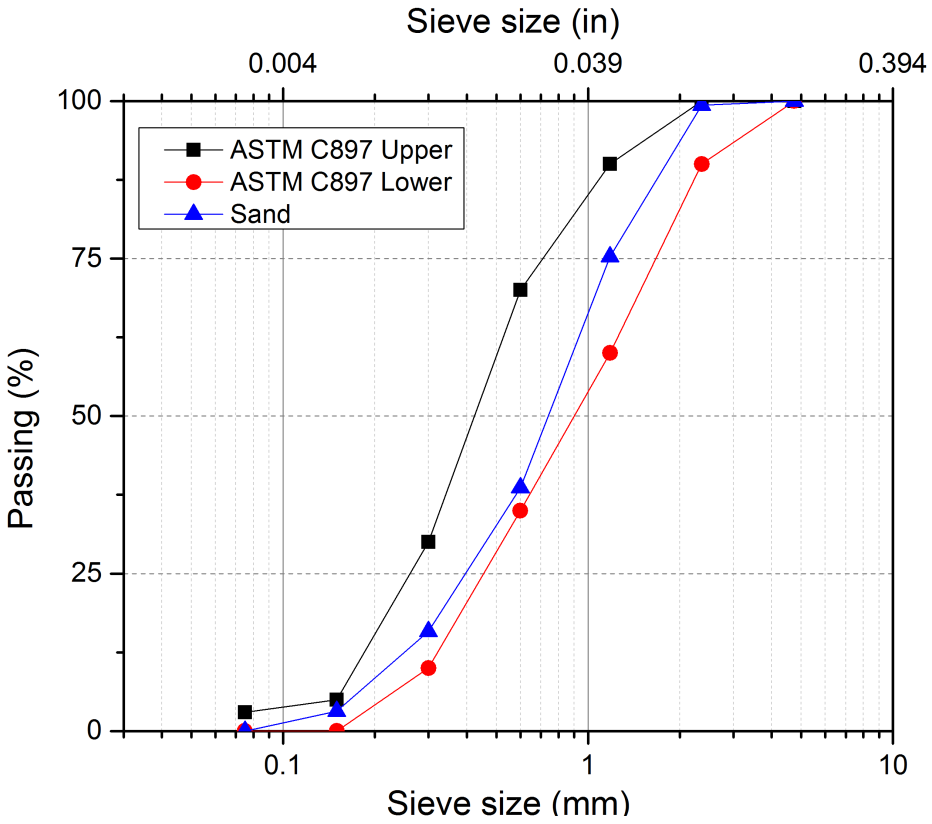

Figure 6.1 – Particle size distribution of the sand used in this study.

Mortars were prepared at a water-to-cement ratio (w/c) of 0.40 and a sand-to-cement volume ratio (s/c) of 1.5. All mix design proportions tested in this study are shown in Table 6.1. Maintaining a consistent w/c, particularly for mortars that contain either of the internal curing agents – USF and SAP – requires that the amount of internal curing water available to the paste be accounted for during mixture proportioning. Therefore, the amounts of “entrained water” (e.g., water available for internal curing

[138]), which depend on the amounts of USF and SAP in the mortar as well as the intrinsic properties of these agents and the cement used [40, 44, 127], were quantified using a consistent method [97] and the mix water masses were adjusted accordingly. The absorption capacity of USF was determined to be 1 while that of SAP was 10. The absorption capacity of SAP was close to that previously reported [154], in which the absorption capacity was determined through measurement of chemical shrinkage. Since a high efficiency polycarboxylate-based superplasticizer, ADVA455 (WR Grace), was added to enhance the workability of the fiber-containing mortar, the same amount was also added to each of the companion samples (3µL per gram of cement).

Table 6.1 – Mixture proportion of mortars in oven-dry basis.

	Ratio by weight of cement			**Percent by weight (and by volume) of cement**	
Mix notation	**Sand[1]**	**Mix water**	**IC water**	**USF**	**SAP**
w/c 0.4	1.248	0.4	-	-	-
0.5% USF	1.248	0.4	0.01	0.96 (0.5)[3]	-
0.75% USF	1.248	0.4	0.015	1.44 (0.75)	-
1% USF	1.248	0.4	0.02	1.93 (1.0)	-
0.1% SAP	1.248	0.4	0.01	-	0.1
0.15% SAP	1.248	0.4	0.015	-	0.15
0.2% SAP	1.248	0.4	0.02	-	0.2

[1]Ratio of sand is presented at SSD condition.
[2]Ratio of sand to cement by volume was 1.5.
[3]Number in parentheses is the percent of USF by volume of total.

6.2.2 Restrained Shrinkage

To evaluate the effect of USF hardwood eucalyptus pulp on early-age cracking, this work employed the restrained ring test (ASTM C1581-09 [155]). Strain development in the steel ring was monitored by attaching two electrical resistance strain gauges, 180^{o} apart, to the inner surface of the steel ring at mid-height. The strain gauges were

connected to a quarter-bridge strain gauge module attached to a data acquisition system. The strain data were recorded every three minutes. The amounts of fiber used in restrained shrinkage studies were 0.5% and 0.75% by volume of the original mix. The role of internal curing on restrained shrinkage was clarified by comparing the test results of mortar with a 0.75% volume of fiber to those of mortar with 0.15% weight of the SAP added to the cement which is equivalent to an entrained water-to-cement ratio (w_e/c = the amount of water absorbed by an internal curing agent) of 0.015.

These mortar samples were cast in two layers, each of which was consolidated by a vibrating rod. The samples were cured and sealed in accordance with the ASTM C1581-09 standard. Testing environment was at a temperature of 22±2ºC and a relative humidity of 60±5%.[**] Under the assumption that uniform shrinkage in the radial direction will occur, the maximum residual tensile stress (σ_{max}) in the mortar specimens was calculated from the known parameters of the strain in the steel ring (ε_{st}), the modulus of the elasticity of steel (E_{st}), the outer radius of the steel ring (R_{os}), the outer radius of the specimen (R_{oc}), and the inner radius of the steel ring (R_{is}) by Eq. 6.1[76]

$$\sigma_{max} = -\varepsilon_{st} \cdot E_{st} \cdot \frac{(R_{OS}^2 + R_{OC}^2) \cdot (R_{OS}^2 - R_{is}^2)}{2R_{OS}^2(R_{OC}^2 - R_{OS}^2)} \qquad \text{Eq. 6.1}$$

The age at cracking was reported as the point at which a sudden decrease in strain occurs. At that time, visible cracks were then labeled and photographed every two days. The widths of the cracks were evaluated by image analysis software (Image J).

[**] The humidity range in this study did not comply with ASTM C1581, in which the humidity is specified at 50±5% RH. However, since the ASTM C1581 is for relative comparison of materials, results obtained in this study still reflect the performance of internal curing agents on crack mitigation of mortar.

6.2.3 Free Drying and Autogenous Shrinkages

Free total and autogenous shrinkages, as companions to restrained shrinkage, were evaluated by casting mortar bars according to ASTM C490-11 standard [156]. These bars were demolded 24±1 hours after casting and remained in the same conditioned room as the ring specimens. To prevent moisture loss, the autogenous shrinkage samples were immediately wrapped with an aluminum tape upon demolding. The first reading for all shrinkage measurements was done within 30 minutes after the samples were demolded. Moisture loss was also monitored by recording the mass of each specimen, using a balance with a tolerance of ± 0.1 g.

6.2.4 Mechanical Testing

Specimens for the splitting tensile strength (ASTM C496-11 [157]) and the dynamic elastic modulus (ASTM C215-08 [158]) tests were cast and tested alongside of shrinkage test specimens. Splitting tensile tests were performed on 76.2 mm x 152.4 mm cylindrical specimens at 3, 5, 7, 14, and 28 days. The dynamic modulus was assessed non-destructively on 100 mm x 200 mm cylindrical specimens every two days. Until the tests were performed, all of these specimens were kept in a condition identical to that of the rings until the time of the test.

The effectiveness of hardwood pulp as reinforcement in mortar was further examined through a comparison of flexural toughness test results for the fiber-cement mortars with those of the unreinforced mortar and SAP-blended mortar. As shown in Table 6.1, the amounts of fiber reinforcement used in this study were 0.5%, 0.75%, and 1% by volume of the original mix. The SAP mortars contained 0.1%, 0.15%, and 0.2%

by weight of cement. Both the USF and SAP mortars were equivalent to the w_e/c of 0.01, 0.015, and 0.02, respectively.

Flexural specimens were cast in two layers in 2.54 x 2.54 x 30.5 cm brass molds, vibrated to minimize entrapped air voids, and then covered by a plastic sheet to prevent moisture loss. After 24 hours, the samples were demolded and cut with a masonry saw to a 10.2 cm length. While the specimens for air curing were kept in an environmental chamber at 24±2ºC and 60±5%RH, those for water curing were placed in a lime-saturated tank at 23±2ºC until the time of the test. Flexural testing was performed at 23±2ºC and 45±5% RH.

Specimens that would undergo a three-point bending test were set up at a span of 7.6 cm, which equals a span-to-depth ratio of 3 [159]. Each data point was obtained from at least six specimens. The test was performed on each sample using a 98 kN screw driven test frame (Satec model 22EMF) with a crosshead displacement of 0.1 mm/min. To capture the deflection of the specimen, an electronic deflectometer (Epsilon model 3540-012M-ST) was placed under the center point of the mortar bar. From the test results, flexural toughness was calculated. The flexural toughness was calculated from post-cracking toughness, or the area under the load-deflection curve beyond the initial cracking [160]. An example of these calculations is demonstrated in Figure 6.2. Moreover, since the moisture state of sample (e.g., oven dry, air dry, and wet states) at the time of testing can be crucial for natural fiber-reinforced cement composites [161], all samples were kept in their curing condition until the time of testing. Limewater-cured samples were removed from the curing tank and surface dried using paper towels and tested immediately.

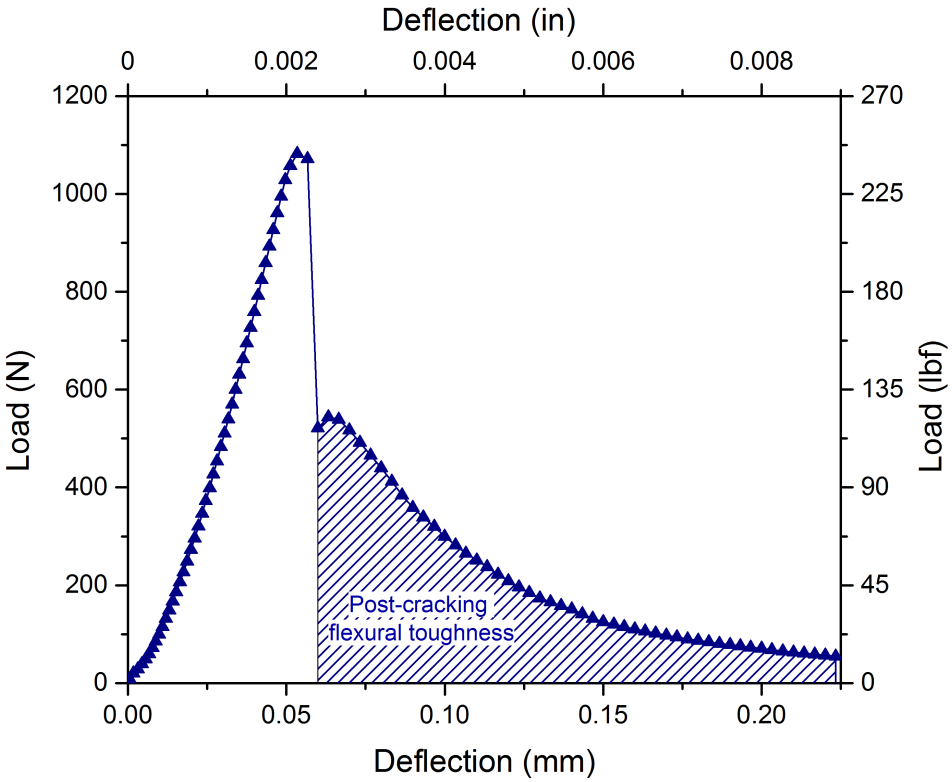

Figure 6.2 – Definition of post-cracking flexural toughness.

6.3 Results

USF hardwood pulp fiber was evaluated as reinforcement and as internal curing agent for mitigation of early-cracking in mortar. The performance of USF pulp was demonstrated through restrained shrinkage, early-age mechanical properties, and microstructure of the composites. For more understanding of the role of USF in an early-age cracking mitigation, additional tests such as autogenous shrinkage, drying shrinkage, dynamic modulus, splitting tensile strength and flexural toughness were performed. Results were then evaluated and analyzed in the context of the effects of USF on mortar properties.

6.3.1 Stress Development and Cracking Potential in Restrained Shrinkage

Tensile stress developed in the mortar ring specimens, as obtained via Eq. 6.1, are shown in Figure 6.3. Compared with plain mortar, internally cured mortar, which contains either of the agents (SAP and USF), exhibited lower tensile stress, a common behavior of internally-cured specimens [154, 162, 163]. From Figure 6.3, the effects of USF reinforcement on pre- and post-cracking behaviors can be distinguished. First, the rates of stress development of the USF-reinforced mortar specimens were slower than those of the plain mortar. After the 0.75% USF-reinforced mortar initially cracked, the tensile stress of this mortar, unlike other mixes, did not immediately approach zero but instead gradually decreased, indicating a transfer of tensile stress from the matrix to the USF, similar to that reported in [11] for pulp-fiber reinforced mortars. In the pre-cracking, the tensile stress of the internally cured mortars was lower than in the control; this disagrees with results reported in [11], in which similar behavior was reported for plain and pulp fiber-reinforced mortar samples prior to cracking.

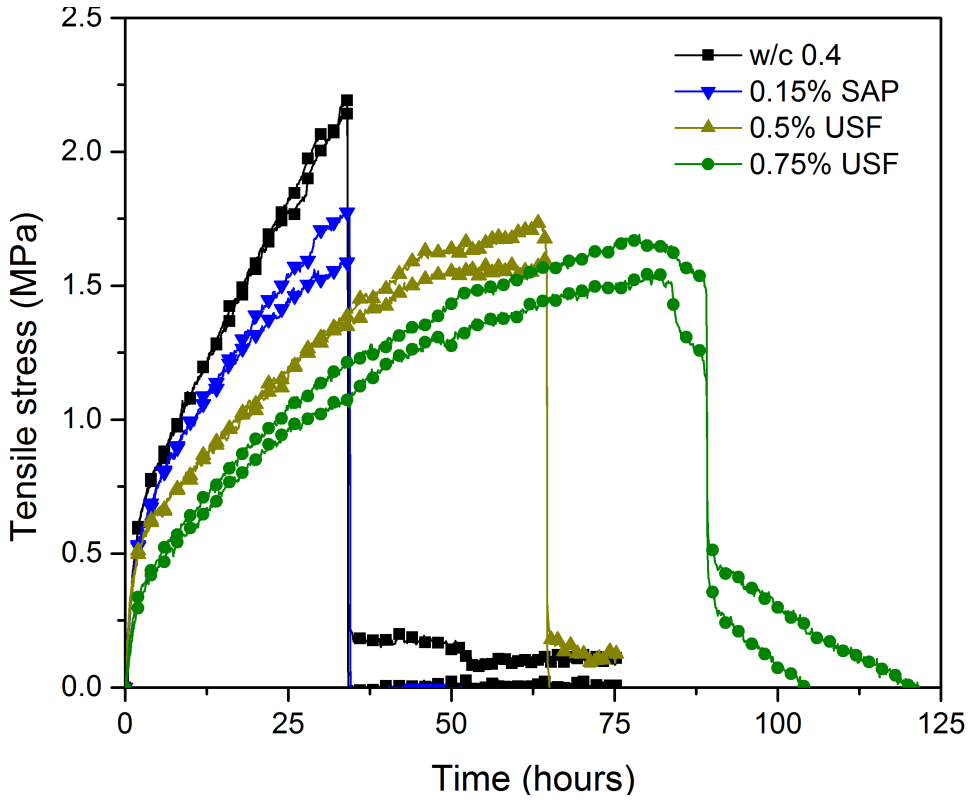

Figure 6.3 – The development of tensile stress in restrained shrinkage specimens with and without USF fiber.

While at the time of cracking the tensile stress was lower in the internally cured mortars (i.e., both SAP and USF), the time-to-cracking (shown in Table 6.2) was extended only for the USF-reinforced cases. The lower tensile stress could derive, at least in part, from the lower modulus of both USF-reinforced and SAP-blended mortars (presented in section 3.3.) Time-to-cracking has been defined as the difference between the age when a sudden decrease in tensile stress occurs and the age of initial drying [127]. The results show that despite the variation in cracking time among the three replicate specimens, the average value is relatively satisfactory in terms of statistical differences. The results also indicate the effectiveness of using USF to mitigate early-age cracking; that is, although the mortar was designed with low s/c and fine sand to exacerbate

cracking, cracks in the USF-reinforced mortar occurred at later ages. Both plain and SAP mortar specimens without USF reinforcement cracked within about 36 hours after initial drying while the 0.5% and 0.75% USF-reinforced mortar cracked at about 57 and 80 hours, respectively.

Figure 6.4 presents the effect of USF on the development of crack width. The initial crack width of the w/c 0.4 mortar was larger than that of USF-reinforced mortar. The average width of the cracks began at about 0.75 mm for w/c 0.4 specimens while that of the 0.5% and 0.75% USF-reinforced mortar began at about 0.35 and 0.09 mm, respectively. Therefore, the initial crack width was decreased by 88% in 0.75% USF reinforcement; it is significant that the crack width can be confined to a size below which self-healing is possible in appropriately designed cementitious matrices [164, 165].

The reduction in the average initial width of cracks indicates that USF pulps, after cracking, effectively bridge microcracks, preventing them from widening. As the width of the cracks developed, the length of the fiber appeared to be crucial. That is, the crack width in 0.75% USF mortar gradually increased in the beginning but dramatically increased as the crack became wider than the average length of the fiber (0.69 ± 0.02 mm). Compared to the crack width of w/c 0.4 mortar, the crack in the 0.75% USF was approximately 25% narrower at later ages (~17 days).

Table 6.2 – Time-to-cracking of restrained ring specimens.

Mixture	Time-to-cracking* (hours)			
	#1	#2	#3	Average (CV %)**
w/c 0.4	41.06	30.80	34.13	35.33±5.23 (14.8)
0.15% SAP	29.47	44.61	34.40	36.16±7.72 (21.4)
0.5% USF	54.15	64.62	53.21	57.33±6.33 (11.0)
0.75% USF	70.87	89.06	82.33	80.75±9.20 (11.4)

* The time-to-cracking of USF-reinforced mortar is defined as the time lapse from initial drying to initial cracking.

**The coefficient of variation is defined as the percentage of the ratio of the standard deviation to the mean.

Upon examination of the SAP-blended specimen, the 0.15% SAP-blended mortar, which had the same nominal amount of entrained water as 0.75% USF-reinforced mortar, did not slow stress development nor delay the cracking time, similar to results reported in [154]. Thus, based solely on the results shown here, one can interpret either that the dosage of SAP at w_e/c of 0.015 did not effectively provide internal curing water to mortar or that internal curing did not mitigate restrained shrinkage. As will be presented subsequently (in Section 6.3.2), at this dosage, the SAP effectively mitigated autogenous shrinkage, suggesting that the dosage was appropriate but did not translate into restrained shrinkage crack mitigation. Recently, Zhutovsky et al. [154] examined the effects of internal curing on restrained shrinkage and demonstrated that despite the reduction of autogenous shrinkage when concrete is subjected to drying, because of water loss, internal curing SAP, without a shrinkage-reducing admixture exhibited only slight reduction of the cracking potential.

Although the delay in time-to-cracking of cellulose-reinforced mortar was not reported in [11], the results in this study demonstrated that hardwood eucalyptus pulp can improve the restrained shrinkage behavior of mortar at early ages. The variation in

behavior for the USF and SAP at the same entrained water dosage rate suggests that further examination of the mechanisms underlying the reduction in shrinkage, time to cracking, and crack width warrant further examination.

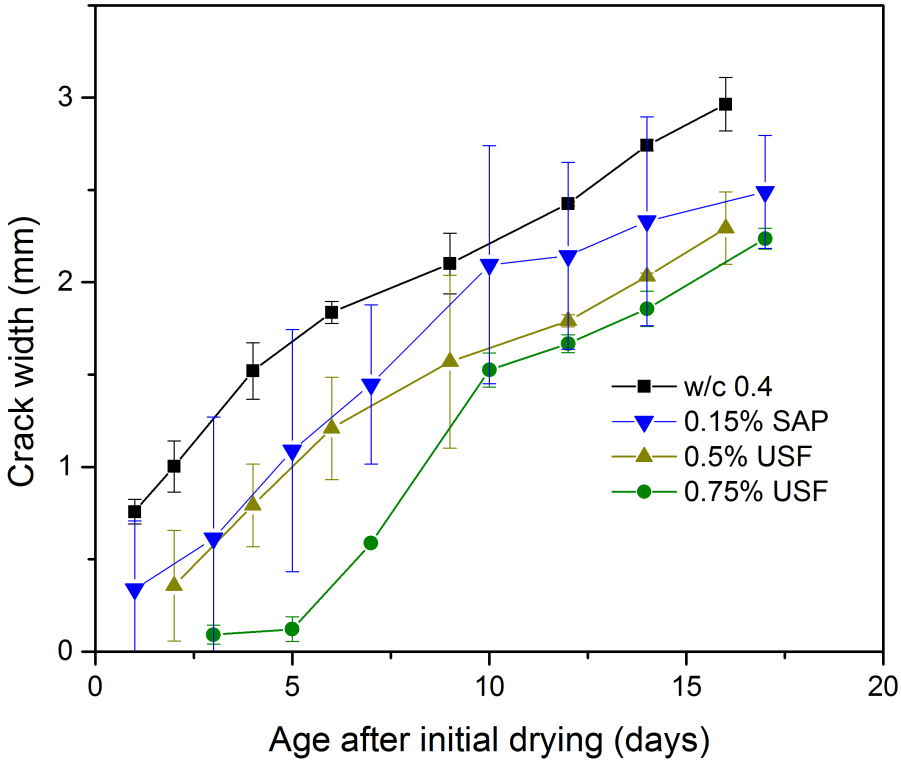

Figure 6.4 – Effects of USF reinforcement on the development of crack width.

6.3.2 Free Drying and Autogenous Shrinkages

Figures 6.5 and 6.6 present the effects of USF fiber on both the free drying and autogenous shrinkages of mortar and the change in mass. The total shrinkage of fiber-reinforced mortar slightly increased compared to ordinary mortar, as has been reported in other studies [11, 89]. The effect of USF on mass loss also agrees with that found in [90]. At 28 days, the loss of mass in the USF-reinforced mortar was about 3.41±0.21% and 3.71±0.24% for the 0.5% and 0.75% volumes of fiber, respectively, whereas that in the plain mortar was about 3.12±0.16%. It is believed that presence of plant-based fiber,

including USF, increased the porosity of the matrix as a result of poorer workability, the effects of which were noted when comparing the specific gravity of USF-reinforced mortar measured immediately after demolding (2.24) to that of plain mortar (2.33). This increased porosity, together with the hygroscopic property of the fiber, contributed to the loss of mass and increased shrinkage.

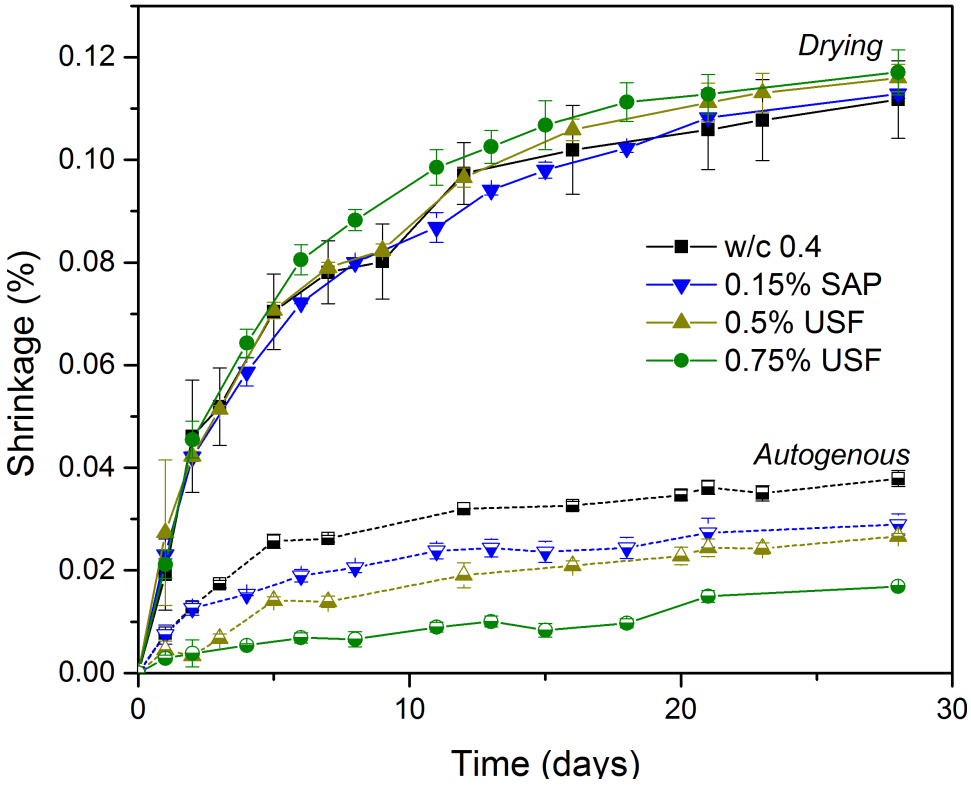

Figure 6.5 – Effects of USF and SAP on free drying and autogenous shrinkage of mortar.

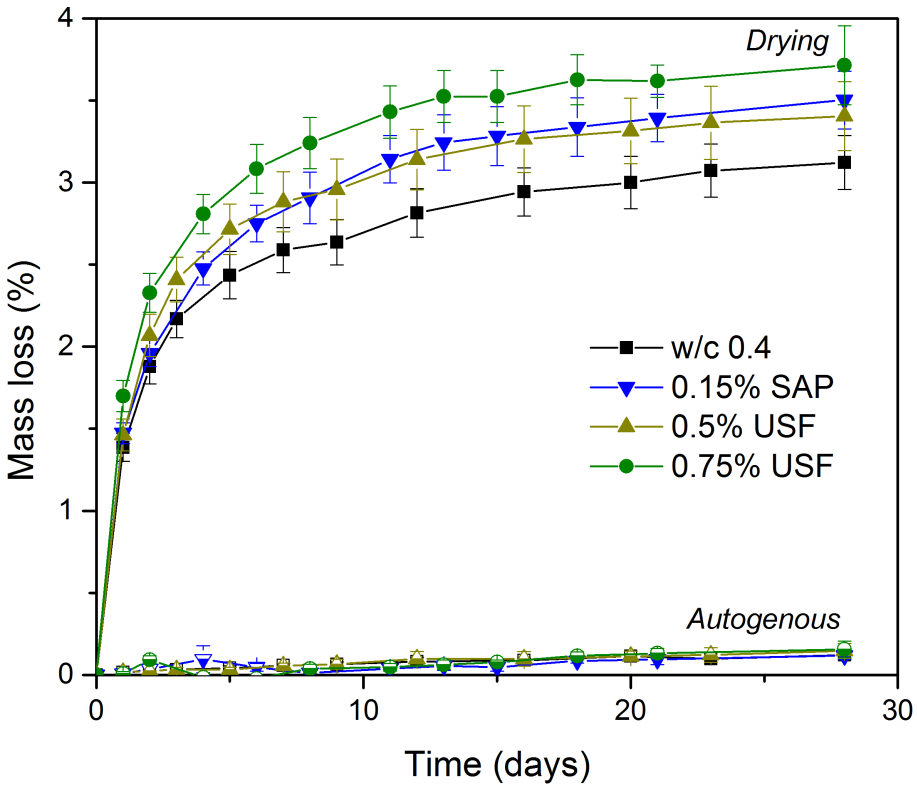

Figure 6.6 – Effects of USF and SAP on the mass loss of mortar.

For comparison, Figures 6.5 and 6.6 also illustrated the shrinkage and mass loss of the companion SAP mortars, respectively. The SAP specimens underwent drying shrinkage similar to but mass loss was higher than the plain mortar specimens, which conformed to that reported in [154, 166]. Zhutovsky et al. [154] also found that although greater mass loss occurred with the incorporation of the SAP, the free shrinkage of the samples remained consistent with that of the control samples.

Here, sealed mortar bars, companions to the drying shrinkage bars, were used to assess autogenous shrinkage. The maximum moisture loss at 28 days was 0.15%, indicating that the bars were effectively subjected to autogenous shrinkage generally in the absence of drying shrinkage. Among the four mortar mix designs examined, the plain mortar exhibited the highest value of autogenous shrinkage. In contrast, the mortar

with the addition of internal curing agents SAP and USF underwent significant reductions in autogenous shrinkage. The percentage reduction in the autogenous shrinkage of internally cured mortar was about 23.7% for 0.15% SAP, 31.6% for 0.15% USF, and 55.3% for 0.75% USF. Although the SAP mortar samples had the same nominal amount of entrained water as the 0.75% USF mortar samples, the addition of the SAP was less effective in mitigating autogenous shrinkage at the dosage rates examined.

In addition to considering the free shrinkage behaviors in Figure 6.5, by subtracting the autogenous shrinkage from the drying shrinkage for each case, as reported in Figure 6.7, the effects of the evaporation of water can be isolated. The trends in these results agree with the trends mass loss, shown in Figure 6.6; that is, the higher the mass loss, the more shrinkage, as expected. Fiber-reinforced specimens experienced more mass loss and shrinkage compared to SAP-blended specimens, which could have resulted from the loss of water from interconnected porosity presenting in the fiber and the shrinkage of the fiber itself.

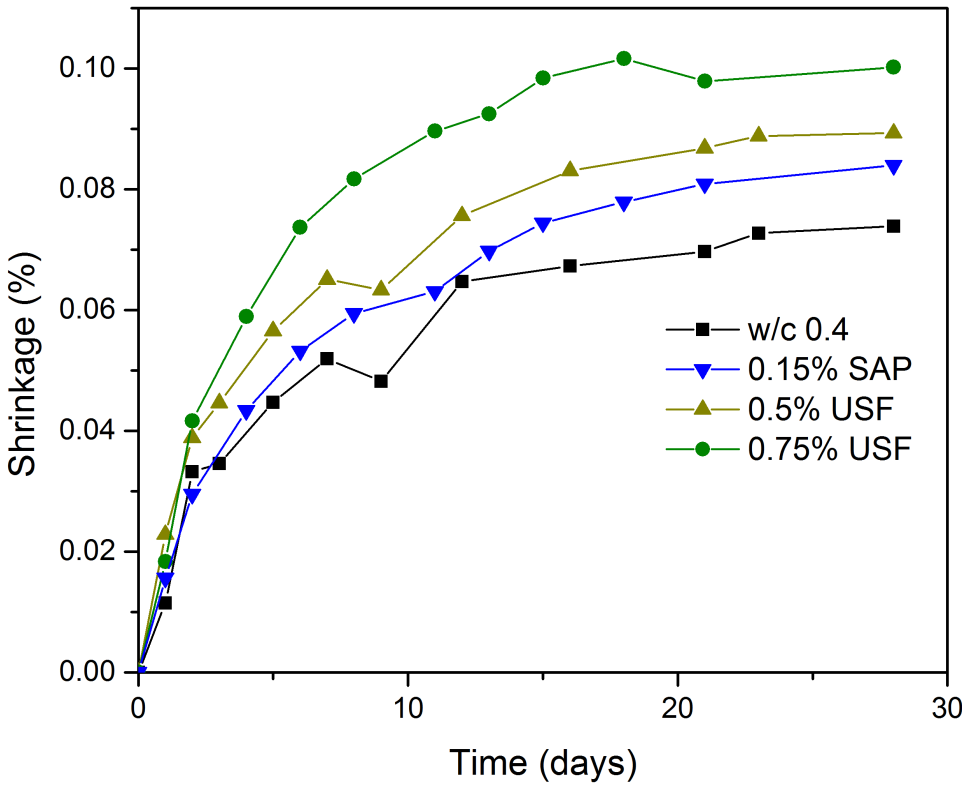

Figure 6.7 – Effects of USF and SAP on the shrinkage caused from the evaporation of water.

6.3.3 Mechanical Properties

To comprehensively evaluate the effects of USF fiber on shrinkage behaviors, shrinkage data – both free and restrained shrinkages – should be examined in the context of the development of tensile strength (Table 6.3) and the stiffness (measured here as dynamic modulus in Figure 6.8). As the length of USF was only about 0.6 mm, this fiber, at the volume fractions range in this study, was not expected to enhance the tensile strength of mortar, which is borne out in the data in Table 6.3. At 28 days, the tensile strength of USF-reinforced mortar was 5.07±0.20 MPa and 5.01±0.1MPa for 0.5% and 0.75% volumes of the fiber, respectively, whereas that of the plain mortar was 5.22±0.31 MPa. However, the tensile strength of the USF-reinforced mortar was slightly higher than

the control at early ages (i.e., 7 days and less), which indicates that USF may have improved the tensile strength of mortar at an early age when the matrix was relatively immature and prone to cracking.

Table 6.3 – Splitting tensile strength of mortar specimens.

Age (days)	Splitting tensile strength (MPa)			
	w/c 0.4	**0.5%USF**	**0.75%USF**	**0.15%SAP**
3	3.41±0.43	3.63±0.29	3.77±0.28	3.66±0.16
5	3.88±0.39	3.84±0.38	4.10±0.12	3.83±0.59
7	4.19±0.41	3.86±0.37	4.34±0.14	4.38±0.28
14	4.82±0.42	4.55±0.41	4.71±0.10	4.46±0.10
28	5.22±0.31	5.07±0.20	5.01±0.10	5.02±0.24

USF may affect not only the tensile strength of mortar but also the dynamic modulus of elasticity, as shown in Figure 6.8.[††] At all ages, all internally cured samples exhibited lower dynamic modulus than that of the plain mortar. At 28 days, the dynamic moduli of the USF-reinforced mortar were 38.71±0.48 GPa and 36.73±0.47 GPa for the 0.5% and 0.75% volumes of fiber, respectively, whereas that of the plain mortar was 45.11±0.29 GPa and that of the SAP-blended mortar was about 42.27±0.63 GPa. From the Figure, the dynamic modulus decreased as the proportion of USF increased. The inclusion of USF could affect the dynamic modulus in 2 ways; 1) the introduction of pre-existing flaws and 2) the lower modulus of the fiber itself compared to the mortar.

[††] Though it should be noted that dynamic modulus not equivalent to static modulus, a good linear relationship is found between dynamic and static values [167]; here, it was advantageous to monitor the evolution of stiffness via non-destructive measurement of the dynamic modulus, which also avoided difficulties in variability in measured mechanical properties among replicate mortars, particularly at early ages.

First, since the dynamic elastic constant is sensitive to material quality and uniformity and the resonant frequency is used to evaluate the damage level in concrete and mortar and often used as an indication of the development of both micro-and macro-cracking [168], the inclusion of USF could introduce some pre-existing flaws and thus decrease the dynamic modulus. Such a flaw might include voids, due to decreased workability, and microcracking, particularly at the fiber/cement interface (as will be examined in Section 6.3.4). Another possible reason is that the modulus of the saturated or near-saturated wood fiber is one order of magnitude lower than it is when dry [110]. Given that the longitudinal modulus of a hardwood kraft pulp in a dry state is approximately 35 GPa [20], the modulus of the wet pulp would be expected to be on the order of 3.5 GPa, which entirely reduces the modulus of mortar based upon composite theory.

The reduction in modulus of elasticity in USF-reinforced mortar would decrease the potential of cracking at early ages of mortar [169], applying the concept of extensibility. That is, assuming linear-elastic behavior, the stress generated during post-setting early-age shrinkage depends on the modulus of elasticity while the resistance to cracking depends on the tensile capacity. For a given shrinkage strain, mortar and concrete with a higher modulus of elasticity and a lower tensile strength will be more prone to cracking. In addition, the stress induced by shrinkage strain is reduced by stress relaxation and, after cracking, is also transferred to the fibers [12, 170]. Thus, restrained cracking relies on both the elastic and viscoelastic properties of a material. The reduction of modulus in USF-reinforced mortars indicates one possible contribution of USF to the mitigation of early-age cracking.

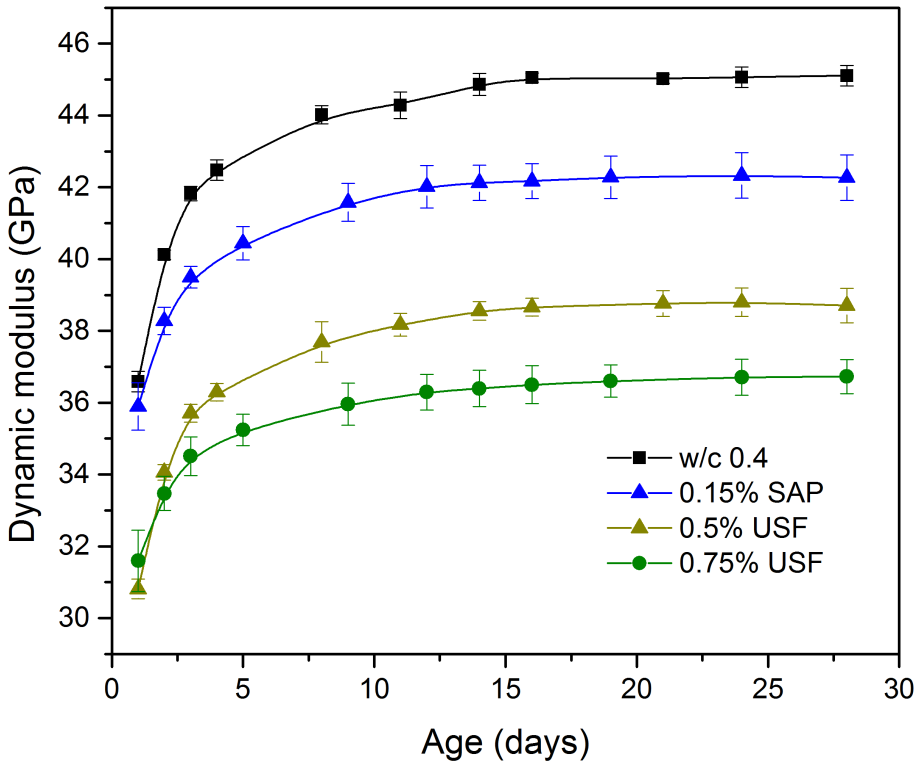

Figure 6.8 – Dynamic modulus of the USF and SAP-reinforced mortar compared with that of plain mortar.

In addition to splitting tension and dynamic modulus, the effects of eucalyptus fibers both as reinforcement and internal curing agents were evaluated through flexural tests. Mortar samples subjected to limewater curing (i.e., no internal curing) and air curing (i.e., with internal curing at 60%RH) were tested in flexure at 7 and 28 days. The (first-cracking) flexural strength of these mortars, as compared to plain mortar with that of internally cured SAP-blended mortars, are shown in Figure 6.9. Generally, these results showed a slight increase in the flexural strength of mortars between 7 and 28 days, as expected. However, with the addition of the USF, flexural strength decreased. That is, the peak flexural strength of the two types of mortar at 28 days decreased by about 17% and 27% for fiber volume fractions of 0.5 and 1%, respectively. This finding contradicts a generally accepted assumption that flexural strength should increase when the fiber

content increases [58, 171]. However, it must be noted that such claims are based on long-length pulp fibers or fiber-cement composites produced by Hatschek or dewatering processes, not on short-length hardwood eucalyptus fibers or cast-in-place mortar. Since increases in flexural strength are particularly sensitive to not only fiber volumes but also aspect ratios, it is often related to the term Wl/d, in which W is the weight percent of the fiber and l/d the aspect ratio [8]. While the aspect ratios of long-length plant-based fibers such as pine pulp are at least 200, the aspect ratio of hardwood fiber is only about 40 to 50. Then, a large amount of hardwood fiber would be necessary to efficiently improve the flexural strength of mortar, which may not lie within the studied range (0 to 1% by volume of fiber). Moreover, for a large amount of fiber inclusion, the mix characteristics tend to become unsatisfactory as a result of inadequate workability and dispersion of fiber, so the non-traditional method of mortar casting (e.g., Hatschek or dewatering) should be employed to maximize the amount of pulp while minimizing void content in the composite. Since this study relied on traditional methods of casting, short lengths of fiber, and small fractions of volume (i.e., less than 2%), the effect of the wood fiber is particularly small before cracking, so no clear contribution can be shown, as in [172]. Therefore, The effects of voids or other pre-existing flaws (e.g., fiber clumps), which result from a decrease in workability likely overshadows any benefit of fiber reinforcement; similar results showing decreases in flexural strength for cast-in-place mortars with longer softwood fibers were found by [118].

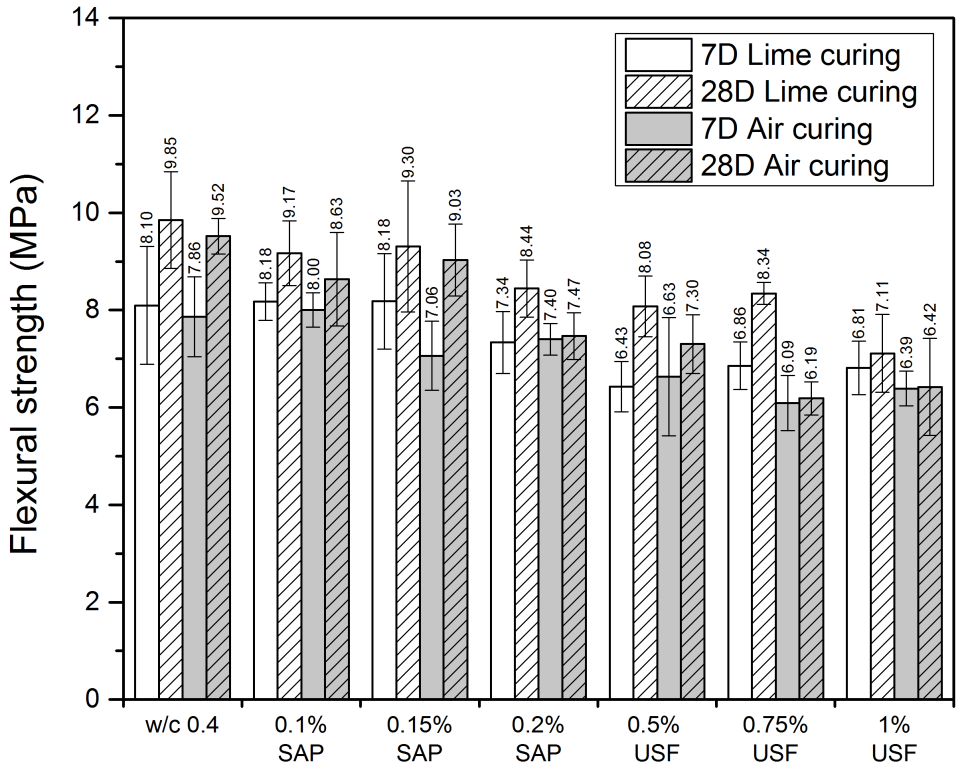

Figure 6.9 – Flexural strength of mortar in lime-water curing and 60% RH curing.

Since the most significant contribution of fiber-reinforcement in concrete or mortar with low to moderate fiber content (i.e., volume fractions of up to 2 percent of fiber) is not to strength but to flexural toughness [12], post-cracking toughness has also been assessed through flexural testing, as shown in Figures 6.10 and 6.11. Although the addition of hardwood fiber within the studied range did not enhance the flexural strength of the mortar, increased toughness was apparent. Figure 6.10 illustrates typical load-midspan deflection curves of USF-reinforced and unreinforced mortar. For SAP-blended and plain mortar, the load rose in a fairly linear manner to a peak value and dropped sharply. For USF-reinforced mortar, the initial behavior was linear, but after the first crack, a sudden load reduction occurred; the load, however, did not approach zero because fibers provided post-cracking ductility. This finding indicates that eucalyptus

fiber may also bridge cracks and potentially improve cracking behavior. All of the tested fiber-reinforced specimens exhibited post-cracking softening behavior in which the strength of the first crack was the peak strength. From Figure 6.11, the flexural toughness of mortar at 28 days increased by about 0.2 to 0.45 kJ/m^2 as fiber volume fraction increased from 0.5 to 1%, respectively. It is also noteworthy that the toughness of mortar cured in air was about 0.5 kJ/m^2 higher than limewater curing, as will be considered in greater detail subsequently. From Figure 6.11, the addition of SAP had slight effect on the post-cracking toughness, but the effect was very small when compared to the USF case, so that it was considered negligible.

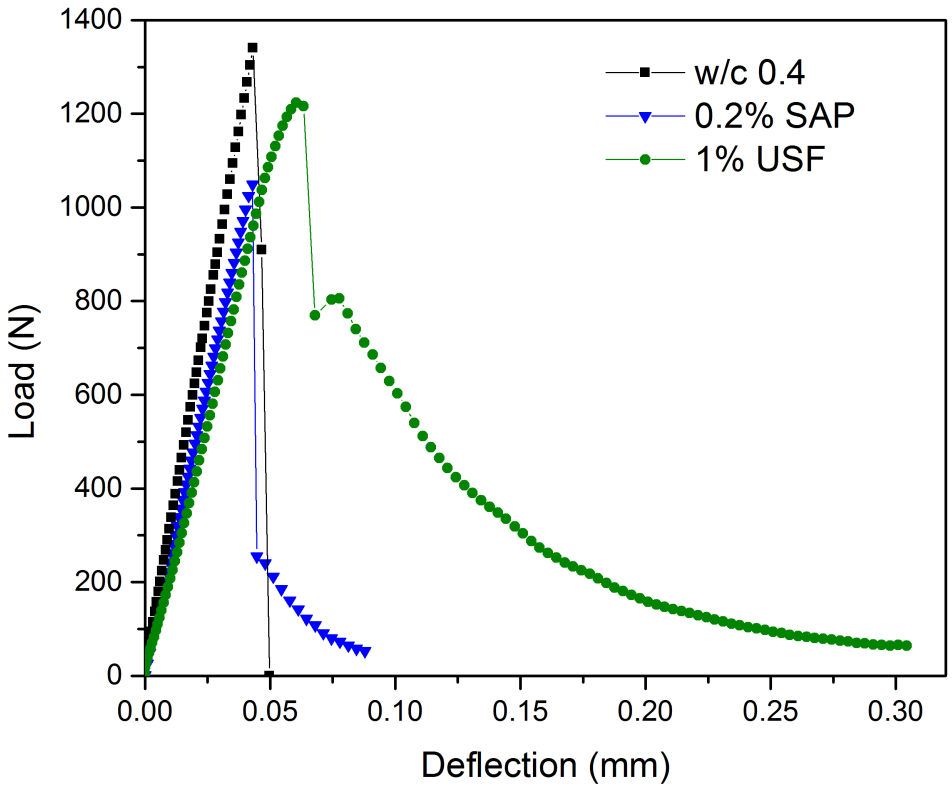

Figure 6.10 – Typical load-deflection curves for USF-reinforced mortar compared with those of SAP-blended and plain mortar.

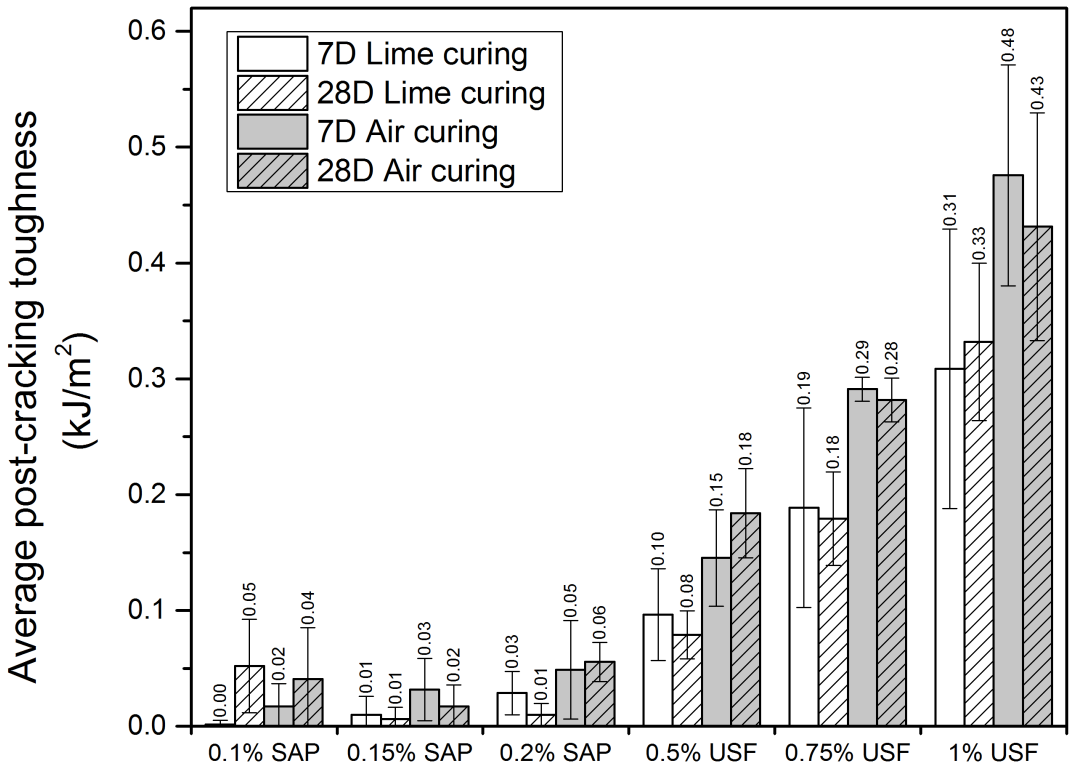

Figure 6.11 – Post-cracking flexural toughness of USF-reinforced mortar and SAP-blended mortar. Note that the post-cracking toughness of the unreinforced control mortars is effectively zero and that of SAP-blended mortar is small so that it can be considered negligible.

These observations generally support prior findings that the inclusion of plant-based fibers can improve the toughness of cementitious materials, with toughness generally increasing with increasing fiber addition rate coupled with well-dispersed reinforcement [58, 172, 173]. These results also show that although eucalyptus pulps are short, like longer fibers, they improve toughness by bridging cracks and undergoing a pull-out process, as demonstrated in Figure 6.12.

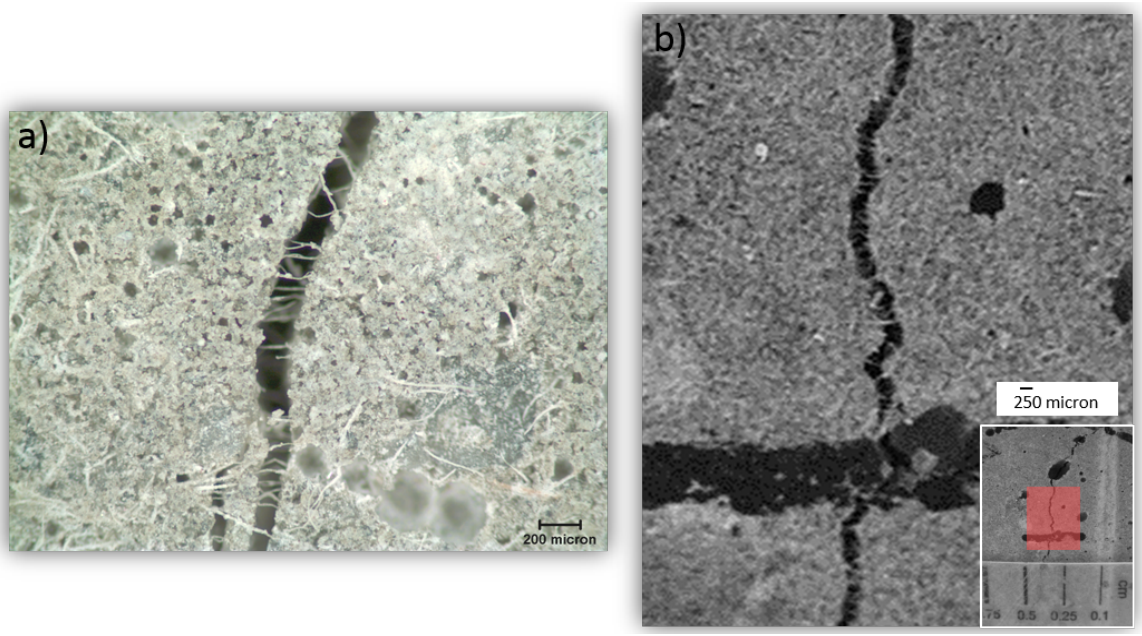

Figure 6.12 – a) Optical micrograph of a crack arresting and bridging in a USF-reinforced mortar after the bending test and b) photograph of a crack in a 0.75%USF restrained ring specimen.

As shown in Figure 6.11, fiber-cement mortars which experienced internal curing were significantly tougher than those cured in limewater. The values of the flexural toughness of mortar cured in air with fiber volume fractions of 0.5, 0.75, and 1% were 0.18±0.04 kJ/m^2, 0.28±0.02 kJ/m^2, 0.43±0.10 kJ/m^2, respectively, while that of mortar cured in limewater were 0.08±0.02 kJ/m^2, 0.18±0.04 kJ/m^2, and 0.33±0.07 kJ/m^2, respectively. This behavior may be related to the influence of curing conditions on the fiber-matrix interface. As reported by Bentur and Akers [174] and Akers and Studinka [175], if the microstructure at the interface between the fiber and cement matrix is dense, representing good bonding, it will result in high strength but low toughness of the cellulose fiber-reinforced composites because of the high extent of fiber failure by fracture rather than by pullout. Although their conclusions are based on a comparison of

air curing and autoclave curing, conceptually they are useful in assessing these data, as similar trends (e.g., higher strength/lower toughness and vice versa) were observed here.

6.3.4 Microstructural Characterization

To better understand the effects of fiber reinforcement and internal curing on shrinkage mitigation, surfaces of fractured mortar samples – both internally cured (i.e., air cured) and limewater cured – were examined using a variable pressure scanning electron microscope (VP-SEM, Hitachi S-3700N). Images were taken immediately following the flexure tests.

Figure 6.13 presents a pair of SEM micrographs of USF-reinforced mortar, showing differences in fracture features for the two curing conditions examined. Dots show fiber failures, and crosses indicate fiber-cement interfaces. For the limewater cured mortar, not only was fiber pullout seen, but fiber breakage and the separation between the primary and secondary cell walls was also clearly observed (in Figure 6.13a). These features, related to energy absorption through fiber damage, are indicative of a stronger bond between the fiber and cement in the case of limewater curing. The fiber/cement interface, shown in Figure 6.13b and indicated by a cross mark, appears denser. In contrast, for the internally cured mortar, shown in Figures 6.13c and 6.13d, hydration products are apparent on the surface of the fiber.

The decrease in bonding between the fiber and matrix in the air-cured mortars likely results from the change in fiber cross-section as a result of drying. The images further suggest that the region around the fibers is perhaps weaker or more porous than in the limewater cured samples, where the fiber surfaces are relatively free of

mineralization. The decreased physical bonding is also suggested by the reduced amount of fiber fracture with internal curing than that of limewater curing.

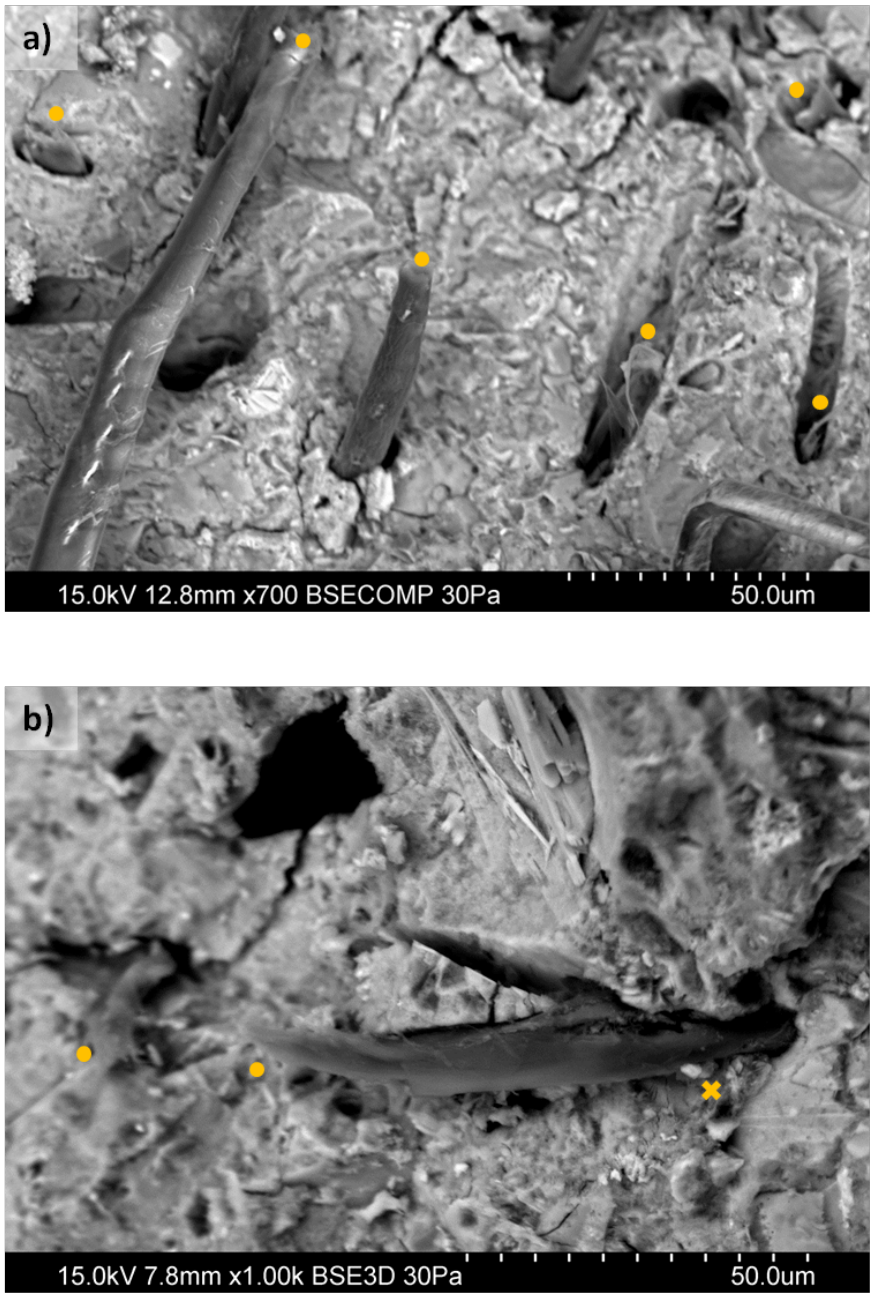

Figure 6.13 – VP-SEM images of the fracture surface of USF-reinforced mortar samples tested at 28 days a), b) limewater curing, and c), d) air curing.

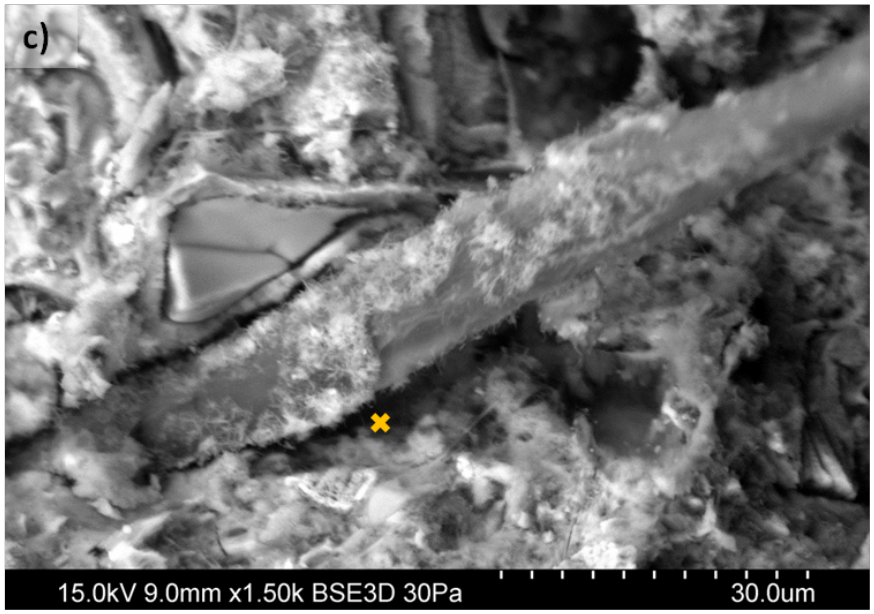

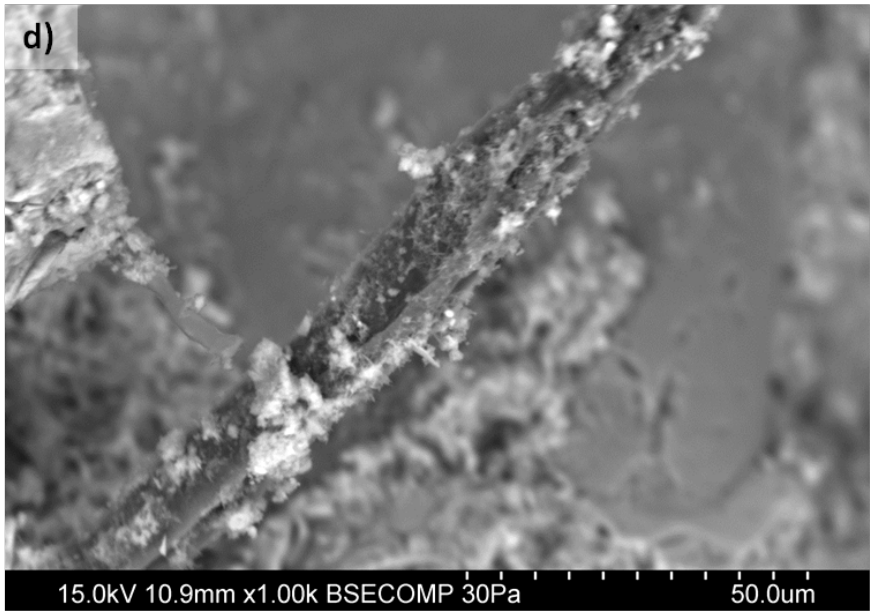

Figure 6.13 – VP -SEM images of the fracture surface of USF-reinforced mortar samples tested at 28 days a), b) limewater curing, and c), d) air curing. (Continued)

6.4 Discussion

The effect of fiber-matrix adhesion or bond strength on the mechanical performance of fiber-cement composites [119, 120, 176, 177], as well as composites in general, is a topic of great interest and importance. Based upon prior work, an abrupt reduction in the toughness of the composite with the progressive improvement of the fiber to matrix adherence is expected. The bonding across the interface can significantly affect the toughness of a composite. In a brittle matrix, a stronger interfacial bond will result in higher strength, but it may lead to lower fracture energy absorption and thus lower toughness [178].

In the case of the USF reinforced mortars, with wet curing, a strong bond is maintained between the fiber and the interface, resulting in relatively higher strength but lower toughness compared to the air-cured mortars. In the air-cured USF mortars, fiber collapse along with slight cell wall shrinkage leaves a weaker interfacial bond which will dissipate more energy than a strong interfacial bond found in limewater curing. This results in the greater post-cracking toughening apparent when comparing the two curing cases for USF mortars.

Overall, however, these results point to several key behaviors which ultimately result in the improved resistance to early-age cracking observed in the restrained shrinkage test for the USF fiber cases. In addition to the ancillary effect of internal curing on the fiber/cement bond strength and composite toughening, the internal curing afforded by the fibers mitigates autogenous shrinkage, apparently more effectively than the SAPs examined. As a result, tensile stresses induced are mitigated. This is then further compounded by apparent beneficial alterations in mechanical properties due to the

presence of the fibers, including an increase in early tensile strength and an increase in compliance in the USF-reinforced mortars. Thus, despite greater mass loss, hardwood fiber mortars display greater resistance to early shrinkage cracking through a combination of internal curing and mechanical reinforcing effects.

6.5 Conclusions

The early-age cracking of mortar and concrete relies on the development and the distribution of tensile stresses, the degree of restraint, the evolution of mechanical properties, and stress relaxation. Since cracking occurs when the combination of the elastic modulus and the shrinkage strain result in a stress state that exceeds its tensile capacity [12], the mechanical properties of mortar and concrete – both the elastic modulus and the tensile strength – are the most significant parameters in the control of cracking. After mortar sets, these parameters are critical at early ages when the mix is immature, shrinkage rates are high, and tensile capacity is developing. A series of experiments clarifies the role of hardwood eucalyptus pulp in the mitigation of early-age cracking by the combination of the increase of early tensile capacity, the reduction of a modulus, and the improvement of post-cracking toughness, all of which mitigates the early-age cracking.

From this study, the inclusion of hardwood eucalyptus pulp influences mortar mechanical properties in several ways while also providing internal curing, ultimately leading to better improved early crack mitigation than the use of SAP at the same entrained water content. The effects of short fiber are summarized as follows:

- Overall, USF pulp has shown to mitigate early-age cracking in restrained mortar. The 0.5% and 0.75% USF-reinforcement extended the time-to-

cracking in mortars by about 1.6 and 2.3 times as compared to the plain mortar, respectively.

- The inclusion of USF reduces the mortar cracking potential at early ages because the greater extensibility provided, along with contribution from stress relaxation and stress transfer to the fibers, which combine to enhance the early tensile capacity of USF-reinforced mortar.
- In addition, despite their short length, USF improves post-cracking toughness of mortar. Microstructural evaluation has also linked the improved toughness to microscale damage at the fiber/cement interface induced during internal curing.
- The addition of USF confines the initial crack width to a size below which self-healing is possible in appropriately designed cementitious matrices. The initial crack width was decreased by 88% in 0.75%. USF reinforcement.

Considering that eucalyptus fibers provide additional tensile capacity and toughness at early ages as well as internal curing capacity which mitigates autogenous shrinkage, these fibers can mitigate early-age crack. In particular, this approach may be especially beneficial in a system with a high cement content and a relatively high rate of drying, where the highest tensile stress-to-strength ratios are exhibited at early ages. Ultimately, the internal curing performance, the early-age enhancement, the extensibility improvement, and the effective crack-bridging of eucalyptus pulp confirm its potential as effective reinforcement in a wide range of fine-structured cementitious composites such as stucco, plaster, and thin overlays, all of which are prone to early-age cracking.

CHAPTER 7

THE EFFECTS OF EUCALYPTUS PULP ON CONCRETE PROPERTIES

7.1 Introduction

While increases in compressive strength due to internal curing might be expected due to enhanced early cement hydration, instead reductions in the compressive strength of cementitious composites with internal curing have been reported [179-181]. For example, when being used as internal curing agents, pulp-based fibers have been shown to reduce compressive strength in cement pastes containing fiber [9], but results are not based on fiber-reinforced concrete. Independent of their potential for internal curing on compressive strength, reductions in compressive strength of pulp fiber-reinforced cementitious composites can result from increased air content, likely due to reduced workability, and their potential to clump, acting as pre-existing flaws. While several studies have reported a significant loss in compressive strength as the fraction of the fiber volume increases [58, 182-184], some have reported little or no significant gain in compressive strength with the addition of a small amount of fiber of as much as 1.2 percent by volume [89, 172, 185]. Since the amount of fiber required for the internal curing application in concrete should not exceed one percent by volume of concrete, the use of pulps for the internal curing application should reduce the compressive strength of concrete only slightly or not at all.

Similarly, a recent publication pertaining to the influence of superabsorbent polymers (SAP) on the compressive strength of concrete has clearly mentioned two opposite mechanisms: an increase in the number of voids (which will decrease strength) and an increase in the degree of hydration (which should enhance strength) [38]. Therefore, to minimize the reduction in compressive strength, the use of SAP in concrete can be optimized by balancing the effect of air voids with the degree of hydration, which implies that the reduction in the compressive strength of internally cured concrete may be eliminated by increasing the degree of hydration. Applying this concept to internal curing with pulp fibers, the use of hardwood pulps as internal curing agents may offer benefits over longer softwood pulps, which are more prone to clumping.

Several studies have demonstrated the benefits of uniformity dispersion on shrinkage and mechanical properties of cementitious composites [11, 186]. Recent studies have demonstrated the benefits of hardwood eucalyptus pulps in cementitious composites that result from the uniformity in the volumetric dispersion of fibers in the matrix [5]. The number of eucalyptus fibers per unit mass is always much higher than, and up to seven or eight times as high as, that of softwood fibers [187]. This higher number of fibers per unit mass contributes to higher specific surface areas [188] that may serve as nucleation sites for hydrating cement and result in a higher strength gain. Therefore, eucalyptus pulp's reinforcing capacity combined with its internal curing performance could offset potential losses of compressive strength caused by the addition of fiber, which could be further compensated for at early ages by increases in the rate of cement hydration due its high number of nucleation sites [189]. The relative short fiber

length (i.e., low aspect ratio) of eucalyptus fibers compared with softwood pulps also reduces the potential for fiber clumping and entanglement.

If the compressive strength of pulp-fiber reinforced concrete can be made adequate, it is also important to understand the implications of this internal curing strategy on long-term performance. Several studies have shown the effects of pulp fibers on the durability of concrete [190-192]. Although cellulose fibers have also been found to reduce the permeability to water, and based upon those results it was calculated that chloride ion diffusion coefficient would also be decreased. However, it should be realized that cellulose-based fibers, unlike polymer and steel fibers, are hygroscopic and also are semi-permeable membranes, properties which may affect the migration of moisture and, ultimately, ions in concrete.

Furthermore, in general, standards recommend that test samples be stored in lime-saturated water or water. As a result, prior examinations of transport in such composites, which have relied upon standard tests, have excluded the effect of drying and internal curing that may alter the microstructure of concrete. That is, results based solely on fully cured specimens, as presented in [193, 194], may not represent actual in-service concrete, where pulp fibers are used for internal curing.

This chapter explores the concept that the use of a proper type of pulp fiber, or hardwood eucalyptus pulp as in this study, at a proper dosage as an internal curing agent should preserve the compressive strength of internally cured concrete. Therefore, one aim is to evaluate the effect of hardwood pulp as an internal curing agent on the compressive strength of concrete. The results of internally cured pulp-cement concrete are compared with those of SAP-blended concrete with the same amount of entrained water. Moreover,

to further elucidate the use of hardwood pulp in concrete, if hardwood pulp-reinforced concrete does not exhibit a significant reduction in compressive strength, the transport properties of the composite are also determined. These results allow users to optimize the application of hardwood pulps in concrete structures to achieve both adequate strength and long-term durability.

7.2 Materials and Methods

7.2.1 Materials

The wood pulp used in this study was conventional unrefined unbleached eucalyptus kraft pulp fiber (UKF) collected from a commercial kraft pulping process in Southeast Asia. The as-received pulp moisture content (dry basis) was 402%, according to the ASTM D4442-07 standard [98]. The apparent specific gravity of dry pulp was assumed at 1.5 g/cm^3 [172]. Since the UKF was chemically treated, it was high in cellulose and low in lignin. The kappa number of the UKF used in this study was 25, which was equal to a total residual lignin content of 3.82 percent.

The superabsorbent polymer was a cross-linked acrylamide/acrylic acid copolymer, the most predominant type of SAP used for internal curing [44]. The SAP (Watersorb®), in powdered form, was added to dry cement prior to mixing. The absorption capacities of UKF and SAP, determined by a consistent method used in [97], were 2 and 10, respectively [139]. The absorption capacity of SAP was close to that found in [154], in which the absorption capacity was determined by the measurement of chemical shrinkage.

Concrete samples were prepared using commercially available portland cement ASTM C150 Type I/II (Lafarge, North America), natural siliceous sand with fineness modulus of 2.4 (Atlanta, Georgia, USA), #67 crushed granite coarse aggregate (Cartersville, Georgia, USA), and tap water. The absorption capacities, the moisture contents, and the specific gravities at the saturated surface dry (SSD) condition of the natural sand and the crushed granite were 0.87% and 0.58%, 0.02% and 0.20%, and 2.5 and 2.65, respectively. The dry rodded unit weight of the crushed granite was 1,570 kg/m^3 (98 lb/ft^3.) The oxide analysis of cement was performed by x-ray fluorescence (XRF, Bruker AXS S8 Tiger) spectrometry and the crystalline phases of cement were determined by performing quantitative x-ray diffraction analysis (QXRD, Bruker AXS D4 Endeavor) with the Rietveld method using TOPAS software. The oxide composition of the cement was (percentage by mass) 19.73% SiO_2, 4.82% Al_2O_3, 3.16% Fe_2O_3, 62.41% CaO, 3.64% MgO, 2.99% SO_3, 0.08% Na_2O, 0.48% K_2O, and 2.27% LOI. The crystalline phase composition of the cement was (percentage by mass): 52.6% alite, 20.7% belite, 3.7% aluminate, 11% ferrite, 0.1% lime, 2.3% portlandite, 2.6% periclase, 0.6% arcanite, 0.4% aphthitalite, 0.9% gypsum, 2.4% bassanite, and 2.7% calcite. To enhance the workability of the concrete mixes, a high efficiency polycarboxylate-based superplasticizer (ADVA140 from WR Grace), was added at various dosages to obtain 7-10 cm (approximately 3-4 in) slump of concrete.

Concrete samples were mixed at a water-to-cement ratio (w/c) of 0.30 and 0.40, according to mix designs shown in Table 7.1. While the mix design of the concrete with w/c of 0.30 was proportioned according to the ACI211.4R-93 procedure, that of concrete with w/c of 0.40 was proportioned according to the ACI211.1-91 procedure. The masses

of water for the concrete samples that contained internal curing agents were adjusted to account for the amount of the water available for internal curing, to maintain a constant "entrained water"-to-cement ratio (w_e/c) of 0.02. The amount of entrained water depends on the amounts of USF and SAP in the mortar as well as the intrinsic properties of these agents [40, 44, 127].

Table 7.1 – Base mixture proportion of concretes on an oven-dry basis (kg/m^3).

Mixture notation	**OPC**	**Water**	**IC water[2]**	**Coarse aggregate[1]**	**Fine aggregate[1]**	**UKF[1,3]**	**SAP[1]**
w/c 0.3	564	169	-	1130	513	-	-
UKF 03	564	169	11.3	1130	513	5.65	-
SAP 03	564	169	11.3	1130	513	-	1.13
w/c 0.4	468	187	-	1035	634	-	-
UKF 04	468	187	9.36	1035	634	4.7	-
SAP 04	468	187	9.36	1035	634	-	0.93

[1] The weights of the coarse aggregate, the fine aggregate, the UKF, and the SAP are oven-dry weights.

[2] Internal curing water (IC water) does not participate in the lubrication of the mix. Therefore, IC water is treated as an addition to mixing water.

[3] The volume fractions of the UKF added to the concrete mixes with a w/c of 0.30 and 0.40 were 0.38 and 0.31 percent, respectively.

7.2.2 Mixing and Curing Methodology

Concrete was mixed in an 85-liter capacity high shear mixer (Eirich Model R 08 W). Dry ingredients were first mixed at 150 rpm for two minutes. Water was then added slowly to the dry premix over a period of two minutes. Then, the mixing speed was raised to 300 rpm and allowed to mix for two minutes. The slump of concrete was then tested, and, if required, the superplasticizer was added to adjust the slump, and the concrete was mixed for another three minutes. For fiber-concrete mixes, the UKF was dispersed in the mixing water at 120 rpm prior to the mixing.

After mixing, the concrete samples were cast in 76.2x152.4 mm (3x6 in) and 101.6x203.2 (4x8 in) cylinder molds for compressive strength and chloride permeability tests, respectively. The samples were compacted in three layers, each tamped 25 times using a compacting rod. These cylinders were demolded at 24 hours and kept in two curing conditions until the time of testing. While the specimens for water curing were placed in a lime-saturated tank at 23±2°C (73.5±3.5°F), those for air curing were placed on open shelving in laboratory conditions, where the temperature averaged 23±2°C (73.5±3.5°F) and the relative humidity averaged 45±5%.

7.2.3 Test Methodology

The compressive strength of concrete was measured at 1, 3, 7, 14, 28, and 56 days. Using a hydraulic compression-testing machine with a load rate that corresponded to a stress rate of 0.25±0.05 MPa/s (35±7 psi/s), the test was conducted in compliance with the ASTM C39-14 [195] standard on 76.2x152.4 mm (3x6 in) cylinders.

In a series of experiments, the effects of the inclusion of UKF and SAP on the resistance of concrete to chloride ingress were determined. The concretes were evaluated by ASTM C1202-12 [196] to assess their rapid chloride ion permeability at 56 days of age on two 50.8 mm (2 in.) thick slices of 101.6 mm (4 in.) diameter concrete cylinders. In addition, the surface resistivity of the limewater curing samples was also nondestructively monitored by a 38 mm (1.5 in) 4-point Wenner probe (Resipod, Proceq) according to ASSHTO TP 95-11. Finally, the bulk diffusion test (ASTM C1556-11 [197]) was performed on the concrete samples with w/c of 0.30. After curing for 180 days, the specimens were cut, their surfaces and the bottoms were sealed with silicone sealant, and they were placed in a limewater bath. After their mass stabilized, they were

placed in a 165 g/L sodium chloride solution for 90 days. After this exposure period, profile grinding was performed on the sample, and the total chloride concentration of each 2 mm (0.079 in) increment was determined according to ASTM C1152-04 (2012) [198]. To determine an apparent diffusion coefficient D_a (m^2/s), the results were analyzed by performing a non-linear regression analysis fitting to the equation of diffusion in concrete, shown in Eq. 7.1, in which known parameters were the chloride concentration of concrete (C (x,t), %), the surface chloride concentration of concrete (C_s, %), the initial chloride concentration of concrete (C_0, %), depth below the exposed surface (x, m), the exposure time (t, s), and the error function (erf).

$$C(x,t) = C_s - (C_s - C_0) \cdot erf\left(\frac{x}{\sqrt{4 \cdot D_a \cdot t}}\right) \qquad \text{Eq. 7.1.}$$

7.3 Results

7.3.1 Compressive Strength of Concrete

Figures 7.1, 7.2, and Table 7.2 present the evolution of the compressive strength of concrete samples with and without internal curing agents, examining two curing conditions (curing in limewater vs. curing in air). For samples cured in limewater, where internal curing effects would be minimized, strengths were similar for the control and UKF concrete at most of all ages, but the addition of SAP produced lower strength. This reduction in compressive strength was more notable in w/c 0.30 concrete mixes than in w/c 0.40 concrete mixes, as about 20% and 10% reductions were found at 56 days in SAP concrete mixes with w/c of 0.30 and 0.40, respectively. Similar severe strength reduction of SAP concrete has been reported in [199] while the increase in compressive strength in

cellulose fiber-reinforced concrete has been reported in [185]. Likely, the variation in strength is related to stress concentrations resulting from these inclusions, which are relatively larger for the SAP, particularly since good dispersion of the fibers was achieved. As the 1 day strength was significantly lower than that of the control sample, it is also possible that some delay in hydration reaction occurred in UKF concrete with w/c of 0.30. However, the compressive strength of UKF 03 concrete at 3 days and beyond was comparable to that of the w/c 0.30 concrete.

In this study, the compressive strength of concrete cured in open-air conditions is used to probe the efficiency of internal curing with USF and SAP at increasing degree of hydration.[‡‡] First, from Figures 7.1 and 7.2, as expected, the curing conditions had a significant effect on the compressive strength of concrete, especially in concrete with w/c of 0.40. Concrete samples with w/c of 0.40 exhibited a greater reduction in strength than concrete samples with w/c of 0.30 when comparing limewater and air curing. The reductions of compressive strength at 56 days were about 31 and 17 percent for concrete samples with w/c of 0.40 and 0.30, respectively. As no significant strength gain appeared in both w/c 0.30 and w/c 0.40 concretes, the benefit of internal curing at increasing the degree of hydration by using SAP was not apparent during this test period.

However, while internal curing did not appear to benefit strength for concrete mixes at w/c of 0.30, its effect was noticeable in the UKF concrete with w/c of 0.40. At w/c of 0.30, the strength of UKF concrete specimens was similar to that of the control.

[‡‡] Due to the hygroscopic nature of wood pulps, one may be concerned that the moisture state of a sample at the time of test might affect its compressive strength. However, at the fiber volume fraction of up to 2 percent, El-ashkar et al. [161] have reported no clear differences between the compressive strength of wood pulp-cement mortar samples tested in wet or air-dry conditions. Therefore, in this study the effect of testing condition on the compressive strength of UKF concrete should be minimal and the test results should reflect the effects of curing on the compressive strength of such concrete.

However, at w/c of 0.40, UKF concrete exhibited the higher strength, approximately up to 11 percent, than that of the control, as shown in Figure 7.3.

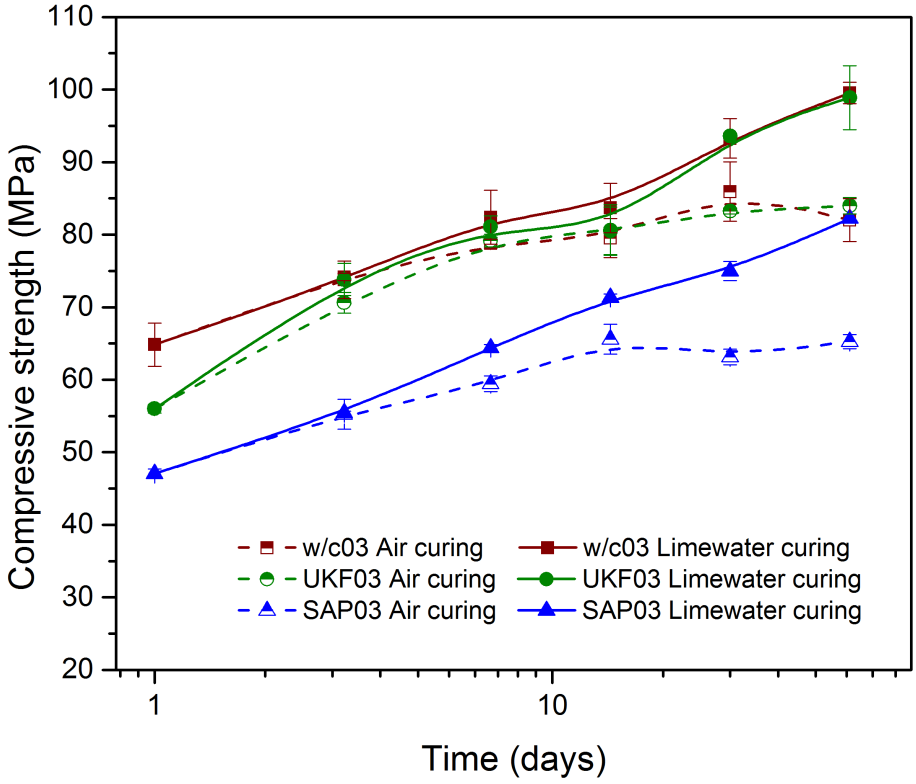

Figure 7.1 – Effects of UKF and SAP on the development of compressive strength of concrete with w/c of 0.30.

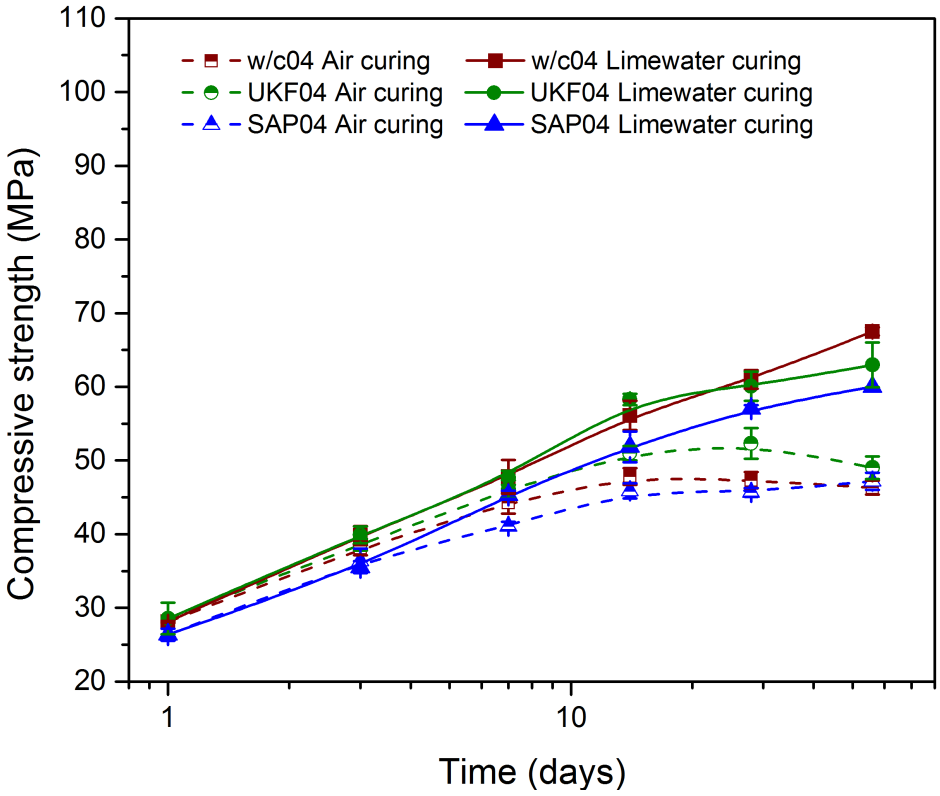

Figure 7.2 – Effects of UKF and SAP on the development of compressive strength of concrete with w/c of 0.4.

Table 7.2 – Compressive strength of concrete samples.

	Time (d)	Compressive strength (MPa)		Ratio to lime cured f_c (%)	Strength gain (%)			Time (d)	Compressive strength (MPa)		Ratio to lime cured f_c (%)	Strength gain (%)	
		Lime cured	Air cured		Lime cured	Air cured			Lime cured	Air cured		Lime cured	Air cured
w/c 0.3	1	64.85	64.85	100.00			w/c 0.4	1	28.10	28.10	100.00		
	3	73.78	74.17	100.53	13.78	14.38		3	39.82	38.13	95.75	41.71	35.69
	7	82.40	78.77	95.60	27.08	21.48		7	47.78	44.27	92.65	70.03	57.54
	14	83.68	79.54	95.06	29.04	22.66		14	56.11	47.83	85.26	99.65	70.22
	28	93.27	85.94	92.14	43.84	32.53		28	60.98	47.31	77.59	117.01	68.37
	56	99.53	82.01	82.40	53.49	26.47		56	67.50	46.31	68.61	140.19	64.80
UKF 03	1	55.99	55.99	100.00			UKF 04	1	28.56	28.56	100.00		
	3	73.82	70.62	95.67	31.85	26.13		3	39.90	38.57	96.68	39.71	35.06
	7	81.10	79.18	97.63	44.85	41.42		7	47.65	46.12	96.78	66.85	61.48
	14	80.63	80.53	99.87	44.02	43.83		14	58.29	51.01	87.51	104.10	78.60
	28	93.60	83.26	88.95	67.18	48.71		28	60.09	52.31	87.06	110.38	83.15
	56	98.89	83.99	84.93	76.63	50.01		56	62.97	49.02	77.85	120.49	71.65
SAP 03	1	47.05	47.05	100.00			SAP 04	1	26.36	26.36	100.00		
	3	55.46	55.24	99.61	17.86	17.39		3	35.53	36.37	102.36	34.80	37.98
	7	64.40	59.43	92.29	36.87	26.31		7	45.34	41.10	90.65	72.02	55.93
	14	71.32	65.57	91.94	51.58	39.36		14	51.87	45.86	88.42	96.79	73.99
	28	74.99	63.15	84.22	59.37	34.22		28	57.07	45.68	80.04	116.53	73.30
	56	82.25	65.26	79.35	74.79	38.70		56	60.00	47.18	78.64	127.66	79.03

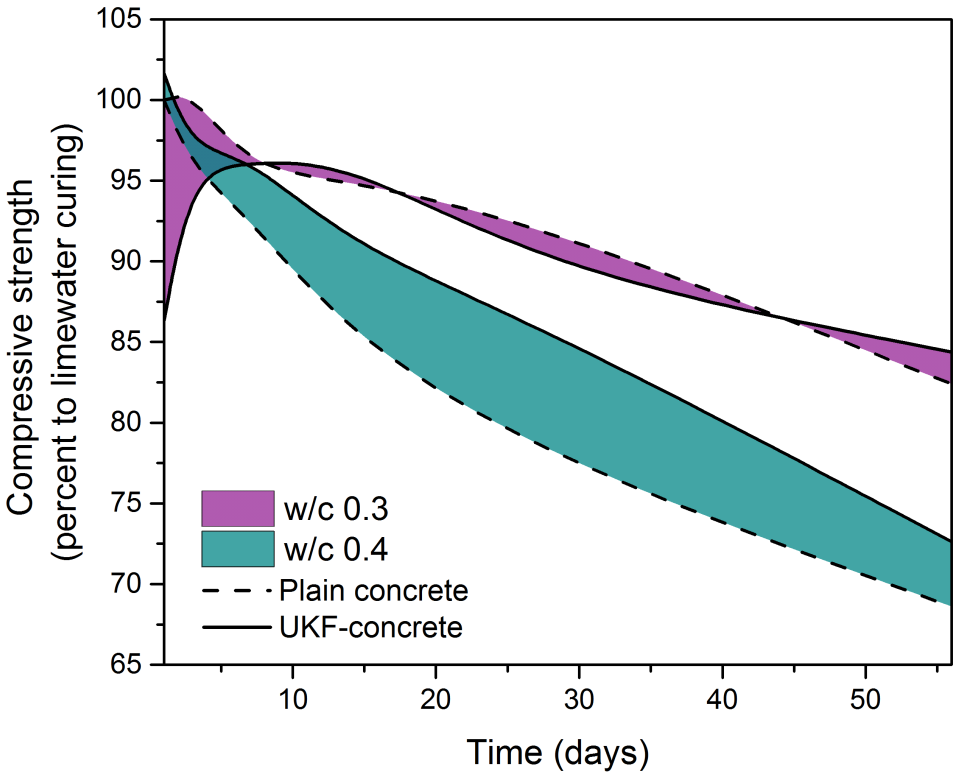

Figure 7.3 – Effects of internal curing provided by UKF on the compressive strength of concrete with w/c of 0.30 and 0.40 as percentage of the compressive strength of control concrete specimens cured in limewater.

Since samples underwent both self-desiccation and drying, the effectiveness of internal curing at increasing degree of hydration might not be apparent. Discussions in previous paragraphs are based on the comparison of the compressive strength of internally cured samples with that of the control sample. However, if we focus on the development of compressive strength after 1 day of age, the results may indicate the effects of curing condition, water-to-cement ratio, and internal curing on the hydration of cement. Table 7.2 presents the ratio of the compressive strength of air cured samples to that of the limewater cured sample (%), and the strength gain of both air cured samples and limewater cured samples (%). As the ratio of the compressive strength of air cured samples to lime water cured samples at w/c of 0.30 are similar, the table confirmed that

the internal curing seems not to benefit strength for concrete mixed with w/c of 0.30. However, since the ratio of the compressive strength of air cured samples to lime water cured samples with w/c of 0.40 are different, the internal curing efficiency of UKF appears to be more effective. At 28 days, the ratios of the compressive strength of air cured samples to that of the limewater cured samples of w/c 0.4, UKF 04, and SAP 04 were about 77%, 87%, and 80%, respectively. After 1 day of age, the development of strength of concrete samples with nominal w/c of 0.40 was better than that of concrete samples with nominal w/c of 0.30, which suggests the effect of a curing condition on the hydration of cement.

Giving that the hydration reaction of cement paste ceases at an internal relative humidity below 80% [200], this perhaps indicates that, for concrete sample with w/c of 0.40, while undergoing air curing, the hydration reaction of UKF-concrete samples proceeded continuously since a higher internal RH was maintained in the specimens. The behavior was also observed in SAP concrete, in which, at w/c of 0.40, the difference of compressive strength between SAP concrete samples and control samples cured in air was lower than that of the samples cured in limewater, as shown in Figure 7.2. Also, at w/c of 0.30, neither the UKF nor SAP concretes exhibited higher compressive strength than control concrete specimens during air curing. It can only be assumed that this is due to inadequacies in the amount of entrained water or the quality of the internal curing in w/c 0.30 concrete samples. From Figure 7.1, it is clearly seen that the strength development occurred quite rapidly at very early age, suggesting that a higher amount of w_e/c than 0.02 is required for concrete at w/c of 0.30 during air curing at 45% RH.

7.3.2 Resistance to Chloride Ingress

Recent studies have demonstrated that supplementary cementitious materials (SCMs) can be used to overcome concerns surrounding potential degradation of wood fibers in cement-based composites [201], providing more confidence in the durability of pulp-fiber reinforced concrete. But, the issue of permeability and chloride ingress – and the potential role (if any) – of the fibers in transport must also be considered.

Recent studies on permeability of pulp fiber-reinforced concrete have suggested that the permeability pulp fiber-reinforced concrete, both in the unstressed and stressed states, is lower than that of plain concrete [191, 192]. Another study has further demonstrated that cellulose fibers bind with chloride ions, which reduces the amount of free chloride in concrete, and thus corrosion of embedded steel is delayed [194]. However, most of the samples in these studies pertaining to permeability of concrete were moist cured in lime-saturated water, which might not simulate the actual curing conditions in the field. Since cellulose-based fibers are hydrophilic, their properties depend on moisture state and also moisture history. Therefore, in this study, to elucidate the effects of moisture history (i.e., curing condition) on the permeability of pulp-reinforced concrete, a series of standard tests to indirectly assess permeability and the resistance to chloride ingress were performed.

Figure 7.4 shows the development of surface resistivity of concrete while experiencing limewater curing. According to AASHTO TP 95-11 [202], the surface resistivity results, in this study, fall in the low, moderate, and high categories. While the w/c 0.30 concrete exhibited the highest surface resistivity at about 25 kOhm-cm, the UKF04 concrete exhibited the lowest at a surface resistivity of about 9 kOhm-cm. The

addition of UKF and SAP led to a decrease in surface resistivity at both w/c. Neglecting any potential effects of internal curing of pore solution composition. Since surface resistivity is inherently related to the electrical conductance (or resistance) of concrete [203], the lower surface resistivity values of both UKF and SAP concrete indicate greater connectivity in the flow path for electrical current than in plain concrete. The reductions in surface resistivity suggest that SAP particles (or resulting void space) and fibers might act as an interconnected flow path for electricity.

The evolution of surface resistivity of mortar samples, containing either SAP or eucalyptus pulp, was monitored, as shown in Figure 7.5. All mortar samples were produced at a sand-to-cement volume ratio (s/c) of 1.5 and had the same nominal w/c of 0.40 but different amount of entrained water. These were obtained by varying the amount of fiber used (i.e., 0.5%, 0.75%, and 1% by volume of the original mix) or the amount of SAP (i.e., 0.1%, 0.15%, and 0.2% by weight of cement). For both the USF and SAP mortars, these are then equivalent to entrained water-to-cement ratios of 0.01, 0.015, and 0.02, respectively. All samples were cast in 101.6x203.2 (4x8 in) cylinder molds and cured in limewater.[§§]

[§§] Since the surface resistivity measurement requires a surface to be saturated or conditioned to nearly saturated for a good correlation between concrete resistivity and chloride diffusivity [204], we did not perform the test on air-cured specimens.

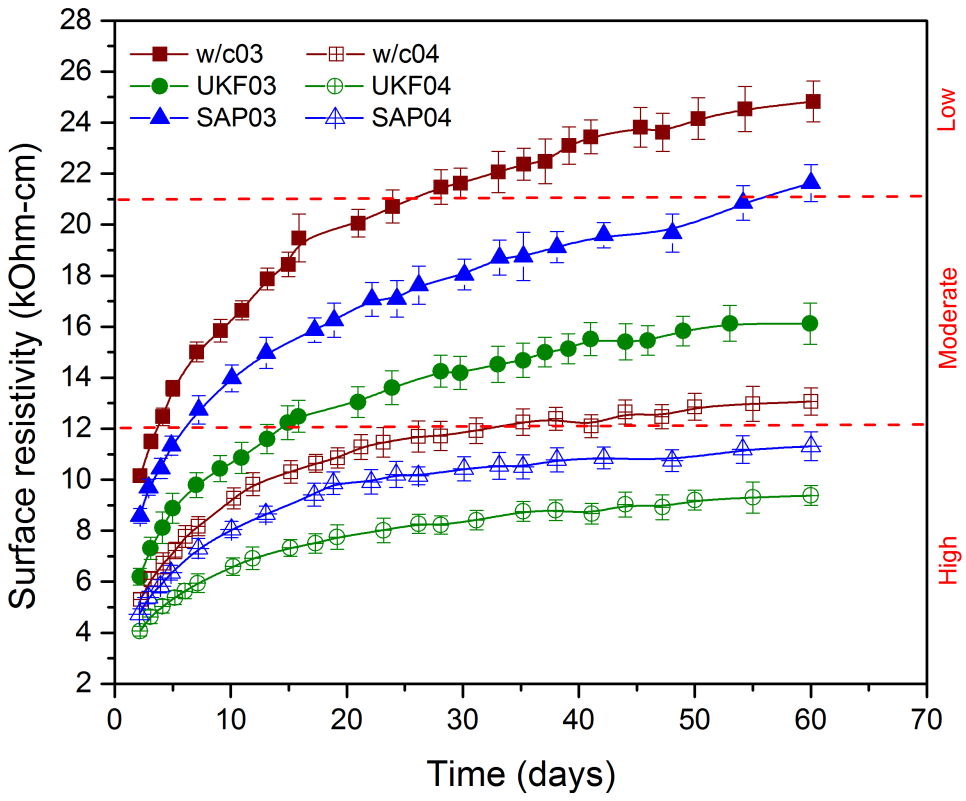

Figure 7.4 – The development of surface resistivity of limewater cured concrete specimens.

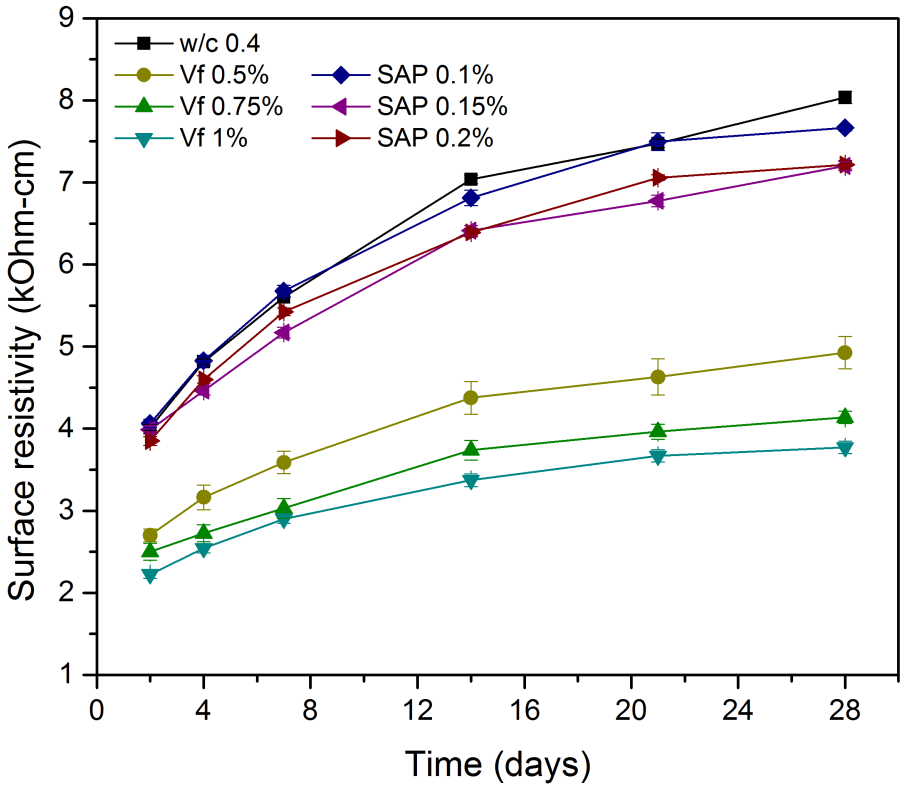

Figure 7.5 – The development of surface resistivity of limewater cured mortar specimens with nominal w/c of 0.40.

From Figure 7.5, at early ages, while the addition of SAP – particularly at rates greater than 0.1% – appeared to slightly impact surface resistivity, the inclusion of eucalyptus pulp decreased the surface resistivity of mortar samples more substantially. At 28 days, the surface resistivity of w/c 0.40 mortar was 8.03±0.07 kOhm-cm, whereas those of the eucalyptus-reinforced mortar at the fiber volume fraction of 0.5%, 0.75%, and 1% were 4.93±0.19, 4.13±0.08, and 3.80±0.07 kOhm-cm, respectively. Results show that the reduction in surface resistivity is related to but perhaps not directly proportional to the volume fraction of fibers.

Dry wood pulp fibers are insulators. However, in a cement matrix, pulp fibers carry electrolytic pore solution ions in their structures (i.e., lumen and cell wall) and act as alternative flow paths for a current applied by Wenner array. Likewise, SAP particles

also interact with the pore solution and influence resistivity. But, the effects of the two agents on resistivity are clearly different, and it is proposed that the internal curing capacity and geometry of these agents are the underlying sources for these variations in resistivity.

Due to its much higher absorption capacity, for the same amount of internal curing water, SAP is added in a much smaller dosage than wood pulp. Therefore, the average distance between SAP particles is higher than that of wood pulp. Moreover, their morphology is another important factor that should be considered. Unlike a SAP particle that has spherical-like shape, higher aspect ratio of a fiber (for this study, the aspect ratio of SAP is ~1, while that of the eucalyptus pulps is ~60-70) contributes to the formation of a continuous or more continuous path. Fibers can also bridge the capillary pores of cement and hence increase the flow of electrons through the concrete or mortar. Therefore, when wood pulps are added to concrete and mortar, the surface resistivity of fiber-blended composites is substantially reduced. Figures 7.6 and 7.7 illustrate the distribution of SAP and UKF in mortar samples. Both samples have the same entrained water-to-cement ratio of 0.015. Samples were polished with silicon carbide grinding paper with sequential grit sizes of 240, 320, 600, and 1200 using Automet lapping oil (Buehler) as a lubricant. Specimens were rinsed with ethanol for 4 minutes and dried in an oven at 40^{o}C. Images of polished samples were acquired with a Hitachi S-3200N variable pressure scanning electron microscope (VP-SEM). From the figures, while the size of SAP particles is in hundreds of a micron, that of the pulp is in tenths of a micron. Only one particle of SAP presents under the field of view whereas several fibers appear. UKF fibers also seem to disperse more evenly over the entire observed area.

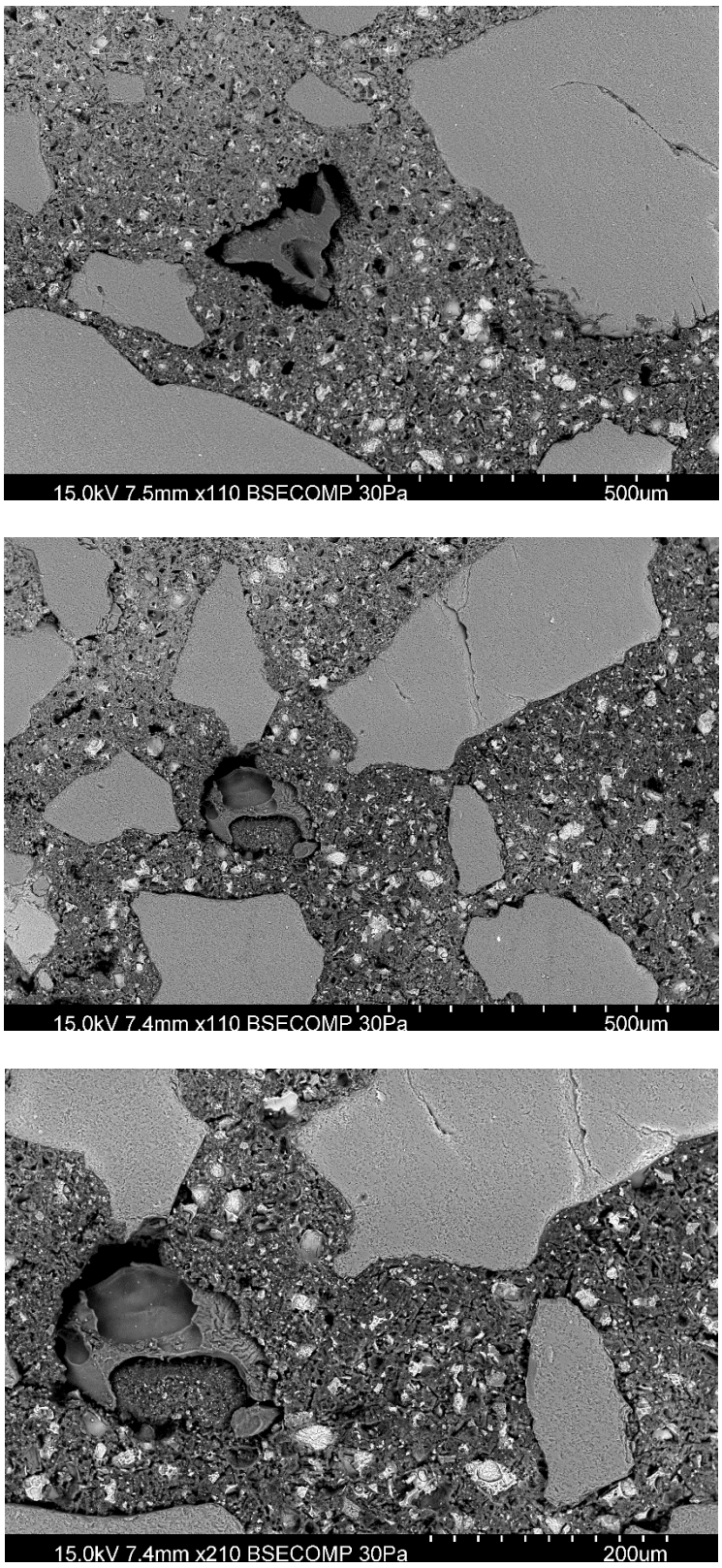

Figure 7.6 – VP-SEM images of 0.15% SAP- mortar samples.

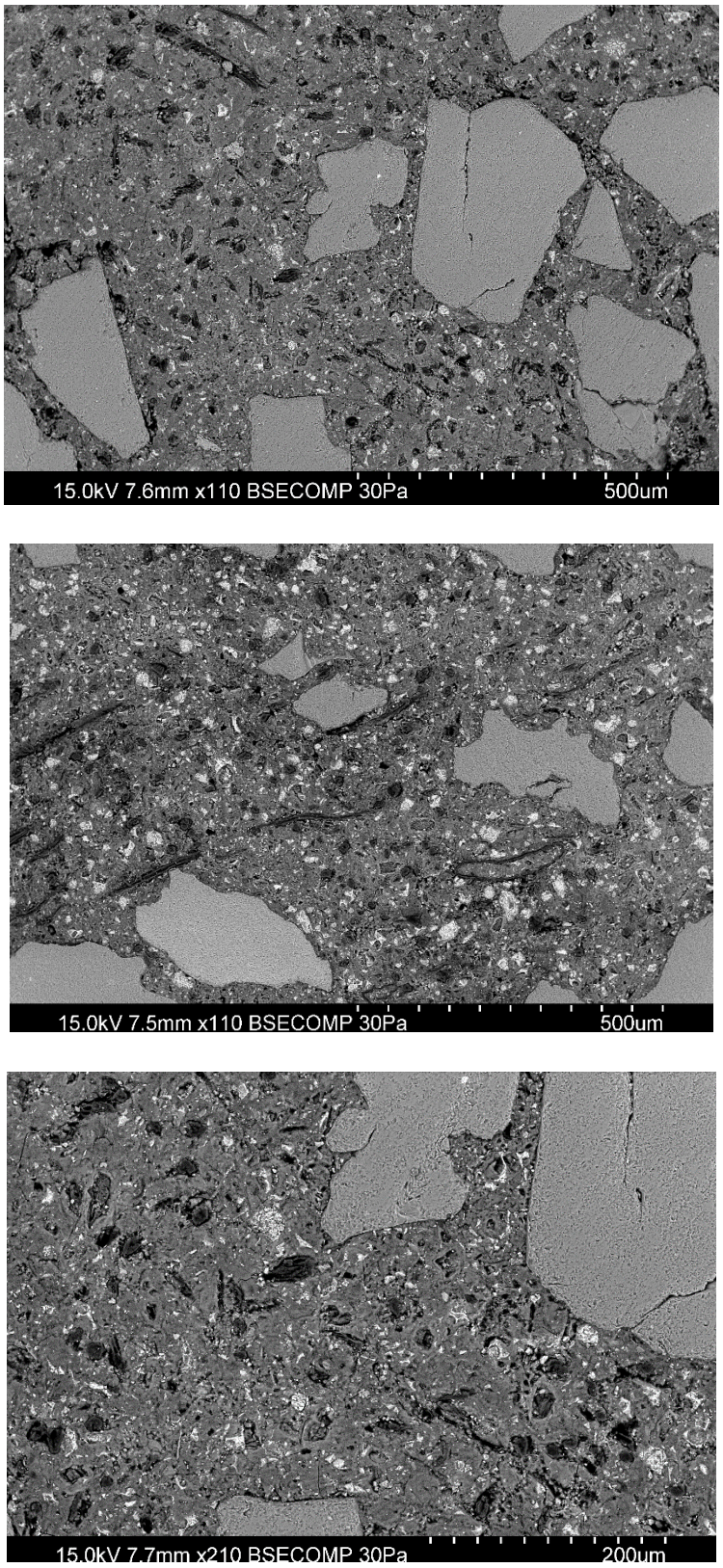

Figure 7.7 – VP-SEM images of 0.75% pulp- mortar samples.

Overall, results from this study suggest that surface resistivity may not be an appropriate test, at least as currently performed, for the indirect assessment of permeability in wood pulp-reinforced concrete. But, it is not clear if this effect is an "artifact" of the test method or if it truly influences moisture and ionic transport in pulp-fiber reinforced cementitious composites in a way which meaningfully alters service life.

To further examine this, results from a different indirect test RCPT performed on concrete specimens, both cured in limewater and air, are shown in Figure 7.8. All air cured specimens exhibited greater charge passed than that of limewater cured specimens, as expected. However, from the figure, at w/c of 0.30, the curing condition does not seem to affect plain and SAP concrete, which agrees with the compressive strength data for these concretes, which showed little effect of curing on strength at w/c of 0.30. But, curing does significantly affect RCPT values for UKF concrete at the lower w/c. In contrast, the effect of curing condition was pronounced in concrete mixes at w/c of 0.40, with limewater curing producing lower RCPT values for each case but with internal curing agents generally resulting in higher RCPT values than the control in the air-cured case.

Similar to the surface resistivity results in Figures 7.4 and 7.5, the RCPT also appears to show sensitivity to the presence of internal curing agents, but especially the pulp fibers. This is likely because wood pulp fibers, particularly given their aspect ratio and relatively large number fraction as well as their capacity for binding water and ions from the pore solution, can contribute to the connectivity forming the electrical path between the two ends of a sample.

Therefore, to more completely assess the effects of the UKF and SAP internal curing agents as well as the effect of curing conditions on transport, the apparent chloride diffusion coefficient of concrete samples at w/c of 0.30 was determined. From the results in Table 7.3, all diffusion coefficients range within an order of magnitude, except for w/c 0.30 concrete cured in limewater, which is lower. The results also showed that air-cured specimens had a higher diffusion coefficient than limewater-cured specimens, as expected [43]. Among concrete mixes, the effect of curing condition seems strongest for ordinary w/c 0.30 and lowest for UKF concrete. That is, the diffusion coefficients of air-cured samples were about 4.87, 1.93, and 2.75 times higher than that of limewater cured samples for w/c 0.3, UKF03, and SAP03 concretes, respectively. Overall, however, the presence of internal curing agents appears to result in a slight increase in chloride diffusion coefficient during air curing, relative to ordinary concrete.

In addition, using the Life 365 service life prediction model, the expected corrosion initiation time of a structure was estimated. With a chloride threshold limit (CTL) of 0.05% by weight of concrete, the Life 365 estimates were based on a 50.8 mm (2 in.) cover distance of a 508 mm (20 in.) square pile exposed in Atlanta, Georgia. Neglecting the effects of chloride binding and the reduction of apparent diffusion coefficient caused by the continued maturation of the concrete, the calculation provides a more conservative estimate of the corrosion initiation time. From Table 7.3, although the w/c 0.30 concrete provided the longest service life, its initiation time decreased significantly when the sample was cured in air. However, the UKF concrete seems to have the shortest service life but it also least affected by curing condition. In fact, the differences between limewater curing and air curing of w/c 0.30 concrete, UKF concrete,

and SAP concrete were about 20, 4, and 8 years respectively. Results also show that the UKF and SAP concretes that underwent air curing initiated corrosion almost at the same time. This suggests that internal curing, producing pore structure refinement through enhanced hydration and contributing to decreased microcracking due to shrinkage mitigation, influences the results for the UKF and SAP concretes.

The role of ion absorption by the internal curing agents, however, should be considered, as this can increase the concentration of chlorides. However, it is not clear if chlorides bound to fibers or SAPs are available to participate in corrosion reactions. As also reported in [194], because they can bind chlorides to their structure although cellulose fibers increase the coefficient of apparent (total) chloride diffusion, they decrease the effective (free) chloride diffusion. Since only free chlorides are responsible for corrosion initiation, giving that the main constituent of UKF pulps is cellulose, the actual values of UKF concrete should be longer than the estimated values shown in Table 7.3.

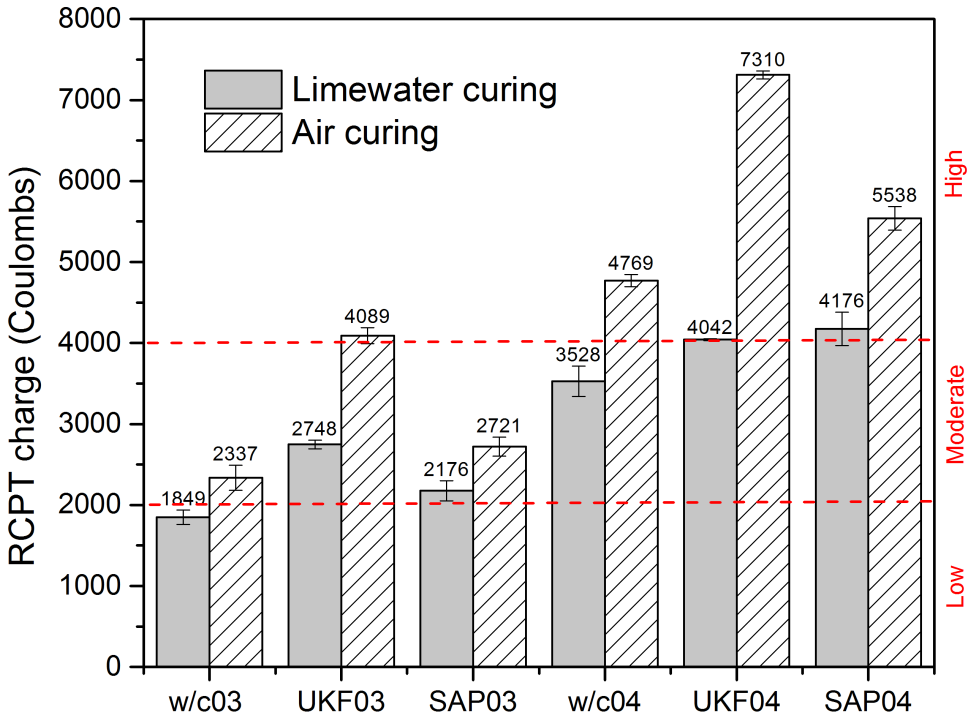

Figure 7.8 – Effects of UKF and SAP on RCPT charge in concrete samples with w/c of 0.30 and 0.40.

Table 7.3 – Diffusion coefficient from bulk diffusion test (m^2/s) and corrosion initiation time from Life 365 model (yrs).

	Diffusion coefficient		**Corrosion initiation time**			
			Parking garages		**Urban highway bridges**	
	Air curing	**Limewater curing**	**Air curing**	**Limewater curing**	**Air curing**	**Limewater curing**
w/c 0.3	3.61E-12	7.41E-13	28	49.4	31.5	54.2
UKF 03	6.96E-12	3.62E-12	23.8	27.9	27.1	31.5
SAP 03	5.95E-12	2.16E-12	24.7	32.7	28	36.5

Because cellulose fibers are hygroscopic and act as semi-permeable membranes, their properties relate to their moisture state and history of exposure to water or solutions. These characteristics can then influence their behavior in fiber-reinforced cementitious

composites such as concrete, as shown in this study. As a result, the curing condition employed in standard testing, while it may follow standard specifications, may not represent the actual curing condition in the field. Further, since wood pulp fibers in cement matrix can also be alternative flow paths for a current that is applied according to surface resistivity and RCPT tests, these experimentally-derived measures tend to overestimate permeability, at least at the fiber contents examined here. Moreover, although cellulose-based fiber appeared to contribute to increase the coefficient of apparent (total) chloride diffusion of a concrete cylinder, one should note that these specimens did not contain visible cracks, which also generate alternate flow paths that allow more water and deteriorating substances into concrete and its reinforcements. Since using cellulose pulp as internal curing reduces early-age cracking potential and hence reduces cracks, if such fibers mitigate cracking in a more restrained condition, it may eventually improve the service life of a concrete structure. Moreover, one study has reported that cellulose fibers can bind the chlorides and reduce the amount of free chlorides, which ultimately decreases the coefficient of effective (free) chloride diffusion of concrete [194]. Together with the findings in this study, it indicates the need for further studies on the role of pulps in corrosion of rebar. Such studies would account for the internal curing performance of pulps, the effects of curing condition, and the effects of cracking on the initiation of corrosion of steel rebar in concrete.

7.4 Conclusions

Since compressive strength is a fundamental property of concrete and often is the primary requirement in the job specification, it is an important parameter to consider when developing internal curing materials and identifying their appropriate dosages. This study evaluates the effects of hardwood pulp, as an internal curing agent, on concrete properties – compressive strength and permeability – both of which are common criteria for performance specifications in concrete. Results from UKF concrete cured in limewater and in air (where internal curing would be more influential) are compared with those gathered from plain concrete and companion SAP concrete that had the same amount of w_e/c of 0.02. From these experiments, these conclusions may be drawn:

- The addition of UKF did not adversely affect the compressive strength of concrete, unlike SAP. In fact, the results suggest some enhancement of the hydration reaction in UKF concrete that compensated for the reduction of compressive strength caused by decreased workability or fiber clumping.
- Because an interconnected flow path for electricity and ions may be occur in the distributed fiber system, standard tests for indirect assessment of permeability may not be appropriate for assessment of durability in systems containing absorptive fibers.

Testing concrete in a saturated condition, as required by most standard direct or indirect tests for diffusion and permeability, can lead to overestimates of these parameters for concretes containing absorptive fibers, because of the potential for wicking and the

formation of an interconnected flow path. Therefore, a new test method is necessary for assessing transport in cellulose-based fiber-reinforced concrete.

CHAPTER 8

CONCLUSIONS AND FUTURE RESEARCH

8.1 Conclusions

The use of hardwood pulps in cementitious materials has been examined in this research. This chapter presents global conclusions, key findings, recommendations and possible future research topics.

Overall, this study demonstrated that eucalyptus pulps can be used for internal curing applications to reduce early shrinkage caused by self-desiccation. The efficiency of such pulp is more strongly related to physical morphology than chemical composition, for the materials and mixture proportions examined. Pulp that has thicker cell wall is more suitable for internal curing than pulp that has thinner cell wall, as suggested by the relation between autogenous shrinkage and the physical morphology and also the NMR measurements. The NMR results indicate that pulps lose free water in their lumen within 25 h of hydration and, thus, only water that is held in the cell wall is available for further hydration. Results from fiber-cement interaction studies suggest that eucalyptus pulps acts as semi-permeable membrane in cement pore solution and serve as nucleation sites for precipitation of hydration products. The ability to improve hydration reaction is confirmed later by compressive strength of concrete. Unlike LWA and SAP, eucalyptus pulps mitigate early-age cracking without compromising the compressive strength, within the range of fiber contents examined.

8.1.1 Internal Curing Performance of Eucalyptus Pulps

Internal curing of eucalyptus pulps is related more strongly to their physical morphology than chemical composition, as measured by cellulose-to-hemicellulose ratio. A slower rate of entrained water release is preferable for internal curing of hardwood pulps. The soda pulps, both unbleached and bleached, with their thicker cell wall and higher HR water content were more effective for internal curing than kraft fibers. Semi-chemical pulp is not suitable for internal curing applications due to damage to the fibers from mechanical treatments during pulping process which resulted in fiber fracture and some fiber bundles. The partial defiberization and the poorly dispersible bundles limit their internal curing capability of semi-chemical pulp.

8.1.2 Early-age Interaction between Eucalyptus Pulps and Cements

From the analysis of T_2 relaxation of internally cured eucalyptus pulp-cement pastes, it was found that free water in the fiber lumen structure is released within 25 h of hydration. This confirms that uniformly dispersed fibers can provide from their lumens entrained free water that is readily available for internal curing. For the hydration beyond 25 hours, free water in small cell wall pores and bound water in the cell wall are responsible for mitigation of self-desiccation of a cementitious matrix. Therefore, the study supports the finding that wood pulp, within the same species, that has a thick cell wall benefits more for internal curing applications as it can retain water in its structure to mitigate further self-desiccation beyond 25 h of hydration.

Results from sorption measurements suggest that chemical wood pulps behave as a semi-permeable membrane, in which the greatest binding – in terms of reduction in concentration – occurred for the most abundant cation. Therefore, their sorption

properties depend on the binder composition (e.g. cement type), which in turn influences the pore solution composition. In both cement pore solution studies, the most abundant cation was preferentially bound by the fiber. That is, in gray cement pore solution, more K^+ was taken up, but in white cement pore solution, more Ca^{2+} was.

The surface analysis also shows the precipitation of small discrete particles on the surface. Observations by XPS show that these particles are calcium-rich phases which may include calcium silicate hydrate, calcium hydroxide and sulfate-containing calcium hydrate phases. These precipitants may facilitate hydration reaction at early ages and thus increase the early chemical shrinkage of wood pulp-cement samples.

Altogether, several mechanisms contribute to early age internal curing. First, when mixed with cement, pulp absorbs pore solution ions in its cell wall, in which selectivity depends on pH and initial ion concentration of the pore solution. Then, when self-desiccation occurs, hydrating cement paste consumes water from wood pulp by capillary draw, water vapor diffusion, and osmosis. Within 25 h of hydration, free water is desorbed from the lumen by capillary draw and water vapor diffusion resulting from humidity gradient between wood pulp and self-desiccating capillary pores. From the study, for the case of eucalyptus pulps, perhaps only free water in small wall pores and bound water are available for further hydration reaction beyond 25 h of hydration. Depending on the type of ions being absorbed in the cell water, since the composition of pore solution changes during hydration reaction, specifically after 25 h of hydration, water can also be transported through the fiber's cell wall by osmosis. In addition, since calcium-containing products will precipitate on the surface of pulp, the presence of pulp may increase the rate of hydration or be involved in osmosis process. The selective

adsorption and precipitation ultimately affect the internal curing performance of such pulps in a cement pore solution and hydration behaviors of pulp-cement composites as the changes in the concentration creates an osmotic flow.

8.1.3 The Effect of Eucalyptus Pulp on Mortar Properties

Eucalyptus pulp improves the restrained shrinkage behavior of mortar at early ages. That is, the 0.5% and 0.75% pulp-reinforced mortars exhibited a lower rate of restrained tensile stress development and lengthened time-to-cracking of about 1.6 and 2.3 times as long as the control mortar, respectively. The initial crack width also decreased by 88% in 0.75% USF reinforcement samples, which suggests the possibility of assisting self-healing in an appropriately designed mix and under appropriate environmental conditions. The key behaviors that contributed to the improved resistance to early-age cracking were identified as the combination of a reduction in self-desiccation shrinkage, an increase of early-age tensile capacity, reduction in composite modulus, and an improvement of post-cracking toughness. Microstructure observation also reveals that, when undergo air curing, fiber collapse along with slight cell wall shrinkage leaves a weaker interfacial bond that can dissipate more energy and, thus, improve post-cracking toughness.

8.1.4 The Effect of Eucalyptus Pulp on Concrete Properties

Unlike superabsorbent polymers, depending on curing conditions, eucalyptus pulp was found not to reduce compressive strength of concrete. However, any enhancements were modest: while the compressive strengths of UKF concrete cured in limewater were similar to that of ordinary concrete, the strengths of UKF concrete cured in air were about 11% higher than that of the control concrete. The improvement of compressive strength

of eucalyptus pulp over SAP can result from its properties that act like semi-permeable membrane and its ability to provide nucleation sites on the surface.

The surface resistivity, RCPT, and bulk diffusion results from air cured samples demonstrate that at dosages of 0.31 to 0.38 % by volume of concrete (or 2% by mass of cement), the hardwood fibers can provide a connected flow path for electron migration. Therefore, values obtained from an electrical migration test may underestimate the anticipated performance of wood pulp concrete. Particularly given the aspect ratio and relatively large number fraction of hardwood pulps as well as their capacity for binding water and ions from the pore solution, pulp can provide a percolation path for election migration during indirect assessments of permeability.

When obtained from saturated cured sample, the addition of eucalyptus pulp increases the coefficient of chloride diffusion because of the potential for wicking and the formation of an interconnected flow path. However, the coefficient of chloride diffusion and the initiation time for corrosion, obtained from air cured samples, confirm pore refinement through enhanced hydration and contributions of decreased microcracking due to shrinkage mitigation.

8.2 Recommendations

The study presents some aspects of using renewable hardwood eucalyptus pulps in cementitious materials and their behaviors. Along with the key mechanisms controlling internal curing efficiency as well as the early-age interaction, the use of eucalyptus pulps as internal curing agents of cement paste, mortar, and concrete is reported. Critical to the result is verification of important characteristics of hardwood pulps that will enhance

their efficiency as internal curing agents. Several techniques have been addressed for the characterization of hardwood pulp in cementitious materials. Based on the study, some recommendations are made as follows.

- For internal curing applications, if wood pulps have similar lumen size range, it is recommended to use wood pulp that has a thicker cell wall. The thick cell wall pulp can retain more water in its structure, as free water in the cell wall pores and bound water in the cell wall to further mitigate self-desiccation beyond 25 h of hydration. Otherwise, pulp that has large and open (un-collapsed) lumen structure should be used because it can hold more free water in its lumen, which is important for internal curing at earlier times.
- Among eucalyptus pulps tested, soda pulps are recommended for internal curing applications and early-age cracking mitigation. In the region in which soda pulps are not available, kraft pulps can also be used as internal curing agents. However, kraft pulps must be added at dosages higher than soda pulps to achieve the same internal curing performance.
- The use of proper methods to determine the absorption capacity of wood pulps is crucial. Since wood pulps interact with cement, even when they are chemically treated, the measurement of absorption capacity when made in water is not accurate for application in cement-based materials. Since the pH of the pore solution and the concentration of ions significantly affect the sorption and precipitation of the pore solution ions in fiber cell wall, the absorption capacity and the efficiency of wood pulp change according to cement composition. Moreover, the use of SCMs and admixtures such as

superplasticizer also affect the chemistry of pore solution ions. Thus, absorption capacity of wood pulps should be determined when wood pulps are dispersed in a cementitious matrix or at least in synthetic pore solution, both of which closely relate to the actual binder. The method suggested by Johansen [97] is recommended for the determination of absorption capacity of wood pulp for internal curing.

- Although drying shrinkage is often used as a primary indicator of shrinkage cracking for an industrial practice, this study found that drying shrinkage alone is not a sufficient indicator for the evaluation of shrinkage cracking in wood pulp-reinforced cementitious materials. However, the restrained shrinkage test is a better test for wood pulp-cementitious paste, mortar, and concrete. More thorough evaluation can be done by the combination of shrinkage tests – free drying and autogenous shrinkage tests and restrained shrinkage test – with mechanical tests such as splitting tensile strength, compressive strength, and elastic modulus to better understand the relative contributions of reinforcement and internal curing to shrinkage crack mitigation.

8.3 Future Research

This study demonstrates the use of hardwood eucalyptus pulp in cementitious materials including mortar and concrete. The present research has also demonstrated the use of new techniques to characterize the properties of wood pulps, which affect their performance in cementitious materials. However, much future research will be necessary

to generalize these techniques. Some key topics that require additional research are listed below.

- Although for eucalyptus pulps, their internal curing performance relates more strongly to their physical morphology. Since it is not clear if the results obtained from this hardwood species would be applicable to softwood species. To apply this assumption to other pulps, further studies on lignin-rich fibers are needed to verify this finding. More research on other types of pulp (i.e., softwood pulp) is necessary for generalization of this finding.
- The use of low-field NMR and MRI for *in situ* monitoring of the migration of the internal curing process in hardwood eucalyptus-cement paste was introduced. Further studies on other internal curing agents such as softwood pulp and SAP should be performed to demonstrate the value of these techniques across a wider range of internal curing agents. In addition, since low-field NMR is highly mobile and inexpensive, it will suit for on-site monitoring and quality assurance of self-curing concrete for industrial practice.
- Time-dependent deformations result from drying and creep phenomena. Therefore, for more thorough understanding of the behaviors of internally cured fiber-reinforced cementitious composites, tensile and flexural creep are other properties that should be evaluated.
- Although cellulose-based fiber appeared to contribute to the increase in the coefficient of apparent (total) chloride diffusion, it should be noted that these specimens did not contain visible cracks, which also generate alternate flow

paths that allow more water and deteriorating substances into concrete and its reinforcements. Since the use of cellulose pulps as internal curing agents reduces early-age cracking potential and hence reduces cracks, therefore, if such fibers mitigate cracking in a more restrained condition, the service life of a concrete structure may be lengthened. Moreover, one study has reported that cellulose fibers can bind the chlorides and reduce the amount of free chlorides, which ultimately decreases the coefficient of effective (free) chloride diffusion of concrete [194]. Together with the findings in this study, further studies on the role of pulps on corrosion of rebar are needed. Such studies would account for the internal curing performance of pulps, the effects of field curing conditions, and the effects of cracking on the initiation of corrosion of steel reinforcement in concrete.

- To ensure the use of eucalyptus pulp in cementitious materials, future research needs to be conducted to identify the role of eucalyptus pulp on durability of composite materials such as its performance on wet/dry cycling, freeze thaw resistance, and salt scaling.
- Based on findings that pulp with ability to hold a large amount of water in its structure after 25 h of hydration has a good performance on mitigation of autogenous shrinkage, future studies on the improvement of the water retention of pulp by perhaps cross-linking cellulose with polymer is another area of interest.
- The analyses of the potential environmental impact of eucalyptus-cementitious composites through a life cycle analysis (LCA) should be

conducted. Such analysis would account for all factors including total embodied energy and emissions of CO_2 to comprehensively quantify the sustainability of eucalyptus-cementitious composites.

REFERENCES

1. Kyrklund, B. and Strandel.G, *Applicability of chlorine number for evaluation of lignin content of pulp.* Paper Ja Puu-Papper Och Tra, 1969. 51(4A): p. 299.

2. Hillis, W.E., *Wood quality and utilization*. Eucalyptus for wood production. 1984, Sydney: Commonwealth Scientific and Industrial Research Organization.

3. ENCE, G.E., *Sustainable forest management and eucalyptus*. 2009.

4. Foelkel, C. *Papermaking properties of eucalyptus trees, woods, and pulp fibers*. 2009.

5. Tonoli, G.H.D., Savastano, H., Fuente, E., Negro, C., Blanco, A., and Lahr, F.A.R., *Eucalyptus pulp fibres as alternative reinforcement to engineered cement-based composites.* Industrial Crops and Products, 2010. 31(2): p. 225-232.

6. Dutt, D. and Tyagi, C.H., *Comparison of various eucalyptus species for their morphological, chemical, pulp and paper making characteristics.* Indian Journal of Chemical Technology, 2011. 18(2): p. 145-151.

7. Shackford, D.L., *A comparison of pulping and bleaching of kraft softwood and eucalyptus pulps*, in *36th International Pulp and Paper Congress and Exhibition*. 2003: Sao Paulo, Brazil.

8. Bentur, A. and Mindess, S., *Fiber-Reinforced Cementitious Composites*. 2007, NewYork: Taylor & Francis.

9. Mohr, B.J., Premenko, L., Nanko, H., and Kurtis, K.E. *Examination of wood-derived powder and fibers for internal curing of cement-based materials* in *Proceedings of the 4th Internatinal Seminar on Self-Desiccation and Its Importance in Concrete Technology*. 2005. Gaithersburg, MD.

10. Mezencevova, A., Garas, V., Nanko, H., and Kurtis, K., *Influence of thermomechanical pulp fiber compositions on internal curing of cementitious materials.* Journal of Materials in Civil Engineering, 2012. 24(8): p. 970-975.

11. Kawashima, S. and Shah, S.P., *Early-age autogenous and drying shrinkage behavior of cellulose fiber-reinforced cementitious materials.* Cement & Concrete Composites, 2011. 33(2): p. 201-208.

12. Mehta, P.K. and Monteiro, P.J.M., *Concrete: microstructure, properties, and materials*. 3 ed. 2006, New York, NY: McGraw-Hill.

13. Siddiqui, M.S., Nyberg, W., Smith, W., Blackwell, B., and Riding, K.A., *Effect of curing water availability and composition on cement hydration.* Aci Materials Journal, 2013. 110(3): p. 315-322.

14. Bentz, D.P. and Weiss, W.J., *Internal curing: A 2010 state-of-the art review*. 2011, National Institute of Standards and Technology.

15. ACI544.1R, *State-of-the-Art report on fiber reinforced concrete*. 2002, American Concrete Institute: Detroit, Michigan, USA.

16. Ferreira, J. and Branco, F.A.B., *The use of glass fiber-reinforced concrete as a structural material.* Experimental Techniques, 2007. 31(3): p. 64-73.

17. ASTM D7508/D7509M-10, *Standard specification for polyolefin chopped strands for use in concrete*. 2010, ASTM international: West Conshohocken (PA).

18. Pacheco-Torgal, F. and Jalali, S., *Cementitious building materials reinforced with vegetable fibres: A review.* Construction and Building Materials, 2011. 25: p. 575-581.

19. Sable, I., Grinfelds, U., Jansons, A., Vikele, L., Irbe, I., Verovkins, A., and Treimanis, A., *Comparision of the properties of wood and pulp fibers from lodgepole pine (Pinus contorta) and Scots pine (Pinus sylvestris)* Bioresources, 2012. 7(2): p. 1771-1783.

20. Neagu, R.C., Gamstedt, E.K., and Berthold, F., *Stiffness contribution of various wood fibers to composite materials.* Journal of Composite Materials, 2006. 40(8): p. 663-699.

21. Whistler, R. and BeMiller, J., *Alkaline degradation of polysaccharides.* Advances in Carbohydrate Chemistry and Biochemistry, 1958. 13: p. 289-329.

22. Miller, D. and Moslemi, A., *Wood-cement composites: effect of model compounds on hydration characteristics and tensile strength.* Wood and Fiber Science, 1991. 23(4): p. 472-82.

23. Govin, A., Peschard, A., Fredon, E., and Guyonnet, R., *New insights into wood and cement interaction.* Holzforschung, 2005. 59(3): p. 330-335.

24. Govin, A., Peschard, A., and Guyonnet, R., *Modification of cement hydration at early ages by natural and heated wood.* Cement and Concrete Composites, 2006. 28: p. 12-20.

25. Pereira, C., Jorge, F.C., and Ferreira, J.M., *Adsorption of cations from a cement suspension onto lignocellulosic substrates and its influence on cement setting.* Journal of Wood Chemistry and Technology, 2005. 25(4): p. 231-244.

26. McDonough, T.J., *Wood chemistry-fundamentals and applications* Journal of the American Chemical Society, 1983. 105(13): p. 4503-4503.

27. Smook, G.A., *Handbook of Pulp & Paper Technologists*. 1982, Atlanta, GA: TAPPI.

28. Klieger, P. *Early high strength concrete for prestressing.* in *Proceedings World Conference on Prestressed Concrete*. 1957. San Francisco.

29. Philleo, R., *Concrete science and reality*, in *Materials Science of Concrete II*, J. Skalny and Mindess, S., Editors. 1991, American Ceramic Society: Westerville, OH. p. 1-8.

30. Castro, J., De la Varga, I., and Weiss, J., *Using isothermal calorimetry to assess the water absorbed by fine LWA during mixing.* Journal of Materials in Civil Engineering, 2012. 24(8): p. 996-1005.

31. Zhutovsky, S. and Kovler, K., *Hydration kinetics of high-performance cementitious systems under different curing conditions.* Materials and Structures, 2013. 46(10): p. 1599-1611.

32. Espinoza-Hijazin, G., Paul, A., and Lopez, M., *Concrete containing natural pozzolans: New challenges for internal curing.* Journal of Materials in Civil Engineering, 2012. 24(8): p. 981-988.

33. Akcay, B. and Tasdemir, M.A., *Effects of distribution of lightweight aggregates on internal curing of concrete.* Cement & Concrete Composites, 2010. 32(8): p. 611-616.

34. Bentur, A., Igarashi, S., and Kovler, K., *Prevention of autogenous shrinkage in high-strength concrete by internal curing using wet lightweight aggregates.* Cement and Concrete Research, 2001. 31(11): p. 1587-1591.

35. Bentz, D.P., Lura, P., and Roberts, J.W., *Mixture proportioning for internal curing.* Concrete International, 2005. 27: p. 35-40.

36. Bentz, D.P. and Snyder, K.A., *Protected paste volume in concrete - Extension to internal curing using saturated lightweight fine aggregate.* Cement and Concrete Research, 1999. 29(11): p. 1863-1867.

37. Justs, J., Wyrzykowski, M., Winnefeld, F., Bajare, D., and Lura, P., *Influence of superabsorbent polymers on hydration of cement pastes with low water-to-binder ratio.* Journal of Thermal Analysis and Calorimetry, 2014. 115(1): p. 425-432.

38. Jensen, O.M., *Use of superabsorbent polymers in concrete: An overview of the possibilities offered by using these smart materials as concrete admixture*, in

Concrete international. 2013, American Concrete Institute: 38800 Country Club Drive, PO Box 9094, Farmington Hills, MI, 48331, United States.

39. ESCSI, *Internal Curing Using Expanded Shale, Clay and Slate Lightweight Aggregate*, in *Publication #4362, Internal Curing Using Expanded Shale, Clay and Slate Lightweight Aggregate* 2006, Expanded Shale Clay and Slate Institute.

40. Siramanont, J., Vichit-Vadakan, W., and Siriwatwechakul, W., *The impact of SAP structure on the effectiveness of Internal Curing*, in *International RILEM Conference on Use of Superabsorbent Polymers and Other New Additives in Concrete*. 2010, RILEM: Denmark.

41. Wyrzykowski, M., Lura, P., Pesavento, F., and Gawin, D., *Modeling of water migration during internal curing with superabsorbent polymers.* Journal of Materials in Civil Engineering, 2012. 24(8): p. 1006-1016.

42. Zhutovsky, S., Kovler, K., and Bentur, A., *Revisiting the protected paste volume concept for internal curing of high-strength concretes.* Cement and Concrete Research, 2011. 41(9): p. 981-986.

43. Siriwatwechakul, W., Siramanont, J., and Vichit-Vadakan, W., *Superabsorbent polymer structures*, in *International RILEM Conference on Use of Superabsorbent Polymers and Other New Additives in Concrete*. 2010, RILEM: Denmark.

44. Siriwatwechakul, W., Siramanont, J., and Vichit-Vadakan, W., *Behavior of superabsorbent polymers in calcium- and sodium-rich solutions.* Journal of Materials in Civil Engineering, 2012. 24(8): p. 976-980.

45. Park, S., Venditti, R.A., Jameel, H., and Pawlak, J.J., *Changes in pore size distribution during the drying of cellulose fibers as measured by differential scanning calorimetry.* Carbohydrate Polymers, 2006. 66(1): p. 97-103.

46. Cheumani, Y.A.M., Ndikontar, M., De Jeso, B., and Sebe, G., *Probing of wood-cement interactions during hydration of wood-cement composites by proton low-field NMR relaxometry.* Journal of Materials Science, 2011. 46(5): p. 1167-1175.

47. Wan, J.Q., Wang, Y., and Xiao, Q., *Effects of hemicellulose removal on cellulose fiber structure and recycling characteristics of eucalyptus pulp.* Bioresource Technology, 2010. 101(12): p. 4577-4583.

48. Wu, N., Hubbe, M.A., Rojas, O.J., and Park, S., *Permeation of polyelectrolytes and other solutes into the pore spaces of water-swollen cellulose: A review.* Bioresources, 2009. 4(3): p. 1222-1262.

49. Bendzalova, M., Pekarovicova, A., Kokta, B.V., and Chen, R.B., *Accessibility of swollen cellulosic fibers.* Cellulose Chemistry and Technology, 1996. 30(1-2): p. 19-32.

50. Lindstrom, T. and Carlsson, G., *The effect of carboxyl groups and their ionic form during drying on the hornification of cellulose fibers.* Svensk Papperstidning-Nordisk Cellulosa, 1982. 85(15): p. R146-R151.

51. Scallan, A.M., *The effect of acidic groups on the swelling of pulps - A review.* Tappi Journal, 1983. 66(11): p. 73-75.

52. Koukkari, P., Pajarre, R., and Pakarinen, H., *Modeling of the ion exchange in pulp suspensions by Gibbs energy minimization.* Journal of Solution Chemistry, 2002. 31(8): p. 627-638.

53. Barneyback, R.S. and Diamond, S., *Expression and analysis of pore fluids from hardened cement pastes and mortars.* Cement and Concrete Research, 1981. 11(2): p. 279-285.

54. Jayme, G. and Buttle, H., *The dependency of water retention value (WRV) and strength properties on the pH value during refining for various bleached and unbleached cellulose pulps.* Wochenblatt Papierfabrik, 1964. 92(23/24): p. 718-727.

55. Stamm, A.J., *Wood and cellulose science*. 1964, New York: The Ronald Press Company. 549.

56. Davidson, G.F. and Nevell, T.P., *8—The acidic properties of cotton cellulose and derived oxycelluloses part IV. Absorption of silver from silver nitrophenate solutions.* Journal of the Textile Institute Transactions, 1948. 39(3): p. T93.

57. Lothenbach, B., Winnefeld, F., Alder, C., Wieland, E., and Lunk, P., *Effect of temperature on the pore solution, microstructure and hydration products of Portland cement pastes.* Cement and Concrete Research, 2007. 37(4): p. 483-491.

58. Soroushian, P. and Marikunte, S., *Reinforcement of cement-based materials with cellulose fibers. Thin-section fiber reinforced concrete and ferrocement*, in *SP-124*. 1990, American Concrete Institute: Detroit. p. 99-124.

59. Kawachi, K., Murakami, M., and Hirahara, E., *The hydration and hardening of cement. The nuclear magnetic absorption of water molecules in cement.* Bulletin of the Faculty of Engineering Hiroshima University, 1955.

60. Gummerson, R.J., Hall, C., Hoff, W.D., Hawkes, R., Holland, G.N., and Moore, W.S., *Unsaturated water flow within porous materials observed by NMR imaging.* Nature, 1979. 281(5726): p. 56-57.

61. Kalliopi, K.A., *Pore structure of cement-based materials: testing, interpretation and requirements*. Modern concrete technology series: A series of books presenting the state-of-the-art in concrete technology, ed. A. Bentur. 2006, New York: Taylor & Francis.

62. Wang, B., Faure, P., Thiéry, M., and Baroghel-Bouny, V., *1H NMR relaxometry as an indicator of setting and water depletion during cement hydration.* Cement and Concrete Research, 2013. 45(0): p. 1-14.

63. Schreiner, L.J., Mactavish, J.C., MiljkoviĆ, L., Pintar, M.M., Blinc, R., Lahajnar, G., Lasic, D., and Reeves, L.W., *NMR line shape-spin-lattice relaxation correlation study of portland cement hydration.* Journal of the American Ceramic Society, 1985. 68(1): p. 10-16.

64. Korb, J.P., *NMR and nuclear spin relaxation of cement and concrete materials.* Current Opinion in Colloid & Interface Science, 2009. 14(3): p. 192-202.

65. Faure, P., Care, S., Po, C., and Rodts, S., *An MRI-SPI and NMR relaxation study of drying-hydration coupling effect on microstructure of cement-based materials at early age.* Magnetic Resonance Imaging, 2005. 23(2): p. 311-314.

66. Kosmac, T., Lahajnar, G., and Sepe, A., *Proton NMR relaxation study of calcium aluminate hydration reactions* Cement and Concrete Research, 1993. 23(1): p. 1-6.

67. Friedemann, K., Stallmach, F., and Kärger, J., *NMR diffusion and relaxation studies during cement hydration—A non-destructive approach for clarification of the mechanism of internal post curing of cementitious materials.* Cement and Concrete Research, 2006. 36(5): p. 817-826.

68. Kosmatka, S.H., Kerkhoff, B., and Panarese, W.C., *Design and control of concrete mixtures*. 14 ed. 2002, Skokie, Illinois: Portland cement association.

69. Greener, J., Peemoeller, H., Choi, C.H., Holly, R., Reardon, E.J., Hansson, C.M., and Pintar, M.M., *Monitoring of hydration of white cement paste with proton NMR spin-spin relaxation.* Journal of the American Ceramic Society, 2000. 83(3): p. 623-627.

70. Jaffer, S.J., Lemaire, C., Hansson, C.M., and Peemoeller, H., *MRI: A complementary tool for imaging cement pastes.* Cement and Concrete Research, 2007. 37(3): p. 369-377.

71. Balcom, B.J., Macgregor, R.P., Beyea, S.D., Green, D.P., Armstrong, R.L., and Bremner, T.W., *Single-point ramped imaging with T1 enhancement (SPRITE).* Journal of Magnetic Resonance, Series A, 1996. 123(1): p. 131-134.

72. Balcom, B., Barrita, J., Choi, C., Beyea, S., Goodyear, D., and Bremner, T., *Single-point magnetic resonance imaging (MRI) of cement based materials.* Materials and Structures, 2003. 36(3): p. 166-182.

73. Mindess, S., Young, J.F., and Darwin, D., *Concrete*. 2 ed. 2003, Upper saddle river: Prentice-Hall.

74. ASTM C157/C157M-08, *Standard test method for length change of hardened hydraulic-cement mortar and concrete*. 2008, ASTM international: West Conshohocken (PA).

75. Radlinska, A. and Weiss, J., *Toward the development of a performance-related specification for concrete shrinkage.* Journal of Materials in Civil Engineering, 2012. 24(1): p. 64-71.

76. Hossain, A.B. and Weiss, J., *Assessing residual stress development and stress relaxation in restrained concrete ring specimens.* Cement and Concrete Composites, 2004. 26: p. 531-540.

77. Weiss, W.J. and Shah, S.P., *Restrained shrinkage cracking: the role of shrinkage reducing admixtures and specimen geometry.* Materials and Structures, 2002. 35(246): p. 85-91.

78. Raoufi, K., Pour-Ghaz, M., Poursaee, A., and Weiss, J., *Restrained shrinkage cracking in concrete elements: role of substrate bond on crack development.* Journal of Materials in Civil Engineering, 2011. 23(6): p. 895-902.

79. Weiss, W.J., Yang, W., and Shah, S.P., *Influence of specimen size/geometry on shrinkage cracking of rings.* Journal of Engineering Mechanics-Asce, 2000. 126(1): p. 93-101.

80. Banthia, N., Azzabi, M., and Pigeon, M., *Restrained shrinkage cracking in fiber-reinforced cementitious composites.* Materials and Structures, 1993. 26(161): p. 405-413.

81. Bloom, R. and Bentur, A., *Free and restrained shrinkage of normal and high-strength concretes.* Aci Materials Journal, 1995. 92(2): p. 211-217.

82. Banthia, N., Yan, C., and Mindess, S., *Restrained shrinkage cracking in fiber reinforced concrete: A novel test technique.* Cement and Concrete Research, 1996. 26(1): p. 9-14.

83. Paillere, A.M., Buil, M., and Serrano, J.J., *Effect of fiber addition on the autogenous shrinkage of silica fume concrete* Aci Materials Journal, 1989. 86(2): p. 139-144.

84. Collins, F. and Sanjayan, J.G., *Cracking tendency of alkali-activated slag concrete subjected to restrained shrinkage.* Cement and Concrete Research, 2000. 30(5): p. 791-798.

85. ASTM C1581/C1581M-09a, *Standard test method for determining age at cracking and induced tensile stress characteristics of mortar and concrete under restrained shrinkage*. 2009, ASTM international: West Conshohocken (PA).

86. Balayssac, J.P., Nicot, P., Ruot, B., Devès, O., and Détriché, C.H., *Influence of admixtures on the cracking sensitivity of mortar layers applied to a mineral substrate.* Construction and Building Materials, 2011. 25(6): p. 2828-2836.

87. Mauroux, T., Benboudjema, F., Turcry, P., Ait-Mokhtar, A., and Deves, O., *Study of cracking due to drying in coating mortars by digital image correlation.* Cement and Concrete Research, 2012. 42(7): p. 1014-1023.

88. Lopez, M., Kahn, L.F., and Kurtis, K.E., *Characterization of elastic and time-dependent deformations in normal strength and high performance concrete by image analysis.* Cement and Concrete Research, 2007. 37(8): p. 1265-1277.

89. Sarigaphuti, M., Shan, S.P., and Vinson, K.D., *Shrinkage cracking and durability characteristics of cellulose fiber reinforced concrete.* ACI Material Journal, 1993. 90(4): p. 309-318.

90. Filho, R.D.T., Ghavami, K., Sanjuan, M.A., and England, G.L., *Free, restrained and drying shrinkage of cement mortar composites reinforced with vegetable fibres.* Cement and Concrete Composites, 2005. 27: p. 537-546.

91. Soroushian, P., *Reinforcing effects on processed cellulose fibers in mortar (stucco), thin sheet products, and concrete,* in *High-performance fiber-reinforced concrete thin sheet products*. 2000, American Concrete Institute: Detroit. p. 203-214.

92. Chinga-Carrasco, G., Lenes, M., Johnsen, P.O., and Hult, E.L., *Computer-assisted scanning electron microscopy of wood pulp fibres: Dimensions and spatial distributions in a polypropylene composite.* Micron, 2009. 40(7): p. 761-768.

93. Reme, P.A., Johnsen, P.O., and Helle, T., *Assessment of fibre transverse dimensions using SEM and image analysis.* Journal of Pulp and Paper Science, 2002. 28(4): p. 122-128.

94. Laine, J., Stenius, P., Carlsson, G., and Strom, G., *Surface characterization of unbleached kraft pulps by means of ESCA.* Cellulose, 1994. 1(2): p. 145-160.

95. Yang, H., Yang, R., Chen, H., Lee, D.H., and Zheng, C., *Characteristic of hemicellulose, cellulose and lignin pyrolysis.* Fuel, 2007. 86(12-13): p. 1781-1788.

96. Park, S., Venditti, R.A., Jameel, H., and Pawlak, J.J., *Hard to remove water in cellulose fibers characterized by high resolution thermogravimetric analysis - methods development.* Cellulose, 2006. 13(1): p. 23-30.

97. Johansen, N.A., Millard, M.J., Mezencevova, A., Garas, V.Y., and Kurtis, K.E., *New method for determination of absorption capacity of internal curing agents.* Cement and Concrete Research, 2009. 39(1): p. 65-68.

98. ASTM D4442-07, *Standard test methods for direct moisture content measurement of wood and wood-base materials*. 2007, ASTM international: West Conshohocken (PA).

99. ASTM C1698-09, *Standard Test method for autogenous strain of cement paste and mortar* 2010, ASTM international: West Conshohocken (PA).

100. ASTM C191-08, *Standard test methods for time of setting of hydraulic cement by vicat needle*. 2008, ASTM international: West Conshohocken (PA).

101. Clark, J.d.A., *Pulp Technology and Treatment for Paper*. 1985, San Francisco: Miller Freeman Publications.

102. Ramezani, O. and Nazhad, M.M. *The effect of coarseness on paper formation. www.tappsa.co.za/archive2/APPW_2004/Title2004. Accessed in June 2012*. 2004 Consulted in June 2012]; Available from: www.tappsa.co.za/archive2/APPW_2004/Title2004.

103. Paavilainen, L., *Fiber structure*, in *Handbook of Physical Testing of paper*, R.E. Mark, et al., Editors. 2002, Marcel Dekker, Inc.: New York. p. 700-725.

104. Pulkkinen, I., Alopaeus, V., Fiskari, J., and Joutsimo, O., *The use of fibre wall thickness data to predict handsheet properties of eucalypt pulp fibres*, in *O Papel*. 2008, ABCTP. p. 71-85.

105. Park, S., Venditti, R.A., Jameel, H., and Pawlak, J.J., *A novel method to evaluate fibre hornification by high resolution thermogravimetric analysis.* Appita Journal, 2006. 59(6): p. 481-485.

106. Stone, J.E. and Scallan, A.M., *The effect of component removal upon the porous structure of the cell wall of wood. II. Swelling in water and the fiber saturation point.* Tappi Journal, 1967. 50(10): p. 496-501.

107. Goring, D.A.I., *A speculative picture of the delignification process*, in *ACS Symposium Series*. 1977, American Chemical Society: Washington, D.C. p. 273-277.

108. Odler, I. and Becker, T., *Effect of some liquefying agents on properties and hydration of portland-cement and tricalcium silicate pastes.* Cement and Concrete Research, 1980. 10(3): p. 321-331.

109. Mohr, B.J. and Hood, K.L., *Influence of bleed water reabsorption on cement paste autogenous deformation.* Cement and Concrete Research, 2010. 40(2): p. 220-225.

110. Coutts, R.S.P., *Wood fibres in inorganic matrices.* Chemistry in Australia, 1983. 50: p. 143-148.

111. Hamad, W., *Cellulosic Materials: Fibers, Networks, and Composites*. 2002, Boston, MA: Kluwer Academic Publishers.

112. Geiker, M., Bentz, D.P., and Jensen, O.M., *Mitigating autogenous shrinkage by internal curing*, in *American Concrete Institute Special Publication 218, High Performance Structural Lightweight Concrete*, J.P. Ries and Holm, T.A., Editors. 2004. p. 143-154.

113. Rowell, R.M. and Stout, H.P., *Jute and kenaf*, in *Handbook of Fiber Chemistry* M. Lewin, Editor. 1998, Marcel Dekker. p. 1103p.

114. Castro, J., Keiser, L., Golias, M., and Weiss, J., *Absorption and desorption properties of fine lightweight aggregate for application to internally cured concrete mixtures.* Cement & Concrete Composites, 2011. 33(10): p. 1001-1008.

115. Schrofl, C., Mechtcherine, V., and Gorges, M., *Relation between the molecular structure and the efficiency of superabsorbent polymers (SAP) as concrete admixture to mitigate autogenous shrinkage.* Cement and Concrete Research, 2012. 42(6): p. 865-873.

116. Herrington, T. and Petzold, J., *Surface area of papermaking woodpulps used by the British paper industry.* Cellulose, 1995. 2(2): p. 83-94.

117. Jayapalan, A.R., Lee, B.Y., and Kurtis, K.E., *Can nanotechnology be 'green'? Comparing efficacy of nano and microparticles in cementitious materials.* Cement & Concrete Composites, 2013. 36: p. 16-24.

118. Mohr, B.J., *Durability of pulp fiber-cement composites*, in *Civil and Environmental Engineering*. 2005, Georgia Institute of Technology: Atlanta.

119. Mohr, B.J., Nanko, H., and Kurtis, K.E., *Durability of thermomechanical pulp fiber-cement composites to wet/dry cycling.* Cement and Concrete Research, 2005. 35(8): p. 1646-1649.

120. Mohr, B.J., Nanko, H., and Kurtis, K.E., *Durability of kraft pulp fiber-cement composites to wet/dry cycling.* Cement and Concrete Composites, 2005. 27(4): p. 435-448.

121. Bentz, D.P., Halleck, P.M., Grader, A.S., and Roberts, J.W. *Four-dimensional X-ray microtomography study of water movement during internal curing*. in *The International RILEM Conference – Volume Changes of Hardening Concrete: Testing and Mitigation*. 2006. Bagneux, France: RILEM

122. Friedemann, K., Schonfelder, W., Stallmach, F., and Karger, J., *NMR relaxometry during internal curing of Portland cements by lightweight aggregates.* Materials and Structures, 2008. 41(10): p. 1647-1655.

123. Friedemann, K., Stallmach, F., and Karger, J., *Carboxylates and sulfates of polysaccharides for controlled internal water release during cement hydration.* Cement & Concrete Composites, 2009. 31(4): p. 244-249.

124. Lura, P., Bentz, D.P., Lange, D.A., Kovler, K., Bentur, A., and van Breugel, K., *Measurement of water transport from saturated pumice aggregates to hardening cement paste.* Materials and Structures, 2006. 39(9): p. 861-868.

125. Barrita, F., Bremner, T.W., and Balcom, B.J., *Use of magnetic resonance imaging to study internal moist curing in concrete containing saturated lightweight aggregate*, in *High-Performance Structural Lightweight Concrete*, J.P. Ries and Holm, T.A., Editors. 2004, American Concrete Institute: Farmington Hills. p. 155-175.

126. Nestle, N., Kuhn, A., Friedemann, K., Horch, C., Stallmach, F., and Herth, G., *Water balance and pore structure development in cementitious materials in internal curing with modified superabsorbent polymer studied by NMR.* Microporous and Mesoporous Materials, 2009. 125(1-2): p. 51-57.

127. See, H.T., Attiogbe, E.K., and Miltenberger, M.A., *Potential for restrained shrinkage cracking of concrete and mortar.* Cement Concrete and Aggregates, 2004. 26(2): p. 123-130.

128. jongvisuttisun, P. and kurtis, K.E., *Chemisorption of pore solution ions in wood pulps during early hydration of cements*. in preparation for submission to journal of the american ceramic society.

129. Tritik, P., Munch, B., Weiss, W., Herth, G., Kaestner, A., and Lehmann, E., *Neutron tomography investigation of water release from superabsorbent polymers*

in cement paste, in *International Conference on Material Science and 64th RILEM Annual Week*. 2010, RILEM: Aachen.

130. Cano-Barrita, P.F.D., Balcom, B.J., Bremner, T.W., MacMillan, M.B., and Langley, W.S., *Moisture distribution in drying ordinary and high performance concrete cured in a simulated hot dry climate.* Materials and Structures, 2004. 37(272): p. 522-531.

131. Menon, R.S., Mackay, A.L., Hailey, J.R.T., Bloom, M., Burgess, A.E., and Swanson, J.S., *An NMR determination of the physiological water distribution in wood during drying.* Journal of Applied Polymer Science, 1987. 33(4): p. 1141-1155.

132. Topgaard, D. and Soderman, O., *Changes of cellulose fiber wall structure during drying investigated using NMR self-diffusion and relaxation experiments.* Cellulose, 2002. 9(2): p. 139-147.

133. Bentz, D.P., *A review of early-age properties of cement-based materials.* Cement and Concrete Research, 2008. 38(2): p. 196-204.

134. Chen, H., Wyrzykowski, M., Scrivener, K., and Lura, P., *Prediction of self-desiccation in low water-to-cement ratio pastes based on pore structure evolution.* Cement and Concrete Research, 2013. 49: p. 38-47.

135. Bohris, A.J., Goerke, U., McDonald, P.J., Mulheron, M., Newling, B., and Le Page, B., *A broad line NMR and MRI study of water and water transport in portland cement pastes.* Magnetic Resonance Imaging, 1998. 16(5–6): p. 455-461.

136. Koptyug, I.V., *MRI of mass transport in porous media: Drying and sorption processes.* Progress in Nuclear Magnetic Resonance Spectroscopy, 2012. 65(0): p. 1-65.

137. Faure, P.F. and Rodts, S., *Proton NMR relaxation as a probe for setting cement pastes.* Magnetic Resonance Imaging, 2008. 26(8): p. 1183-1196.

138. Jensen, O.M. and Hansen, P.F., *Water-entrained cement-based materials I. Principles and theoretical background.* Cement and Concrete Research, 2001. 31(4): p. 647-654.

139. Jongvisuttisun, P., Negrello, C., and Kurtis, K.E., *Effect of processing variables on efficiency of eucalyptus pulps for internal curing.* Cement and Concrete Composites, 2013. 37(0): p. 126-135.

140. Jongvisuttisun, P., Negrello, C., and Kurtis, K.E., *Efficiency of eucalyptus pulps for internal curing.* ACI SP290, 2012. 03: p. 1-12.

141. Duong, T.D., Nguyen, K.L., and Hoang, M., *Competitive sorption of Na+ and Ca2+ ions on unbleached kraft fibres—A kinetics and equilibrium study.* Journal of Colloid and Interface Science, 2006. 301(2): p. 446-451.

142. Duong, T.D., Hoang, M., and Nguyen, K.L., *Sorption of Na+, Ca2+ ions from aqueous solution onto unbleached kraft fibers—kinetics and equilibrium studies.* Journal of Colloid and Interface Science, 2005. 287(2): p. 438-443.

143. Duong, T.D., Hoang, M., and Nguyen, K.L., *Extension of Donnan theory to predict calcium ion exchange on phenolic hydroxyl sites of unbleached kraft fibers.* Journal of Colloid and Interface Science, 2004. 276(1): p. 6-12.

144. ASTM C1301-95(2009)e1, *Standard test method for major and trace elements in limestone and lime by inductively coupled plasma-atomic emission spectroscopy (ICP) and atomic absorption (AA)*. 2009, ASTM international: West Conshohocken (PA).

145. Hocking, M.B., *15 - Production of pulp and paper*, in *Handbook of Chemical Technology and Pollution Control (Third Edition)*, M.B. Hocking, Editor. 2005, Academic Press: San Diego.

146. Buchanan, C.E., *Rapid determination of the predominant form of calcium sulfate found In portland cement and Its effect on premature stiffening.* Cement Concrete and Aggregates, 1980. 2(2): p. 84-88.

147. Lerch, W., *The influence of gypsum on the hydration and properties of portland cement pastes - discussion.* Proceedings-American Society for Testing and Materials, 1946. 46: p. 1252-1297.

148. Su, P.P., Granholm, K., Harju, L., and Ivaska, A., *Binding affinities of different metal ions to unbleached hardwood kraft pulp.* Holzforschung, 2011. 65(4): p. 619-622.

149. Yuan, G.X., Dai, H.Q., Ye, C.H., Zhang, Y.J., and Wang, Z.L., *Absorption of Ca(II) from aqueous solution onto cellulosic fibers and its impact on the pepermaking process.* Bioresources, 2011. 6(3): p. 2790-2804.

150. Peled, A., Castro, J., and Weiss, W.J., *Atomic force and lateral force microscopy (AFM and LFM) examinations of cement and cement hydration products.* Cement & Concrete Composites, 2013. 36: p. 48-55.

151. Gartner, E.M., Kurtis, K.E., and Monteiro, P.J.M., *Proposed mechanism of C-S-H growth tested by soft X-ray microscopy.* Cement and Concrete Research, 2000. 30(5): p. 817-822.

152. Cusson, D. and Hoogeveen, T., *Internal curing of high-performance concrete with pre-soaked fine lightweight aggregate for prevention of autogenous shrinkage cracking.* Cement and Concrete Research, 2008. 38(6): p. 757-765.

153. ASTM C897-05, *Standard specification for aggregate for job-mixed portland cement-based plaster*. 2005, ASTM international: West Conshohocken (PA).

154. Zhutovsky, S., Kovler, K., and Bentur, A., *Effect of hybrid curing on cracking potential of high-performance concrete.* Cement and Concrete Research, 2013. 54(0): p. 36-42.

155. ASTM C1581-09, *Standard test method for determining age at cracking and induced tensile stress characteristics of mortar and concrete under restrained shrinkage*. 2009, ASTM international: West Conshohocken (PA).

156. ASTM C490/C490M-11, *Standard practice for use of apparatus for the determination of length change of hardened cement paste, mortar, and concrete*. 2011, ASTM international: West Conshohocken (PA).

157. ASTM C496/C496M–11, *Standard test method for splitting tensile strength of cylindrical concrete specimens*. 2011, ASTM international: West Conshohocken (PA).

158. ASTM C215-08, *Standard test method for fundamental transverse, longitudinal, and torsional frequencies of concrete specimens*. 2008, ASTM international: West Conshohocken (PA).

159. ASTM C348-08, *Standard test method for flexural strength of hydraulic-cement mortars*. 2008, ASTM international: West Conshohocken (PA).

160. Mohr, B.J., Nanko, H., and Kurtis, K.E., *Aligned kraft pulp fiber sheets for reinforcing mortar.* Cement and Concrete Composites, 2006. 28(2): p. 161-172.

161. El-Ashkar, N.H., Nanko, H., and Kurtis, K.E., *Effect of moisture state on mechanical behavior and microstructure of pulp fiber-cement mortars.* Journal of Materials in Civil Engineering, 2007. 19(8): p. 691-699.

162. De la Varga, I., Castro, J., Bentz, D., and Weiss, J., *Application of internal curing for mixtures containing high volumes of fly ash.* Cement & Concrete Composites, 2012. 34(9): p. 1001-1008.

163. Henkensiefken, R., Bentz, D., Nantung, T., and Weiss, J., *Volume change and cracking in internally cured mixtures made with saturated lightweight aggregate under sealed and unsealed conditions.* Cement & Concrete Composites, 2009. 31(7): p. 427-437.

164. Şahmaran, M., *Effect of flexure induced transverse crack and self-healing on chloride diffusivity of reinforced mortar.* Journal of Materials Science, 2007. 42(22): p. 9131-9136.

165. Yang, Y.Z., Lepech, M.D., Yang, E.H., and Li, V.C., *Autogenous healing of engineered cementitious composites under wet-dry cycles.* Cement and Concrete Research, 2009. 39(5): p. 382-390.

166. Swamy, N. and Rigby, G., *Dynamic properties of hardened paste, mortar and concrete.* Matériaux et Construction, 1971. 4(1): p. 13-40.

167. Lamond, F.J. and Pielert, H.J., *Significance of tests and properties of concrete and concrete-making materials*. ASTM special technical publication ;. 1978, ASTM: Philadelphia.

168. Zhang, Z.Z., Olek, J., and Diamond, S., *Studies on delayed ettringite formation in early-age, heat-cured mortars. I. Expansion measurements, changes in dynamic modulus of elasticity, and weight gains.* Cement and Concrete Research, 2002. 32(11): p. 1729-1736.

169. Shin, K.J., Bucher, B., and Weiss, J., *Role of Lightweight Synthetic Particles on the Restrained Shrinkage Cracking Behavior of Mortar*. Journal of Materials in Civil Engineering, 2011. 23(5): p. 597-605.

170. Troxell, G.E., Davis, H.E., and Kelly, J.W., *Composition and properties of concrete*. 1968, New York: McGraw-Hill.

171. Coutts, R.S.P. and Warden, P.G., *Air cured wood pulp, fiber cement composites.* journal of materials science, 1985. 4: p. 117-119.

172. El-Ashkar, N.H., *Wood pulp microfibers in cement-based composites: improving fiber distribution and characterizing composite behavior*, in *Civil and Environmental Engineering*. 2002, Georgia Institute of Technology: Atlanta. p. 343.

173. Soroushian, P., Marikunte, S., and Won, J.-P., *Wood fiber reinforced cement composites under wetting-drying and freezing-thawing cycles.* Journal of materials in civil engineering, 1994. 6(4): p. 595-611.

174. Bentur, A. and Akers, S.A.S., *The microstructure and ageing of cellulose fibre reinforced cement composites cured in a normal environment.* The International Journal of Cement Composites and Lightweight Concrete, 1989. 11(2): p. 99-109.

175. Akers, S.A.S. and Studinka, J.B., *Ageing behaviour of cellulose fibre cement composites in natural weathering and accelerated test.* Int J Cem Compos Lightweight Concr, 1989. 11: p. 93-97.

176. Coutts, R.S.P., *A review of Australian research into natural fibre cement composites.* Cement and Concrete Composites, 2005. 27: p. 518-526.

177. Yurtdas, I., Peng, H., Burlion, N., and Skoczylas, F., *Influences of water by cement ratio on mechanical properties of mortars submitted to drying.* Cement and Concrete Research, 2006. 36(7): p. 1286-1293.

178. Kim, J.K. and Mai, Y.W., *High-strength, high fracture-toughness fibre composites with interface control-A review*. Composites Science and Technology, 1991. 41(4): p. 333-378.

179. Hasholt, M.T., Jensen, O.M., Kovler, K., and Zhutovsky, S., *Can superabsorent polymers mitigate autogenous shrinkage of internally cured concrete without compromising the strength?* Construction and Building Materials, 2012. 31: p. 226-230.

180. Piérard, J., Pollet, V., and Cauberg, N. *Mitigating autogenous shrinkage in HPC by internal curing using superabsorbent polymers*. in *Volume changes of hardening concrete: testing and mitigation*. 2006. Bagneux (France): RILEM.

181. Keskin, S.B., Sulaiman, K., Sahmaran, M., and Yaman, I.O., *Effect of Presoaked Expanded Perlite Aggregate on the Dimensional Stability and Mechanical Properties of Engineered Cementitious Composites.* Journal of Materials in Civil Engineering, 2013. 25(6): p. 763-771.

182. Bentchikou, M., Guidoum, A., Scrivener, K.L., Silhadi, K., and Hanini, S. *Effect of cellulose fibre on the thermal and mechanical properties of cement paste*. in *International RILEM Conference on the Use of Recycled Materials in Buildings and Structures*. 2004. Barcelona, Spain: RILEM.

183. Lin, X., Silsbeeb, M.R., Roy, D.M., Kessler, K., and Blankenhorna, P.R., *Approaches to improve the properties of wood fiber reinforced cementitious composites.* Cement and Concrete Research, 1994. 24(8): p. 1558-1566.

184. Blankenhorn, P.R., Blankenhorn, B., Silsbeeb, M.R., and DiCola, M., *Effects of fiber surface treatments on mechanical properties of wood fiber-cement composites.* cement and Concrete Research, 2001. 31: p. 1049-1055.

185. Soroushian, P. and Ravanbakhsh, S., *High-early-strength concrete: Mixture proportioning with processed cellulose fibers for durability.* ACI Material Journal, 1999. 96(5): p. 593-599.

186. Chung, D.D.L., *Dispersion of short fibers in cement.* Journal of Materials in Civil Engineering, 2005. 17(4): p. 379-383.

187. Coutts, R.S.P., *Wood fibre reinforced cement composites*, in *Natural fibre reinforced cement and concrete*, R.N. Swamy, Editor. 1988, Blackie: Glasgow. p. 143-172.

188. Risen, J., Hulten, A.H., and Paulsson, M., *Influence of fiber properties on the network strength of softwood and hardwood kraft pulp fibers from different stages of a bleaching sequence.* Journal of Wood Chemistry and Technology, 2004. 24(4): p. 289-306.

189. Jongvisuttisun, P., Florencio-Aleman, C., and Kurtis, K.E., *Chemical interactions between natural fibers and cement examined at the nanoscale*, in *10th fib International PhD Symposium in Civil Engineering*. 2014: Quebec, Canada.

190. Chun, Y., *Investigation on the use of pulp and paper mill residual solids in producing durable concrete*. 2002, University of Wisconsin-Milwaukee. p. 256.

191. Banthia, N. and Bhargava, A., *Permeability of stressed concrete and role of fiber reinforcement.* Aci Materials Journal, 2007. 104(1): p. 70-76.

192. Bhargava, A. and Banthia, N., *Permeability of concrete with fiber reinforcement and service life predictions.* Materials and Structures, 2008. 41(2): p. 363-372.

193. Sappakittipakorn, M., *Microstructural refinements in concrete due to fiber reinforcement and its influence on corrosion initiation of reinforcing steel*. 2010, The University of British Columbia: Vancouver.

194. Sappakittipakorn, M. and Banthia, N., *Corrosion of Rebar and Role of Fiber Reinforced Concrete.* Journal of Testing and Evaluation, 2012. 40(1): p. 127-136.

195. ASTM C39/39M-14, *Standard test method for compressive strength of cylindrical concrete specimens*. 2014, ASTM international: West Conshohocken (PA).

196. ASTM C1202-12, *Standard test method for electrical indication of concrete's ability to resist chloride ion penetration*. 2012, ASTM international: West Conshohocken (PA).

197. ASTM C1556-11a, *Standard test method for determining the apparent chloride diffusion coefficient of cementitious mixtures by bulk diffusion*. 2011, ASTM international: West Conshohocken (PA).

198. ASTM C1152/C1152M-04(2012)e1, *Standard test method for acid-soluble chloride in mortar and concrete*. 2012, ASTM international: West Conshohocken (PA).

199. Kovler, K., *Effect of Superabsorbent Polymers on the Mechanical Properties of Concrete*, in *Application of Super Absorbent Polymers (SAP) in Concrete*

Construction, 2012 State-of-the-Art Report Prepared by Technical Committee 225-SAP, V. Mechtcherine and Reinhardt, H.-W., Editors. 2012, RILEM.

200. Flatt, R.J., Scherer, G.W., and Bullard, J.W., *Why alite stops hydrating below 80% relative humidity.* Cement and Concrete Research, 2011. 41(9): p. 987-992.

201. Mohr, B.J., Biernacki, J.J., and Kurtis, K.E., *Supplementary cementitious materials for mitigating degradation of kraft pulp fiber-cement composites.* Cement and Concrete Research, 2007. 37: p. 1531-1543.

202. AASHTO TP95-11, *Standard method of test for surface resistivity indication of concrete's ability to resist chloride ion penetration*. 2011, American Association of State and Highway Transportation Officials.

203. Nadelman, E. and Kurtis, K.E., *A resistivity-based approach to optimizing concrete performance.* Ci Concrete international, 2013. submitted for pulbication.

204. Liu, Y., Suarez, A., and Presuel-Moreno, F.J., *Characterization of new and old concrete structures using surface resistivity measurements*. 2010, Florida Department of Transportation Research Center: Tallahassee, Florida.